TRACE HYDROGEN IN MINERALS

Thesis by

Roger Deane Aines

In Partial Fulfillment of the Requirements

for the Degree of

Doctor of Philosophy

California Institute of Technology

Pasadena, California

1984

(Submitted April 9, 1984)

Acknowledgments

Acknowledgments to individuals who aided the progress of each of the projects included in this thesis are included at the end of each chapter. However, I would like here to acknowledge those individuals who aided or influenced a greater portion of my thesis and graduate studies.

George Rossman, my thesis advisor, has been an understanding supervisor, an invigorating source of ideas and new outlooks, and has always allowed me the independence to proceed and learn on my own while still providing advice and assistance whenever required. Ed Stolper has supplied much of the impetus and assistance required for me to begin applying the techniques and findings of my study of trace water to important problems of petrologic interest. I would like to thank C.C. Patterson for supporting me before I had settled on a thesis topic, for introducing me to the problem of lead pollution and for teaching me the precise attitudes required to work in a clean lab which have served me well in later scientific studies under other conditions. Sam Epstein has watched over my scientific and academic progress with a much appreciated concern for my best interests.

Much of my work has been done in conjunction with undergraduate students working both over the summer and during the year. Chris Finch, Bill Gould, Martin Ruzek, Darrel Schlom, Mary Yang, and Phil Ihinger have all both aided and stimulated my studies of trace hydrogen. Martin Ruzek deserves special thanks for constructing and maintaining much of the equipment used in this study. My conversations, collaborations and interactions with my fellow graduate students have been of inestimable

value, providing an undercurrent of understanding and continuity of techniques and interpretations. I would like to gratefully acknowledge Stephanie Mattson, Anne Hofmeister, Gerry Fine, Cleve Solomon, Jim Conca, Julie Paque and Lynn Silver for providing their help, support, ideas and criticisms without which this thesis would not have been accomplished.

Some of my work applying the study of trace hydrogen to problems of geologic interest has been done in conjunction with investigators from other institutions. I would like to thank Steve Kirby and Andreas Kronenberg (U.S.G.S, Menlo Park), John Holloway (Arizona State University), Werner Schreyer (Ruhr-Universität, Bochum), and W. Johannes (Technischen Universität, Hannover) for their assistance and collaboration.

Abstract

Trace hydrogen in minerals most frequently occurs bonded to oxygen. The resulting water and hydroxyl (OH^-) affect and play a role in a variety of mineral properties and reactions. This thesis examines the occurrence of trace hydrogen in nominally anhydrous minerals, the mechanisms by which trace hydrogen participates in reactions and controls properties, and the changes that occur in hydrogen speciation and siting as a function of temperature. The principal tool used in this study is infrared (IR) spectroscopy because of its sensitivity to the highly polar O-H bond, yielding quantitative information on concentration, and symmetry, speciation, and siting information.

The speciation of trace hydrogen in garnet and low temperature natural and synthetic quartz is examined in detail. In garnet hydrogen occurs as the hydrogarnet substitution, four hydroxyl groups replacing a silicate tetrahedron. This substitution is extremely common among natural garnets. Concentrations range from 0.05 to 0.20 wt. % (as H_2O) in garnets from most occurrences, including garnets from the mantle. This trace hydrogen is truly dissolved. The hydrogen found in natural and synthetic quartz formed at low temperature can occur as either hydroxyl or molecular water. The molecular water is the active participant in hydrolytic weakening of quartz, but it is not truly dissolved. It occurs as small groups of molecules (approximately 5 to 200) which were trapped during rapid growth.

Two properties of minerals affected by trace hydrogen are strength and radiation response. Molecular water may be responsible for weakening of other minerals as well as quartz. Both water and hydroxyl participate in radiation response of minerals. In metamict zircon,

water stabilizes local charge imbalance formed when bonds are broken. Water enters the crystal after a threshold of damage occurs, and reacts with broken bonds to form hydroxyl groups. These must reform molecular water and be expelled before recrystallization occurs during heating. In quartz, molecular water is strongly correlated with the formation of citrine color during irradiation, but inhibits the formation of the amethyst color center Fe^{4+}. Apparently molecular hydrogen forms during radiolysis of the water, and reduces the Fe^{4+}. Several hydroxyl sites in topaz are strongly correlated with the formation of brown color upon irradiation. The unifying theme in all these reactions is the extreme mobility of hydrogen and the ease with which different oxygen-hydrogen species may be formed in silicates.

The behavior of trace hydrogen at temperatures of geologic interest has been examined using high temperature infrared spectroscopy. Direct observations of speciation, concentration, and properties have been made up to 1200°C. In muscovite there is no change in hydrogen speciation or site up to the dehydration point, as expected. However, in cordierite and beryl water reversibly partitions into a gas-like state above 400°C, and the formation of this new state controls the dehydration behavior. In topaz, hydroxyl groups have been observed converting to new sites at temperatures above 500°C. In orthoclase feldspar, one type of molecular water dehydrates at 200°C, while a second type converts irreversibly to a new hydrous species above 600°C.

There is no evidence for the existence of hydrogen species other than hydroxyl and water in silicate minerals. The hydrogarnet substitution (four hydroxyl groups in a tetrahedral configuration) is common in garnets and may be important in other orthosilicates. The

most common hydrous species in nominally anhydrous silicates (aside from fluid inclusions and alteration) are: small groups of trapped water molecules; individual water molecules occupying voids in the structure of minerals; hydroxyl occurring in a charge balancing role such as AlO_3OH substituting for SiO_4; hydroxyl neutralizing substitutional atoms, e.g., LiOH; and hydroxyl groups formed from the reaction of broken bonds with water as in radiation damaged minerals. There is no evidence for the presence of the oxonium ion, H_3O^+, in common minerals, and the existing evidence for the occurrence of molecular hydrogen may better be explained by the presence of water or hydroxyl groups.

Preface

Each of the chapters of this thesis (with the exception of the introduction and summary) are intended as articles for publication, and as such each contains an introduction, experimental section, and references at the end of the chapter. This has resulted in a certain amount of duplication of material, but I believe that the additional ease with which each chapter may be read more than makes up for this disadvantage. All the material in this thesis will be published with George Rossman as coauthor; the three chapters that have been accepted for publication reflect this in the use of the 1st person plural (we), while the remaining chapters have been written using the singular.

Table of Contents

Extended Table of Contents

Chapter 1

Introduction

Water is a very important substance in geology. The behavior of water as a separate phase is well known, and in this form it is responsible for the deposition of major ore bodies, it is an important product and reactant in metamorphic reactions, and it covers the greater part of the earth in the oceans. However, water is also very important when it occurs not as a separate phase but as a trace constituent in other phases. In the common silicate minerals trace water need not remain as molecular H_2O, but can also take the form of hydroxyl groups and as such it is better to consider the behavior of trace hydrogen in minerals rather than trace water. Trace hydrogen is known to affect many processes of geologic importance, and its ubiquitous participation as both a reactant and catalyst calls for a generalized understanding of the sites, speciation, thermodynamics and reactions of trace hydrogen.

The interaction between trace hydrogen and silicates has only been studied for a few systems, among them silicate melts and quartz. The melting point depression brought about in many silicate compositions by the addition of a small amount of water is well known, and it is apparent that the presence or absence of water can control the formation of magmas in many instances (e.g., Wyllie, 1979; Mysen, 1977; Ringwood, 1975). It is also apparent that water may have a substantial effect on the physical properties and structure of silicate melts. This is currently a field of great interest, but is not properly a topic applicable to this thesis although the results presented here may be generalized to aid understanding of the interactions of hydrogen with melts and glasses. One mineral in which trace hydrogen has been

extensively studied is quartz, and the findings and problems of previous studies of hydrogen in quartz exemplify both the importance of trace water to the physical properties of minerals and also the difficulty in studying and interpreting trace hydrogen. Quartz commonly contains trace hydrogen in a variety of sites and the trace hydrogen in natural quartz was first correctly described by Kats (1962). Perhaps the most dramatic effect of trace hydrogen in quartz is its control of the mechanical properties of quartz. Both the mechanical strength of quartz and its value as an oscillator can be affected by the presence of small amounts (less than 0.1% as H_2O) of hydrogen. The effect on oscillator quality was first noticed in the 1950's. Anelastic losses in synthetic quartz crystals were found to be associated with a trace hydrogen impurity (e.g., Dodd and Fraser, 1965; Chakraborty and Lehmann, 1976).

In 1965, Griggs and Blacic discovered that synthetic quartz was considerably weaker under uniaxial compression than was similar natural quartz, and they associated this weakness with the presence of trace hydrogen. Further experiments by them suggested that strong quartz could be weakened by the addition of trace hydrogen, and this led to the conceptually important idea of hydrolytic weakening of silicates (Griggs 1967). Much controversy and research has followed the original discovery, motivated by the possible importance of this effect in controlling the rheology of the deep crust and mantle. However, while the correlation between trace water and weakening has been established, the mechanisms and species responsible have not previously been adequately determined despite a considerable expenditure of effort

(e.g., Griggs et al. 1974). The effect has only been conclusively demonstrated in synthetic quartz and in natural amethystine quartz grown at low temperatures (Kekulawala et al. 1978). Considerable attention has been drawn to the effects of hydrogen related defects and their interaction with the external environment (Hobbs, 1981) but the actual defects present must first be correctly identified. Trace hydrogen also affects the radiation damage behavior of quartz, and this has been extensively studied (see Weil, 1975 for a review) in the case of smoky quartz coloration.

Although trace hydrogen has not been extensively studied in minerals other than quartz, there has been no lack of speculation about its possible importance. One area of interest is the water content of the mantle. The importance of water in generating certain mantle-derived magmas has been experimentally investigated, but the possible sources of water in the mantle are not known. Martin and Donnay (1972) suggested that substitutional hydroxyl in nominally anhydrous minerals is an important sink for water in the mantle. Ackermann et al. (1983) suggest a similar role for hydrogarnet, and Sclar et al. (1967) synthesized a new hydrous phase at high pressures which they suggest is a hydrated pyroxene. Ringwood and Major (1967) synthesized several hydrous high pressure phases that they suggest may be important in the deep mantle. Clearly it is important to determine what hydrous phases are stable, and to what extent nominally anhydrous phases can take up hydrogen under mantle conditions. This problem is additionally complicated by the calculations of Delany and Helgeson (1978) which show

that the hydrous phases present in subducting oceanic slab material all dehydrate at relatively shallow levels in the crust and mantle, and do not provide a mechanism to recycle water into the deep mantle. The dehydration of slab materials has also been suggested to control seismicity in subduction zones (Anderson et al. 1980).

In order to study the importance of trace hydrogen in minerals it is clearly unacceptable to rely on total water analyses of the type commonly seen in the literature, for instance those lumping together all hydrogen released upon heating the sample above 100°C and calling that quantity H_2O^+. A working understanding of trace hydrogen requires that both the concentration and the speciation of the hydrogen be known. It is also important to distinguish between water that is truly dissolved in silicates, that which has been trapped as a separate phase, and that which is metastably contained in the mineral lattice. Previous work has defined what sorts of hydrogen speciation may be expected to occur when trace hydrogen is dissolved in a mineral. The most important is certainly hydroxide, and this has been studied most extensively in quartz where the hydrogen frequently takes a charge balancing role when Al^{3+} substitutes for Si^{4+}. This type of charge compensation appears to be common in silicates. The second important species is molecular water, which has been shown to occur for instance in cordierite. These two species appear to be the only important hydrogen species in silicates. It has been frequently suggested that the hydronium or oxonium in H_3O^+ is important in minerals (e.g., White and Burns, 1963) but studies of synthetic compounds indicate that this ion only occurs in

extremely acidic environments not reproducible in silicates, and the spectroscopic characteristics of hydronium in these synthetic compounds are well known and have not been seen in hydrous silicates (Ferriso and Hornig, 1955; Savoie and Giguere, 1964; Lundgren and Williams, 1973). Friedman Freund has currently popularized the concept of atomic and molecular hydrogen occurring in substantial concentrations in minerals, and he and his co-workers have published many papers in which the properties of minerals are suggested to be affected by this hydrogen (e.g., Freund and Wengeler, 1982, and references therein). However, the only proven examples of the occurrence of either of these species involve either intense gamma-ray radiolysis (see chapter 6) or the heating of hydroxyl-bearing MgO in a hydrogen atmosphere, which produced hydrogen gas bubbles (Briggs and Bowen, 1967). Freund, and Henderson and Sibley (1971), have based their assignment of the infrared spectra of oxides and silicates upon Briggs and Bowen's work even though they are using infrared spectra rather than the raman spectra used by Bowen and Briggs, and accordingly must assert without proof that molecular hydrogen is an infrared active species. There is no collaborative evidence of this assertion, and it appears likely that the peaks observed are in fact combination modes involving hydroxyl groups. There is no direct evidence for the presence of molecular hydrogen in minerals except when produced under extreme conditions as stated above, and certainly no evidence that it occurs naturally except possibly as a result of natural radiolysis (Chapter 6). The last hydrogen species to consider is the hydrogarnet substitution, four hydroxyl groups in a

tetrahedral configuration. This may be an important hydrogen species in silicates, but is a subclass of hydroxyl speciation. The importance of this substitution has not previously been determined, although in conjunction with the hydronium ion, hydrogarnet substitution is frequently used to explain the presence of trace hydrogen in a mineral with the only evidence presented being the bulk analysis of trace water.

Goals of this study.

My study of trace hydrogen in minerals was undertaken with four major goals. These are:

(1) To identify the possible sites and species for trace water in silicate minerals. What species occur commonly in different silicate types and chemistries, and what understanding can be achieved which will allow the prediction of hydrogen speciation in minerals? What concentrations of hydrogen species can be expected to occur in silicates?

(2) To quantify the relationship between trace hydrogen content of minerals and their origin or conditions of equilibration. One possible goal is the development of water fugacimeters using the hydrogen concentration of minerals. The predictive understanding of trace water speciation and siting can be used to understand the possible sites for water in the mantle and to predict what effect hydrogen will have on mantle minerals.

(3) To understand the relationship between trace hydrogen and the reactions that occur in minerals and the properties of minerals, including radiation damage and hydrolytic weakening. Why does hydrogen play such a common role as a mediator and catalyst of geologic reactions?

(4) To understand the sites and speciation of trace hydrogen at temperatures of geologic interest by direct observation at high temperature. To what extent are $25^{o}C$ measurements of trace hydrogen relevant in considering its behavior in nature?

Outline of This Thesis.

In this thesis I describe some of the progress that has been made in accomplishing these goals. To begin this discussion, Chapter 2 describes the basic techniques that I have used in studying trace hydrogen, and also establishes some of the basic problems that may be addressed using these techniques. Chapter 3 deals with theoretical aspects of the shapes and positions of O-H stretching modes in the infrared, and how they may be used to provide structural information about trace hydrogen. Chapters 4 and 5 discuss the existence of the hydrogarnet substitution in pyralspite garnets, and the significance of the occurrence of this substitution in mantle garnets. In Chapter 6 the effect of trace water on the radiation damage characteristics of minerals is discussed. Chapters 7 and 8 deal with the characteristics and properties of trace water, hydroxyl and carbon dioxide at high temperatures more typical of conditions of geologic interest than the $25^{o}C$ measurements typical of laboratory work in mineralogy. Chapter 9 concludes this thesis by summarizing my results, discussing the extent to which my stated goals have been accomplished and the current state of understanding of trace hydrogen in minerals.

References

Ackermann, L., Cemic, L., and Langer, K. (1983) Hydrogarnet substitution in pyrope: a possible location for "water" in the mantle. Earth and Planetary Science Letters, 62, 208-214.

Anderson, R.N., DeLong, S.E., and Schwarz, W.M. (1980) Dehydration, asthenospheric convection, and seismicity in subduction zones. Journal of Geology, 88, 445-451.

Briggs, A. and Bowen, D.H. (1967) Cavity formation in magnesium oxide. U.S. National Bureau of Standards, Special Publication 296.

Chakraborty, D., and Lehmann, G. (1976) Distribution of OH in synthetic and natural quartz crystals. Journal of Solid State Chemistry, 17, 305-311.

Delany, Joan M. and Helgeson, H.C. (1978) Calculation of the thermodynamic consequences of dehydration in subducting oceanic crust to 100 KB and >800^{o}C. American Journal of Science, 278, 638-686.

Dodd, D.M., and Fraser, D.B. (1965) The 3000-3900 cm^{-1} absorption bands and anelasticity in crystalline α-quartz. Journal of Physics and Chemistry of Solids, 26, 673-686.

Ferriso, C.C., and Hornig, D.F. (1955) Infrared spectra of oxonium halides and the structure of the oxonium ion. Journal of Chemical Physics, 23, 1464-1468.

Freund, F. and Wengeler, H. (1982) The infrared spectrum of OH-compensated defect sites in C-doped MgO and CaO single crystals. Journal of Physics and Chemistry of Solids, 43, 129-145.

Griggs, D. (1967) Hydrolytic weakening of quartz and other silicates. Geophysical Journal, 14, 19-31.

Griggs, D. (1974) A model of hydrolytic weakening in quartz. Journal of Geophysical Research, 79, 1653-1661.

Griggs, D. and Blacic, J.D. (1965) Quartz: anomalous weakness of synthetic quartz crystals. Science, 147, 292-295.

Henderson, B. and Sibley, W.A. (1971) Studies of OH^- and OD^- ions in magnesium oxide. I. Distribution and annealing of hydroxyl and deuteroxyl ions. Journal of Chemical Physics, 55, 1276-1285.

Hobbs, B.E. (1981) The influence of metamorphic environment upon the deformation of minerals. Tectonophysics, 78, 335-383.

Kats, A. (1962) Hydrogen in alpha-quartz. Philips Research Reports, 17, 133-195 and 201-279.

Kekulawala, K.R.S.S., Paterson, M.S., and Boland, J.N. (1978) Hydrolytic weakening in quartz. Tectonophysics, 46, T1-T6.

Lundgren, J.O., and Williams, J.M. (1973) The hydrated proton $H^+(H_2O)_n$. I. A single crystal neutron diffraction study of the oxonium ion in p-toluensulfonic acid monohydrate, $H_3O^+CH_3C_6H_4SO_3^-$. Journal of Chemical Physics, 58, 788-796.

Martin, R.F. and Donnay, G. (1972) Hydroxyl in the mantle. American Mineralogist, 57, 554-570.

Mysen, B.O. (1977) The solubility of H_2O and CO_2 under predicted magma genesis conditions and some petrological and geophysical implications. Reviews of Geophysics and Space Physics, 15, 351-361.

Ringwood, A.E. (1975) Composition and Petrology of the Earth's Mantle. McGraw-Hill, New York.

Ringwood, A.E. and Major, A. (1967) Some high pressure transformations of geophysical interest. Earth and Planetary Science Letters, 2, 106-110.

Savoie, R. and Giguere, P.A. (1964) Infrared study of the crystalline monohydrates of nitric, perchloric, and sulfuric acids. Journal of Chemical Physics, 41, 2698-2705.

Sclar, C.B., Carrison, L.C., and Stewart, O.M. (1967) High pressure synthesis of a new hydroxylated pyroxene in the system $MgO-SiO_2-H_2O$ (abstract). Transactions of the American Geophysical Union, 48, 226.

Weil, J.A. (1975) The aluminum centers in α-quartz. Radiation Effects, 26, 673-686.

White, J.L. and Burns, A.F. (1963) Infrared spectra of hydronium ion in micaceous minerals. Science, 141, 800-801.

Wilkins, R.W.T., and Sabine, W. (1973) Water content of some nominally anhydrous silicates. American Mineralogist, 58, 508-516.

Wyllie, P.J. (1979) Magmas and volatile components. American Mineralogist, 64, 469-500.

Chapter 2

Water in Minerals?

A Peak in the Infrared

(Text of article accepted for publication in

The Journal of Geophysical Research,

George Rossman coauthor.)

Abstract

The study of water in minerals with infrared spectroscopy is discussed with emphasis on natural and synthetic quartz. Water can be recognized in minerals as fluid inclusions and as isolated molecules, and can be distinguished from hydroxide ion. The distinction between very small inclusions and aggregates of structurally bound molecules is difficult. New studies of synthetic quartz using near infrared spectroscopy are reported. These demonstrate that water molecules are the dominant hydrogen containing species in synthetic quartz, but that this water is not in aggregates large enough to form ice when cooled.

Introduction

Hydrogen in minerals most frequently occurs bonded to oxygen. The resulting OH group is highly polar. Because this directed dipole is an efficient absorber of light in the infrared region, infrared spectroscopy is a powerful tool in the study of hydrogen in minerals.

In this paper we review the use of infrared spectroscopy (IR spectroscopy) with emphasis on the study of hydrogen in the silicate minerals and with a detailed examination of the hydrogen found in quartz. We also present new results regarding the spectrum of hydrogen in synthetic quartz. We distinguish two major categories of hydrogen in minerals: 1) stoichiometric hydrogen-bearing minerals which contain hydrogen that is generally considered to be essential to the structure of the mineral, and which appears explicitly in the chemical formula of the mineral; and 2) trace hydrogen-bearing minerals which includes all cases where hydrogen can be detected in a mineral, but where it is not essential to the structural identity of the mineral. Stoichiometric hydrogen occurs in gypsum as H_2O and in mica as OH^-. Examples of trace hydrogen include the hydrogen in cordierite (H_2O) and quartz (OH^-).

Minerals containing hydrogen, whether trace or stoichiometric, are commonly referred to as "hydrous" or "water-bearing." This nomenclature reflects the fact that the neutral species H_2O is what is actually measured by common analytical techniques. We follow this convention when the speciation of the hydrogen is not known or we are referring to actual analytical measurements. The most important uses of IR spectroscopy in the study of hydrous minerals are: 1) determining the actual speciation of hydrogen, 2) determining the crystallographic environment of that species, and 3) analytically determining its concentration.

The identification of hydrogen species in minerals.

The most common species of hydrogen is H_2O. The spectrum of liquid H_2O is shown in Figures 1 and 2. The lower abscissa scale is in wavenumbers, a linear energy scale proportional to the frequency of the light exciting the absorption in units of cm^{-1}. The upper scale is a wavelength scale. The major features in Figure 1 are bands at 1630 wavenumbers and ~3400 wavenumbers. These are the fundamental absorptions of the molecule H_2O. The 1630 wavenumber absorption is due to the bending of the H_2O molecule, and the 3400 wavenumber band consists of a symmetric stretching absorption at 3220 wavenumbers and an antisymmetric stretching absorption at 3445 wavenumbers. The absorptions at higher wavenumbers in Figure 2 arise from linear combinations and multiples (overtones) of the fundamental vibrations. The spectral region below 4000 wavenumbers is referred to as the infrared (IR) and the region above 4000 wavenumbers is the near infrared (NIR). Absorption in the 3800-3000 wavenumber region is typical of the O-H stretching vibration.

Water in the crystalline environment, free of the extended hydrogen bonded networks typical of liquid water, can produce sharper absorptions than occur in the liquid water spectrum. Figure 3 is the spectrum of gypsum, $Ca_2SO_4 \cdot 2H_2O$. The two stretching modes near 3400 wavenumbers are well-resolved from each other, and are displaced from their position in liquid water. The bending modes near 1620 wavenumbers are proof that the molecule H_2O is present. They contain additional structure not found in the liquid water spectrum because of interactions between water molecules. The existence of water is further confirmed by the combination modes at ~1900 nm (~5200 wavenumbers) which involve bending motions (Figure 4). Muscovite mica contains only OH^- groups and no molecular H_2O, so the

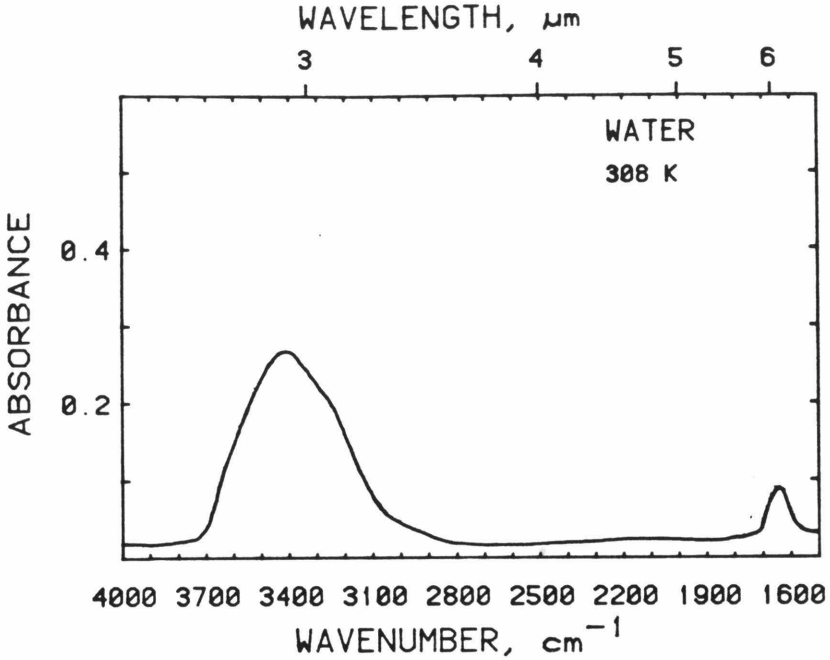

Fig. 1. Infrared absorption spectrum of a film (~1 μm thick) of liquid water showing the two overlapping stretching modes near 3400 wavenumbers and the bending mode near 1630 wavenumbers.

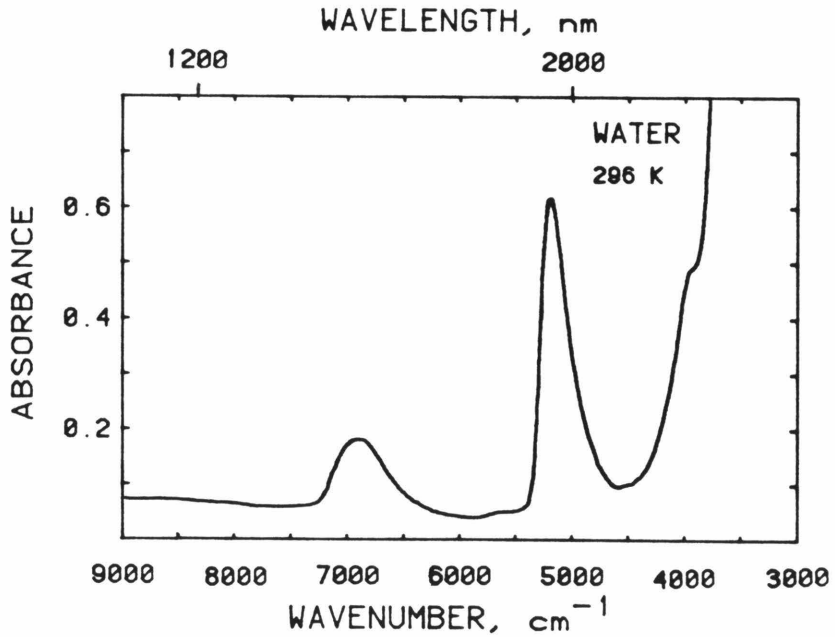

Fig. 2. Near-infrared absorption spectrum of film (100 μm thick) of liquid water showing the first O–H stretching overtone near 7000 wavenumbers and the stretch + bend combination mode near 5000 wavenumbers.

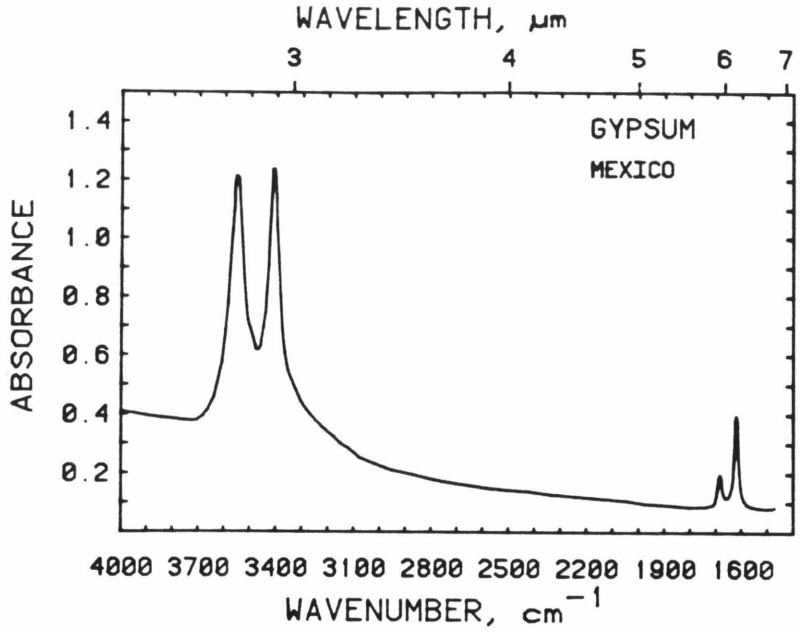

Fig. 3. IR spectrum of 0.50 mg powdered gypsum in a KBr pellet showing the separation between the two O-H stretching modes near 3500 wavenumbers and the bending modes of H_2O near 1600 cm^{-1}.

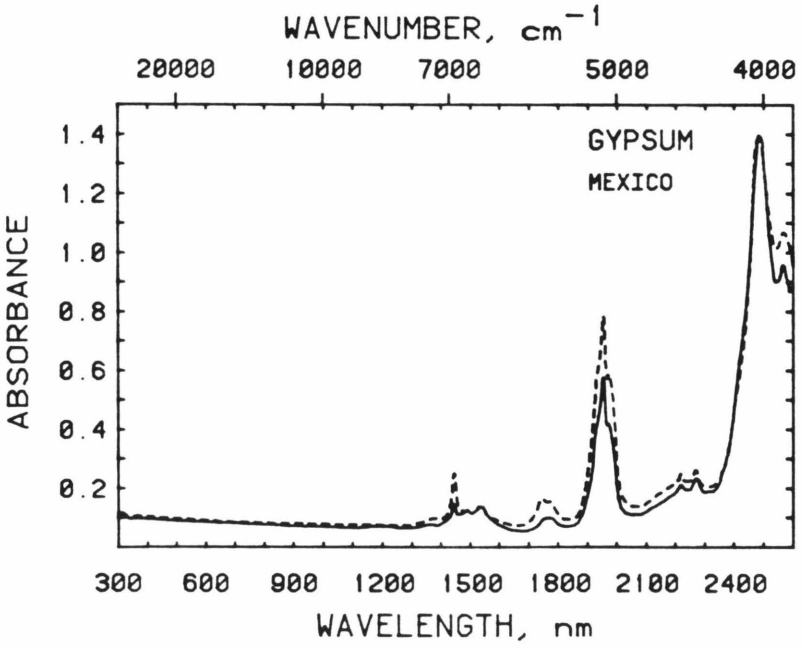

Fig. 4. Near-IR spectrum of a 0.34 mm thick cleavage plate of gypsum showing overtone and combination modes, including the mode near 5000 wavenumbers (1900 nm) which is caused by the molecule H_2O. Taken with light polarized in the optical X (---) and Z (---) direction.

bending vibration should be absent. This is frequently most readily verified in the 1900 nm region (Figure 5) because of interference from silicate absorption in the 1600 wavenumber region when thick samples are examined. The presence or absence of the bending-related absorptions is the primary distinction between the two major hydrogen species, H_2O and OH.

Water commonly exists in minerals as fluid inclusions. To distinguish fluid water from crystallographically-bound water, spectra are obtained at cryogenic temperatures. Figure 6 compares the IR spectrum of water and ice in an artificial "fluid inclusion" formed by sandwiching water between two Al_2O_3 windows. The 78 K spectrum demonstrates the utility of low temperature measurement in identifying hydrogen as fluid inclusions. The band at 3200 wavenumbers that forms at 78 K is characteristic of ice [Eisenberg and Kauzmann, 1962, Ch. 3].

Case studies.

H_2O in cordierite and beryl

Beryl and cordierite have structures consisting of sixfold rings of silicate tetrahedra joined by other octahedrally and tetrahedrally coordinated cations in such a way that open channels exist parallel to the c axis. Both minerals also commonly yield H_2O upon analysis. Schreyer and Yoder [1964] demonstrated that the hydrogen speciation in cordierite was in fact as H_2O, and that it resided in the channels. Wood and Nassau [1967] showed that the hydrogen speciation in beryl was also as H_2O, and showed from the polarization dependence of the absorption that it occupied two distinct sites. Absorption of light by an O-H bond occurs when the electric vector of the light is oriented parallel to the direction of the dipole. When more than one O-H is involved in

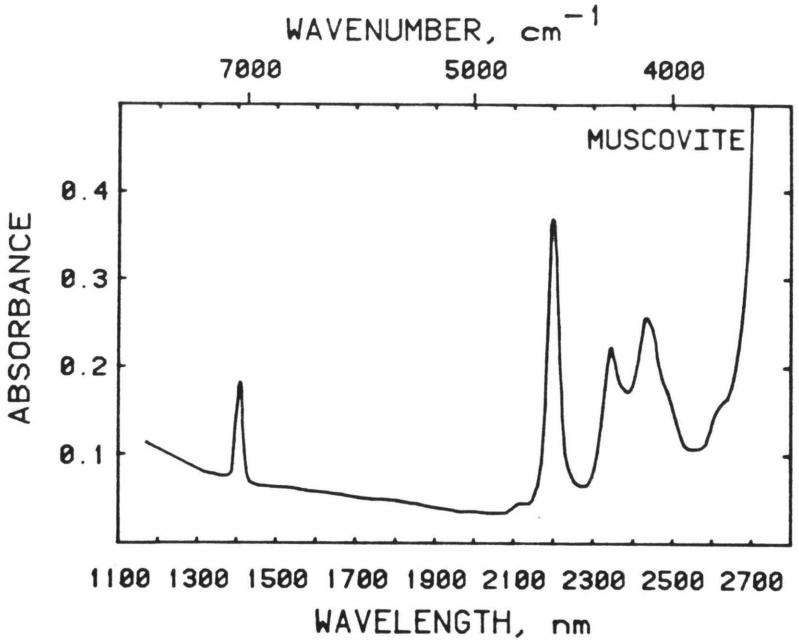

Fig. 5. Unpolarized NIR spectrum of a cleavage plate of muscovite showing the overtone of the O-H stretch near 1400 nm and the absence of an H_2O combination mode near 1900 nm. Thickness = 0.25 mm; sample oriented 45° to the incident beam.

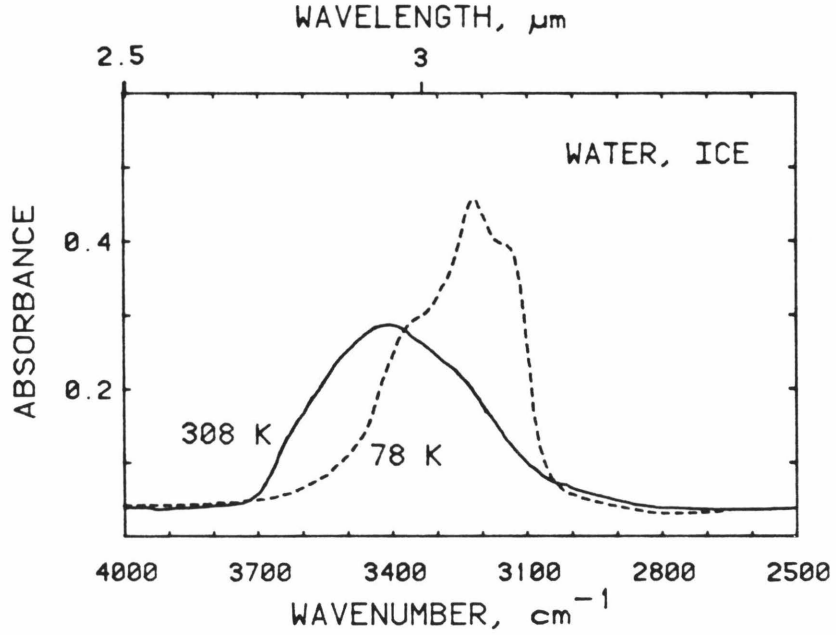

Fig. 6. Comparison of the infrared spectra of a thin film (~1 μm thick) of liquid water (---) to the same thickness of ice at 78 K (---).

absorbing the light, symmetry considerations determine the directions in which light is absorbed. In order to understand the spectrum of H_2O in beryl and cordierite, we first consider the detailed nature of the IR absorption of isolated H_2O molecules.

Figure 7 shows schematically the type of motion constituting the vibrations of H_2O. There are 3 atoms in the molecule, and therefore the motions of these atoms have 3x3 = 9 degrees of freedom. Three of these are translations of the entire molecule ($T_{x,y,z}$) and three are rotations of the entire molecule ($R_{x,y,z}$) around mutually perpendicular axes. This leaves three degrees of freedom representing internal vibrations of the molecule, where the atoms move relative to each other. These three vibrations are labeled ν_1, ν_2, and ν_3. They are, respectively, the symmetric stretching, bending, and asymmetric stretching of the H_2O molecule. Group theory shows that ν_1 and ν_2 occur when the incident light is polarized in the direction of the 2-fold symmetry axis of the H_2O molecule, and ν_3 occurs when the incident light is perpendicular to this direction but in the plane of the molecule. The most intense absorption bands of H_2O are the fundamentals. The combination modes have very low intensity. It is also possible for bands which are "not allowed" by symmetry to have a small but observable intensity due to limitations in the assumptions used to calculate selection rules.

Wood and Nassau determined that there are two distinct groups of bands in the beryl spectrum that vary according to the chemistry of the sample. From the polarization behavior of these groups of bands, they were able to deduce that one type of molecule is oriented with the H-H vector parallel to c, and that the other H_2O molecule is oriented with its H-H vector perpendicular to the c axis. Goldman, et al. [1977]

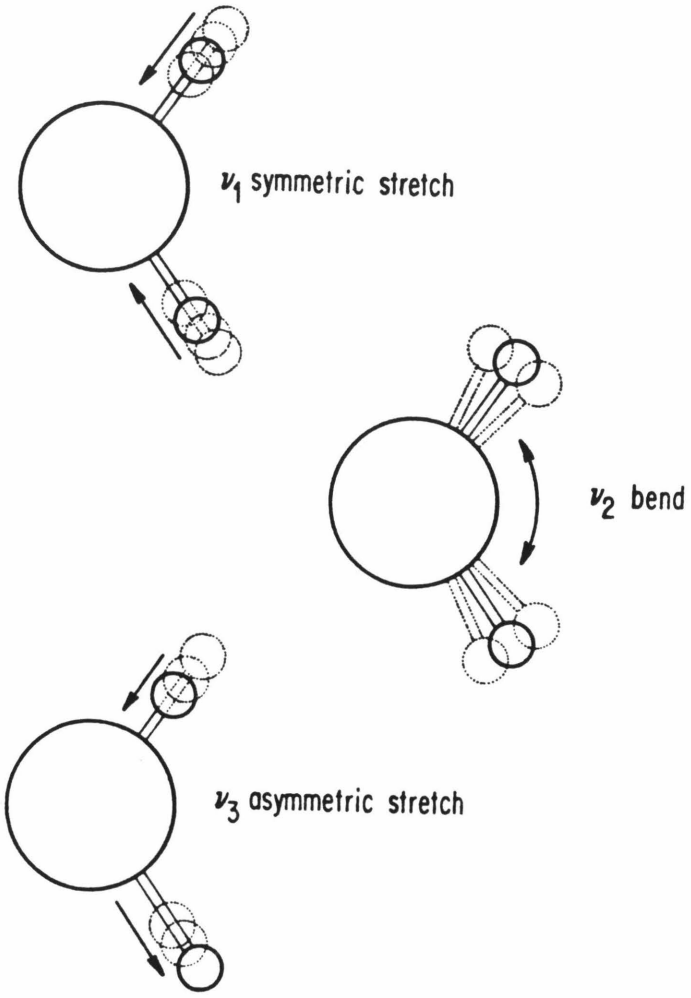

Fig. 7. Modes of vibration of the H_2O molecule.

demonstrated that a similar situation exists in cordierite. In both minerals the frequencies of the absorptions (Figure 8) occur at lower energies than in the vapor H_2O indicating that interaction occurs with the other constituents of the mineral. However, the shifts are not great, and the close correlations with the spectrum of water vapor, the sharpness of the bands, and the presence of bands identified as rotation + vibration indicate that the H_2O molecules in beryl and cordierite are only weakly hydrogen-bonded.

Hydrogen in Quartz

Quartz is the most extensively studied natural system containing trace hydrogen. Hydrogen is ubiquitous in quartz, usually at levels of tens to hundreds of ppm. The most important tool in this field of study has been IR spectroscopy, due to its sensitivity to the O-H bond.

Figure 9 shows the spectrum of a natural, clear quartz taken at 78 K. Most quartz spectra show a complexity of sharp peaks at low temperature. Figures 10 and 11 are the spectra of a natural amethyst crystal measured at room temperature and 78 K. The broad band (near 3400 wavenumbers) superimposed upon the sharp band spectrum is characteristic of synthetic quartz and natural quartzes formed at low temperatures [Frondel, 1982]. These two spectra exemplify the two important classes of absorption spectra in the quartz IR spectrum: sharp band absorption and broad band absorption. Kats [1962] conclusively showed that the sharp band absorptions are due to O-H stretching vibrations. In a study that remains the classic work in the field, Kats showed that the great variety of absorptions are primarily due to the presence of Al^{3+} substitution for Si^{4+} and coupled charge-balancing alkali cations, as well as other alkali cation defects in the crystal. Table 1 summarizes Kats' results and his

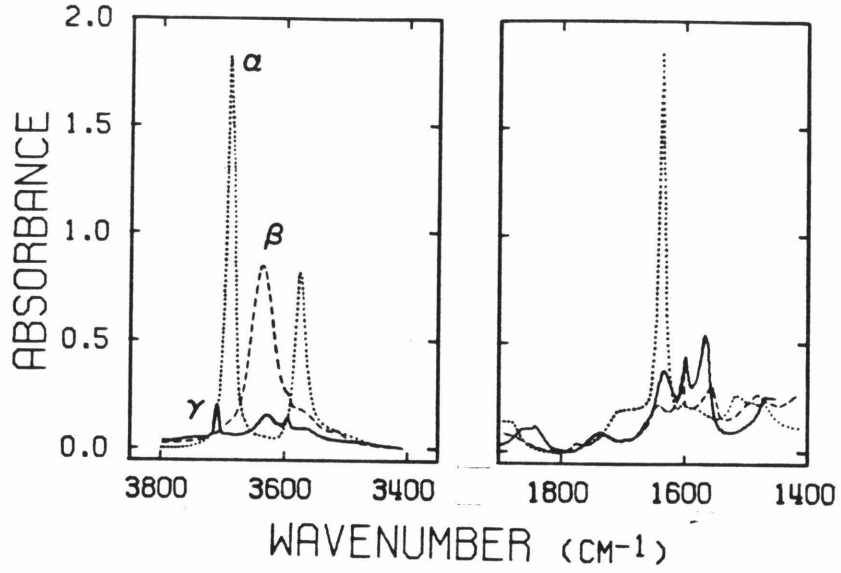

Fig. 8. IR spectrum of water in cordierite. The spectrum, taken in polarized light shows more than two features in the 3600 wavenumbers region because water occurs in more than one site. Figure 7 from Goldman et al. 1977.

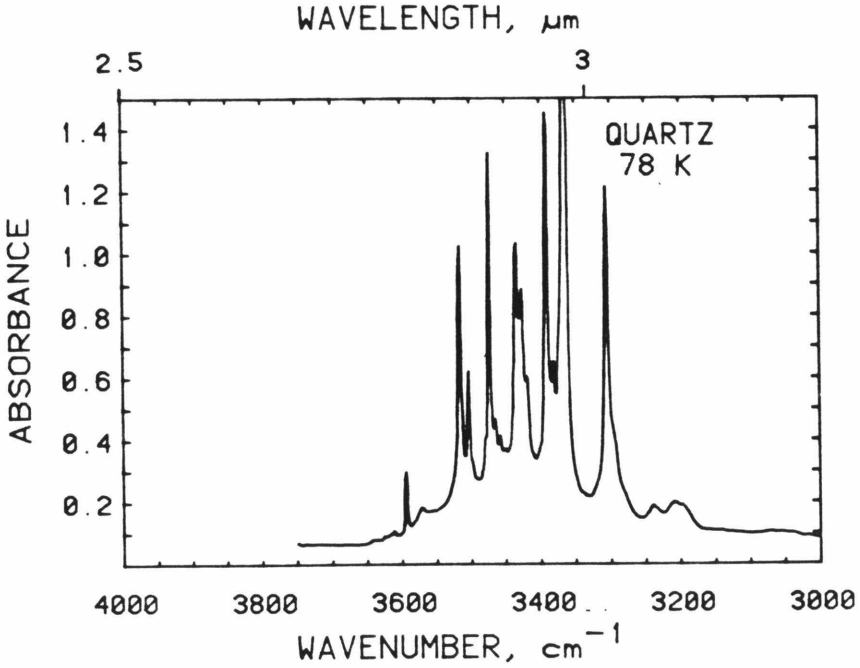

Fig. 9. IR spectrum of a 5 mm thick natural Brazilian quartz crystal showing the complexity of the O-H stretching region. Sample temperature, 78 K, polarized perpendicular to c.

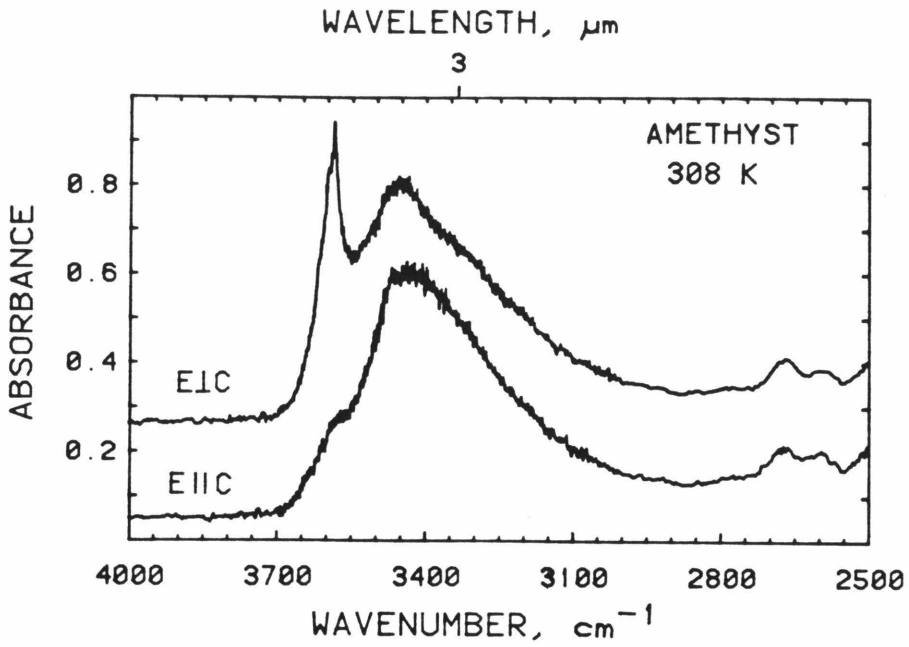

Fig. 10. Room temperature IR spectrum of Brazilian amethyst (1.41 mm thick) taken with polarized light vibrating perpendicular to c axis (upper trace) and parallel to c (lower trace).

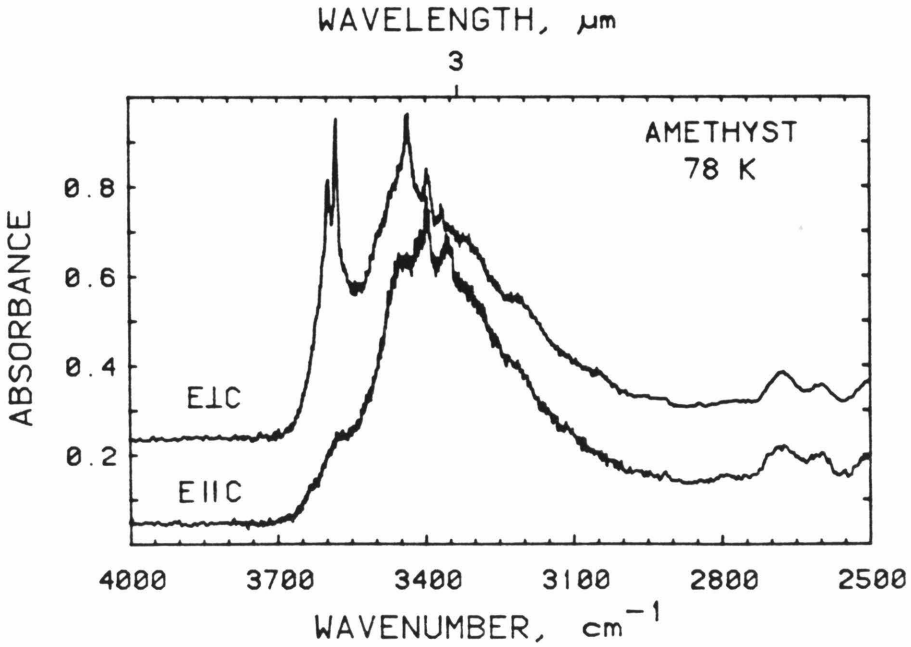

Fig. 11. Low temperature IR spectrum of the sample whose spectrum appears in Figure 10.

peak assignments, as well as additions that have been made by subsequent workers. Despite the assignment of 57 peaks in this table, this is still not a complete description of the quartz O-H vibrational spectrum.

The major tools used by Kats and later workers to index these peaks are electrolytic exchange and high-temperature diffusion. Kats obtained the data in Table 1 by exchanging Na^+, K^+, Li^+, Ag^+, and Cu^+ into clear, natural quartz crystals. He verified that the resulting absorptions were due to hydrogen defects by duplicating all the cationic exchanges under conditions where deuterium defects were formed. Three types of defects may be distinguished: 1) those in which alkali and hydrogen ions are associated, 2) defects involving two or more hydrogens, and 3) associations of aluminum-hydrogen. Aluminum-hydrogen defects are the most stable type, persisting to over 1200°C at 1 atm. Kats distinguishes three major Al(H) peaks at 3310, 3374, and 3440 wavenumbers. They are all due to H^+ occurring in a charge compensating role for Al^{3+} in an Si^{4+} site. They are stable at high temperatures because they are an intrinsic part of the crystal structure. These centers can be destroyed by intense electrolysis in a vacuum, resulting in oxygen vacancies forming the charge compensation for Al^{3+} [Kats, 1962; Krefft, 1975]. Kats demonstrates that there are two important Al(H) defects in quartz, one giving rise to the 3310 wavenumber peak and one giving rise to the 3370-3345 wavenumber pair. They are separate defects since the intensities of their infrared absorptions vary independently. He concludes, based largely on the orientation of the O-H vectors in these defects, that the 3310 wavenumber peak arises from H^+ bound between the two nonequivalent oxygens in an aluminum tetrahedron, and the 3370-3345 wavenumber pair arises from an hydroxide in the aluminum tetrahedron with the O-H vector pointing into

TABLE 1. Peak Assignments for O-H Stretch in Quartz

Peak Location at 78 K[a] cm^{-1}	Assigment or Observed Association[b]	Intensity Relative to Associated Peaks[c]	Method of Assignment[d]	Comments: Type of Quartz Where Found[e]	Reference[f]
3610	K^+	k = 6	A.E.	natural clear	1
3600	?	α = 0.1	—	synthetic	1
3590	H^+	α = 0.5	A.E	natural clear	1
3585	K^+	k = 4	A.E	natural clear	1
3585	?	α = 1.3	—	synthetic, amethyst	1,2
3578	K^+	k = 6	A.E.	natural clear	1
3573	$Li^+ + \gamma$	α = 1.0	X ray	natural clear[g]	1
3567	K^+	k = 4	A.E.	natural clear	1
3556	Na^+	k = 8	A.E.	natural clear	1
3553	$Cu^+ + \gamma$	—	X ray	natural clear	1
3551	$Ag^+ + \gamma$	—	X ray	natural clear	1
3550	K^+	k = 7	A.E.	natural clear	1
3546	$Na^+ + \gamma$	—	X ray	natural clear	1
3540	Cu^+	k = 15	A.E.	natural clear	1
3535	Ag^+	k = 8	A.E.	natural clear	1
3538	K^+	k = 12	A.E.	natural clear	1
3534	Na^+	k = 12	A.E.	natural clear	1
3530	H^+	α = 0.5	A.E.	natural clear	1
3524	Ag^+	k = 7	A.E.	natural clear	1
3520 [3517]	Li^+	k = 30	A.E.	natural clear	1
3514	Cu^+	k = 12	A.E.	natural clear	1
3513	Na^+	k = 18	A.E.	natural clear	1
3510 [3510]	Li^+	k = 14	A.E.	natural clear	1
3500	Ag^+	k = 6	A.E.	natural clear	1
3485	H^+	α = 1.0	A.E.	natural clear	1
3478 [3485]	Li^+	k = 17	A.E.	natural clear	1
3470 [3474]	?	α = 0.5	nat.	h	1,3
3462	Cu^+	k = 9	A.E.	natural clear	1
3462	H^+	α = 0.5	A.E.	natural clear	1
3460	K^+	k = 12	A.E.	natural clear	1
3454	Ag^+	k = 7	A.E.	natural clear	1
3453	Na^+	k = 48	A.E.	natural clear	1
3440	i	α = 0.5	—	synthetic, amethyst	1,2
3440 [3443]	Li^+	k = 15	A.E.	natural clear	1
3435 [3432]	Al^{3+}	α = 1.5	nat.	Fermi pair with 3373[j]	1
3422	H^+	α = 0.5	A.E.	natural clear	1
3415	Cu^+	k = 8	A.E.	natural clear	1
3414	K^+	k = 7	A.E.	natural clear	1
3408	$Li^+ + \gamma$	weak	X ray	>2 Mrads[k]	1
3400	H^+	α = 0.5	A.E.	natural clear	1
3400	Ag^+	k = 9	A.E.	natural clear	1
3400	Na^+	k = 7	A.E.	natural clear	1
3400	i	α = 0.3	—	synthetic, amethyst	1
3396 [3405]	Li^+	k = 36	A.E.	natural clear	1
3382	Na^+	k = 42	A.E.	natural clear	1

TABLE 1. (continued)

Peak Location at 78 K[a] cm^{-1}	Assigment or Observed Association[b]	Intensity Relative to Associated Peaks[c]	Method of Assignment[d]	Comments: Type of Quartz Where Found[e]	Reference[f]
3380	?	weak	nat.	natural clear	1
3375	?	medium	nat.	amethyst	1,2
3371 [3383]	Al^{3+}	α = 9.0	nat.	Fermi pair with 3435[j]	1
3365	?	α = 0.2	—	synthetic	1
3355	i	α = 0.3	—	synthetic, amethyst	1,3
3310 [3318]	Al^{3+}	α = 3.0	nat.	natural clear	1
3305	H^+	α = 0.5	A.E.	natural clear	1
3240	H_2O	weak	A.E.	very broad[ℓ]	1
3222	H_2O	weak	A.E.	very broad[ℓ]	1
3205	?	weak	nat.	natural clear	1

[a]Peak locations measured at 78 K by Kats [1962]; room temperature values in brackets where available.

[b]Most assignments by Kats; (+ γ) means after irradiation of alkali exchanged material; '?' where peak is reported in literature but not assigned or assigned with doubts by the authors.

[c]Intensities from Kats. These should only be used to compare like associations, for instance, comparing one Cu^+ peak to another. k is the integral absorbance per 10^{-2} m; α is the absorbance per 10^{-2} m.

[d]Usually alkali exchange (A.E.) and deuteration by Kats. Dashes indicate where not assigned. 'nat.' where assigned on the basis of occurrence in natural material and other criteria without alkali exchange.

[e]Type of quartz listed as "natural clear" when that is what Kats used to make initial assignment. Many of these peaks also occur in amethyst and synthetic quartz.

[f]References: 1, Kats [1962]; 2, Chakraborty and Lehmann [1976a]; 3, Krefft [1975]; 4, Chakraborty and Lehmann [1978].

[g]Observed only in clear samples that color yellow upon irradiation and not in those coloring brown. Peak disappears if dose exceeds 5 Mrads.

[h]This band was observed by Kats to persist above 1000°C, along with bands assigned to Al^{3+}. Krefft [1975] produced this band by prolonged electrolysis in H_2O or H_2 atmosphere; it was accompanied by a yellow coloration in the sample.

[i]Chakraborty and Lehmann [1976a] assign these bands to "H^- bonded directly to Si." However, later papers by the same authors make no mention of this assignment.

[j]These peaks are assigned by Kats as due to H^+ in a charge compensating role for Al^{3+} substitution for Si^{4+}. They are stable to above 1000°C, unlike all the other peaks in this table. The peaks at 3435 and 3373 are a fermi resonance pair formed by a lattice mode and an O-H mode at about 3410.

[k]Occurs in quartz coloring yellow by irradiation, as in footnote g but only after dose exceeds 2 Mrads.

[ℓ]Kats assignment of these bands is based on their breadth and the fact that they are formed at the expense of bands he interprets as due to LiOH under hydrogen exchange.

the c-axis "channel," making an angle of 75 degrees with the c axis.

Much less can be said about the structure of the alkali-hydrogen and hydrogen-hydrogen defects. The overall stoichiometry of these defects is neutral, since they can be entirely removed and reintroduced by electrolysis. This suggests overall stoichiometries such as LiOH and HOH. The occurrence of new peaks when hydrogen is exchanged into the crystal suggests reactions such as LiOH to HOH, but any number of other geometries could be proposed where the introduced H^+ perturbs another O-H group without being directly bonded to it. Kats is of the opinion that several of the hydrogen defect bands are due to H_2O based largely on the greater width of the bands compared to the other sharp bands (Table 1). However, the characteristic overtone at 1900 nm due to bending and simultaneous stretching of an H_2O molecule has not been correlated with these IR bands, and probably cannot be due to low intensity.

There are associations in the alkali-defect data indicating that several classes of defects occur. For instance, the peaks at 3396(Li^+), 3382(Na^+), and 3354(Ag^+) have identical shifts upon deuteration, suggesting that they have the same structure. The Li(H) peaks at 3520 and 3396 wavenumbers always behave together, and are independent of the Li(H) peaks at 3478 and 3440 wavenumbers. The second pair are also stable to higher temperatures. Chakraborty and Lehmann [1976a] conclude, based on orientation of O-H vectors, that there are no molecules of the type LiOH existing in the c-axis channels of quartz, the most logical opening in the structure. A number of plausible structures for defects in quartz have been proposed [Kats, 1962; Kirby, 1982; Chakraborty and Lehmann, 1976b] but the actual structures are still not known.

Hydrogen in Low-Temperature Quartz. Amethyst, chalcedony, opal, citrine, and synthetic quartz are all characterized by IR spectra in the O-H stretching region showing a broad band with superimposed sharp bands. While there are substantial differences in their IR spectra, the similarities merit discussing them simultaneously.

In some cases, the sharp bands in these low temperature silicas are almost certainly due to the same factors discussed previously. For instance, Hosaka and Taki [1981a,b,c,d] report an intense band at 3450 wavenumbers in a synthetic quartz grown in NaCl solution. This band is probably the same band reported by Kats as the most intense natural quartz Na(H) band, at 3453 wavenumbers (Table 1). The shift may be due to instrumental calibration. Hosaka and Taki also consistently find bands at 3364 and 3304 wavenumbers in quartz grown in NaCl, KCl and pure water solutions. These correlate with Kats' Al(H) defects. (The source of aluminum is the source quartz material.) Koop and Staats [1970] also report these bands for synthetic quartz; Chakraborty and Lehmann [1978] report bands in these positions and with similar intensities for synthetic quartz and citrine. They are absent from chalcedony [Frondel, 1982] and at least some amethyst [Chakraborty and Lehmann, 1976a]. Frondel suggests that this is due to the low Al content of low-temperature natural quartz.

Aside from these instances, there is little correlation between the sharp bands in low-temperature quartzes and their trace constituents. Many authors, for example, Kats [1962] and Koop and Staats [1970], cite this lack of correlation. Koop and Staats succeeded in growing Rb-doped quartz, but observed no new peaks as a result of an RbOH component. They confirmed a result of Kats which is crucial to understanding synthetic quartz. In a wide range of synthetic crystals doped with alkalies and

other monovalent impurities, the sum of the molar concentrations of monovalent cations is approximately equal to the concentration of Al^{3+}. It appears that all the alkalies are involved in charge compensation for aluminum and cannot compensate for OH groups, so alkali hydrogen defects cannot form. Hosaka and Taki show that Al(H) centers are allowed by an excess of Al^{3+} over alkalies in their crystals.

We are left with two types of unexplained absorption in low-temperature quartzes: the majority of the sharp band absorptions, and the characteristic broad band absorption, which is correlated with a variety of physical properties. The nature of the broad band absorption is of substantial economic and scientific interest. Many structures and mechanisms of formation have been proposed for the hydrogen defect(s) responsible for the broad band absoprtion (see Kirby [1984] for a review). The outstanding problem is to establish which structures are consistent with the observed spectra.

Kats established that the broad band in synthetic quartz is related to hydrogen impurity by observing the spectrum of quartz grown in D_2O. Calibration curves now exist [Kirby, 1984] relating the total hydrogen content of synthetic quartz to the intensity of this band. The concentration of hydrogen in synthetic quartz is known to increase with growth rate, along with the concentration of other impurites [Frondel, 1982; Barnes et al., 1976]. The concentration decreases with increasing growth temperature, suggesting that the broad band in natural low temperature quartz has a similar origin, and that it's absence in pegmatitic quartz such as that commonly obtained from Brazil is due to the higher growth temperature of such quartz.

Frondel [1982] studied the IR spectra of chalcedony and determined

that the majority of its hydrogen is contained in two major species: surface hydroxyl groups and water molecules hydrogen bonded to those surface hydroxyls. The similarities between the behavior of chalcedony and synthetic fumed silica [McDonald, 1956] were used by Frondel to make these assignments. The adsorbed water appears to be responsible for the broad band absorption, and the hydroxyls for the sharp bands. When chalcedony is heated, a sharp band appears at 3744 wavenumbers. By analogy to fumed silica, Frondel assigns this to nonhydrogen-bonded surface hydroxyl. Frondel notes that in geodes, crystalline α-quartz growing on chalcedony has a spectrum similar to the chalcedony in the O-H region, which is also the spectrum found in other low-temperature quartz such as amethyst and synthetic. These are not fibrous, so the fumed silica analogy is not entirely applicable unless the c-axis "channels" are capable of creating a similar situation. No band above 3700 wavenumbers has been reported in crystalline α-quartz. Flörke, et al. [1982] studied the NIR spectra of several types of fibrous and microcrystalline natural silicas. The major hydrogen species in them was found to be water, interpreted as liquid water between grains and fibers.

Figure 12 shows the IR spectrum of a typical synthetic quartz. The spectrum does not change substantially when the sample is cooled to 78 K. Figure 13 is a typical NIR spectrum of synthetic quartz. This spectrum is dominated by the 1920 nm (bend + stretch) band for molecular H_2O [Aines, Kirby, and Rossman, in preparation]. There is a minor absorption in the 2250 nm region due to (bend + stretch) of SiOH groups. Molecular H_2O appears to be the dominant speciation for the hydrogen in synthetic quartz. The spectra of natural amethyst (Figures 10 and 14) are very similar to that of synthetic quartz (Figures 12 and 13). The major

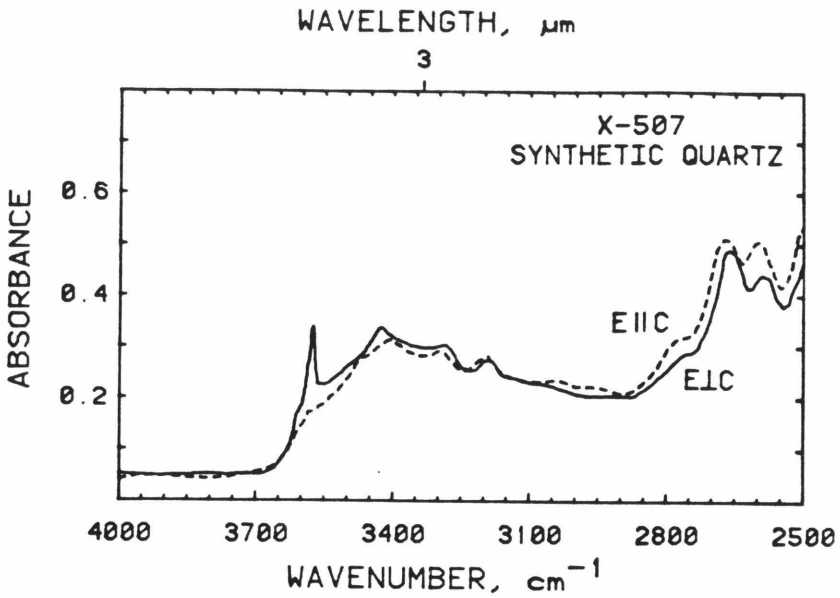

Fig. 12. Room temperature IR spectrum of synthetic quartz. Sample 3.97 mm thick. Dashed trace polarized parallel to c, solid trace perpendicular to c. From block E of crystal X-507.

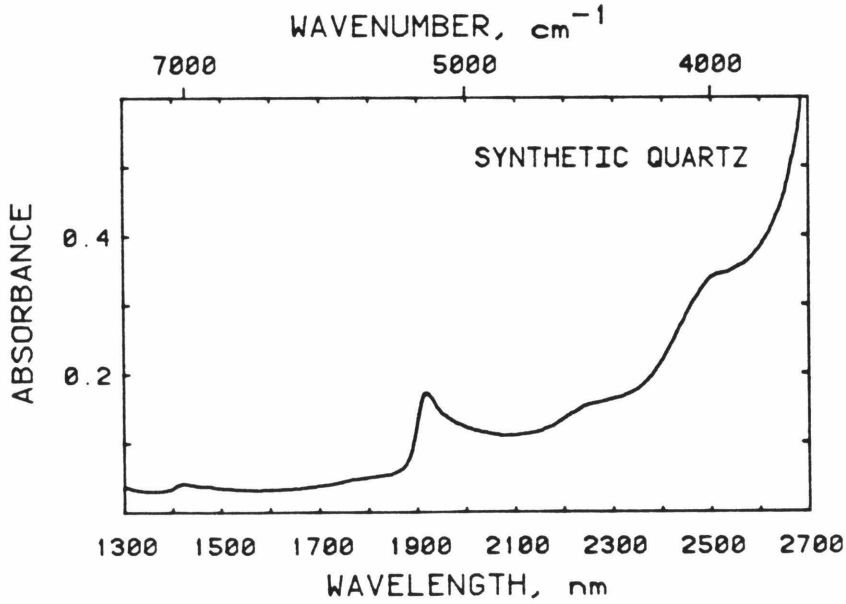

Fig. 13. Room temperature NIR spectrum of synthetic quartz X-13, 47.5 mm thick, showing the molecular H_2O band near 1900 nm. Taken with light polarized parallel to c axis. The perpendicular spectrum has an additional peak at 2215 nm of absorbance 0.01, but is otherwise identical.

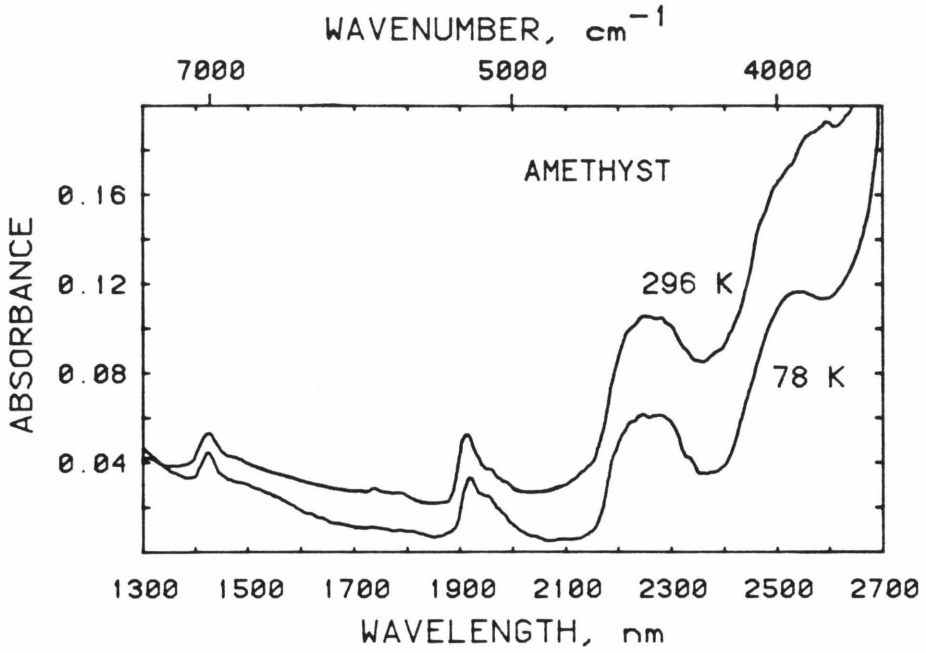

Fig. 14. Unpolarized NIR spectra of Brazilian amethyst, 5.72 mm thick. Upper trace: room temperature; lower trace cooled to 78 K.

difference between the synthetic quartz and the amethyst shown here is in the SiOH region; SiOH is the dominant hydrogen defect in this amethyst.

Opals may contain up to 8 wt% "H_2O." In the near infrared spectra of opals, Langer and Flörke [1974] recognized the presence of both molecular water and SiOH groups. The 1900 nm region of the 296 K opal spectrum (Figure 15) shows two overlapping components. Langer and Flörke assigned the sharper, higher energy absorption to isolated water molecules encased in the silica structure, and the broader one at 1957 nm to liquid-like, hydrogen bonded water. The absorption at 2220 nm was assigned to SiOH groups in the silica which were not interacting with other H_2O groups, whereas the absorption at 2260 nm was assigned to SiOH groups at the interface with the water-like H_2O and which are hydrogen-bonded to the H_2O.

The spectrum of opal taken at 78 K shows substantial peak shifts for Langer and Flörke's liquid-like water. This is consistent with the formation of ice. Figures 16 and 17 show the IR and NIR spectra of milky quartz. Here there is very similar behavior upon freezing. The fluid inclusions in this sample, and the liquid-like water in opal, represent large agglomerations of water molecules that are spectroscopically distinct from the non-freezable water in opal, amethyst, and synthetic quartz.

Summary: Proposed Hydrogen Defects in Low-Temperature Quartz.

Kirby [1983] discusses a number of mechanisms proposed for the incorporation of hydrogen in synthetic quartz. Two mechanisms that he favors are substitution of an $H_4O_4^{4-}$ group for SiO_4^{4-} (the hydrogarnet substitution), and a model involving chains of OH groups. The second model would result in a broad band absorption due to

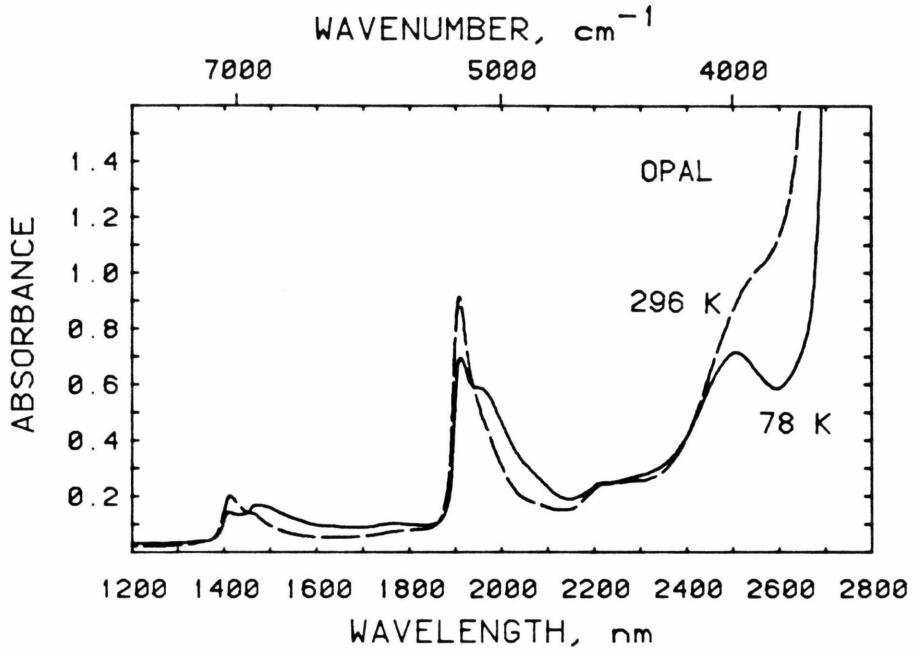

Fig. 15. NIR spectrum of an opal from Opal Mt., San Bernardino County, California, 1.288 mm thick. Solid line - 78 K; dash line - 296 K. The molecular H_2O bands at 1900 nm are prominent.

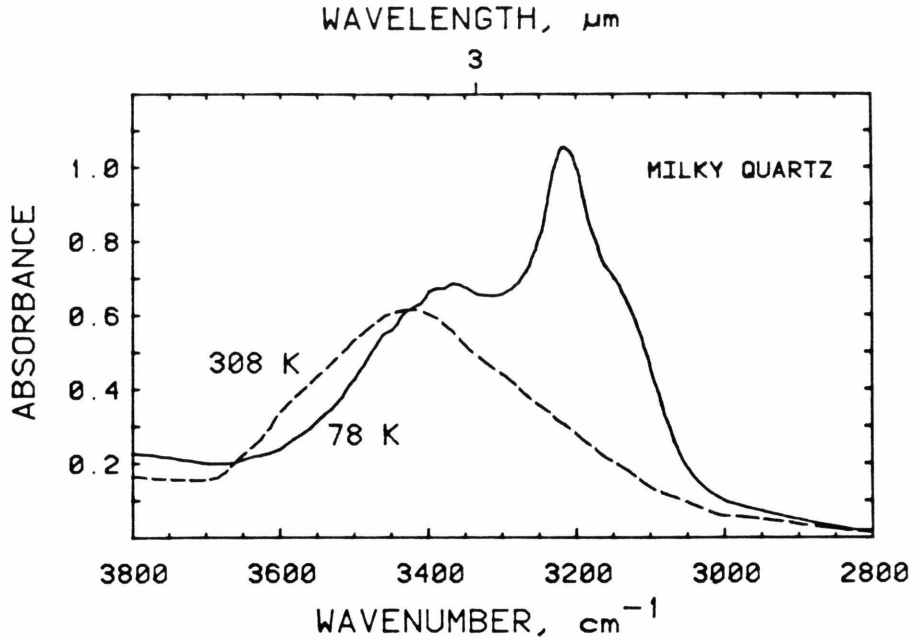

Fig. 16. IR spectrum of milky quartz from Dillsburg, Pennsylvania, 1 mm thick, showing water bands at 308 K (dash line) and ice bands at 78 K (solid line).

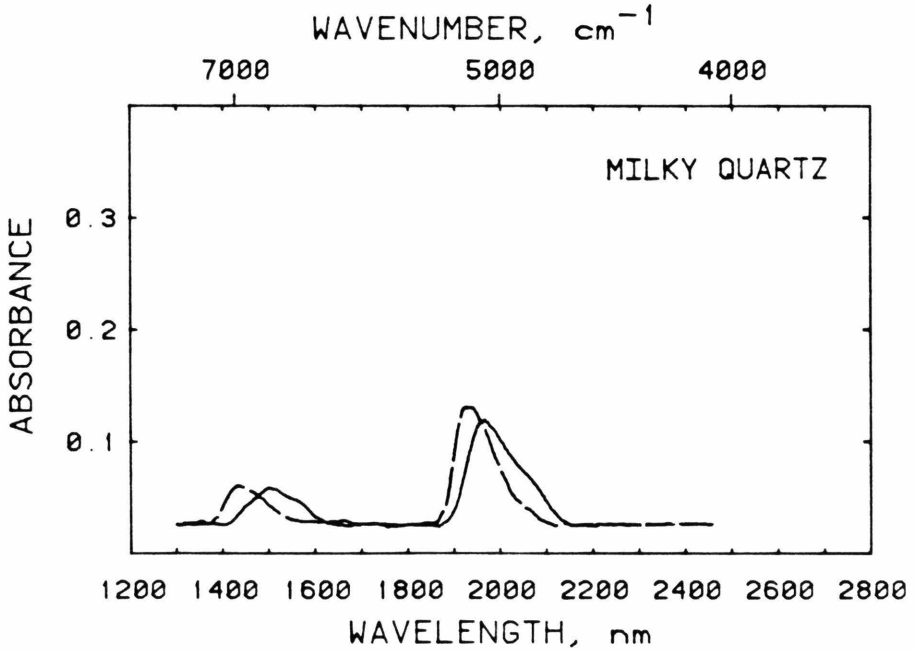

Fig. 17. Near IR spectrum of milky quartz from Dillsburg, Pennsylvania, at 296 K (dash line) and 78 K (solid line) showing ice bands. A sloping baseline due to scattering has been subtracted out. Thickness 3 mm.

interactions among the OH groups through hydrogen bonds in the following fashion:

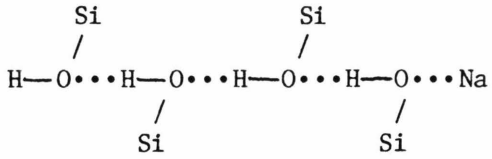

The spectroscopic features of $H_4O_4^-$ are not well established experimentally. However, the hydrogarnet substitution does not yield an absorption at 1900 nm, since all the hydrogens are attached to different oxygens [Aines and Rossman, 1982]. In fact, the presence of molecular H_2O as indicated by the 1920 nm band in synthetic quartz indicates that neither proposed substitution is the major hydrogen defect in synthetic quartz. However, the minor absorptions at 2250 nm (Figure 13) could be due to these substitutions.

The Effects of Water on the Properties of Quartz. The effect of water on the mechanical properties of quartz is well known, and the subject of several papers in this volume. Water also has a strong correlation with radiation damage in quartz. The most spectacular form of radiation damage in quartz is the removal of an electron from a substitutional Fe^{3+} to yield Fe^{4+} and amethyst [Cox, 1977]. No change in the O-H vibrational spectrum accompanies this oxidation, and no Fe^{3+}(H) defect has been identified analogous to the Al(H) defects [Chakraborty and Lehmann, 1978]. However, other changes in the O-H spectrum are associated with radiation damage in quartz. These are interesting in terms of understanding both the nature of hydrogen defects and radiation damage mechanisms in quartz.

Kats [1962] performed radiation experiments on synthetic and natural clear quartz. Two effects are noted on the IR spectrum. Associated with each cation is at least one new band that forms upon irradiation (Table 1). Also, the intensity of the bands assigned to Al(H) defects increase in natural quartz at the expense of the prevalent alkali-hydrogen defect. In synthetic quartz, the bands assigned to Al(H) defects grow, sometimes with accompanying decrease of other sharp bands. These results are in agreement with current thought about the nature of radiation damage to Al(H) and Al(alkali) defects obtained from other methods reviewed by Weil [1975]. The common manifestation of radiation damage of this kind is the formation of smoky coloration [Weil, 1975] due to the presence of $[AlO_4]^{4-}$ centers. They are formed by the removal of an electron and an alkali ion from the vicinity of the aluminum tetrahedron. This can be duplicated by electrolysis in vacuum [Krefft, 1975]. When such a crystal is heated, the alkali diffuses back and destroys the color center. Al(H) defects do not form smoky centers when irradiated at room temperature, apparently because the proton can diffuse back too easily. When irradiated and observed at 78 K [Mackey, 1963], smoky centers form which are destroyed upon warming.

The effects of radiation on the IR spectrum of quartz may largely be explained by the mechanism just discussed. The growth of Al(H) absorptions at the expense of other absorptions is accordingly due to alkalies being removed from their charge compensating position around an Al tetrahedron, but an H^+ diffuses to that site making an Al(H) defect. Presumably an alkali-alkali defect is also formed which may have a spectroscopic manifestation if it is a complex one with hydrogen. However, the new alkali-hydrogen defects that arise upon irradiation could have many

origins. One possible origin in synthetic quartz arises from a mechanism as follows: ionizing radiation dissociates an HOH group, giving neutral H and OH which interact with an Al-alkali defect, giving an Al(H) defect and an alkali-hydrogen defect. Hosaka and Taki [1981d] noted that in quartz crystals grown from increasingly pure solutions, i.e., NaCl solution and pure water, the pure water grown crystal showed essentially no radiation change while the NaCl grown crystal showed changes of the type discussed above.

The association of water speciation with a physical property of quartz is well-illustrated by Figures 18 and 19. They show the spectra of two zones of different color in a single quartz crystal zoned with both the amethyst and citrine color varieties. The broad band in the spectrum of the citrine zone is due to molecular H_2O similar to that in synthetic quartz. The amethyst zone in this crystal has only sharp band absorption in its spectrum indicative of OH^-. Whether water inhibits amethyst formation, promotes citrine formation, or is coincidentally associated with another substituent cannot be determined from these data alone. However, Maschemeyer, et al. [1980] have proposed, based on EPR evidence, that the citrine color center is composed of a Li-Al smoky-type hole center, adjacent to a silicon vacancy. They suggest that one way to generate such a vacancy is by incorporating H_2O in the Si site, with adjacent Si atoms moving to interstitial sites to minimize charge imbalance.

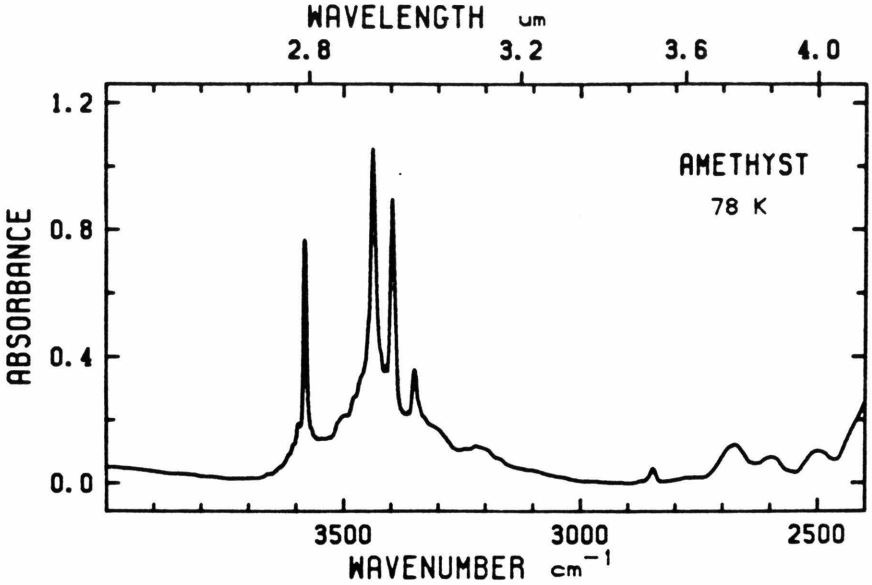

Fig. 18. IR spectrum of zoned amethyst-citrine in the amethyst zone showing absorption from OH ions, 78 K, 2 mm thick.

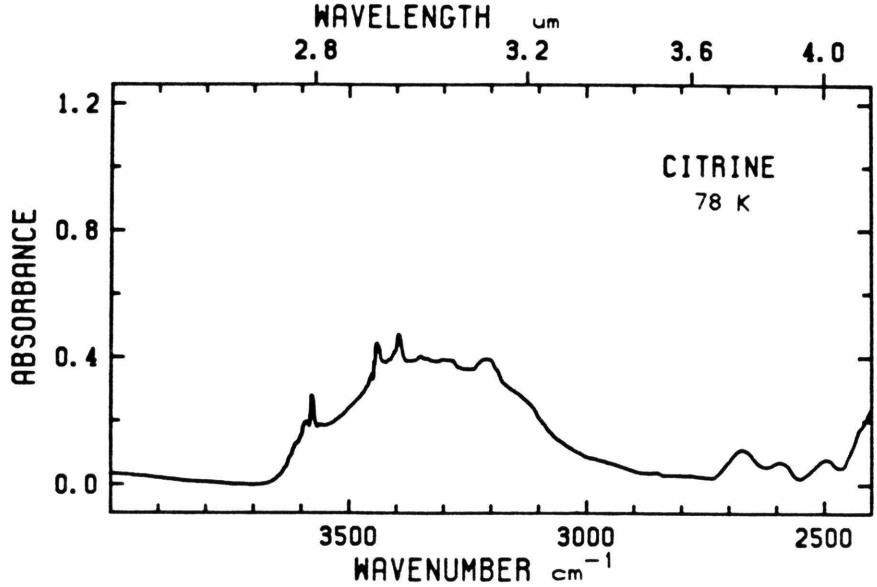

Fig. 19. IR spectrum of zoned amethyst-citrine in the citrine zone showing the broad band absorption from H_2O molecules, 78 K, 2 mm thick.

Spectroscopy of Fluid Inclusions

Fluid inclusions are an important site for hydrogen in minerals. In principle, there should exist a continuum between an isolated water molecule and a large fluid inclusion containing millions of water molecules. It would be desirable to differentiate between single water molecules, small clusters of water molecules which are crystallographically constrained, and "bulk" water in fluid inclusions of the classical definition.

We have already discussed some examples (cordierite, gypsum) of the spectroscopic behavior of isolated water molecules in a crystal structure. An interesting model system for small groups of water molecules was studied by Van Thiel, et al. [1957]. They froze varying concentrations of H_2O in an argon matrix at 8 K, creating "pockets" containing varying numbers of H_2O molecules. In this system, the pockets are expected to be completely "filled" by H_2O; that is, the matrix conforms to the H_2O it entraps. This system should be a reasonable model for H_2O trapped in a locally-neutral silicate lattice. No attempt was made to directly characterize the shapes and sizes of the entrapping volumes.

Van Thiel, et al. recognized four polymeric species of H_2O. Their assignments of the IR absorption patterns are given in Table 2. The assignments for the tetramer are tentative because of the spectral complexity at high H_2O concentrations. In the bending region, the formation of higher polymers resulted in a shift of complex absorptions toward 1650 wavenumbers from the monomer frequency of 1595 wavenumbers; the actual peaks could not be assigned for the polymeric species in the bending region. As the concentration was raised to the point where tetramers and higher polymers predominated, the O-H stretch region was

TABLE 2. Vibrational Bands for Polymeric Water Species Entrapped in Solid Argon Matrix

Polymeric Species	Stretching Frequency ν_{OH}, cm^{-1}
Monomer	3725 , 3627
Dimer	3691 , 3546
Trimer	3510 , 3355
Tetramer	3318?, 3322?

From Van Thiel et al. [1957].

dominated by a broad band in the 3400 to 3200 wavenumber region. This study suggests what type of behavior should be expected from small groups of H_2O molecules in a mineral such as quartz. Interestingly, as the H_2O concentration increases, the total integrated absorption increases nonlinearly. The ε value increases sharply as more H_2O is bound in polymers where hydrogen bonding occurs. This is in accord with Paterson's [1982] appraisal of ε values in minerals and glasses.

The next model system to be considered is one in which the water molecules are coordinated directly or indirectly to a cation, providing a contrast to the neutral argon matrix. Clays such as hectorite contain exchangable Na^+ or Mg^{++} between layers formed by silicate tetrahedra and octahedra of other cations. The inter-layer cations serve to balance charge deficiencies within the layers, but in contrast to the otherwise similar cations in micas, these cations will readily become hydrated by up to 24 water molecules [Farmer and Russell, 1971].

Hectorite can exist in three states of hydration: completely hydrated with multiple H_2O per cation, tri-hydrated, and mono-hydrated. The fully hydrated form is characterized by a broad band absorption centered at 3370 wavenumbers and a sharper band superimposed at slightly higher frequencies. Farmer and Russell interpret this spectrum and the spectra of the partially deuterated clays as being due to extended chains of water molecules in the fully hydrated forms extending from the cation to an oxygen adjoining the site of charge imbalance in the layer, i.e., for the fully deuterated form:

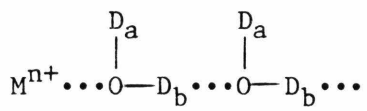

They state that the OD_a groups are mostly directed towards the oxygens of the silicate lattice and form weak hydrogen bonds with those surface oxygens which carry little or no charge. They give rise to the sharp band while the OD_b groups give rise to the broad band. Sharper, more resolved patterns were obtained for the lower hydrates.

A third model system is water in classic fluid inclusions. These are possible in all minerals and have been extensively studied. Kekeluwala et al. [1981] studied fluid inclusions in synthetic quartz, integrating results from IR, TEM, and strain measurements. Hydrous synthetic quartz becomes cloudy if heated or strained. Kekelulawa, et al. demonstrated that this cloudiness is due to the precipitation of the hydrogen in the sample into fluid inclusions. Once this occurs, the quartz behaves similarly to natural milky quartz which has much higher ductility and Q value than synthetic quartz. These physical properties in synthetic quartz only correlate when the hydrogen is in some more dispersed form than fluid inclusions.

Figures 6 and 20 show the IR and NIR regions of an artificial "fluid inclusion" formed by sandwiching water between two Al_2O_3 windows. They are shown at room temperature and 78 K to demonstrate the utility of low temperature measurement in identifying hydrogen in fluid inclusions. Kekeluwala et al. [1981] discovered that the broad band absorption at 3400 wavenumbers does not disappear totally as the 3200 wavenumbers band forms, as it does in pure ice [Eisenberg and Kauzmann, 1962]. This behavior is also seen in the spectra of the 2 μm-thick artificial inclusion and the milky quartz [Figures 6 and 16]. They interpreted the persistence of this band as a result of the H_2O monolayer at the edge of the fluid inclusion. This water still in contact with the silicate

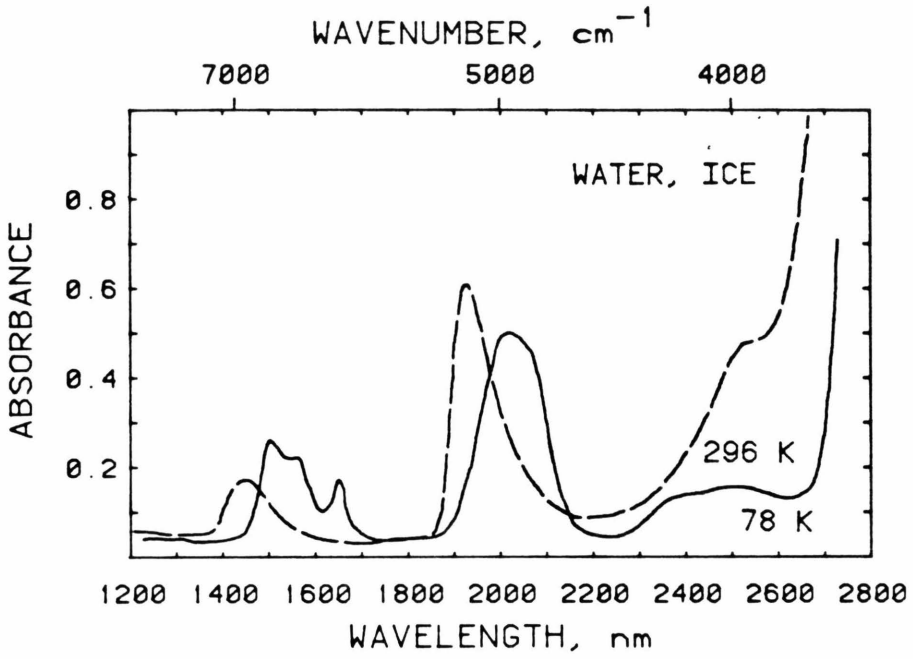

Fig. 20. NIR spectrum of water at 296 K (dash line) and ice at 78 K (solid line). Sample 100 μm thick.

lattice never attains the ice structure. They measured the diameters of the fluid inclusions by TEM and calculated the extent of the monolayer for a 60 nm inclusion at two internal pressures. AT 180 MPa it would be 10% of the inclusion; at 50 MPa it would be 30%. It does not appear that IR spectroscopy can accurately identify extremely small fluid inclusions, given the current understanding of their behavior. All the H_2O would be involved in the monolayer; it would not form "ice" at low temperature. This limit may extend to hundreds of molecules in a cavity.

Before heat treatment, Kekeluwala's sample contained small contrast features observed in TEM which they describe as having the "characteristics of sources of hydrostatic pressure." Heating diminishes their number, with an increase in the number of identifiable fluid inclusion bubbles. If these small contrast features are very small fluid inclusions, it is probable that they will not give the infrared spectrum of a fluid inclusion at 78 K because of the monolayer effect described above.

Trace "Water" in Other Minerals

Most minerals show OH absorption in their infrared spectrum. Usually the amounts are low, but it is present even in gem quality crystals. Examples are shown in Figures 21, 22, and 23. The crystallographic details of the location of this "water" have been established in only a few of the minerals [Beran, 1969, 1970, 1971; Beran and Zemann, 1969, 1971; Beran and Putnis, 1983; Wilkins and Sabine, 1973]. In many of these studies, spectroscopic results have been reported for only one crystal so that it is not possible to distinguish between OH present in foreign phases from OH which is crystal chemically bound in the host phase. Studies in progress in our laboratory indicate that OH is a common substituent in garnet [Aines and Rossman, 1982], and that minor

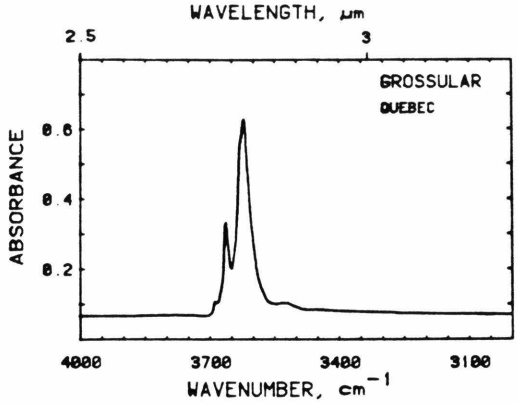

Fig. 21. IR spectrum of grossular garnet showing OH stretching absorptions. Sample 150 μm thick.

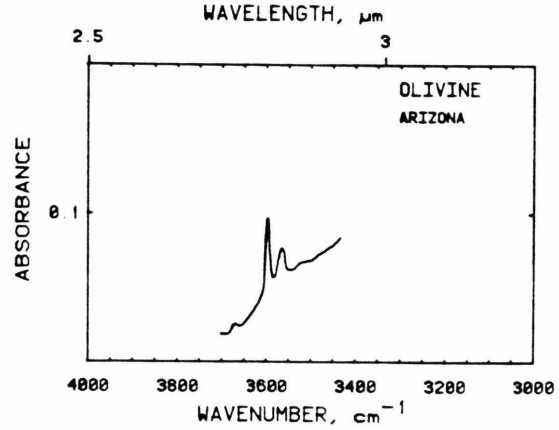

Fig. 22. IR spectrum of olivine showing O-H stretching absorptions. Sample 9.5 mm thick.

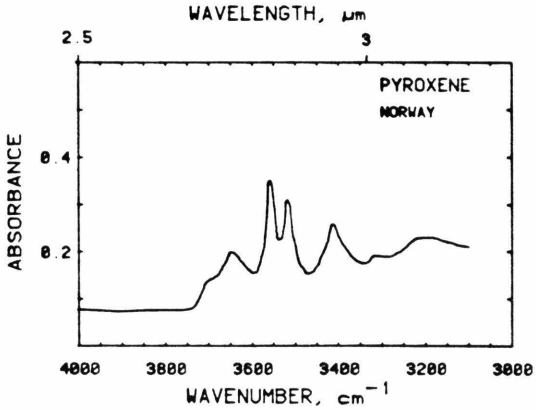

Fig. 23. IR spectrum of the orthopyroxene bronzite showing O-H stretching absorptions. Sample 410 μm thick.

amounts of water are commonly found in feldspars [Solomon and Rossman, 1982]. In natural feldspars higher water content is associated with a greater extent of Al/Si ordering, an observation which parallels results from laboratory Al/Si disordering experiments. Water in feldspar is also intimately associated with radiation damage processes which generate the colored amazonite variety of potassium feldspar [Hofmeister and Rossman, 1981].

An example of concentration determination.

The concentration of molecular water in fluid inclusions in the milky quartz, whose spectrum is illustrated in Figure 16, can be estimated by the following procedure:

1) From the room temperature spectrum the absorbance of the ~3400 wavenumbers band is determined. To correct for the sloping baseline (a result of wavelength dependent scattering in the sample), a sloping straight line baseline is connected to lower portions of the data trace at the left and right hand sides. From the spectrum the peak of the absorption at 3400 wavenumbers is read to be 0.50 absorbance units above the baseline.

2) Using the Beer's Law relationship, defined as $A = \varepsilon \times p \times c$

where A = absorbance from the spectrum (0.50 in this case)

p = optical path length through the sample (in 10^{-2}m)

c = concentration of the species of interest (in moles per liter)

ε = molar absorptivity constant obtained from a standard substance.

Using the ε value of this band for H_2O in liquid water, 81 liters per mole per 10^{-2}m [Thompson, 1965], the following calculation gives the concentration:

$$0.50 = 81\ \ell\ mol^{-1}\ (10^{-2}m)^{-1} \times 0.0195 \times 10^{-2}m \times c$$

$$c = 0.317 \text{ moles per liter}$$

3) The concentration can be converted to wt% as follows: From the density of quartz, 2.65, a sample weight of 2.65 kg per liter is obtained. The water content is:

$$0.317 \text{ moles} \times 0.018 \text{ kg mole}^{-1} = 5.70 \times 10^{-3} \text{ kg } H_2O$$

or:

$$(5.70 \times 10^{-3} \text{ kg}/2.65 \text{ kg} \times 100 = 0.215\%\ H_2O.$$

Two major difficulties in determing concentrations are the determination of appropriate ε values for all the different types of H_2O and OH which occur in minerals, and dealing with spectra with several overlapping bands. Paterson [1982] surveys available calibrations for the IR determination of water in quartz, glasses, and related substances. He provides his tabulations in terms of integrated absorption profiles which have a smaller temperature dependence than ε values.

Acknowledgments

This work has benefited from discussions with Stephen Kirby (USGS) who also provided the synthetic quartz samples used in this study, and from Clifford Frondel (Harvard) who provided the results of his study of low temperature silica in advance of publication.

This study was in part funded by the National Science Foundation (Grant EAR-7919987).

References

Aines, R. D. and G. R. Rossman, The hydrous component in garnets, (abstract) Geol. Soc. Am. Abstracts with Programs, 14, 430, 1982.

Barnes, R.L., E.O. Kolb, R.A. Laudise, E.E. Simpson, and K.M. Kroupa, Production and perfection of z-face quartz, J. Crystal Growth, 34, 189-197, 1976.

Beran, A., Über (OH)-Gruppen in Olivin. Anz. Osterr. Akad. Wiss., Math.-naturwiss., Kl., 106, 73-74, 1969.

Beran, A., Messung des Ultrarot-Pleochroismus von Mineralen. IX. Der Pleochroismus der OH-Streckfrequenz in Titanit, Tschermaks Miner. u. Petrogr. Mitt., 14, 1-5, 1970.

Beran, A., Messung des Ultrarot-Pleochroismus von Mineralen. XII. Der Pleochroismus der OH-Streckfrequenz in Disthen. Tschermaks Min. Petr. Mitt., 16, 129-135, 1971.

Beran, A. and J. Zemann, Messung des Ultrarot-Pleochroismus von Mineralen. VIII. Der Pleochroismus der OH-Streckfrequenz in Andalusit. Tschermaks Min. Petr. Mitt., 13, 285-292, 1969.

Beran, A. and A. Putnis, A model of the OH positions in olivine, derived from infrared-spectroscopic investigations. Phys. Chem. Minerals, 9, 57-60, 1983.

Beran, A. and J. Zemann, Messung des Ultrarot-Pleochroismus von Mineralen. Der Pleochroismus der OH-Streckfrequenz in Rutil, Anatas, Brookit, und Cassiterit. Tschermaks Min. Petr. Mitt., 15, 71-80, 1971.

Chakraborty, D. and G. Lehmann, On the structures and orientations of hydrogen defects in natural and synthetic quartz crystals, Phys. Stat. Sol. (a), 34, 467-474, 1976a.

Chakraborty, D. and G. Lehmann, Distribution of OH in synthetic and natural quartz crystals, J. Sol. S. Chem., 17, 305-311, 1976b.

Chakraborty, D and G. Lehmann, On the fine structure in the infrared spectra of clear natural quartz, amethyst, citrine, and synthetic quartz crystals, Z. Naturforsch., 33a, 290-293, 1978.

Cox, R.T., Optical absorption of the d^4 ion Fe^{4+} in pleochroic amethyst quartz, J. Phys. C.: Solid State Physics, 10, 4631-4643, 1977.

Eisenberg, O. and W. Kauzmann, The structure and properties of water, Oxford U. Press, 296 pp., 1962.

Farmer, V.C. and J.D. Russell, Interlayer complexes in layer silicates. The structure of water in lamellar ionic solutions, Trans. Faraday Soc., 67, 2737-2749, 1971.

Flörke, D.W., B. Köhler-Herbertz, K. Langer, and I. Törges, Water in microcrystalline quartz of volcanic origin: agates, Cont. Min. Pet., 80, 329-333, 1982.

Frondel, C., Structural hydroxyl in chalcedony (Type B quartz), Am. Min., 67, 1248-1257, 1982.

Goldman, D.S., G.R. Rossman, and W.A. Dollase, Channel constituents in cordierite, Am. Min., 62, 1144-1157, 1977.

Hofmeister, A.M. and G.R. Rossman, Effects of radiation on water and lead in potassium feldspar (abstract) Geol. Soc. Amer., Abstracts with Programs, 13, 474, 1981.

Hosaka, M. and S. Taki, Hydrothermal growth of quartz crystals in NaCl solution, J. Crystal Growth, 52, 837-842, 1981a.

Hosaka, M. and S. Taki, Hydrothermal growth of quartz crystals in KCl solution, J. Crystal Growth, 53, 542-546, 1981b.

Hosaka, M. and S. Taki, Hydrothermal growth of quartz crystals in pure water, J. Crystal Growth, 51, 640-642, 1981c.

Hosaka, M. and S. Taki, Synthetic quartz crystals grown in NaCl, KCl solutions and pure water, and their low temperature infrared absorption, 35th Annual Symposium on Frequency Control, 1981d.

Kats, A., Hydrogen in alpha quartz, Philips Research Reports, 17, 133-195 and 17, 201-279, 1962.

Kekulawala, K.R.S.S., M.S. Paterson, and J.N. Boland, An experimental study of water in quartz deformation, in Mechanical Behavior of Crustal Rocks, Geophysical Monograph 24, edited by N.L. Carter, pp. 49-60, Am. Geophys. Union, Washington, DC, 1981.

Kirby, S.H., Hydrogen-bonded hydroxyl in synthetic quartz: analysis, mode of incorporation and role in hydrolytic weakening, Phys. Chem. Min., (in press) 1984.

Koop, O.C. and P.A. Staats, Characterization of Rb-OH grown quartz by infrared and mass spectroscopy, J. Phys. Chem. Solids, 31, 2469-2476, 1970.

Krefft, G. B., Effects of high temperature electrolysis on the coloration characteristics and OH-absorption bands in alpha-quartz, Radiation Effects, 26, 249-259, 1975.

Langer, K. and O.W. Flörke, Near infrared absorption spectra (4000-9000 cm^{-1}) of opals and the role of "water" in these $SiO_2 \cdot nH_2O$ minerals, Fortschr. Miner., 52 (1), 17-51, 1974.

Mackey, J.H. Jr., EPR study of impurity-related color centers in germaniumdoped quartz, J. Chem. Phys., 39, 74-80, 1963.

Maschemeyer, D., K. Niemann, H. Hake, and G. Lehmann, Two modified smoky quartz centers in natural citrine, Phys. Chem. Min., 6, 145-156, 1980.

McDonald, R.S., Study of the interaction between hydroxyl groups of Aerosil silica and adsorbed non-polar molecules by infrared spectrometry, J. Am. Chem. Soc., 79, 850-854, 1956.

Paterson, M., The determination of hydroxyl by infrared absorption in quartz, silicate glasses and similar materials, Bull. Miner., 105, 20-29, 1982.

Schreyer, W. and H.S. Yoder, The system Mg-cordierite-H_2O and related rocks, Neues. Jahrb. Mineral. Abh., 101, 271-342, 1964.

Solomon, G.C. and G.R. Rossman, Water in feldspars, (abstract), Geol. Soc. Amer., Abstracts with Programs, 14, 622, 1982.

Thompson, W.K., Infrared spectroscopic studies of aqueous systems: I, Trans. Faraday Soc., 61, 1635-1640, 1965.

Van Thiel, M., E.D. Becker, and G.C. Pimental, Infrared studies of hydrogen bonding by the matrix isolation technique, J. Chem. Phys., 27, 486-490, 1957.

Weil, J. A., The aluminum centers in α-quartz, Radiation Effects, 26, 261-265, 1975. Wilkins, R.W.T. and W. Sabine, Water content of some nominally anhydrous silicates, Am. Min., 58, 508-516, 1973.

Wood, D.L. and K. Nassau, Infrared spectra of foreign molecules in beryl, J. Chem. Phys., 47, 2220-2228, 1967.

Chapter 3

The Significance of Infrared Band Shapes and Positions in Hydrogen Bonded Systems

Abstract

The band shape and position of an infrared absorption due to water or hydroxyl in a mineral are measures of the bonding and site distribution of that species. The absorption energy (position) of the band is a well known indicator of the O-H--O distance in a hydrogen bonded system. I have combined this with hypothetical distributions of O-H--O bond lengths in order to obtain a predictive model of the spectroscopic behavior of hydrogen-bonded systems which contain a variety of sites. Using simple gaussian distributions of bond lengths I have modeled the absorption behavior of several "broad band" systems including synthetic quartz and metamict zircon.

Introduction

Infrared spectroscopy has been extensively used to study hydrogen in minerals because of its sensitivity to O-H bonds. Through the application of information obtained at various energies in the infrared region it is now a relatively straightforward process to identify hydrogen species and their orientation in many minerals (e.g. Chapter 2, Aines and Rossman, 1984a, and references therein.) These techniques are most easily applied to systems in which hydrogen occupies discrete sites, and are more difficult to apply to systems in which the hydrogen occupies a continuum of sites. In this paper I discuss the expected spectroscopic behavior of such a continuum of sites and I present a quantitative model which may be used to interpret the spectra of minerals containing such a continuum. Two systems of interest are synthetic quartz and hydrous metamict zircon (Figure 1). Figure 1 also shows the spectrum of amorphous solid water, which is of interest for modelling the behavior of very small fluid inclusions whose structure is controlled by the surrounding silicate lattice, and which never attain the ice structure. The basis of my model is the variation in absorption energy of an O-H bond with O-H--O distance, in other words, the strength of hydrogen bonding. This model can also be applied to understand the spectral changes anticipated due to changes in pressure or temperature which cause O-H--O distances to change.

Manifestations of Hydrogen Bonding

The effects of hydrogen bonding on the spectra of O-H species have been extensively studied. I will review briefly the results of these

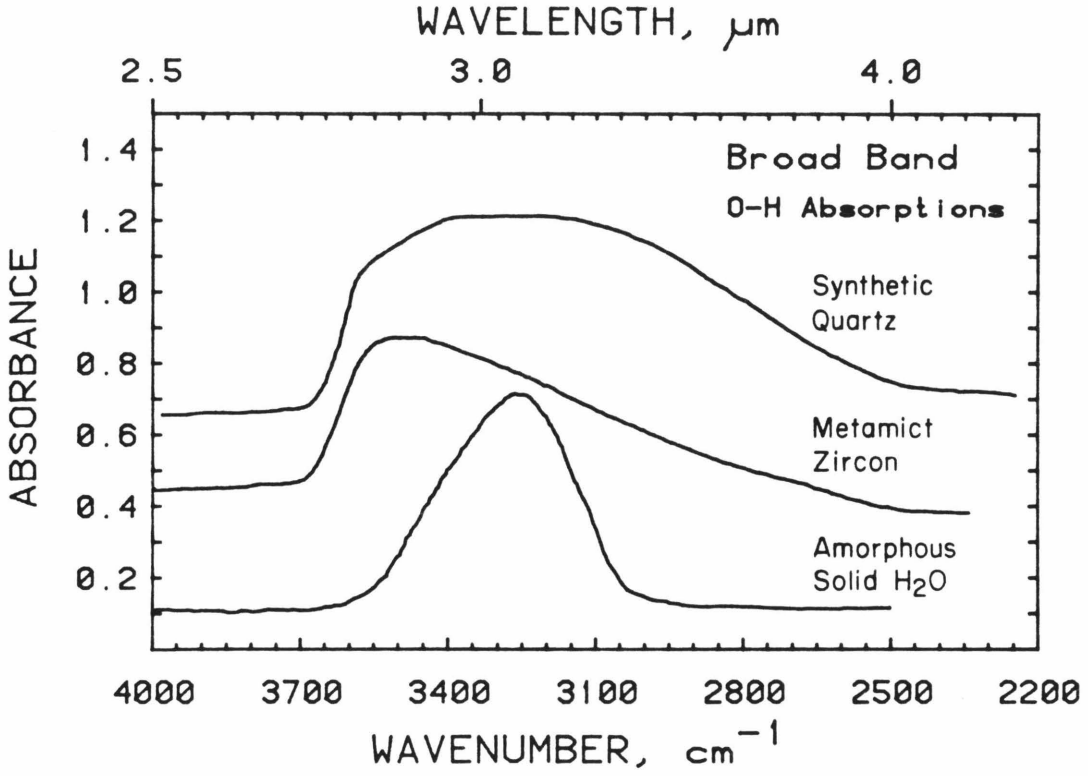

Figure 1. Infrared spectra of two systems containing hydrogen in an apparent continuum of sites, and amorphous water. Synthetic quartz, X-O reference slab 1.06 mm thick (Aines et al., 1984). Metamict Zircon, Ceylon 6500, 0.6 mm thick (Chapter 6, Aines and Rossman, 1984c). Amorphous solid water, (Hagen, et al., 1981).

studies in order to establish the basis for my model and the interpretation of broad band spectra as seen in Figure 1, and also shifts caused by pressure and temperature changes.

Absorption Frequency. Perhaps the most useful manifestation of hydrogen bonding is the strong correlation between the length of a hydrogen bond and the corresponding O-H vibrational energy (Figure 2). The upper limit of 3.4 Å corresponds to no hydrogen bonding. The lower limit corresponds to a symmetric hydrogen bond, which most authors agree has a limiting length of approximately 2.40 Å (e.g. Olovsson and Jönsson, 1976; see discussion of short hydrogen bonds below). This relationship is obeyed for all linear O-H--O bonds, and a similar relationship is found for hydrogen bonds involving N, F, and Cl (Nakamoto et al., 1955; Novak, 1974). This relationship is very useful as a spectroscopic tool for determining the length of hydrogen bonds, particularly those longer than 2.7 Å. Considerable uncertainty remains concerning the spectroscopic behavior of very short hydrogen bonds, less than 2.7 Å in length, because of the difficulty in separating stretching absorptions from other modes in the 1500-500 cm^{-1} region.

The results of Figure 2, and most other data on O-H--O hydrogen bonds, may be conveniently described by a potential model for the hydrogen bond first described by Lippincott and Schroder (1955; see also Hadzi and Bratos, 1976; Sandorfy, 1976). Their model assumes that a potential well described by

$$V = D[1-\exp(-n\Delta r^2/2r)] \qquad (1)$$

(where D = bond dissociation energy, r = O-H distance, $\Delta r = r-r_0$, the O-H length when free of hydrogen bonding), exists between each of the

Figure 2. Relationship between O-H vibration frequency and O-H--O bond length. Data from Nakamoto et al.,(1955).

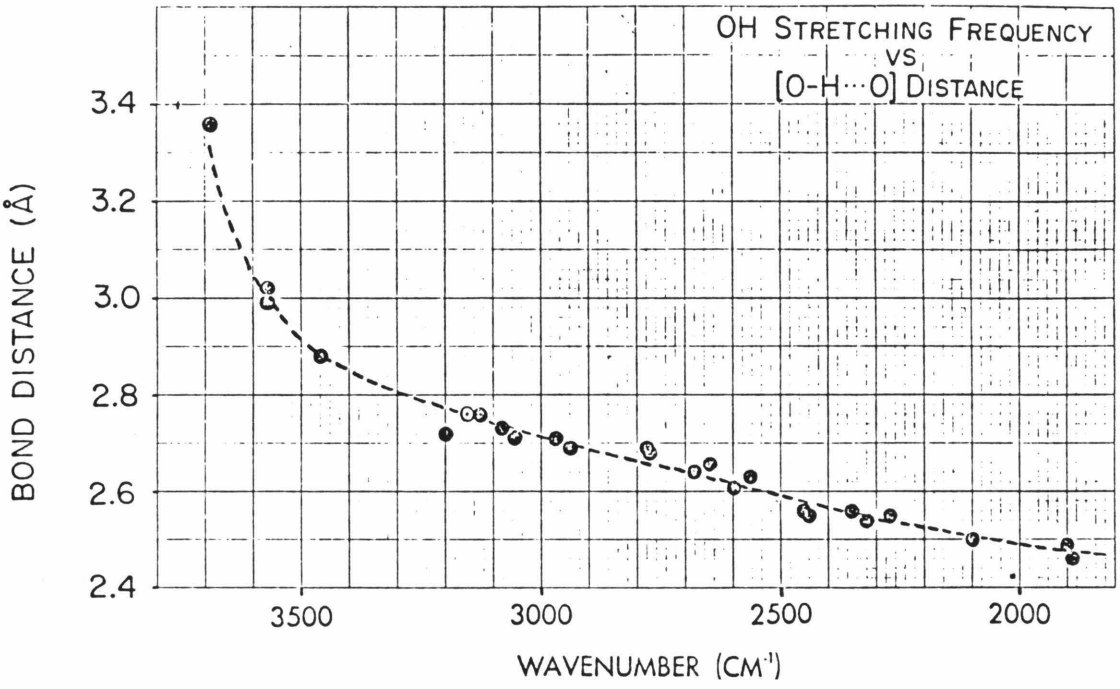
OH STRETCHING FREQUENCY
VS
[O-H···O] DISTANCE
BOND DISTANCE (Å)
3.4
3.2
3.0
2.8
2.6
2.4
3500
3000
2500
2000
WAVENUMBER (CM⁻¹)

oxygens and the hydrogen. Additional terms are used to describe the attractive and repulsive interactions of the oxygens but they are not important except for very short bonds. Using known bond dissociation energies this model accurately predicts the absorption frequencies shown in Figure 2. It is important to note that this implicitly includes D as a function of r because the bond dissociation energies are not measured independently of the bond length. As a result the results are best applicable to systems at 1 bar, 25°C and may not be applicable when the O-O distance is changed independently of the dissociation energy by changing either pressure or temperature.

Bandwidth. Comparatively large half-widths are characteristic of hydrogen-bonded OH groups in gases, liquids, and solids. Some broadening may be attributed to causes such as doppler shifting in gases, however when these are removed from consideration it is apparent that the broadening is an intrinsic result of hydrogen bonding (e.g. Hadzi and Bratos, 1976). Although considerable controversy exists concerning the possibility of the existence of a single unified theory of broadening, several plausible mechanisms have been suggested which appear to adequately explain specific cases. All the mechanisms suggested, however, involve asymetric O-H potential wells of the type given by Lippincott and Schroeder (eq. 1). The fluctuation theory (see Hadzi and Bratos, 1978; Lascombe et al., 1973) and the anharmonicity theory particularly as described by Rice and Wood, 1973, and Azman et al., 1971, seem to account for most of the observed phenomena. Other treatments have been given by Rösch and Ratner, 1974, and Mikhailov et al., 1973.

The fluctuation theory is based on the time dependency of O-H--O distances. Relative time scales and coupling coefficients are important in this theory, but the result is that the breadth of the O-H absorption in hydrogen bonded materials can be due to the existence of a distribution of O-H--O lengths. I have applied a similar theory to calculate the O-H--O length distributions associated with broad-band absorptions in minerals. A requirement of the fluctuation theory is that the motions of the individual molecules be strongly coupled. Jakobsen et al. (1967) showed that in solid alcohols the broadening was due to coupled motion in adjacent molecules and that there was no broadening in isotopically substituted systems because the molecules are decoupled. The anharmonicity theories are actually extensions of the fluctuation theories (Hadzi and Bratos, 1976). These theories explicitly consider the effect of coupling of the O-H, O-H--O stretches and external vibrations, all of which are anharmonic. As a result, the potential surface for the O-H vibration is extremely sensitive to molecular interactions and temperature changes (Sandorfy, 1976). When molecular motions are coupled, broad band absorption will result.

Band Intensity. The relationship between integral band intensity and O-O distance is almost as good a measure of hydrogen bonding as is the frequency shift. As hydrogen bonding increases, so does the integrated intensity of the O-H stretching vibration (Pimental and McClellan, 1960; Hadzi and Bratos, 1976.) This is due to the increase in the transition dipole along the normal coordinate ν_1 caused by the effective charge transfer of the hydrogen bond (Lippincott and Schroeder, 1955; Sandorfy, 1976.) Paterson (1982) has established a calibration of $\Delta\nu_1$ vs.

integral intensity which is useful in calculating molar concentrations when individual molar absorptivities have not been determined.

Non-Linear Hydrogen Bonds. It is convenient to assert that hydrogen bonds are linear. This is because of the difficulty of actually locating the proton by X-ray diffraction methods. The advent of neutron diffraction studies, however, allows the direct determination of the hydrogen position, and while linear bonds are dominant, deviations of up to 30° occur commonly (Olovsson and Jönsson, 1976). Short hydrogen bonds tend to be more linear than long ones, rarely deviating more than 10° from linear when O-H--O distances are less than 2.6 Å. Both theoretical and experimental studies show that bent hydrogen bonds will show smaller O-H stretching frequency shift than those given in Figure 2 (Schroeder and Lippincott, 1956; Nakamoto et al. 1955). These reductions in shift are experimentally observed to be as much as 700 cm^{-1} less than the linear hydrogen bond value (Nakamoto et al. 1955). Similarly, bifurcated hydrogen bonds (hydrogen bonds shared by two oxygens) are expected to show greater shifts than Figure 2, but in O-H--O systems, these rare and not well characterized experimentally (Olovsson and Jönsson, 1976; Luck, 1976).

Short Hydrogen Bonds. Considerable controversy surrounds the spectroscopic behavior of very short and symmetrical hydrogen bonds. From both theoretical and experimental results, the minimum O-H-O distance to be expected is about 2.40 Å (Lippincott and Schroeder, 1955; Olovsson and Jönsson, 1976). The infrared spectra of these systems have proved to be very difficult to interpret. It is common for symmetric, intra-molecular hydrogen bonds to show no detectable O-H stretching

absorption (Ellison and Levy, 1965; Hadzi and Orel, 1973; Hadzi and Bratos, 1976) despite theoretical predictions of absorption intensity increasing with decreasing O-H-O distance. Absorptions related to the O-H bond are detectable for many systems where the two oxygens are not symmetrically equivalent, but the assignment of vibrational modes is difficult. The slope of the frequency vs. O-H--O distance curve (Fig. 2) is very shallow below 2.7 Å, and sensitive to experimental uncertainties. Acceptable correlations to experimental data have been given placing the OH frequency of a 2.5 Å O-H--O system from 2050 cm^{-1} (Nakamoto et al., 1955) to 1500 cm^{-1} (Novak, 1974). Lippincott and Schroeder's potential well model predicts a value of ~1700 cm^{-1} at 2.5 Å, and because of oxygen-oxygen interactions (this is close to the Van der Waals radii) this is the predicted minimum frequency. Novak's correlation suggests that for a symmetric bond of 2.35 Å the frequency will be 0 cm^{-1}; Nakamoto et al. predict ~1400 cm^{-1}. Novak's work makes it very clear, however, that assignment of stretching modes is very difficult for short hydrogen bonds. The "best fit" to the type of data presented in Figure 2 cannot, therefore, be obtained, and the quantitative aspects of the spectroscopy of short hydrogen bonds must be considered an open question.

Effects of Pressure and Temperature

In the context of mineralogy and geology it is desirable to understand the properties of earth materials at various pressures and temperatures. It is also interesting to study the effects of pressure and temperature on hydrogen bonds purely as a test of hydrogen bonding

theory. Both types of studies have been undertaken, and two effects may be distinguished: quantum mechanical effects that are purely the result of temperature, and physical effects resulting from changing the O-O distance through external means.

The effect of pressure on O-H vibrations is straightforward in most cases; as pressure increases, O-O distance decreases, and O-H stretching frequency is reduced in accord with Figure 2 and the results of the Lippincott-Schroeder (1955) potential surface (eq. 1). Experimental studies of ice VII to 360 kbar (Walrafen et al., 1982), ice clathrates to 1.5 kbar (Johari and Chew, 1983) and gypsum to 7 kbar (Corty et al., 1983) confirm this behavior. However, it is important to note that while the general trend of Figure 2 is followed with pressure (see esp. Walafen et al, 1982), the value of $\partial\nu/\partial p$ hence $\partial\nu_{OH}/\partial r_{OH(O-O)}$ need not follow the trend of Figure 2 since in the Lippincott-Schroeder potential (eq. 1) D is an implicit function of r. In fact, a family of curves like Figure 2 must exist at varying pressures and although presently their relationships are not known, the evidence of Walrafen et al. is that the $\partial\nu_{OH}/\partial r_{(O-O)}$ due to pressure is less than $\partial\nu_{OH}/\partial r_{(O-O)}$ due to changes in bonding.

It is interesting to note that the effect of compression on O-H frequencies is the opposite of that commonly found for other bonds. Most atoms in solids vibrate in anharmonic potential wells similar to that given by eq. (1), and are not strongly coupled to other vibrations. The effect of pressure is, therefore, that expected of a single oscillator, that is the frequency <u>increases</u> with pressure. O-H vibrations are unusual in decreasing frequency with pressure because of

strong coupling of the stretching frequency with the hydrogen bond.

Similar changes in ν_{OH} in minerals due to the effects of thermal expansion have been noted by Velde (1983) Johari and Chew, (1983), and Aines and Rossman (1984b; Chapters 7 and 8), and the effect is well known in synthetic materials (e.g. Pimental, 1960, p.76; Rice and Wood, 1973; Hadzi and Bratos 1976.) The thermal behavior of OH stretching frequently follows the O-O distance behavior shown in Figure 2. However, it is also common for them to show negative temperature coefficients (Chapter 7). Rice and Wood (1973) quantitatively describe a mechanism that will cause a different temperature shift in broad bands which are significantly coupled to other anharmonic vibrations of low frequency. In this case, the frequency shift with increasing temperature will be positive. The basic mechanism responsible for this is the excitation of low-freqeuncy strongly anharmonic vibrations. These bands become increasingly anharmonic at higher excited states, forcing the coupled O-H stretching frequency to higher energies. Rice and Wood (1973) worked out this relationship in general terms using a quantum mechanical treatment; treatment using classical anharmonicity theory yields the same result (Romanowski and Sobczyk, 1978).

These treatments suggest that for broad OH bands (greater than 100 cm^{-1}) where the breadth is due to coupling to other OH groups or lattice modes, a positive temperature coefficient is expected. Velde (1983) and Aines and Rossman (Chapter 7) report that the OH stretching vibrations in micas may have temperature coefficients of both signs despite their apparently similar natures. The crystallographic work has not been done to establish the angular relationships for the hydrogen bonds, but it

seems likely that the signs of the temperature coefficients can be dominated by the bending of hydrogen bonds. These are all weak bonds (>2.9 Å in length) and may be considered to be subject to bending (Olovsson and Jönsson, 1976). The weak hydrogen bonds involving these OH groups may also not interact significantly with the O-H vibration, giving negative temperature coefficients (from simple thermal expansion) of the same sort seen in single oscillators.

Model for O-H Stretching Bands Due to Distributions of O-H--Lengths

In order to understand the nature of O-H groups contributing to broad bands of the type seen in Figure 1, and to understand the general frequency, intensity, and bandwidth relationships for O-H groups in minerals, I have developed a model for O-H absorption based on gaussian distributions of O-H--O bond lengths and the frequency relationships shown in Figure 2. The basic premise of this model is that for all O-H groups in minerals, some distribution of O-H--O lengths exists representing slightly different sites. In the case of O-H distributions resulting in broad bands, there is a sizable difference between the longest and shortest bonds. The purpose of this model is to quantify that difference.

By assuming a static distribution of O-H--O lengths, this model is similar to the fluctuation theory but has no time dependency. Therefore, I can model the absorption band resulting from a distribution by calculating a sum of individual bands resulting from individual O-H groups. These bands were assumed to be of Laurentian shape with a half-width (full width at half height) of 5-20 cm^{-1}. For distributions of O-

H--O lengths resulting in broad bands, the shape of the band is insensitive to the width of the component peaks.

The following steps are used to calculate a spectrum based on an assumed O-H--O distribution:

(1) A peak location for each of a finite number of points in the O-H--O distribution is calculated.

(2) A Laurentian peak of given half-width is established at each of those points.

(3) The absorption band is calculated by summing the intensity under the Laurentian peak at each calculated wavenumber. The intensity is scaled by the original gaussian distribution of O-H--O length intensity, and by an absorption coefficient for that frequency from Paterson's 1982 calibration.

This model assumes that all broadening of O-H stretching absorptions is due to the static existence of different O-H--O bond lengths. The temperature coefficient associated with such bands should be small and positive, similarly the pressure coefficient should be negative, in accord with the discussion in the last section. The only cause of frequency shifts inherent in this model is changes in O-O distance. Similarly, bandwidth and intensity changes should follow the previously discussed relationships. This model does not account for bent hydrogen bonds, nor does the present version allow for more than one distribution of O-H--O lengths. However, the fact that broad band absorption spectra may be modeled successfully using only one distribution is a strong argument that I am using a realistic algorithm.

Results

The model for simulating peak shapes is useful both for deriving the O-H--O distributions responsible for broad band absorptions and also for understanding thermal effects on well defined O-H--O sites. If a single OH site exists in a mineral the width of the absorption band will be determined by relaxation phenomena and by thermal motion of the oxygens. I will not attempt to evaluate relaxation phenomena but the effect of thermal motion may be easily evaluated by investigating the bandwidths resulting from different O-H--O distributions. This assumes that the absorption phenomena occur much faster than thermal motion, a similar assumption to those of the fluctuation theory. Figure 3 shows the spectra resulting from gaussian distributions of O-H--O lengths centered at 2.8 Å and ranging in width at half height from 0.01 to 0.1 Å. As the O-H--O distribution becomes broader so do the resultant peaks. Asymmetry becomes apparent in the broadest peak. This asymmetry is caused by the asymmetry of the relationship between O-H--O distance and frequency (Fig. 2).

The asymmetry of the frequency - O-H--O relationship also results in O-H stretching peaks at low wavenumbers being inherently broader than high-wavenumber peaks. Figure 4 shows the peaks generated by a gaussian O-H--O distribution of constant width (0.01 Å) at successively shorter O-H--O lengths. It is apparent that short O-H--O bonds yield inherently broad absorptions even with very well defined O-H--O distances, and that long O-H--O bonds can result in comparatively much sharper peaks even with broad O-H--O distributions. When sites are well defined and not

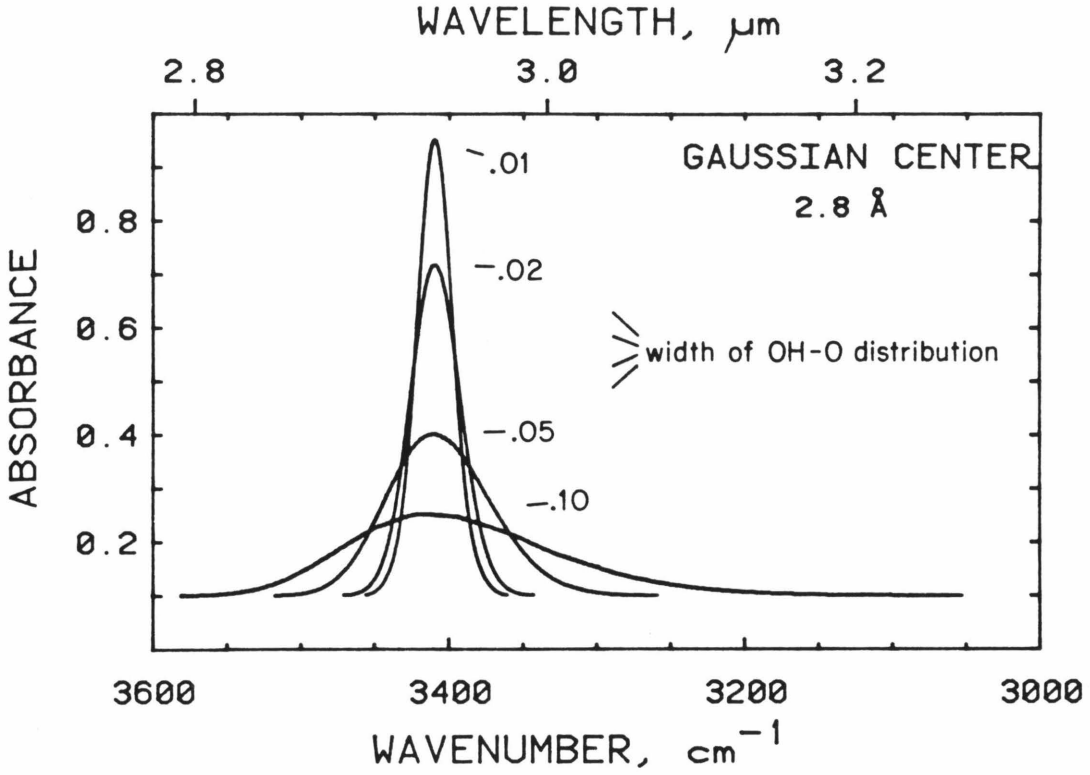

Figure 3. Model-generated spectra of an OH--O distribution centered at 2.8 Å showing the spectroscopic effects of different distribution widths. Each peak is composed of 200 Laurentian component peaks with widths at half height of 10 cm^{-1}.

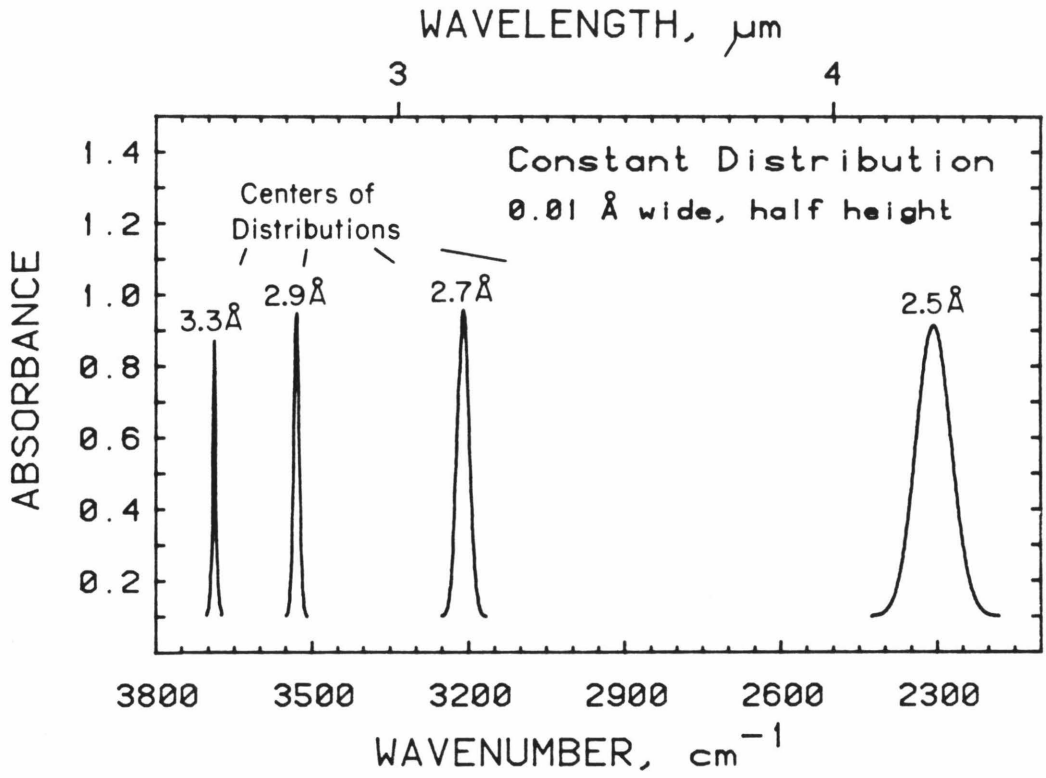

Figure 4. Model-generated spectra of OH--O distributions with a constant half-width of 0.01 Å, centered at the OH--O lengths shown. 200 component peaks 4 cm^{-1} wide.

subject to extensive thermal motion, the asymmetry seen in Figure 3 is not apparent. This asymmetry is entirely a function of the present of a number of different O-H--O distances.

Model-generated spectra for the broad bands shown in Figure 1 are given in Figure 5. The best fit is obtained for zircon (Fig. 5a). This sample contains approximately 0.06 wt% H_2O, all in the form of OH - groups. Water content was calculated from an absorbance of 7.56/cm, assumed $\varepsilon = 60\ell\ mol^{-1}\ cm^{-1}$, assumed density = 4.0 g/cc.) The spectrum may be accurately modeled with an average O-H--O distribution of 2.82 Å and a width at half height of 0.4 Å. The spectrum of amorphous ice (Fig. 5b) may be modeled using an O-H--O distribution centered at 2.75 Å with a half width of 0.13 Å. This is in good agreement with the known O-H--O distance of 2.76 Å. The amorphous ice spectrum shown in Figure 5b has been corrected slightly to remove a low frequency component due to ice I. It did not prove possible to fit both the high and low frequency parts of the amorphous ice broad band with a single gaussian distribution of O-H--O lengths.

The broad band present in synthetic quartz proved to be the most difficult to model. Two attempts are shown in Figures 5c and d. It does not appear possible to fit the synthetic quartz broad band spectrum with a single O-H--O distribution.

Discussion

The model I have presented here provides a quantitative description of the O-H--O bond distributions responsible for O-H broad bands in minerals. The description is not necessarily complete, however, since

Figure 5. (Following pages) Comparison of real (dashed line) to model generated (solid line) broad band spectra. The O-H--O distribution used in the model is shown to the right. A) Metamic zircon. B) Amorphous ice. C) Synthetic quartz X-0, fit 1. D) Synthetic quartz X-0, fit 2. 200 Laurentian peaks 20 cm^{-1} wide used for all plots.

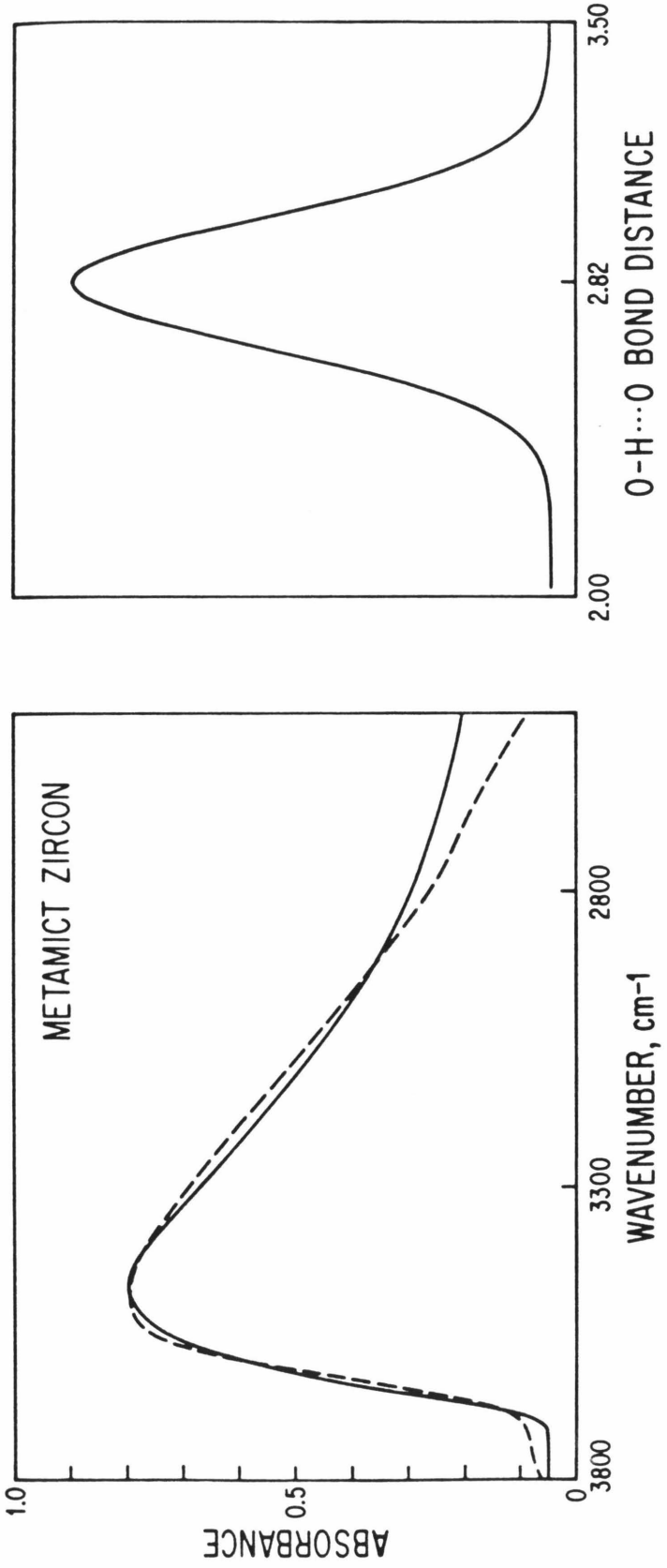
METAMICT ZIRCON
ABSORBANCE
1.0
0.5
0
3800
3300
2800
WAVENUMBER, cm-1
2.00
2.82
3.50
O-H···O BOND DISTANCE

(5A)

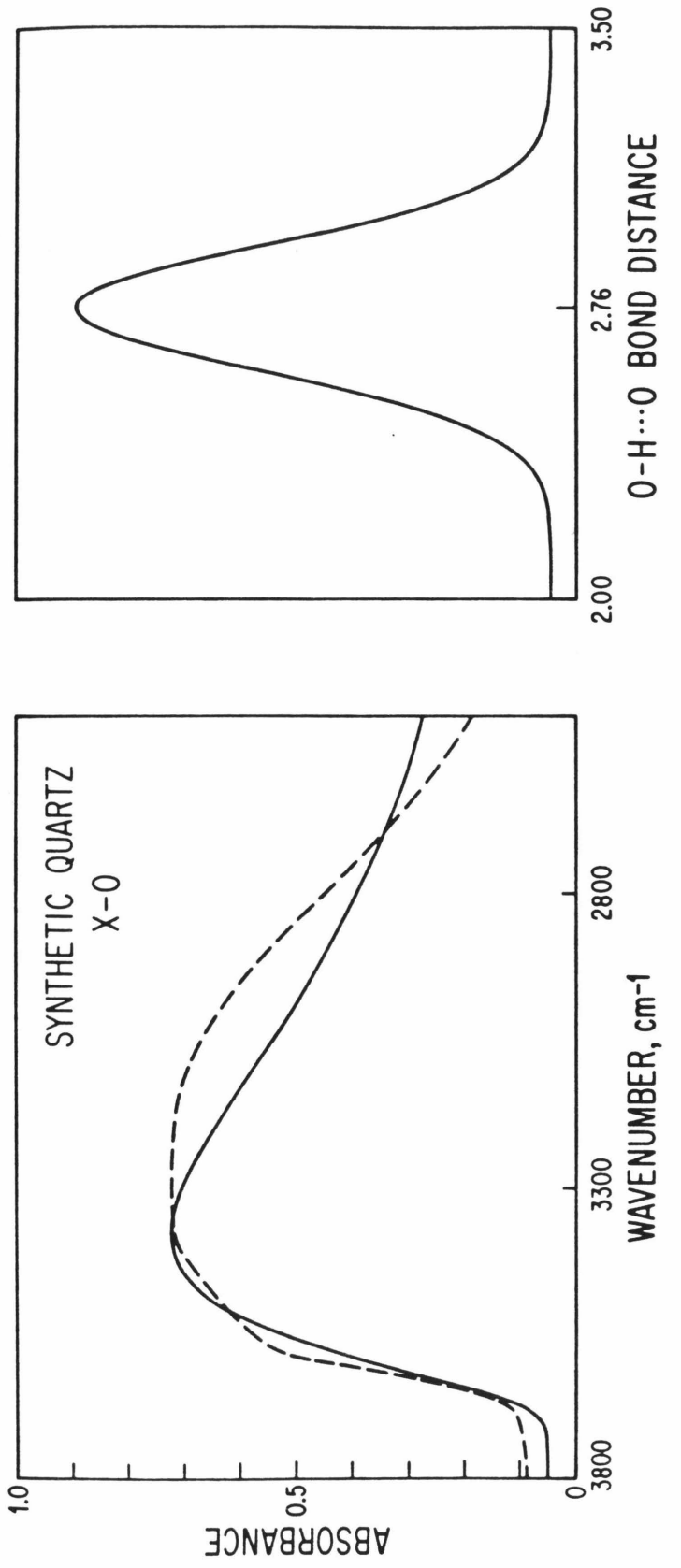
SYNTHETIC QUARTZ
X-O
ABSORBANCE
1.0
0.5
0
3800
3300
2800
WAVENUMBER, cm-1
2.00
2.76
3.50
O-H···O BOND DISTANCE

(5B)

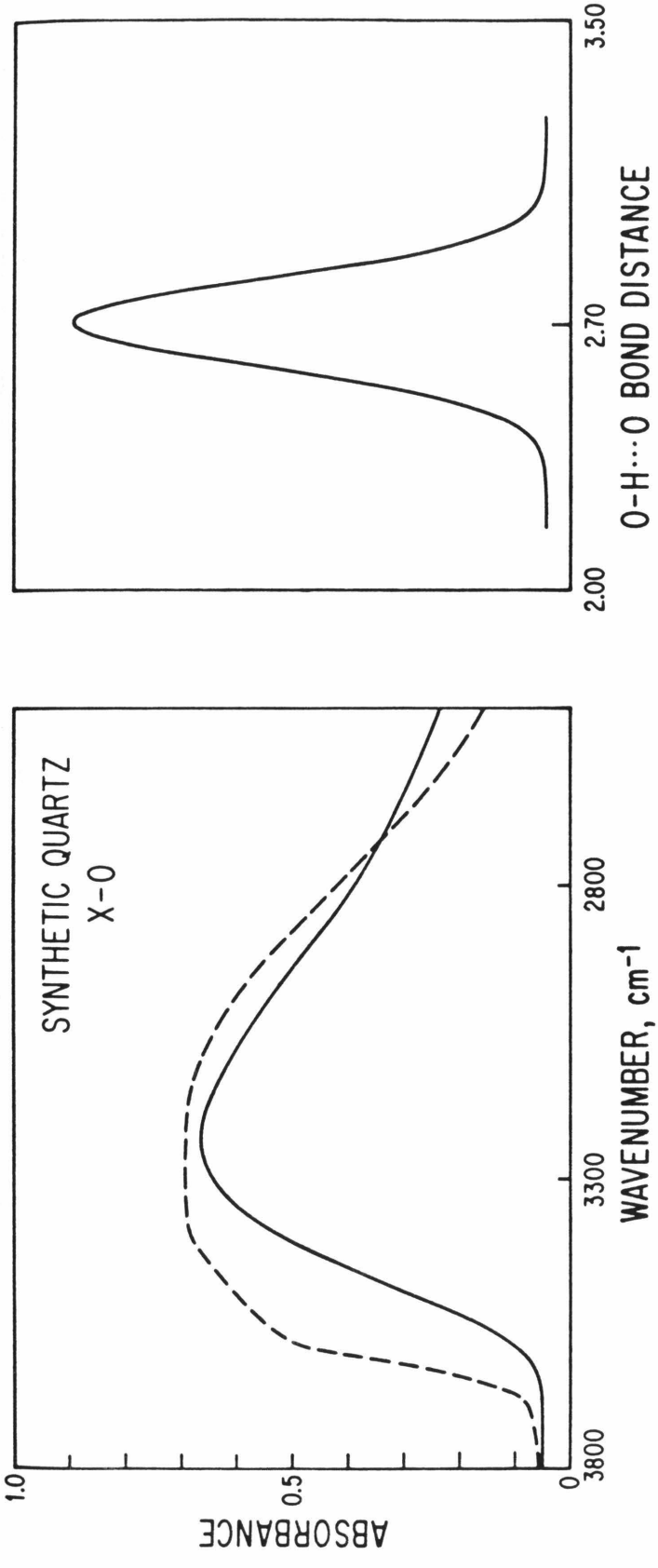
SYNTHETIC QUARTZ
X-O
ABSORBANCE
1.0
0.5
0
3800
3300
2800
WAVENUMBER, cm-1
2.00
2.70
3.50
O-H···O BOND DISTANCE

(5C)

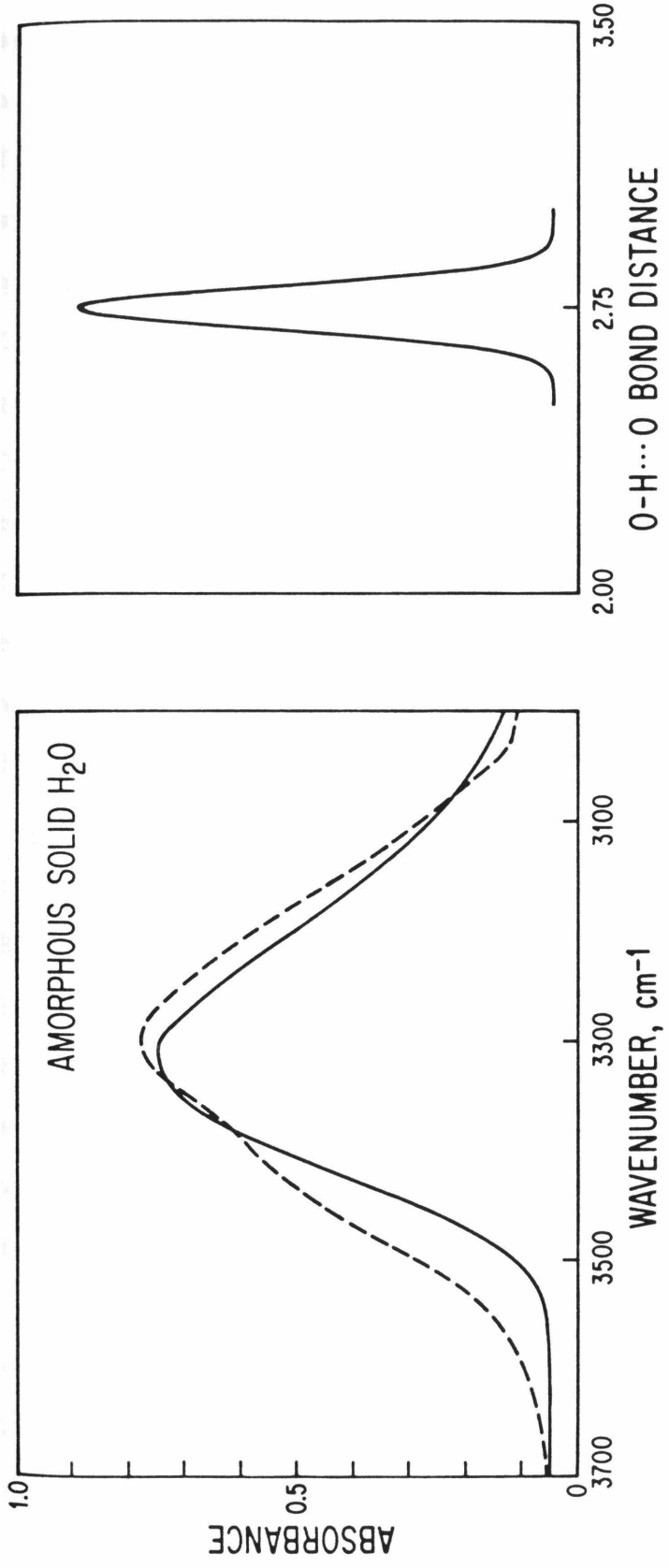
AMORPHOUS SOLID H_2O
ABSORBANCE
1.0
0.5
0
3700
3500
3300
3100
WAVENUMBER, cm^{-1}
2.00
2.75
3.50
O-H···O BOND DISTANCE

(5D)

other distributions than gaussians might provide a better fit to the spectra. In particular, it appears that synthetic quartz could be more accurately modeled with two distributions. This is a significant finding, suggesting that there are two types of O-H--O bonds in synthetic quartz. Aines et al. (1984) showed that water in synthetic quartz is contained in small groups of 5 to 100 molecules. The two O-H--O distributions may represent water molecules on the edge of such groups, and in the center, the two bond types being $O\text{-}H\text{--}O_{water}$ and $O\text{-}H\text{--}O_{silicate}$. The O-H--O distribution in metamict zircon appears to be very simple. This may be interpreted by suggesting that the OH^- groups in the metamict zircon are in charge-compensating sites at broken bonds caused by alpha particles and recoiling nuclei (Yada et al., 1981). Because of the random nature of this process, a gaussian distribution O-H--O bond lengths results in a good fit to the spectrum.

The fit to the amorphous ice spectrum is relatively good and is consistent with the O-O distances derived from diffraction work. However, the breadth of this band might more accurately be described by coupling of H_2O molecules through hydrogen bonds in a process similar to that seen in alcohols (Jakobsen et al., 1967). This process has a similar effect to the effect of thermal motion in tha the O-H potential well is changed in the same way, but the O-O distances are not affected in the same way as in my model.

The gaussian distributions used in my model are clearly not entirely meaningful since they can suggest the presence of bonds shorter than 2.4 Å, as in the examples of Figure 5. This is an indication that the gaussian distribution is not entirely appropriate. It results in my

fits having slightly larger intensities at low wavenumbers than do the actual spectra. The intensities in this region may also be high due to the assumption that Paterson's (1982) molar-absorptivity relationship is applicable to short hydrogen bonds. This relationship predicts high intensities for short O-H--O bonds, but there is evidence particularly for symmetrical bonds that the intensities can actually be extremely low. An example is the hydrogen bond in potassium hydrogen chloromaleate, which gives no infrared absorption at all (Ellison and Levy, 1965).

My model should be able to accurately predict the effects of temperature on O-H absorption frequency when the only temperature-dependent variable is O-H distance. There is not yet sufficient experimental evidence to test this. The initial results discussed in the introduction suggest that factors such as bending of O-H--O bonds, and interactions with excited low energy modes may be more commonly important than simple changes in O-O distance. Pressure effects appear to also be subject to the uncertainty of bending. Unambiguous determinations can only be made if a neutron diffraction study has been done to locate the hydrogen. However, the presently available experimental work suggests that bending can only be responsible for fairly small shifts (2-20 cm^{-1}) and that large shifts represent changes in O-O distance.

Acknowledgments

I would like to thank Jim Woodhead and Ed Stolper (Caltech) and Steve Kirby (U.S.G.S Menlo Park) for helpful discussions. Steve also provided the synthetic quartz sample. This work supported in part by NSF Grant EAR 7919987 AOI.

References

Aines, R.D., and Rossman, G.R. (1984a) Water in Minerals? A Peak in the Infrared. Journal of Geophysical Research, in press.

Aines, R.D. and Rossman, G.R. (1984b) The high temperature behavior of water and carbon dioxide in cordierite and beryl. American Mineralogist, in press.

Aines, R.D. and Rossman, G.R. (1984c) Radiation damage and water in minerals. American Mineralogist, in press.

Aines, R.D., Rossman, G.R., and Kirby, S. (1984) Hydrogen speciation in synthetic quartz. Physics and Chemistry of Minerals, in press.

Azman, A., Borstnick, B., and Hadzi, D. (1971) Intensity and width of infrared A-H stretching bands in hydrogen-bonded systems. Journal of Molecular Structure, 8, 315-318.

Couty, R., Velde, B., Besson, J.M. (1983) Raman spectra of gypsum under pressure. Physics and Chemistry of Minerals, 10, 89-93.

Detoni, S., Hadzi, D., Jurani, M. (1973) A study of proton donor-acceptor systems in the overtone region. Spectrochimica Acta, 30A, 249-253.

Ellison, R. D. and Levy, H.A. (1965) A centered hydrogen bond in potassium hydrogen chloromaleate: a neutron diffraction structure determination. Acta Crystallographica, 19, 260-268.

Hadzi, D., and Orel, B. (1973) The "OH stretching" band of acid salts of carboxylic acids and the symmetry of the hydrogen bond. Journal of Molecular Structure, 18, 227-239.

Hadzi, D., and Bratos, S. (1976) Vibrational spectroscopy of the hydrogen bond. In P. Schuster, et al. (eds.) The Hydrogen Bond, Recent Developments in Theory and Experiments, 567-611. North-Holland, Amsterdam.

Hagen, W., Tielens, A.G.G.M., and Greenberg, J.M. (1981) The infrared spectra of amorphous solid water and ice I_c between 10 and 140 K. Chemical Physics, 56, 367-379.

Jakobsen, R.J., Brasch, J.W. and Mikawa, Y. (1967) Hydrogen bonding in solids. Journal of Molecular Structure, 1, 309-321.

Janoschek, R. (1976) Calculated vibrational spectra of hydrogen bonded systems. In P. Schuster, et al. (eds.) The Hydrogen Bond, Recent Developments in Theory and Experiments, 167-216. North-Holland, Amsterdam.

Johari, G.P. and Chew, H.A.M. (1983) O-H stretching vibrations in ice clathrate. Nature, 303, 604-605.

Lascombe, J., Lasseques, J.C., and Huong, P.V. (1973) A new explanation of the infrared and raman ν(xH) band shape of hydrogen-bonded complexes. Journal of Physical Chemistry, 77, 2779-2782.

Lippincott, E.R., and Schroeder, R. (1955) One-dimensional model of the hydrogen bond. Journal of Chemical Physics, 23, 1099-1106.

Luck, W.P. (1976) The angle dependence of hydrogen bond interactions. In P. Schuster, et al. (eds.) The Hydrogen Bond, Recent Developments in Theory and Experiments, 529-562. North-Holland, Amsterdam.

Mikhailov, I.D., Saualev, V.A., Sokolov, N.D. and Bokii, N.G. (1973) Effect of deuteration on the Davydov splitting and on the shape of the absorption band of OH stretching vibrations in alcohol monocrystals. Physica Status Solidii (b), 57, 719-732.

Nakamoto, K., Margoshes, M., and Rundle, R. E. (1955) Stretching frequencies as a function of distances in hydrogen bonds. Journal of the American Chemical Society, 77, 6480-6486.

Novak, A. (1974) Hydrogen bonding in solids. Correlation of spectroscopic and crystallographic data. Structure and Bonding, 18, 177-216.

Olovsson, I. and Jönsson, P. (1976) X-ray and neutron diffraction studies of hydrogen bonded systems. In P. Schuster, et al. (eds.) The Hydrogen Bond, Recent Developments in Theory and Experiments, 395-456. North-Holland, Amsterdam.

Paterson, M.S. (1982) The determination of hydroxyl by infrared absorption in quartz, silicate glasses and similar materials. Bulletin de Minéralogie, 105, 20-29.

Pimental, G.C., and McClellan, A.L. (1960) The Hydrogen Bond. W.H. Freeman, San Francisco.

Rice, S.A., and Wood, J.L. (1973) Effect of temperature on the hydrogen bond ν_s band. Chemical Society Transactions of the Faraday Society, 69, 87-90 and 91-96.

Romanowski, H., and Sobczyk, L. (1977) A stochastic approach to the IR spectra of the symmetrical OHO hydrogen bond. Chemical Physics, 19, 361-370.

Romanowski, H., and Sobczyk, L. (1978) The temperature effect on the OH stretching vibration band of hydrogen bonded complexes. Chemical Physics Letters, 58, 73-78.

Rösch, N., and Ratner, M.A. (1974) Model for the effects of a condensed phase on the infrared spectra of hydrogen bonded systems. Journal of Chemical Physics, 61, 3344-3351.

Sandorfy, C. (1976) Anharmonicity and hydrogen bonding. In P. Schuster, et al. (eds.) The Hydrogen Bond, Recent Developments in Theory and Experiments, 616-654. North-Holland, Amsterdam.

Schroeder, R. and Lippincott, E.R. (1957) Potential function of hydrogen bonds. II. Journal of Physical Chemistry, 61, 921-928.

Van Thiel, M., Becker, E.D., and Pimental, G.C. (1957) Infrared studies of hydrogen bonding of water by the matrix isolation technique. Journal of Chemical Physics, 27, 486-490.

Velde, B. (1983) Infrared OH-stretch bands in potassic micas, talcs and saponites; influence of electronic configuration and site of charge compensation. American Mineralogist, 68, 1169-1173.

Walrafen, G.E., Abebe, M., Mauer, F.A., Blocks, S., Piermarini, G.J., and Munro, R. (1982) Raman and x-ray investigations of ice VII to 36.0 GPa. Journal of Chemical Physics, 77, 2166-2174.

Williams, J.M. (1976) Spectroscopic studies of Hydrated proton species, $H^+(H_2O)_n$, in crystalline compounds. In P. Schuster, et al. (eds.) The Hydrogen Bonds, Recent Developments in Theory and Experiments, 657-682. North-Holland, Amsterdam.

Yada, K., Tanji, T., and Sunagawa, I. (1981) Application of lattice imagery to radiation damage investigation in natural zircon. Physics and Chemistry of Minerals, 7, 47-52.

Chapter 4

The Hydrous Component in Pyralspite Garnets

(Text of article accepted for publication in

The American Mineralogist.

Coauthor George Rossman)

Abstract

Natural pyralspite garnets have been found to commonly contain a hydrous component, ranging in concentration from 0.02 to 0.25 wt% as H_2O. Anhydrous pyralspites of crustal origin are rare. Of forty crustal garnets examined, only two were anhydrous. The most-hydrous garnets were spessartines from igneous pegmatites. Metamorphic garnets had lower water contents, and frequently also contained hydrous inclusions. The infrared absorptions of the hydrous component in the garnet end members are characteristic, and consist of 2 to 4 narrow bands centered at 3640 cm^{-1} in spessartine, 3500 cm^{-1} in almandine, and 3670 cm^{-1} in pyrope. The IR spectra indicate that the hydrous component is not in the form of molecular H_2O; the most likely form is $H_4O_4^{4-}$ substituting for SiO_4^{4-} but other substitutions involving multiple OH^- groups on one site are consistent with the data. The concentration of OH (as H_2O) in garnets may be determined from the integral absorptivity (K) in the 3700-3400 cm^{-1} region, although K varies with chemistry from 3700-6000 ($\ell\ mol^{-1}_{H_2O}\ cm^{-2}$) in end members to 120-600 in intermediate compositions.

Introduction

The hydrous component found in many garnets is routinely ascribed to the hydrogarnet substitution, $H_4O_4^{4-} \rightleftarrows SiO_4^{4-}$. The characteristics of this substitution are poorly defined in natural garnets, however. This is particularly true of the pyralspite garnets, the pyrope-almandine-spessartine series. In this paper we discuss the nature and extent of the hydrous component commonly found in pyralspite garnets. In a forthcoming paper, we will discuss the grandite series. These papers address the questions of the degree to which all natural garnets may be expected to contain a hydrous component, and whether that hydrous component is the classic hydrogarnet substitution, other substitutional hydroxide, molecular water or fluid inclusions, or alteration and included hydrous phases. Previous studies have concentrated on rare garnets containing 1 % H_2O or more; we have instead concentrated on understanding the hydrous component in common garnets.

Hydrogarnets were first described by Cornu (1906) and Foshag (1920). Winchell (1933), Flint *et al.* (1941), Pabst (1937, 1942), and Belyankin and Petrov (1941) brought understanding of the natural hydrogarnets to the point where it was realized that the $H_4O_4^{4-} \rightleftarrows SiO_4^{4-}$ substitution accounted for the chemistries of hydrous grandites known at that time. Modern research has focused almost exclusively on synthetic hydrogrossular. A series of papers by Cohen-Addad and co-workers proved, using neutron diffraction and other techniques, that in several synthetic compounds including hydrogrossular there are, in fact, tetrahedral groups of $4OH^-$ replacing the SiO_4^{4-} tetrahedron (Cohen-Addad *et al.*, 1964, 1967; Cohen-Addad 1968, 1969). These results were

confirmed by Foreman (1968). There are, however, no direct determinations of the H_4O_4 tetrahedral grouping in natural garnets. The proton positions in hydrogarnet type substitutions have only been verified by neutron diffraction in natural materials in henritermierite (Aubry et al., 1969), and by X-ray diffraction in bicchulite (Sahl, 1980) and zunyite (Baumer, et al., 1974).

The pyralspite series is not well known for containing a hydrous component. Ackermann et al. (1983) describe the synthesis of hydrous pyropes, which they assume contain the hydrogarnet substitution. Wilkins and Sabine (1973) reported that two spessartines from Sterling Hill, New Jersey, contained up to 2.5 wt% H_2O. Hsu (1980) synthesized hydrospessartine, but the garnets were reported to be metastable.

In this paper we discuss the extent to which natural pyralspite garnets contain a hydrous component, and the evidence for the speciation of that component. The hydrogarnet substitution ($H_4O_4^{4-} \rightleftarrows SiO_4^{4-}$), or other substitutional hydroxides would constitute a structural hydrous component. They are part of the crystal structure and their properties are linked to those of the basic garnet structure. Other forms for a hydrous component are basically inclusions of a foreign phase: fluid inclusions, alteration, or included hydrous phases. Regardless of the actual speciation, we report the content of hydrous component as H_2O because that is the species actually measured by our analytical methods. We have tabulated the total amounts of H_2O present in pyralspites from a variety of occurrences and localities, and determined calibrations for structural H_2O content in pyralspites. The major tool used in this study was infrared (IR) spectroscopy, because of its

sensitivity to the O-H bond. The use of IR spectroscopy to determine the speciation of trace hydrous components in minerals is discussed in Aines and Rossman, (1983). Water contents were obtained from infrared integral absorptivity, calibrated by thermogravimetry, P_2O_5 cell coulometry, and H_2 gas manometry.

Methods

Infrared spectra were obtained on doubly polished, single crystal slabs of garnet, using techniques described by Goldman et al., 1977. A Perkin-Elmer model 180 grating infrared spectrometer was used for both room temperature and cryogenic measurements. Near infrared (NIR) measurements were obtained using a Cary 17I grating spectrometer. IR spectra were recorded digitally using an interface with a DEC MINC-11 computer. These spectra were corrected for baseline and then used to determine integrated areas under absorption bands.

Water contents were calculated by calibrating the integrated IR intensities against the water content measured with a DuPont moisture evolution analyzer (MEA). Reagent grade $Mg(OH)_2$ was used as a standard material; its water content was calibrated using thermogravimetry. The carrier gas used was N_2 or 99% N_2:1% O_2 for samples containing ferrous iron. In these samples it is possible for H_2O to oxidize the iron, evolving H_2 gas which is not detected by the cell. The oxygen gas is added to react with H_2 to regenerate H_2O prior to reaching the electrolytic cell.

100 to 200 mg of coarsely powdered garnet was used for MEA analysis. Samples were held at 110°C until no more moisture was

measurable, then heated at ~500°/minute to 1000°C. The moisture evolved was taken as the water content of the garnets. The blank for this technique is 30 ±10 μg H_2O, as determined from empty boat runs, and runs using identically prepared anhydrous garnet. The precision is approximately 5% of the measurement (exclusive of the error in the blank) as measured using the $Mg(OH)_2$ standard. The primary errors in this measurement are due to adsorbed water on furnace walls and tightly bound water on particle surfaces that was added during grinding. The water added during grinding ranged up to 0.04 wt%. It was kept below 0.02% for the analyses reported here by thoroughly drying the mortar and pestle in a vacuum oven at 160°C and by not overgrinding the samples. The average particle size was 25 μm.

Water contents were also estimated by thermal gravimetric analysis using a Mettler TA2000 TGA system. The lower detection limit is ~100 μg with a precision of approximately ±50 μg. Up to 100 mg of powdered sample was used per run. The primary error in this measurement is due to bouyancy changes in the sample during the course of the run, which is made with constant flow of N_2 gas. Measurements were made up to 1200°C.

Samples 13 and 49 were analyzed by gas volumetric methods. 500 mg of the powdered samples were heated to 1400° and the evolved gas was converted to H_2, then measured manometrically. This analysis was performed in James O'Neil's laboratory at the U.S.G.S., Menlo Park, California, facility.

Major element analyses were performed using the Caltech MAC5 automated microprobe, with data reduction methods described by Bence and Albee (1968) and the alpha factors of Albee and Ray (1970). A pyrope

collected by T. McGetchin from the Moses Rock diatreme, Utah, was used as a secondary standard (Champion et al. 1975). This garnet is homogeneous and has been extensively used as a microprobe secondary standard. It is included in Table 1, Sample #110. In no instance was there sufficient H_2O in these garnets for the microprobe analyses to be significantly silica deficient.

Samples

A total of 75 pyralspite garnets were surveyed for the presence of a hydrous component. A summary of the localities and occurrences of samples that were analyzed in detail is given in Table 1. The garnets were museum specimens, and details of associated phases can not be obtained directly. Table 1 contains references to the detailed petrology of the localities, where available. Only representative samples from several diatreme and kimberlite localities are listed in Table 1. A more complete discussion of the hydrous mantle garnets encountered during the course of this project will be published later. Samples were chosen to represent the common range of natural chemistries of pyralspite garnets, to represent the common occurrences, and to be of sufficient size (and lacking inclusions) for accurate analysis.

The necessary size of gemmy material is approximately 250 μm in diameter by 1 mm in thickness for spectroscopic analysis. More material is required for the analytical techniques used for H_2O concentration. Accordingly, analytical results on large samples were used to calibrated the infrared integral absorptivity so that water contents could be measured on extremely small samples. The effects of

Table 1. Localities and Occurrences of Garnets Used in This Study.

Sample Number	Locality	Type	Occurrence, Comments	Caltech Number	Reference
2	Minas Gerais, Brazil	Spess	Igneous pegmatite	7765	
4	Rutherford #2, Amelia, Va	Spess	Igneous pegmatite	6725	Sinkankas, 1968
5	Rutherford #2, Amelia, Va	Alm-Spess	Igneous pegmatite	6725	Sinkankas, 1968
10	Tanzania	Spess-Alm		15001	
11	Unknown, East Africa (?)	Py-Alm		15002	
12	Minas Gerais, Brazil	Spess-Alm	Igneous pegmatite (?)	15003	
13	Asbestos, Quebec	Gross	Altered ultramafic body	15004	Grice & Williams, 1979
19	Franklin, N. Jersey	Gross-Spess		N.M.N.H.#11318*	Frondel, 1972
21	Unknown	Py-Alm		15005	
22	Brazil	Alm-Spess		15006	
23	Wrangell, Alaska	Alm	Metamorphic, schist	15007	Sinkankas, 1976
27	Spruce Pine, N. Car.	Spess-Alm	Igneous pegmatite. Zoned.	1738	Parker, 1952
28			Other zones in Sample 27;		
29			27 rim, 28 middle, 29 core		
32	Rincon, Calif.	Spess-Alm	Igneous pegmatite	15008	Jahns & Wright, 1951
33	Mt. San Jacinto, Calif.	Alm	Xenolith in tonalite	9968	Hill, 1984
34	Ugelvik, Norway	Py	Ultramafic body	15009	Carswell, 1968
35	Gore Mt. New York	Alm-Pyr	Metamorphic gneiss	15010	Levin, 1950
49	Green Knobs, N. Mex.	Py	Diatreme megacryst	15011	Smith & Levy, 1976
55	Anakapelle, India	Py-Alm	Metamorphic, granulite	Ed Grew #3080L	Grew, 1982
56	Casey Bay, Antarctica	Py-Alm	Metamorphic, granulite	Ed Grew #2434E	Grew, 1981
57	North River, N. York	Py-Alm	Metamorphic, granulite	10244	Levin, 1950
61	Garnet Ridge, Ariz.	Py-Alm	Diatreme megacryst	15013	Hunter & Smith, 1981; Swizter, 1977
64	Garnet Ridge, Ariz.	Py	Diatreme megacryst	15013	Hunter & Smith, 1981; Switzer, 1977
65	Garnet Ridge, Ariz.	Py-Alm	Diatreme megacryst	15013	Hunter & Smith, 1981; Switzer, 1977
78	Minas Gerais, Brazil	Spess	Igneous pegmatite (?)	15014	
89	Wesselton Mine, S. Afr.	Py	Kimberlite megacryst	Harvard #12528	
95	Roberts Victor Mine, South Africa	Gross-Py	Kyanite bearing eclogite nodule	N.M.N.H.#87375	
104	Rock Mica Mine, Yancy Co., N. Car.	Alm-Spess	Igneous pegmatite	1731	Parker, 1952
105	Broken Hill, Australia	Alm-Spess		11826	
110	Moses Rock, Utah	Py	Diatreme megacryst	15016	McGetchin & Silver, 1972
111	Chanthaburi, Thailand	Alm-Py	Nodules in alkali basalt	9964	
112	Podsedice, Czech.	Py		15017	Hintze, 1897, p. 63
113	Garnet Ridge, Ariz.	Py	Diatreme	15013	Hunter & Smith, 1981; Switzer, 1977
114	Garnet Ridge, Ariz.	Py	Diatreme	15013	Hunter & Smith, 1981; Switzer, 1977
118	St. Lawrence, N.York	Alm	Metamorphic, granulite	15012	Levin, 1950

*National Museum of Natural History.

inclusions on spectroscopic results were determined by studying samples which contained zones of high and low inclusion content.
All samples were doubly polished for IR analysis, and the same sample was then analyzed by microprobe utilizing the existing polished surface.

Results

Forty pyralspite garnets of crustal origin were studied; all but two were hydrous, as indicated by the presence of absorption bands in the 3400 to 3700 cm^{-1} region. Peaks in this region are typical of O-H stretching absorptions (e.g. Aines and Rossman, 1983). Typical "water" contents are 0.1 wt %, ranging up to 0.25 wt %. This hydrous component is structural, not due to inclusions or alteration which may considerably increase the apparent water content. Pyralspites of mantle origin are also frequently hydrous.

Figures 1 and 2 show the major element chemistry of the garnets studied, and the integrated IR absorptivity due to structural hydrous component. Water contents may be calculated from integrated IR absorption as shown in the scale bar in Figure 1 which was calibrated using MEA and TG results. Only the concentration of structural hydrous component is shown in Figures 1 and 2. Some samples also contained hydrous inclusions or were altered and the relative amount of water held in structural versus non-structural site could not be determined. These are shown as squares containing a cross in Figures 1 and 2. Samples that were badly altered, largely metamorphic garnets, are not included in these figures. The pyrope-almandine and spessartine-almandine series

Figure 1. (Next page) Chemistries and "water" contents of pyrope-almandine garnets studied. Cation contents are plotted as mole %. None of the garnets deviate significantly from $M_3^{2+}Al_2Si_3O_{12}$, M = Ca,Mg,Fe. The vertical axis is integral infrared absorbance in the region 3750 to 3400 cm^{-1}, which is related to water content as shown in the scale and in Table 2. Squares with no vertical extension and which are filled with a cross represent samples that were too badly altered to determine the content of structural hydrous component, even though the IR pattern indicated that one was present. Sample numbers refer to Table 1.

1)

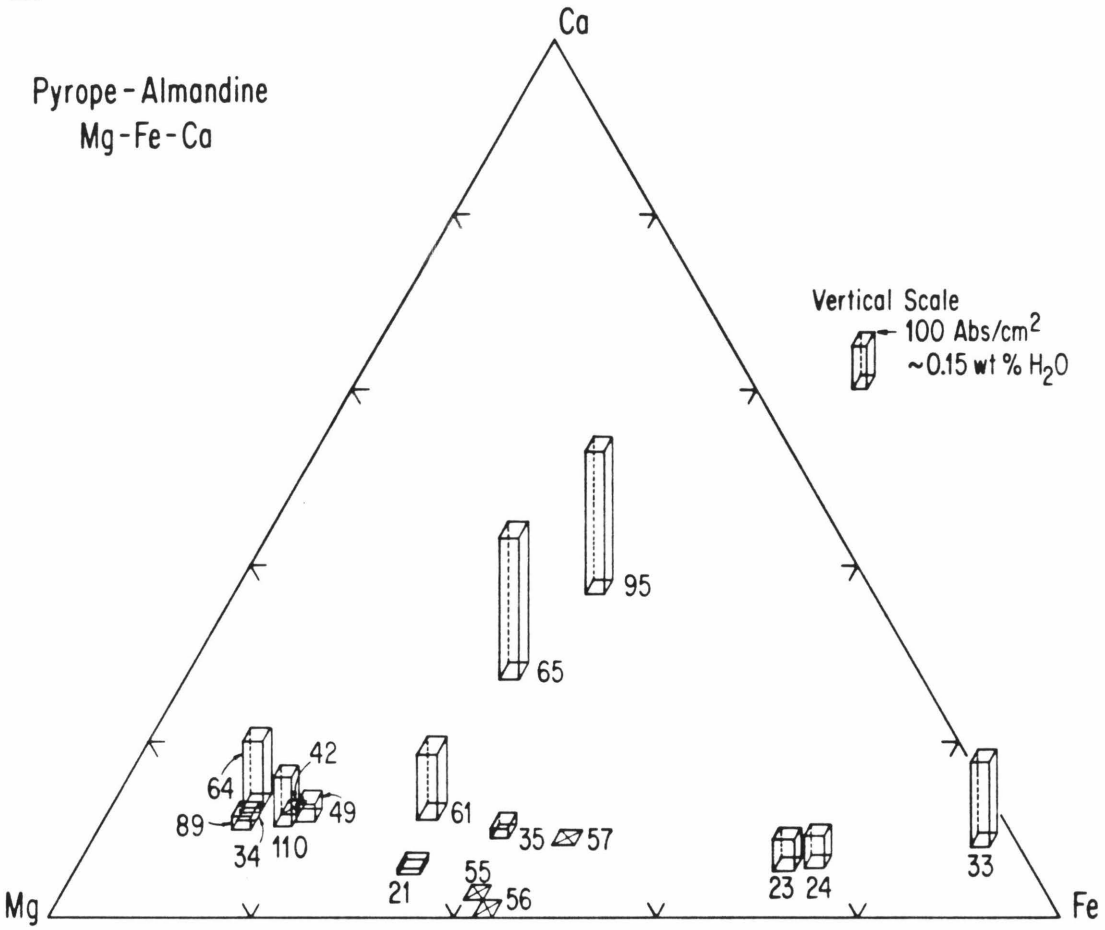
Ca
Pyrope - Almandine
Mg - Fe - Ca
Vertical Scale
100 Abs/cm²
~0.15 wt % H₂O
95
65
42
64
89
34
110
49
61
35
57
21
55
56
23
24
33
Mg
Fe

Figure 2. (Next page) Chemistries and "water" contents of spessartine-almandine garnets studied. Same scale as Figure 1. None of these samples differs significantly from $M_3^{2+}Al_2Si_3O_{12}$, M = Mn,Fe,Ca. Vertical extension has not been shown for samples 4 and 13, which have very large integral absorbances due to the large molar absorptivity of these end member garnets; their water contents are similar to those of the other samples (see Table 2).

2)

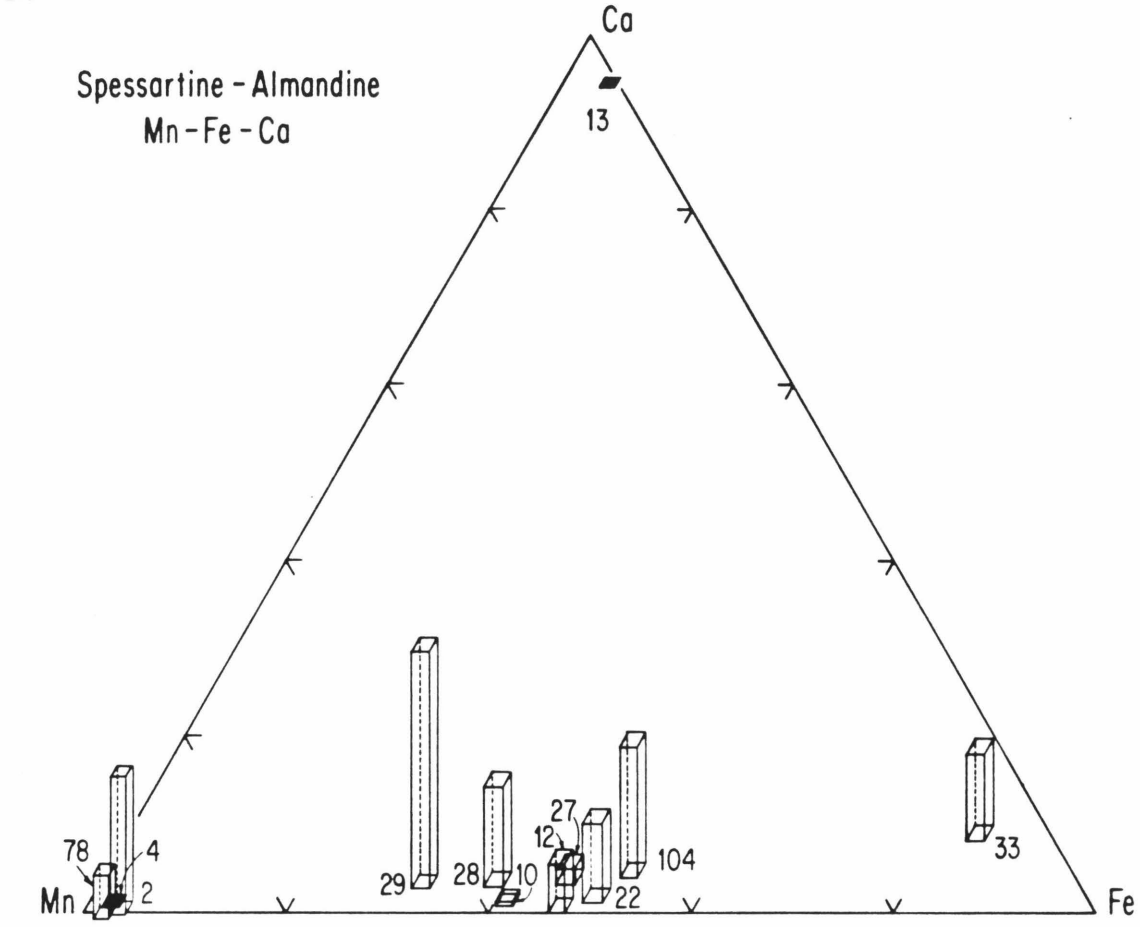
Spessartine - Almandine
Mn - Fe - Ca
Ca
13
Mn
Fe
78
4
2
29
28
10
27
12
22
104
33

are plotted against grossular because most pyralspites contain some calcium. In many respects it is appropriate to consider the octahedral Al^{3+} garnets (pyrope, almandine, spessartine, grossular) as a single group. One representative end-member grossular is included in Table 1. A discussion of the grossular-andradite series is in preparation.

"Water" Contents

Figures 1 and 2 show the content of hydrous component in the garnets studied in terms of integrated infrared absorption measured from 3750 cm^{-1} to 3400 cm^{-1}. This method of measuring the hydrous component is very sensitive, limited only by the sample thickness available, but must be calibrated by another method in order to obtain absolute "H_2O" concentrations. The primary calibration method used was P_2O_5 cell coulometry using the moisture evolution analyzer. Table 2 shows the results of MEA calibration of the IR integrated absorbance. Samples listed here were analyzed first by IR, then ground for MEA. The strong zoning present in some samples (for example up to a factor of 10 for points separated by 4 mm in sample numbers 27-29) required that the identical area used for IR be powdered for MEA.

The result of primary interest in Table 2 is the large variation in integral molar absorptivity seen between end-member and intermediate chemistry garnets. Spessartine and grossular have a molar absorptivity (K) of around 5000 to 6000 (ℓ $mole^{-1}$ cm^{-2}) while the spessartine-almandines and pyrope-almandines have absorptivities of 200 to 500. Some of the variability seen in Table 2 may be ascribed to analytical error. Major sources of error include alteration in the sample and

Table 2. Integral Molar Extinction Coefficients

Sample Number	H_2O* (wt %)	K# (liter $mol^{-1} cm^{-2}$)	Composition (mole %)
2	0.084 ±.04	3700	Mn_{97}
4 ##	0.25 ±.01	5900	Mn_{97}
5	0.36 ±.02	5820	Mn_{95}
10	0.059 ±.03	116	$Mn_{60}Fe_{40}$
12 ##	0.17 ±.02	620	$Mn_{55}Fe_{45}$
13 ##	0.18 ±.01 **	8000	Ca_{97}
35	0.06 ±.01	180	$Mg_{45}Fe_{55}$
49	0.08 ±.02 **	260	$Mg_{75}Fe_{25}$
104	0.27 ±.02	1103	$Mn_{45}Fe_{55}$
113 ##	0.15 ±.03	340	$Mg_{75}Fe_{25}$
114	0.22 ±.03	320	$Mg_{75}Fe_{25}$

* Determined by MEA analysis. Errors based on duplicate measurements and known error in MEA measurement which is largely a function of the amount of sample available.

** Determined by H_2 gas volume. For Sample 13, MEA gave identical results. No MEA available for Sample 49.

\# Determined from integral absorption from 3750 to 3400 cm^{-1}.

These samples were checked for complete dehydration at 1000°C by heating a slab in air for four hours. All lost at least 95 % of their original IR intensity.

surface hydroxyl which forms during grinding even in a low humidity atmosphere. This averaged 0.02 to 0.04 wt%. These problems may account for the variability among each group, but the extreme difference between the end-members and intermediate chemistries is considerably larger than any possible error.

Two of the samples in Table 2 were analyzed by the H_2 gas volume technique. Sample 49 was not analyzed by MEA because of small sample size. Sample 13 was analyzed by both techniques and both gave identical results within error: MEA (two analyses) 0.18% (±0.01); H_2 gas 0.17% (±0.02). Sample 13 is from the same locality as the material used by Westrum, et al. (1979) in a study of the thermophysical properties of grossular. They obtained a water content of 0.19 wt%. Several samples were also measured using thermogravimetry. The errors due to buoyancy for small samples were considerably larger than the corrected weight losses, and all samples studied in this way gave considerably greater weight losses than indicated by MEA. Sample 13, for instance, lost 0.53 wt% from 100 to 1100°C. The sample weighed 112 mg. Considerably larger samples are required for accurate TG work, and no single sample was large enough. An average sample of 500 purple and red garnets from the Garnet Ridge, Arizona, diatreme was ground and sieved to pass 200 mesh but not pass 325 mesh. In this way a 1-gram sample was available for TG, and it yielded a weight loss of 0.14%. The same sample gave an MEA result of 0.12%, confirming that the values in Table 2 are not artifacts of small sample size. Individual garnets from the same locality yielded from 0 to 0.22 wt% H_2O by MEA, in accord with their integrated IR absorbances (Table 2).

The complete dehydration of the garnets measured by MEA was verified in four cases (Table 2) by heating a doubly polished slab at 1000°C for four hours. All four showed greater than a 95% loss of integrated intensity in the infrared spectrum of the O-H region after this treatment, indicating that the MEA analysis at 1000°C is valid. TG curves for single samples and the 500-stone average Garnet Ridge sample show continuous weight loss from 200° to 1000° when heated at 5°C/min. The structural hydrous component in pyralspites is not stable to very high temperatures, if at all, at P_{tot} = 1 bar.

Infrared Analysis

IR spectroscopy was used to determine the nature of the hydrous component, if present, and to calculate the total water content from the integral absorption intensity.

End-Members. The IR absorption patterns for typical end-members of the octahedral Al^{3+} garnets are shown in Figure 3. Only the grossular and spessartine are true end-members. The pyrope and almandine both contain ~20 mol% of almandine and pyrope component, respectively. The examples shown in Figure 3 are all gemmy crystals with no hydrous inclusions or alteration.

Two important results of the infrared analysis of pyralspites are exhibited in Figure 3. (1) End member patterns are composed of multiple absorption peaks. (2) The location of the center of the multiple peaks varies with the chemistry. The grossular and spessartine end-member patterns are best known since multiple examples of them were available. All end-member grossulars and spessartines studied have IR spectra similar to those in Figure 3. The multiple peaks in almandine

Figure 3. (Next page) Typical single crystal infrared spectra of end-member pyralspite garnets obtained at -196°C. From bottom to top: grossular, sample 13, 0.14 mm thick; spessartine, sample 4, 0.06 mm thick; almandine, sample 23, plotted as 11.0 mm thick; pyrope, sample 49, plotted as 10.0 mm thick. End-member hydrous garnets of these chemistries always give IR patterns like these with the exception of the peaks shown here of absorbance less than 0.2, which are not reproducible and are due to inclusions or alteration. These spectra have been corrected for a sloping baseline due to an Fe^{2+} electronic absorption at 4200 cm^{-1}, with the exception of the pyrope which is uncorrected to show the baseline. In the absence of a hydrous component, all garnets are featureless in the 3700-3400 cm^{-1} region.

3)

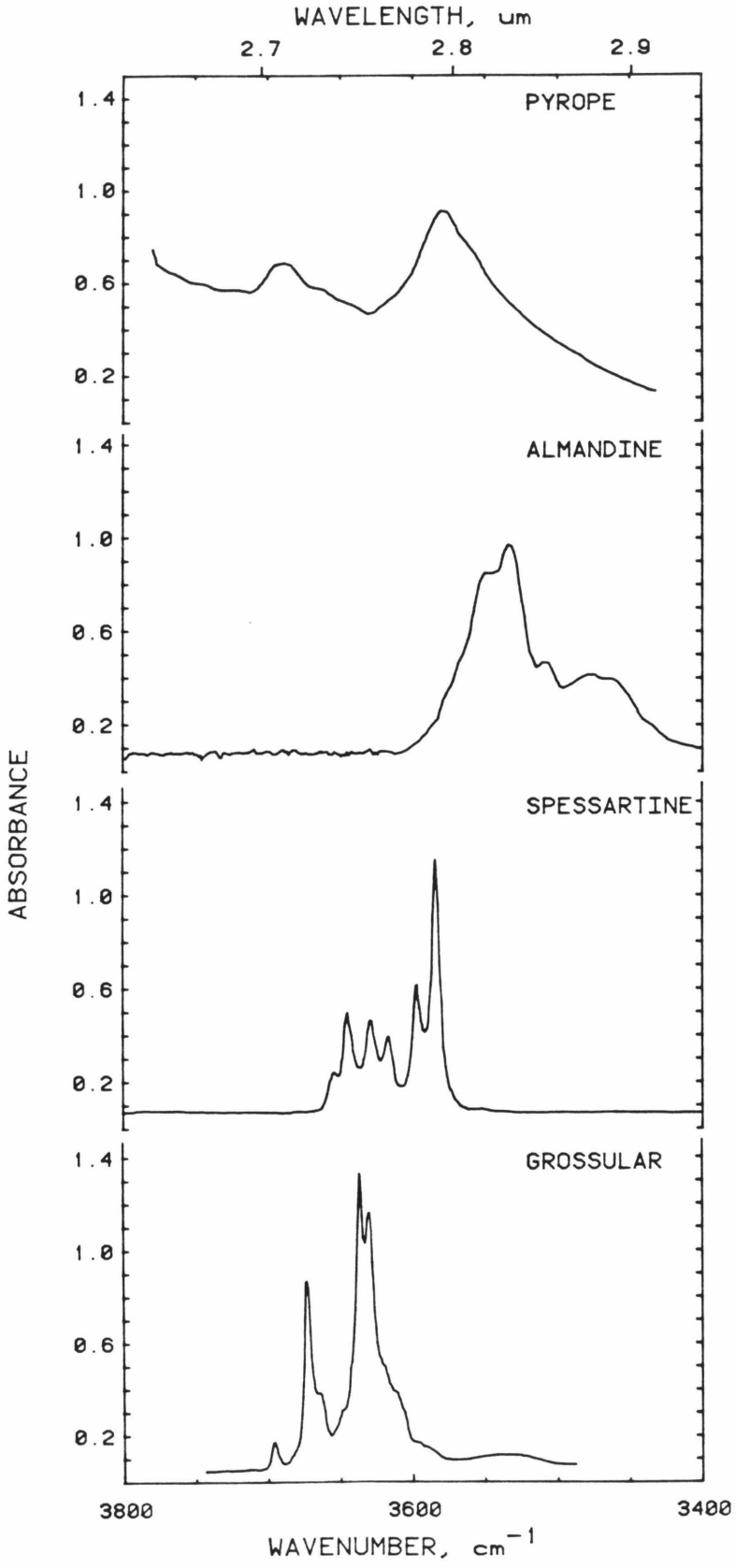
WAVELENGTH, um
2.7
2.8
2.9
PYROPE
ALMANDINE
SPESSARTINE
GROSSULAR
ABSORBANCE
1.4
1.0
0.6
0.2
3800
3600
3400
WAVENUMBER, cm⁻¹

are not as well-resolved as those in grossular and spessartine. All pyropic garnets studied have patterns similar to that seen in Figure 3, but as discussed below this is probably not an end-member spectrum. The end-member pyrope pattern is not well determined because of the absence of stoichiometric pyropes in nature and the low water content of common Mg^{2+}-rich garnets.

The spectra shown in Figure 3 were obtained at -196°C to enhance the separation between peaks. At room temperature the spectra differ only in appearing less well resolved; all the peaks may be identified but may occur as shoulders rather than distinct peaks. The spectra in Figure 3, as well as the other spectra in this paper, have been corrected to remove the effects of a broad Fe^{2+} absorption centered at 4240 cm^{-1}. The Fe^{2+} absorption produces a strongly sloping background which was removed using a scaled baseline obtained from a rigorously anhydrous garnet, sample #111.

The consistent nature of the IR spectra of the end-member pyralspites is striking. No exceptions to this behavior were observed in this study; if end-member garnets were hydrous, they gave the IR spectra seen in Figure 3. This is strong evidence that the absorption pattern is intrinsic to garnet rather than from an alteration product or included phase. In other words, there is a structural hydrous component in natural pyralspites.

Alteration. Many pyralspites contain a hydrous component that is clearly not structural and, in fact, is not part of the garnet but rather part of an included phase. Water of this type may be recognized by two methods. (1) In garnets with varying concentrations of inclusions or altered regions, any component of the IR spectrum that

changes from region to region in the same manner as the inclusion concentration is assumed to be due to the alteration or included phases. (2) Any component of the IR spectrum of a garnet that is inconsistent with the spectra expected for a garnet of that chemistry is assumed to be due to alteration. Criterion (2) could only be applied after many garnets were studied and the patterns of spectral behavior were established.

Figure 4 shows how these criteria are applied to two actual cases. The top two spectra are of an almandine from Wrangell, Alaska. The upper trace is in a region of many inclusions, some of which appear to be chlorite, based on microprobe analysis. The lower spectrum is of an inclusion-free, gemmy region of the crystal. Identical spectra are obtained in all inclusion-free portions of this crystal. The intrinsic, structural hydrous component in this garnet gives rise to the peak at 3550 cm^{-1}, a peak seen in other almandines, while the higher wavenumber peaks are due to included hydrous phases. The lowermost spectrum in Figure 4 is of a spessartine-almandine garnet in which there is incipient alteration. The extremely broad band (~400 cm^{-1} in width) seen underlying the sharper peaks is characteristic of incipient alteration in which crystallites have not yet formed. It is similar to the spectra seen for fluid inclusions (Aines and Rossman, 1983). This garnet has obvious cloudy zones of alteration extending several hundred micrometers inward from large cracks.

Intermediate Chemistries. The spectral patterns of the intermediate composition pyralspites are more complex than those of the end-members. Once alteration and included phases are removed from consideration, two common factors are seen in the behavior of the

Figure 4. (Next page) Example of two altered almandine garnets showing the spectral features which allow alteration and inclusions to be distinguished from a structural hydrous component. The upper two traces are both from a single crystal of sample 23. The uppermost trace shows a region of inclusions, the lower trace a gemmy area which gives a typical pattern for almandine structural hydrous component. The peaks in the upper trace in the 3700-3600 cm^{-1} region are due to the inclusions or alteration. The sample is plotted as 3.8 mm thick. The lowermost trace shows a 0.7 mm thick almandine from a crustal eclogite, sample 118. The extremely broad band underlying the sharp peaks is characteristic of incipient alteration. It extends to 3000 cm^{-1}. All three of these spectra have a sharp peak at 3625 cm^{-1} which is the characteristic O-H stretching frequency of muscovite, and may be attributed to muscovite inclusions.

4)

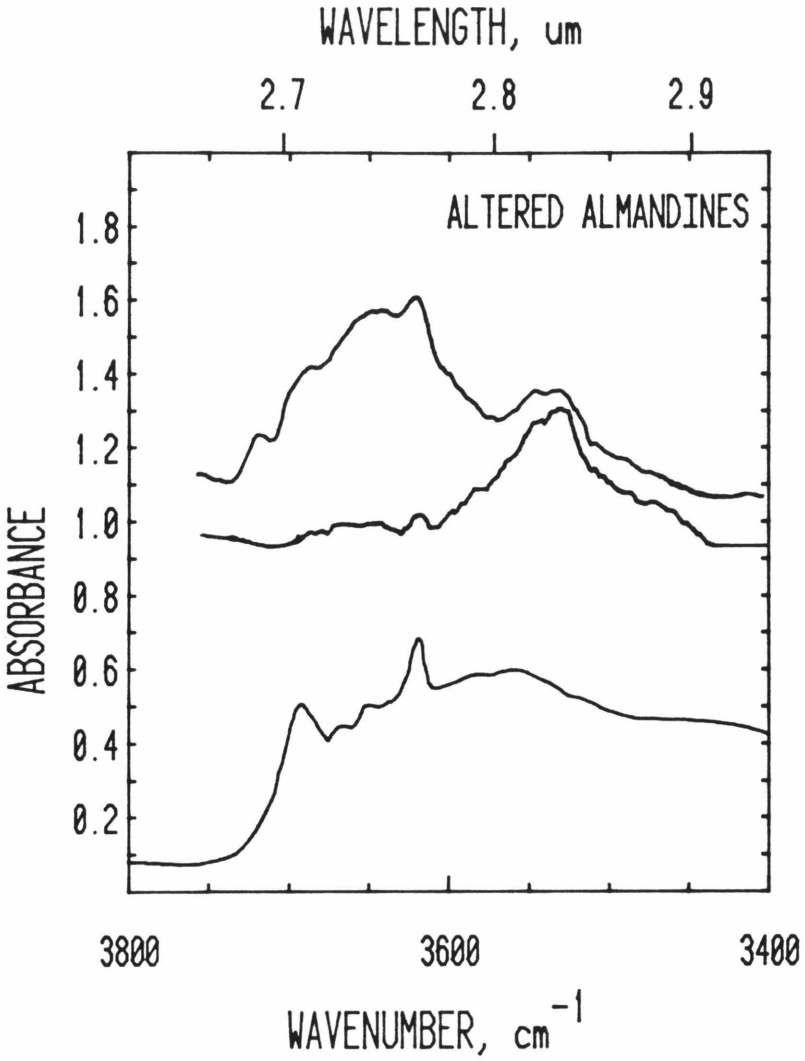
WAVELENGTH, um
2.7
2.8
2.9
ALTERED ALMANDINES
1.8
1.6
1.4
1.2
1.0
0.8
0.6
0.4
0.2
ABSORBANCE
3800
3600
3400
WAVENUMBER, cm-1

intermediate garnets. (1) Multiple peaks occur, and (2) sharp bands of the sort seen in Figure 3 do not occur. The sharpest peaks seen in end-member spessartine are ~10 cm^{-1} in width (at half height) while the sharpest bands seen in intermediate compositions are 40-50 cm^{-1} wide, as broad as the entire set of sharp bands seen in the end-members.

Figure 5 shows the infrared spectra of typical members of the spessartine-almandine series. The chemistries of these samples are shown in Figure 2. Although the spectra of the intermediate compositions are complex, they appear to be simple combinations of the end-member patterns. The broad bands of the intermediate compositions appear to be averaged versions of the multiple sharp bands seen in the end-members as, for instance, the two most spessartine-rich samples at the top of Figure 5.

Despite a consistency of spectral behavior in the Mn^{2+}-Fe^{2+} series, the transition between spectral patterns is not entirely a smooth function of chemistry. Mn^{2+}-rich samples are always dominated by the bands at ~3640 cm^{-1} and ~3600 cm^{-1}, and Fe^{2+} garnets are dominated by the bands at ~3470 cm^{-1} and ~3540 cm^{-1}. However, as seen in the Mn^{2+}-rich samples of Figure 5 (the top two), the relative intensities of the 3640 cm^{-1} and 3600 cm^{-1} bands may vary widely. This behavior is also seen for the Fe^{2+}-related peaks at ~3470 cm^{-1} and 3540 cm^{-1}. Several spessartines of near end-member chemistry contain minor peaks in the region observed for Fe^{2+}-related peaks. (These samples contain lamellar bands, ~200 μm across, that are slightly more brown than the bulk sample.) The consistent peak locations and slightly variable peak intensities suggest that there is a structural hydrous substitution present, but that factors other than the bulk chemistry may control the

Figure 5. (Next page) Infrared spectra of typical members of the spessartine-almandine series showing the progression of spectral patterns at intermediate chemistries. From bottom to top: sample 23, plotted as 5.5 mm; sample 104, plotted as 1.8 mm; sample 27, plotted as 13 mm; sample 29, plotted as 0.7 mm; sample 5, 0.06 mm thick, and sample 4, 0.06 mm thick. All spectra recorded at -196°C.

5)

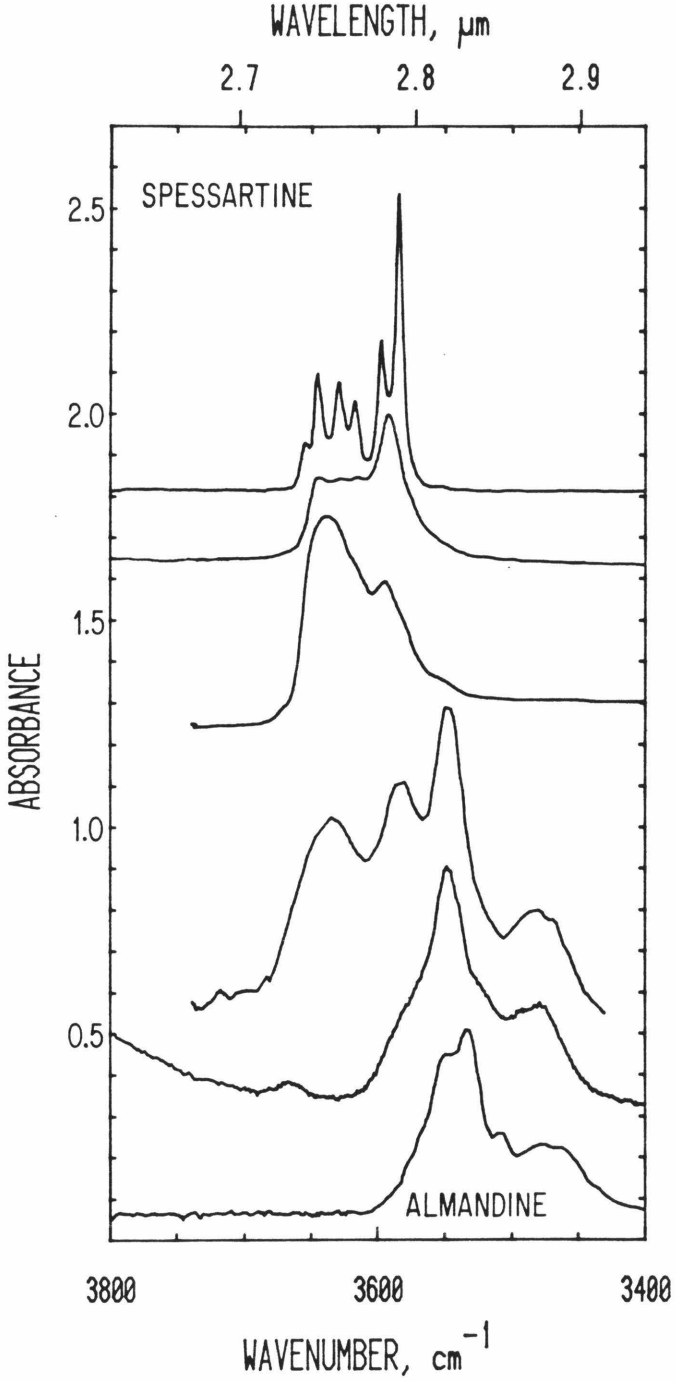
WAVELENGTH, μm
2.7
2.8
2.9
SPESSARTINE
2.5
2.0
1.5
1.0
0.5
ABSORBANCE
ALMANDINE
3800
3600
3400
WAVENUMBER, cm-1

extent or structure of the substitution.

Similar behavior is seen in the Mg^{2+}-Fe^{2+} series (Fig. 6) but the smooth progression of spectral pattern with chemistry seen in Figure 5 is not present. Again, there are four fundamental bands, and the high wavenumber pair at ~3660 cm^{-1} and 3560 cm^{-1} are associated with Mg^{2+}-rich garnets, and the low wavenumber pair at 3470 cm^{-1} and 3540 cm^{-1} are associated with Fe^{2+}-rich garnets. At the intermediate chemistries (middle trace of Fig. 6), however, the highest and lowest wavenumber bands are greatly diminished in intensity. The IR pattern is dominated by a band that appears to be a combination of the 3560 cm^{-1} and 3540 cm^{-1} bands.

Near Infrared Spectroscopy. The 5200 cm^{-1} overtone band of molecular water allows one to distinguish between molecular H_2O and OH^- ions . This band arises from combined bending and stretching, and cannot occur for OH^- ion (e.g. Aines and Rossman, 1983). Figure 7 shows the near infrared (NIR) spectrum of a hydrous spessartine. Superimposed upon three broad bands (~1000 cm^{-1} wide) are a number of sharp bands (~20 cm^{-1} wide). The broad bands are electronic transitions of Fe^{2+}. The sharp bands are overtone and combination modes related to the fundamental O-H modes seen at ~3600 cm^{-1} (Fig. 5). None occur at ~5200 cm^{-1}, the diagnostic H_2O frequency. All the O-H is in the form of OH^- ions. The NIR region is difficult to study in detail because of very low intensities in the hydrous pyralspites, but no band at ~5200 cm^{-1} has been seen.

Figure 6. Infrared spectra of typical members of the pyrope-almandine series showing the progression of spectral pattern with chemistry. From bottom to top: sample 23, plotted as 15 mm; sample 21, plotted as 20 mm; sample 49, plotted as 9.5 mm thick. Spectra recorded at -196°C.

6)

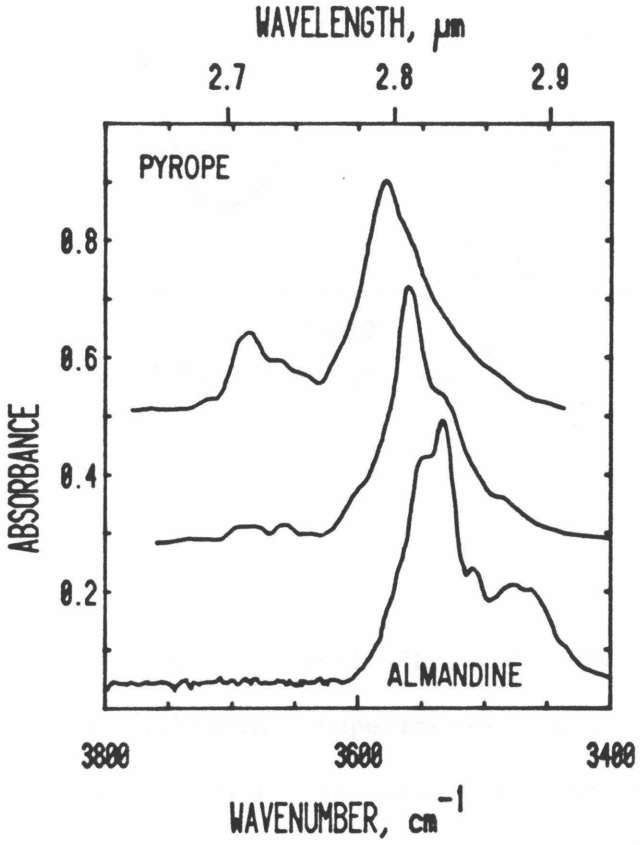
WAVELENGTH, μm
2.7
2.8
2.9
PYROPE
0.8
0.6
0.4
0.2
ABSORBANCE
ALMANDINE
3800
3600
3400
WAVENUMBER, cm-1

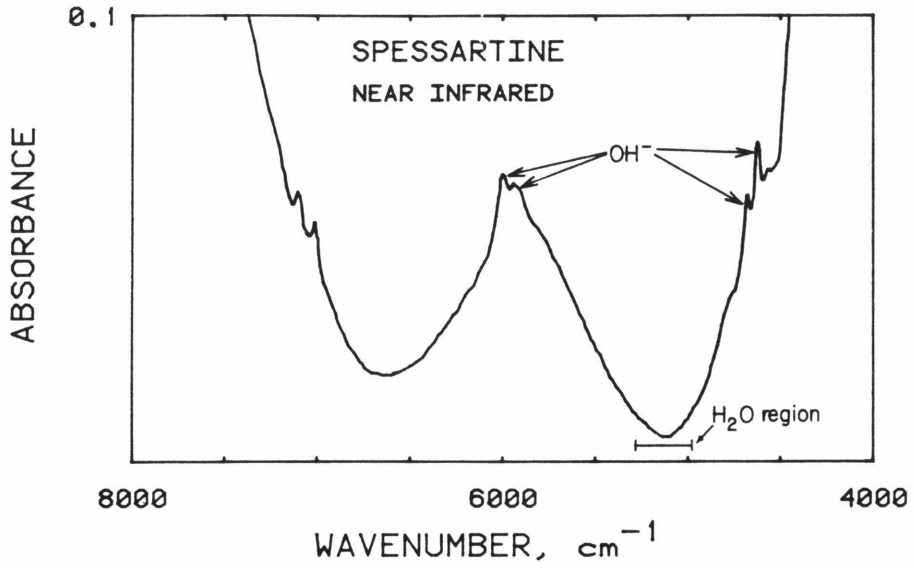

Figure 7. Near-infrared spectrum of sample 78 showing the sharp overtone absorptions of O-H vibrations superimposed upon the extremely broad absorptions of trace Fe^{2+} in the sample, which occur at 7900, 5900 and 4200 cm^{-1}. The overtone O-H absorptions occur at 7000, 6000, and 4600-4000 cm^{-1}. No O-H absorption peaks occur in the 5200 cm^{-1} region, indicating that there is no molecular water present.

Discussion

Structure of the Hydrous Defect

The pyralspite garnets contain two classes of hydrous component: a structural component, and alteration-related water. The alteration-related hydrous component also includes hydrous inclusions and will not be discussed further. The structural hydrous component is of interest because: (1) the "water" contained in the garnet is a record of the environment of formation or events, and (2) the garnet structure must be changed to accommodate a hydrous component and this may also change the physical properties of the garnet.

The criteria used to distinguish the structural hydrous component from alteration and inclusions, and the spectroscopic features that we have observed for the structural component, provide considerable information about its character.

(1) The O-H defect responsible for the hydrous component is OH^-, not H_2O; the diagnostic 5200 cm^{-1} H_2O band is not seen.

(2) The IR spectra depend only on the chemistry of the garnet, not its origin. There is only one type of structural hydrous component.

(3) Multiple OH^- groups occur in close enough proximity to force them all to vibrate simultaneously, resulting in multiple peak patterns in which the relative intensities of the peaks are constant.

These facts provide the basis for a structural interpretation of the hydrous component. It would be a mistake to automatically assume that the hydrogarnet substitution is present in natural pyralspites simply

because they are hydrous. However, the above facts all fit an interpretation based on hydrogarnet.

In the hydrogarnet substitution, four OH^- groups replace SiO_4^{4-} tetrahedra (Cohen-Addad et al., 1967; Foreman, 1968). The four protons are slightly outside the volume of the tetrahedron as defined by the oxygen centers. These four O-H groups can be expected to yield a total of 3N-6 = 18 vibrations, four of which are stretching vibrations and would occur near 3400 to 3700 cm^{-1}. Not all four must occur, depending on the exact symmetry of the group. The presence of hydrogarnet substitution in an end-member garnet should be evidenced by an infrared spectrum in the 3500 cm^{-1} region with up to four peaks. If complete garnet symmetry is maintained there will be two peaks.

The spessartine end-member pattern contains six peaks (Fig. 3) in violation of the four peak limit. However, the two lower-wavenumber peaks vary independently of the four high-wavenumber peaks (Fig. 5). They apparently arise from a separate defect. The grossular and almandine end-member patterns do not violate the four peak limit, and are consistent with the possibility of hydrogarnet substitution. Intermediate chemistry pyralspites are more complex, however. This complexity could be caused by multiple, non-hydrogarnet O-H defects. The simple behavior in binary systems suggests, however, that the multiple peaks are a reflection of site occupancy in the dodecahedral sites which contain the divalent ions. Figure 8 shows a portion of the garnet structure, a tetrahedral site and its two dodecahedral neighbors. Not shown are four octahedral neighbors that share corners with the tetrahedral site. The presence of different cations sharing edges with a tetrahedral site "filled" by $H_4O_4^{4-}$ may be expected to

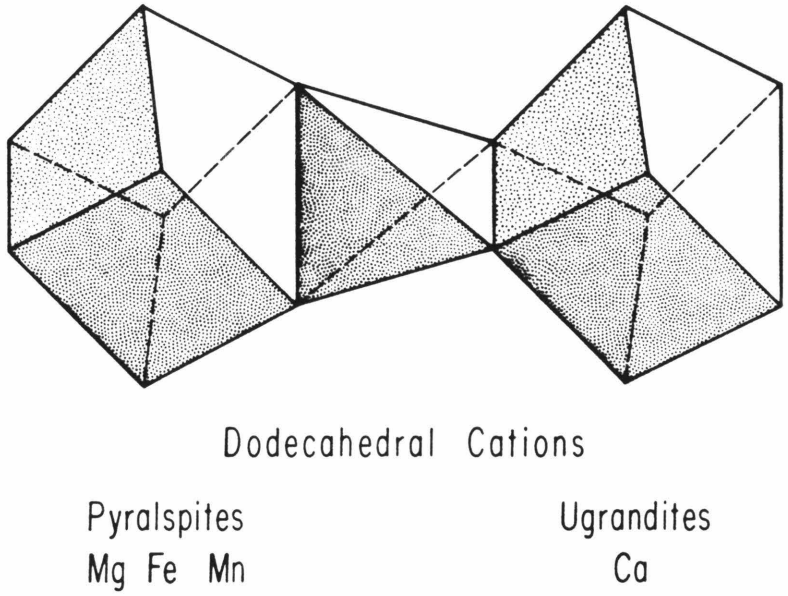

Figure 8. Portion of the garnet structure showing the two dodecahedral sites that share edges with the tetrahedral site that may contain H_4O_4.

significantly alter the spectra of the H_4O_4 group by reducing the symmetry of the site and because of the large differences in cation size and cation oxygen bond lengths in the pyralspite garnets (Novak and Gibbs, 1971). The consistent change in the spectra in accord with the dodecahedral cation chemistries strongly suggests that the hydrous defect is located in the tetrahedral site.

Since the H_2O contents of the garnets studied are extremely low, considerably fewer than one H_4O_4 substitution would occur per unit cell. Accordingly, there should be no coupling of vibrations between possible H_4O_4 tetrahedra, and each may be considered independently. In a garnet of intermediate chemistry in a binary system, three combinations of dodecahedral neighbors (for instance, Mn-Mn, Mn-Fe, Fe-Fe) are possible and should yield three distinct infrared spectra. The intermediate-chemistry garnets' spectra can be described as composed of three components: one for each end-member, and a new component only seen in the intermediate chemistry samples. This new component appears to be due to mixed-neighbor pairs around tetrahedral sites. The spectral complexity in Figures 5 and 6 may be explained by this. The sites with neighboring Mg-Fe may give rise to absorption at ~3580 cm^{-1} in pyrope-almandines, and the 3585 cm^{-1} peak in spessartine-almandine may be assigned to sites with Mn-Fe neighbors.

The absence of resolvable fine structure in the intermediate garnets makes the assignment of actual O-H defect structures difficult. This apparent blurring of the fine structure arises as a result of intermediate chemistries, apparently due to the large number of local environments that are slightly different giving rise to a similarly large number of O-H defects that are slightly different and whose O-H

absorption frequencies are offset by a few wavenumbers. The juxtaposition of many of these in an IR spectrum would result in a blurring of the sharp end-member pattern. This may be most clearly seen in the top three spectra of Figure 5.

The presence of three sets of peaks in intermediate-chemistry garnets is consistent with the hydrogarnet substitution, but is not compelling evidence. An example of one problem with this interpretation is seen in the spessartine spectra in Figures 3 and 5. The postulated Mn,Fe band at 3585 cm^{-1} is seen in the supposedly end-member spectra. This sample is approximately $Mn_{95}Fe_5$, so some Mn-Fe pairs are expected, but the intensity of the 3585 cm^{-1} peaks are far too large to be the result of random mixing of Mn^{2+} and Fe^{2+} dodecahedra with H_4O_4 tetrahedra. If the postulated H_4O_4 defects exist, they must heavily favor association with Mn-Fe neighbors. A similar effect is seen for Mg-Fe (Fig. 6) where the Mg^{2+} end-member pattern is never seen alone, and the postulated Mg-Fe pattern is dominant in all pyropes studied.

Occurrence and "Water" Content.

The most hydrous pyralspite garnets encountered were spessartines and spessartine-almandines from igneous pegmatites. Garnets from metamorphic occurrences were much lower in structural H_2O, but frequently contained hydrous inclusions. Garnets of mantle origin were frequently hydrous, and will be discussed in detail in Aines (in preparation). The majority of the garnets studied which were anhydrous were from the mantle, but only two samples of "crustal" origin were rigorously anhydrous. Sample 112 is from a region known for garnets occurring in metamorphosed mafic rocks, and sample 111 is from an alkali-olivine basalt flow. Both samples may have dehydrated as the

host rock was cooling. Anhydrous crustal pyralspites are rare.

The garnets used in this study were chosen to represent the range of occurrences of pyralspites, but the range of water contents that we observed is quite limited, from 0.0 to 0.25 wt. % clustering around 0.1 to 0.15 wt. %. This suggests that the solubility of water in pyralspites is limited, and that the garnets we observed with greater than 0.2 wt. % may be saturated with water. The range that we observe, however, suggests that the water content of garnets may be a useful indicator of water fugacity pending experimental calibration of water solubilities.

Limitations to "Water" Concentrations in Pyralspites

The hydrogarnet substitution has not been previously recognized as an important component of natural pyralspite garnets. The garnets studied here indicate that this lack of identification is due to the extremely low level of the substitution, and not to its frequency of occurrence. Two hypotheses have been previously advanced for the apparent lack of hydrogarnet substitution in pyralspite, and may be applied instead to explain the consistently low levels. The first is that the $H_4O_4^{4-} \rightleftarrows SiO_4^{4-}$ substitution results in a large volume increase (Cohen-Addad, 1967; Meagher, 1980; Martin and Donnay, 1972) and as such is not favored at the high pressures typical of pyralspite formation. The second hypothesis (Zabinski, 1966) is that Mg-O and Fe-O bond lengths in pyralspites are slightly longer than the average lengths for these bonds in silicates, and that the additional increase in length that would occur during unit cell expansion associated with hydrogarnet substitution de-stabilizes the hydrous pyralspites. Ca-O bond lengths are comparatively short, favoring hydrogarnet formation in

grossular-andradite garnets.

These theories may serve to explain the lack of pyralspites containing large amounts of water, such as the 2 to 6 % H_2O hydrogrossulars described by Zabinski (1966). The relatively constant H_2O contents of the garnets in this study suggest that low solubility limits are indeed the controlling factor in H_4O_4 substitution in pyralspites. Two studies of synthetic, hydrothermal pyralspites have been made in which the solubility was tested. Hsu, 1980, synthesized grossular-spessartines at P_{H_2O} = 2 Kb, T = 420-750°C. The hydrogrossular she generated gave IR spectra identical to those in this study, with peaks at 3660 and 3620 cm^{-1}. The hydrospessartines were identified on the basis of cell volume expansion (Hsu, 1968) analogous to the grossular-hydrogrossular expansion (e.g., Shoji, 1974; Ito and Frondell, 1967) and are reported to be metastable. However, the sharp bands reported by Hsu as related to H_4O_4 in hydrospessartine appear to be due to oil contamination (Ackermann et al., 1983), a conclusion with which we agree. Thus, there is no spectroscopic evidence of the hydrogarnet substitution given by these hydrothermally produced spessartines and their exact nature remains undetermined. This, combined with the metastability of the synthetic hydrospessartines, makes it difficult to determine the expected extent of $H_4O_4^{4-}$ substitution in natural spessartines.

Ackermann et al., 1983, studied hydrothermally produced pyropes. They found a single, sharp IR absorption band at 3600 cm^{-1}, and a broad band centered near 3470 cm^{-1} due to fluid inclusions. They report that the 3600 cm^{-1} band is due to hydrogarnet substitution based on the peak location in synthetic hydrogrossular. Based on the evidence presented

here, this seems unlikely because of the dependence of peak location on chemistry. While the pyrope end-member pattern is not well defined by this study, it occurs in the 3670 cm^{-1} region based on the spectra of the Mg-rich garnets we studied. The presence of fluid inclusions leaves open the possibility of hydrous alteration products in their pyropes. Fluid inclusion IR absorption dominates the spectra of their pyropes. Ackermann et al. report that the intensity of their 3600 cm^{-1} band corresponds to a water content of 0.05% based on the muscovite peak-height molar absorptivity (ε) of 170 ℓ $mole^{-1}H_2O$ cm^{-1}. That value is based on peak height, not integral absorbance as reported here, but on the same basis the ε from this study would be ~5 ℓ $mole^{-1}H_2O$ cm^{-1} for intermediate chemistries, to ~150 ℓ $mole^{-1}H_2O$ cm^{-1} for end members, measured using the most intense peak in the spectrum. Peak height molar absorptivities were not used in this study because of the ambiguity introduced by multiple peaks due to a single hydrous species.

Further work is required to determine the extent and nature of the hydrous component in synthetic pyropes, but the hydrous component seen by Ackermann et al. is present at similar concentrations to those in natural garnets. If they were in fact the same defects, this would be strong evidence of solubility being the limiting factor in natural hydrogarnet substitution. However, the infrared spectra observed by Ackerman et al. do not seem to be consistent with those we observed, and it is unlikely that both represent the same hydrous defect.

Conclusions

Natural pyralspite garnets commonly contain a hydrous component at levels of 0.01 to 0.25 wt%. Anhydrous pyralspites are rare. The hydrous component has the following characteristics:

(1) The hydrogen speciation is OH^-, not H_2O.

(2) Multiple hydroxides (2 to 4) vibrate together, indicating close proximity in the structure.

(3) IR absorption spectra of different chemistry pyralspites are consistent with dodecahedral cation occupancy affecting a hydrogen defect in the tetrahedral site.

These characteristics are suggestive of the hydrogarnet substitution, $H_4O_4^{4-} \rightleftarrows SiO_4^{4-}$, but other structural forms for the hydrogen defect(s) which have the above characteristics cannot be ruled out. Natural garnets also frequently contain a hydrous component in the form of alteration or included hydrous phases. The presence of a structural hydrous component may be best differentiated from these by infrared spectroscopy. The presence of hydrogarnet substitution in natural garnets may prove to be a useful indicator of water fugacity. However, the effects of alteration and hydrous inclusions must be carefully considered, particularly in metamorphic garnets where they are common.

Acknowledgments

We would like to thank Doug Smith (U. Texas), Ed Grew (UCLA), Georg Amthauer (Marburg), Stein Jacobsen (Caltech), Larry Edwards (Caltech), L. T. Silver (Caltech), John White (Washington, DC) and Mary Johnson (Harvard) for generously providing samples used in this study, and Anne Hofmeister (Caltech) and Robert Criss (USGS) for conducting the hydrogen manometry. This study was in part funded by the National Science Foundation (Grant EAR-7919987).

References

Ackermann, L., Cemic, L., and Langer, K. (1983) Hydrogarnet substitution in pyrope: a possible location for "water" in the mantle. Earth and Planetary Science Letters, 62, 208-214.

Aines, R. D. and Rossman, G. R. (1983) Water in minerals? A peak in the infrared. Journal of Geophysical Research, in press.

Albee A. L. and Ray, L. (1970) Correction factors for electron microprobe analysis of silicates, oxides, carbonates, phosphates, and sulfates. Analytical Chemistry, 42, 1408-1414.

Aubry, A., Dusausoy, Y., Laffaille, A., and Protas, J. (1969) Détermination et étude de la structure crystalline de l'henritermiérite, hydrogrenat de symétrie quadratique. Bulletin de Minéralogie, 92, 126-133.

Baumer, A., Gimenez, H., Caruba, R., and Turio, G. (1974) Remplacements de regroupments atomiques dans la structure zunyite. Bulletin de Minéralogie, 97, 271-277.

Belyankin, D. S. and Petrov, V. P. (1941) The grossularoid group (hibschite, plazolite). American Mineralogist, 26, 450-453.

Bence, A. E. and Albee, A. L. (1968) Empirical correction factors for electron microanalysis of silicates and oxides. Journal of Geology, 76, 382-403.

Beran, A. and Putnis, A. (1983) A model of the OH positions in olivine, derived from infrared-spectrosopic investigations. Physics and Chemistry of Minerals, 9, 57-60.

Carswell, D. A. (1968) Possible primary upper mantle peridotite in Norwegian basal gneiss. Lithos, 1, 322-355.

Champion, D. E., Albee, A. L., and Chodos, A. A. (1975) Reproducibility and operator bias in a computer-controlled system for quantitative electron microprobe analysis. Proceedings of the Tenth Annual Conference of the Microbeam Analysis Society, Las Vegas 1975, 55A-55F.

Cohen-Addad, C. (1968) Étude structurale des hydroxystannates $CaSn(OH)_6$ et $ZnSn(OH)_6$ par diffraction neutronique, absorption infrarouge et résonance magnétique nucléaire. Bulletin de Minéralogie, 91, 315-324.

Cohen-Addad, C. (1969) Substitution des groupement $(OH)_4$ par (GeO_4) dans l'hydrogrenat $Ca_3Al_2(OH)_{12}$. Formation de nouveaux composés. Bulletin de Minéralogie, 92, 308-310.

Cohen-Addad, C., Ducros, P., and Bertaut, E. F. (1967) Étude de la substitution du groupement SiO_4 par $(OH)_4$ dans les composés $Al_2Ca_3(OH)_{12}$ et $Al_2Ca_3(SiO_4)_{2.16}(OH)_{3.36}$ de type Grenat. Acta Crystallographica, 23, 220-230.

Cohen-Addad, C., Ducros, P., Durif, A., Bertaut, E. F., and Delapalme, A. (1964) Détermination de la position des atomes d'hydrogéne dans l'hydrogrenat $Al_2O_3,3CaO,6H_2O$ par résonance magnétique nucléaire et diffraction neutronique. Le Journal de Physique, 25, 978-483.

Cornu, F. (1906) Hibschit, ein neues kontaktmineral. Tschermaks Mineralogische und Petrographische Mitteilungen, 26, 457-468.

Flint, E. P., McMurdie, H. F., and Wells, L. S. (1941) Hydrothermal and x-ray studies of the garnet-hydrogarnet series and the relationship of the series to hydration products of Portland cement. Journal of Research of the National Bureau of Standards, 26, 13-33.

Foreman, D. W., Jr. (1968) Neutron and X-ray diffraction study of $Ca_3Al_2(O_4D_4)_3$, a garnetoid. Journal of Chemical Physics, 48, 3037-3041.

Foshag, W. F. (1920) Plazolite, a new mineral. American Mineralogist, 5, 183-185.

Frondel, C. (1972) The Minerals of Franklin and Sterling Hill. Wiley, New York.

Goldman, D. S., Rossman, G. R., and Dollase, W. A. (1977) Channel constituents in cordierite. American Mineralogist, 62, 1144-1157.

Grew, Edward S. (1981) Surinamite, taaffeite, and beryllian sapphirine from pegmatites in granulite-facies rocks of Casey Bay, Enderby Land, Antarctica. American Mineralogist, 66, 1022-1033.

Grew, Edward S. (1982) Sapphirine, kornerupine, and sillimanite plus ortho-pyroxene in the Charnockite region of southern India. Journal of the Geological Society of India, 23, 469-505.

Grice, J. D., and Williams, R. (1979) The Jeffrey mine, Asbestos, Quebec. Mineralogical Record, March-April 1979, 69-80.

Hill, R. I. (1984) Petrology and petrogenesis of batholithic rocks, Mt. San Jacinto, CA. Ph.D. thesis, California Institute of Technology.

Hunter, W. C., and Smith, D. (1981) Garnet peridotite from Colorado Plateau ultramafic diatremes: hydrates, carbonates, and comparative geothermometry. Contributions to Mineralogy and Petrology, 76, 312-320.

Hsu, L. C. (1968) Selected phase relationships in the system Al-Mn-Fe-Si-O-H, a model for garnet equilibria. Journal of Petrology, 9, 40-83.

Hsu, L. C. (1980) Hydration and phase relations of grossular-spessartine garnets at P_{H2O} = 2Kb. Contributions to Mineralogy and Petrology, 71, 407-415.

Ito, J. and Frondel, C. (1967) New synthetic hydrogarnets. American Mineralogist, 52, 1105-1109.

Jahns, R. H. and Wright, L. A. (1951) Gem and lithium bearing pegmatites of the Pala district, San Diego Co., California. California Division of Mines Special Report, 7A.

Levin, S. B. (1950) Genesis of some Adirondack garnet deposits. Bulletin of the Geological Society of America, 61, 519-565.

Martin, R. F., and Donnay, G. (1972) Hydroxyl in the mantle. American Mineralogist, 57, 554-570.

McGetchin, T. R., and Silver, L. T. (1972) A crustal-upper-mantle model for the Colorado Plateau based on observations of crystalline rock fragments in the Moses Rock dike. Journal of Geophysical Research, 77, 7022-7037.

Meagher, E. P. (1980) Silicate garnets. In P. H. Ribbe, Ed., Reviews in Mineralogy Volume 5, Orthosilicates, p. 25-66. Mineralogical Society of America, Washington, D. C.

Novak, G. A. and Gibbs, G. V. (1971) The crystal chemistry of the silicate garnets. American Mineralogist, 56, 791-825.

Pabst, A. (1937) The crystal structure of plazolite. American Mineralogist, 22, 861-868.

Pabst, A. (1942) Re-examination of hibschite. American Mineralogist, 27, 783-792.

Parker, J. M. (1952) Geology and structure of a part of the Spruce Pine district, North Carolina. North Carolina Department of Conservation and Development Bulletin, 65.

Sahl, K. (1980) Refinement of the crystal structure of bicchulite, $Ca_2[Al_2SiO_6](OH)_2$. Zeitschrift für Kristallographie, 152, 13-21.

Shoji, T. (1974) $Ca_3Al_2(SiO_4)_3$-$Ca_3Al_2(O_4H_4)_3$ series garnet: composition and stability. Journal of the Mineralogical Society of Japan, 11, 359-372.

Sinkankas, J. (1968) Geology and mineralogy of the Rutherford pegmatites, Amelia, Virginia. American Mineralogist, 53, 373-405.

Sinkankas, J. (1976) Gemstones of North America. Van Nostrand Reinhold, New York.

Smith, D., and Levy, S. (1976) Petrology of the Green Knobs Diatreme and implications for the uppermantle below the Colorado Plateau. Earth and Planetary Science Letters, 29, 107-125.

Switzer, G. S. (1977) Composition of garnet xenocrysts from three kimberlite pipes in Arizona and New Mexico. Smithsonian Earth Sciences, 19, 1-21.

Westrum, E. F., Essene, E. J., and Perkins, D. (1979) Thermophysical properties of the garnet, grossular: $Ca_3Al_2Si_3O_{12}$.

Wilkins, R. W. T. and Sabine, W. (1973) Water content of some nominally anhydrous silicates. American Mineralogist, 58, 508-516.

Winchell, A. N. (1933) Elements of Optical Mineralogy, Part II, 3rd edition. John Wiley and Sons, New York.

Zabinski, W. (1966) Hydrogarnets. Polska Akademia Nauk, Komisja Nauk Mineralogicznch, Prace Mineralogiczne, 3, 1-61.

Chapter 5

The Water Content of Mantle Garnets

ABSTRACT

Garnet megacrysts from Colorado plateau diatremes (Green Knobs, Garnet Ridge) and the Wesselton kimberlite, South Africa, commonly contain a structural hydrous component. The Colorado plateau samples range from 0.0 to 0.26 wt. % H_2O, and the Wesselton samples contain from 0.01 to 0.07 %. Concentrations were measured using P_2O_5 cell coulometry, H_2 gas manometry, and thermogravimetry. These were used to calibrate infrared integrated absorbance in the 3 μm region, which is a more sensitive measure of total O-H content than the other analytical methods. Infrared absorbance patterns were also used to differentiate structural hydrous component from water contained in alteration and included phases. The structure of the hydrous component in these garnets appears to be the classic $H_4O_4^{4-} = SiO_4^{4-}$. Profiles at 100 μm intervals across these samples show flat concentration profiles or slightly increasing concentration toward the center. A large range of water contents among samples appears to represent real differences in water fugacity at the point where the garnets equilibrated. Garnets in eclogite nodules from South Africa and the Solomon Islands were also studied, but were either anhydrous or too badly altered to determine the content of structurally bound water. The high concentration of hydrous component in the Colorado Plateau samples is consistent with other indicators of high volatile content in that region of the mantle. The water content of mantle garnets may prove to be an accurate indicator of mantle water fugacities.

INTRODUCTION

The occurrence of a structural hydrous component has been shown to be common in pyralspite (pyrope-almandine-spessartire) garnets (Chapter 4, Aines and Rossman, 1984). In this paper I discuss the occurrence of that hydrous component in garnets of mantle origin. I have studied suites of garnet megacrysts from two Colorado Plateau diatremes (Garnet Ridge, Arizona, Green Knobs, New Mexico) and from the Wesselton Kimberlite, South Africa. I have also examined individual samples from an alnoite body in the Solomon Islands; the Kimberly, Roberts Victor, and Lesotho Thabu Putsoa Kimberlites South Africa, and the Moses Rock diatreme, Utah.

The possible importance of water in the processes occurring in the mantle is well known from experimental work, but the sources and sinks for water in the mantle are not well known. Martin and Donnay (1972) suggested that substitutional hydroxide in nominally anhydrous minerals could be an important water site in the mantle. Ringwood and Major (1967) synthesized several hydrous high pressure phases that may be important in the mantle, and Sclar et al., (1967) synthesized a new hydrous phase at high pressures which they suggest is a hydrated pyroxene. However, demonstrable hydrous phases in the mantle are rare, among them phlogopite and humite (e.g. Hunter and Smith, 1981; McGetchin and Silver, 1970). Ackermann, et al., (1983) produced a hydrous synthetic pyrope garnet at 25 kbar P_{H_2O}, and suggest that this may be an important water site in the mantle. However, as was pointed out in chapter 4 (Aines and Rossman, 1984) it is not clear that Ackermann et al. have produced a dissolved, structural hydrous component and not alteration associated with fluid inclusions.

In the previously reported infrared (IR) study of pyralspites I investigated mantle pyropes anticipating that they would be rigorously anhydrous. Instead, they were found to commonly contain similar water contents to garnets formed near the surface (0.02 to 0.25 wt % as H_2O). It became apparent that garnet may serve as a water site in the mantle, and that the present water content of the mantle garnets might prove to be an indicator of water fugacity in the mantle. In order to examine this I have studied a variety of mantle-dervied garnets, in particular suites of stones from several diatremes. My goals were to establish the range of common water contents and its relationship to occurrence, and to determine the origin of that water.

EXPERIMENTAL METHOD AND SAMPLES

Sample preparation and analytical methods have been previously described (Aines and Rossman, 1984). Total H_2O concentrations are determined from the integral intensity of OH-stretching absorptions in the infrared 3400-3700 cm^{-1} region (Figure 1), which has been calibrated using H_2 gas manometry, P_2O_5 cell coulometry, and thermogravimetry. IR spectroscopy is a very precise technique for this type of water analysis, conservatively capable of measuring 0.01 wt % H_2O with an error of ± 20%. As such the values I report here are very accurate relative to each other but the total water content value is dependent on the external calibrations and may be in error by as much as 50% (Chapter 4, Aines and Rossman, 1984).

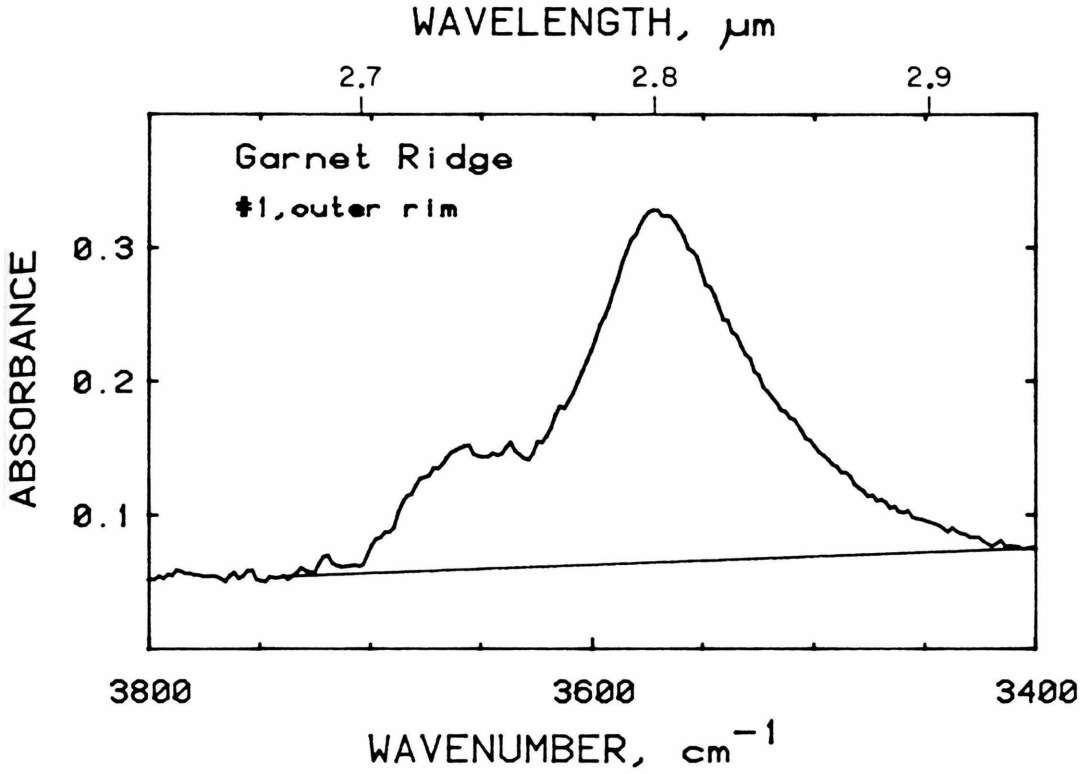

Figure 1. Typical infrared spectrum of a mantle pyrope in the OH stretching region. The baseline used for integrating peak area is shown. Sample thickness 1.79 mm. Garnet Ridge, CIT #15013-C-3 (see Figure 5c)

Samples used are largely individual megacrysts at least 1 mm in the smallest dimension. These provide adequate alteration-free path length for accurate IR analysis. Samples from the Colorado Plateau diatremes are 'ant hill' garnets, collected at the surface from ant hills. The Wesselton mine garnets are concentrator separates from diamond mining operations. Two samples from the Solomon Islands Malaita alnoite body (Nixon and Boyd, 1979) were used, one a megacryst (PHN 3986A), and one a garnet-orthopyroxene-clinopyroxene nodule (PHN 3861). One sample from the Roberts Victor Mine, South Africa, contains a grossular-pyope in an eclogite nodule containing kyanite and rutile (U.S. National Museum # 87375). An eclogite nodule from the Kimberly mine was also examined, as was a sample from the Lesotho Thabu Putsoa pipe, from a garnet lherzolite nodule (Green and Gueguen, 1983)

RESULTS AND DISCUSSION

Megacryst Suites

Figure 1 shows a typical infrared spectrum in the OH stretching region of a mantle garnet. The integrated area is determined using the baseline shown. This integrated area has been plotted for the three megacryst suites in Figures 2, 3 and 4 as the vertical scale on a Mg-Ca-Fe (mol %) triangular plot base. Samples with more than 1% Cr_2O_3 are plotted with shaded tops and bottoms. The vertical scale for the Wesselton suite (Fig. 4) is expanded 10X compared to the Colorado Plateau samples.

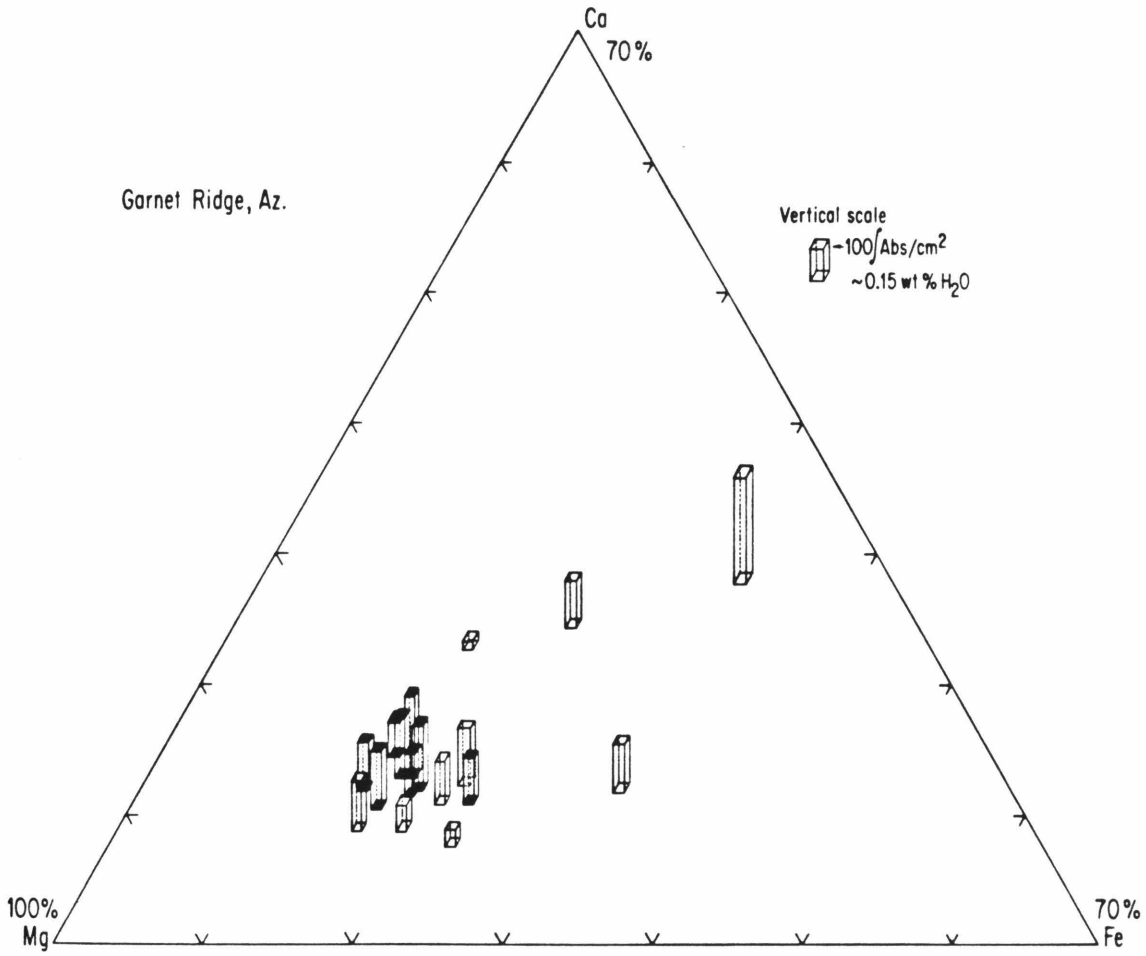

Figure 2. Comparison of dodecahedral site chemistry to water content. Fe-Mg-Ca in mol %. Water content vertical scale in integrated absorbance (cm^{-2}) in the 3700-3400 cm^{-1} region (Figure 1). Samples with filled tops and bottoms contain >1% Cr_2O_3 (by weight).

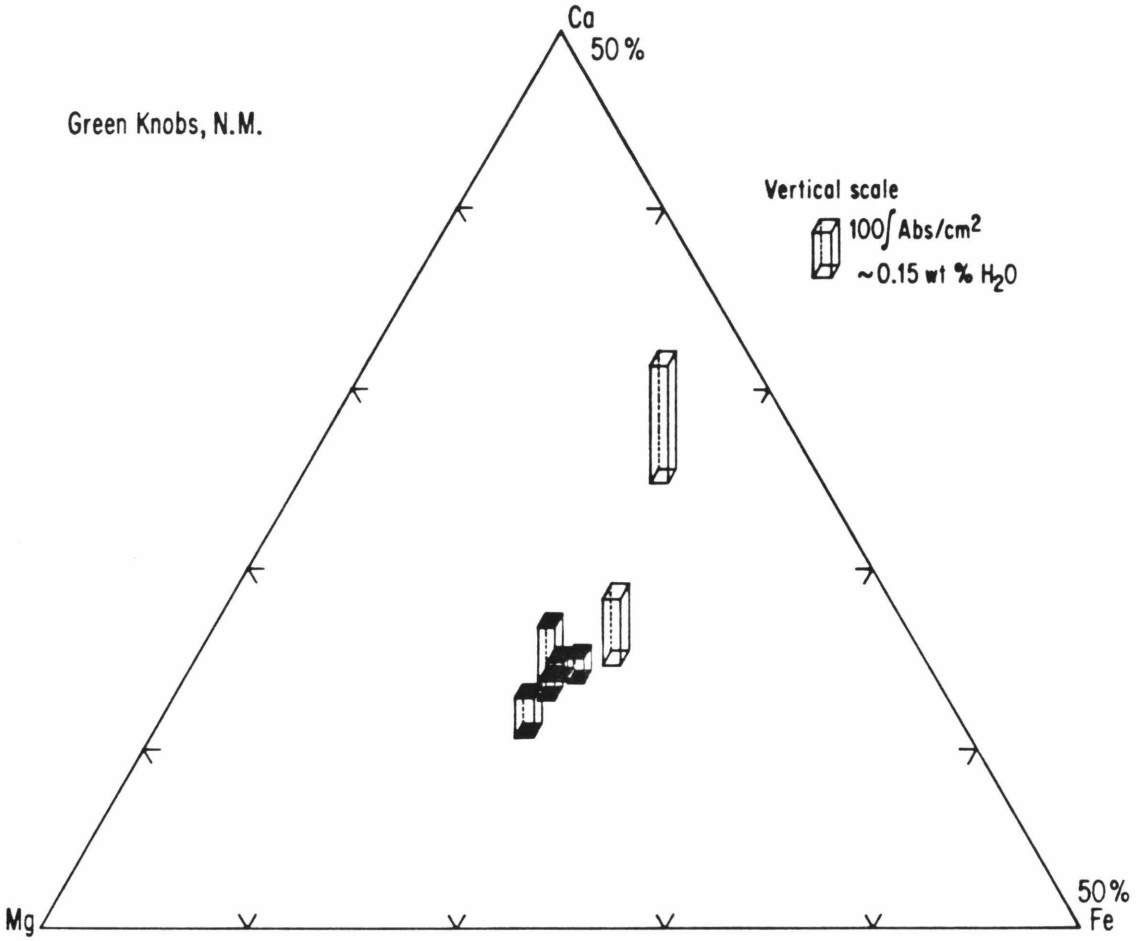

Figure 3. Green Knobs, New Mexico samples. Same as Figure 2 except plot is only extended to 50% Fe and Ca.

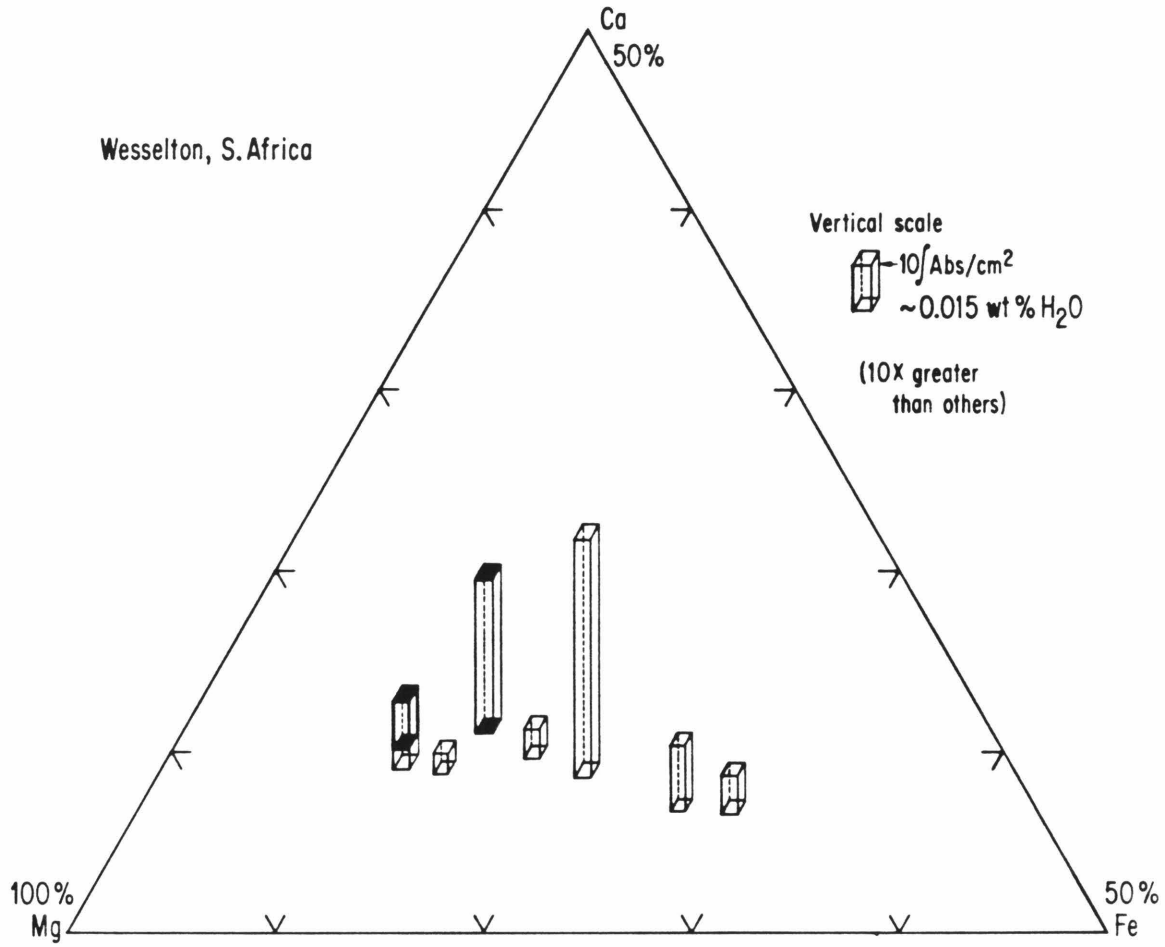

Figure 4. Wesselton, South Africa samples. Same as Figure 3 except vertical scale (H_2O) is 10X expanded.

The majority of the samples cluster tightly in the range of chemistries ascribed to mantle derived garnets (e.g. Smith and Levy, 1976). There is a wide range of water contents from all three localities, from 0.02 to 0.25% at Garnet Ridge, from 0.03 to 0.26% at Green Knobs, and 0.006 to 0.07% at Wesselton. There is no significant variation with the chemistry of the garnets. These samples are all free of alteration, and there is no correlation between inclusion content and water content. In all cases tested, inclusions in these garnets are anhydrous based upon comparison of spectra which include inclusions with spectra of inclusion-free zones in the same crystal. The observed variation in water concentration is intrinsic to the garnets. There is no significant variation among the Colorado Plateau localities, including a single sample from Moses Rock which contains 0.12% H_2O (sample 110, Chapter 4, Aines and Rossman, 1984). This sample is the same used as a microprobe standard (Champion, et al., 1977), collected by T. McGetchin. There is also no difference in water content between garnets of apparent crustal origin, such as the three most Ca rich samples in Figure 2, and those of mantle origin (Smith and Levy, 1975).

Zoning

The extreme variation in water contents among samples from a single suite may be due to real variations in equilibrated water content before the emplacement of the diatreme, or it may represent disequilibrium brought on by differential dehydration or hydration. In order to examine this problem, I have studied water zonation within individual samples as a function of distance from the rim of the crystal. If

either hydration or dehydration was occurring during emplacement and cooling, then individual stones should still contain concentration profiles reflecting diffusion of water. Three samples were chosen that had remaining original surfaces that were perpendicular to the polished surfaces, and spectra were taken at intervals using an aperture 150 μm wide by 2 mm long. In two cases no concentration profile was detectable. Figure 5A shows four overlaid spectra of a Green Knobs sample beginning at the rim of the crystal (0 to 150 μm) and continuing to the core (700 to 850 μm). They are identical in integral area to within 2%. A similar result is seen in 5B for a Wesselton sample. These results are in accord with results obtained when studying the effect of inclusions on spectra. In that case, numerous spectra were taken in different areas of individual samples. These were not characterized with respect to distance from the crystal rim, but no variation was observed to within ± 5%.

One instance of slight zonation was found in a sample from Garnet Ridge (Fig. 5c). Here there was 12% more H_2O at the core of the crystal than at the rim. The concentration profile is localized at the rim of the crystal; there was no change in concentration from 400 μm from the rim to the core in a 2000 μm wide sample. (The average distance for the center of the aperture from the rim is the stated value, + 75μm. This sample's spectrum is also seen in Figure 1.) This concentration profile apparently indicates quenched dehydration.

The results of the zoning studies indicate that the present water concentrations in the garnets equilibrated before emplacement of the diatreme, since they dehydrate readily at 1 bar and 250 - 500°C

Figure 5. (Next two pages) Infrared spectra showing zoning. Aperture 150 μm X 2mm. A) Green Knobs, four points from rim to core of a crystal 1.5 mm wide. Thickness .942 mm, $Ca_{.38}$ $Mg_{2.06}Fe^{+2}_{.54}$ Harvard #12528-J. B) Wesselton, two points at opposite rims and two points at core of .4 mm wide sample. Thickness .913 mm, $Ca_{.26}$ $Mg_{2.21}$ $Fe^{2+}_{.48}$, CIT # 15011-D. C) Garnet ridge, three points at 0, 200 and 400 μm from rim of 2 mm wide sample. Sample 1.79 mm thick, $Ca_{.38}$ $Mg_{2.07}$ $Fe^{2+}_{.51}$, CIT # 15013-C-3.

5A)

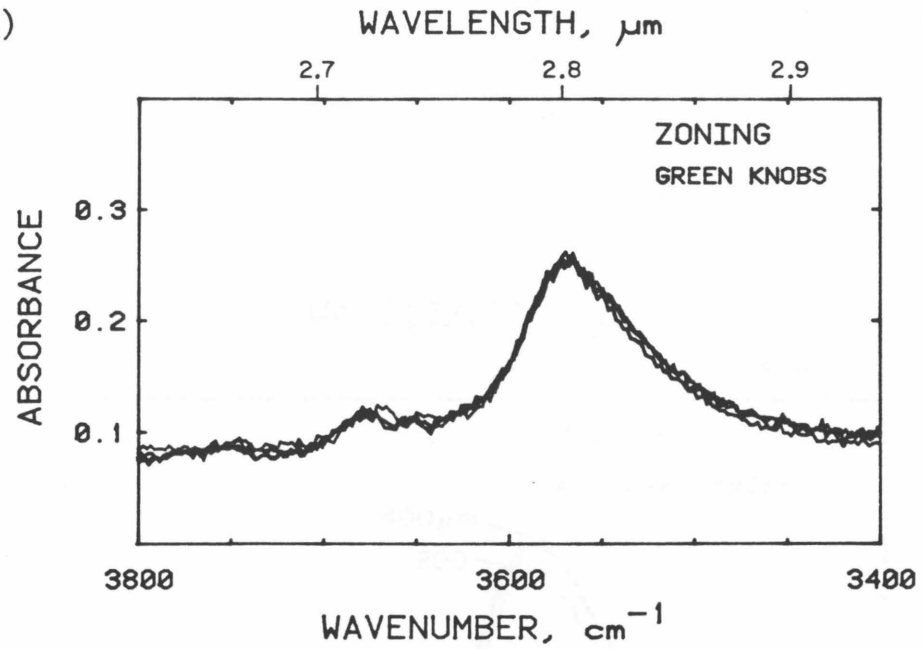
WAVELENGTH, μm
2.7
2.8
2.9
ZONING
GREEN KNOBS
ABSORBANCE
0.3
0.2
0.1
3800
3600
3400
WAVENUMBER, cm⁻¹

5B)

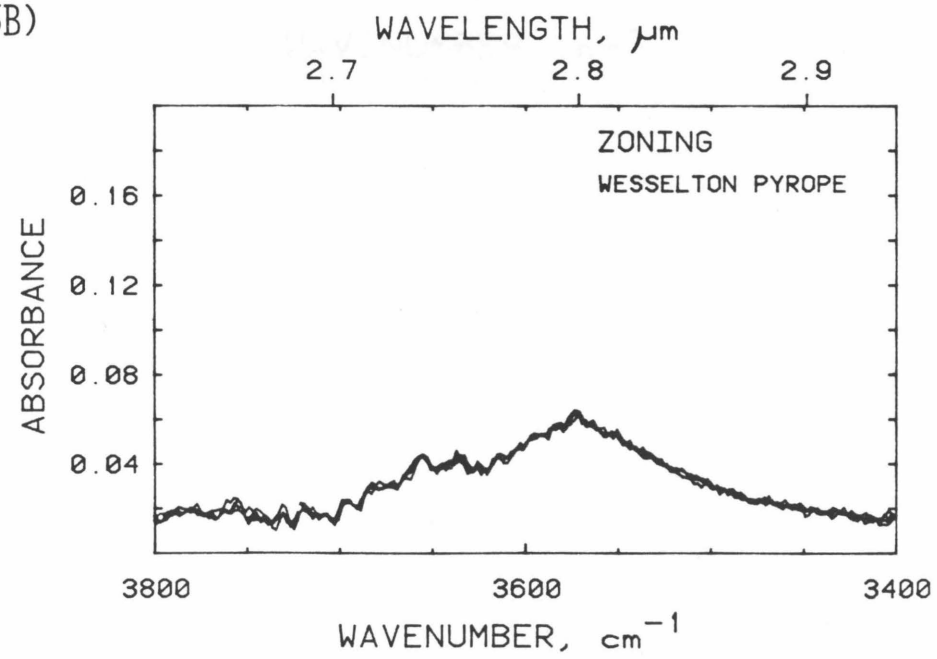
WAVELENGTH, μm
2.7
2.8
2.9
ZONING
WESSELTON PYROPE
ABSORBANCE
0.16
0.12
0.08
0.04
3800
3600
3400
WAVENUMBER, cm⁻¹

5C)

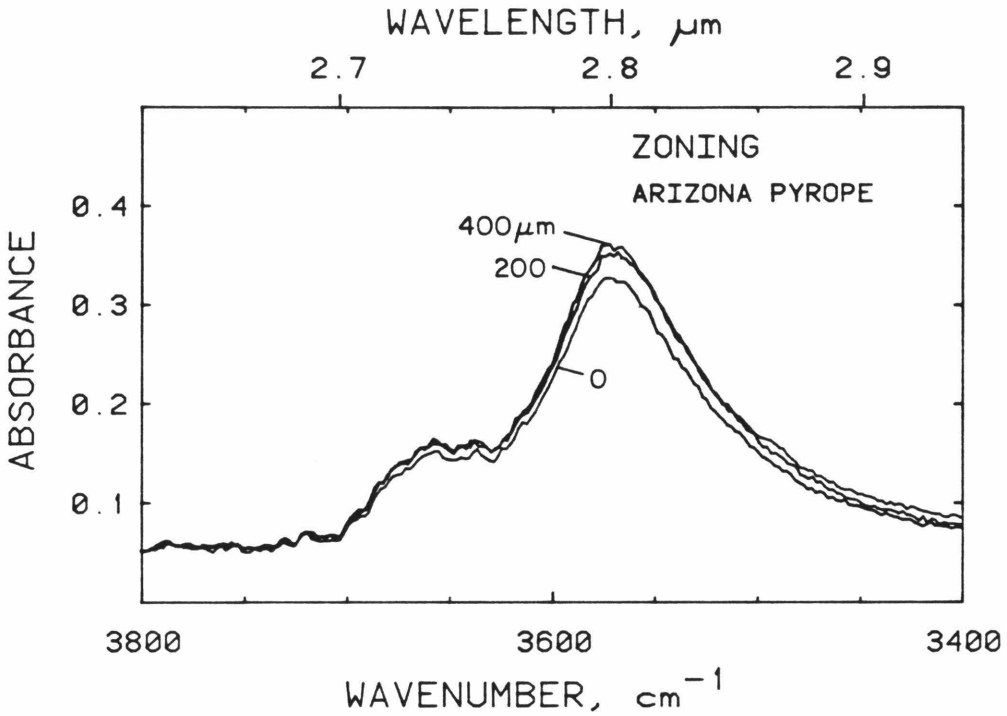
WAVELENGTH, μm
2.7
2.8
2.9
ZONING
ARIZONA PYROPE
400μm
200
0
ABSORBANCE
0.4
0.3
0.2
0.1
3800
3600
3400
WAVENUMBER, cm⁻¹

(Chapter 4, Aines and Rossman, 1984). The slight dehydration apparent in the Garnet Ridge sample might represent a short dehydration period during or after emplacement, but the diatremes apparently cooled rapidly enough that the original water concentrations were quenched in. As such, these garnets record the water fugacity at the point in the mantle where they equilibrated and the large differences noted must be due to differences in temperature or the coupled oxygen-hydrogen-water fugacities.

Other Samples

Solomon Islands Alnoite. The garnets from this occurrence are interesting since they come from oceanic mantle which is presumably depleted relative to continental mantle, and which appears to have an unusually high-gradient geotherm (Nixon and Boyd, 1979). The garnet from the gt-cpx-opx nodule (PHN 3861) was too altered to analyze, however. The infrared spectrum was dominated by a broad, featureless band at ~ 3600 - 3000 cm^{-1} which varied with the optical turbidity of the sample. There appeared to be no constant component in the spectra of different regions, indicating that the sample was anhydrous before alteration. The garnet megacryst (PHN 3986A) contained gemmy areas between altered cracks of approximately 1 mm^2; these area yielded spectra with no detectable absorptions. I conclude that these samples are both anhydrous.

South Africa Kimberlites. The most interesting sample from the South Africa occurrences is a grossular-pyrope from the Roberts Victor Mine (Chapter 4, Aines and Rossman, 1984, sample # 95.). This sample contains ~ .45 wt % H_2O, provided the calibration done on pyrope garnets

is applicable to this sample. If the calibration for grossular-andradites is used. it yields an answer of 0.12 wt %. No zonation was detectable over 2 mm of the sample, which was wholly contained in a kyanite-rutile bearing eclogite nodule. Regardless of the calibration used to assess the data, this is the wettest South Africa sample studied.

Two other samples from nodules were studied. An eclogite nodule from the Kimberly Mine contained substantial hydrous alteration, but superimposed upon the alteration pattern were peaks due to structural water. The amount could not be quantitatively determined but was similar to the Wesselton suite. Garnets from the Lesotho Thabu Putsoa Kimberlite garnet lherzolite nodule yielded sharp bands near the expected pyrope absorptions but slightly shifted to higher wavenumbers. The primary peak occurred at 3785 cm^{-1} with a subsidiary peak at 3600 cm^{-1}. Peaks are anticipated at 3760 cm^{-1} and 3560 cm^{-1} for pyrope-almandine garnets (Chapter 4, Aines and Rossman, 1984). This is not a typical alteration pattern, but was strongly zoned within the sample. The core of the 750 μm diameter sample yielded peaks twice as intense as the rim. Pending further study I conclude that these are due to alteration (an incipient hydrous phase). If they were due to the same structural component seen in the other samples, the water content would be 0.1 to 0.2 %.

CONCLUSIONS

Garnets of mantle origin frequently contain a structural hydrous component, ranging up to 0.26 wt % in samples from the Colorado Plateau diatremes. This hydrous component equilibrated before emplacement and as such is a record of the temperature-water fugacity at the point of equilibration. An obvious drawback to this study is the lack of samples for which pressure-temperature data are available. This is due in part to the necessity of using large, gemmy samples in this initial survey work in order to avoid problems with alteration and hydrous included phases. In all of the polyphasic nodules studied, alteration of the garnets was prevalent.

The presence of water in mantle garnets is somewhat surprising. I previously showed that this water appears to be the classic hydrogarnet substitution, $(SiO_4)^{4-} \rightleftarrows (H_4O_4)^{4-}$ (Chapter 4, Aines and Rossman, 1984). However, at 1 bar this substitution causes an increase in molar volume of about 10% and as such should be disfavored at high pressure (Martin and Donnay, 1972; Addad, et al., 1967). Ackermann, et al., (1983) point out that the relative volumes of other water sinks must be considered also, and that the hydrogarnet substitution may be of lower net volume. However, the compressibility of the hydrogarnet substitution has not been measured, and if the H_4O_4 group is relatively more compressible than a SiO_4 group, this could easily explain its existence in the mantle.

Although garnets contained up to 0.25% H_2O in this study, they are perhaps more interesting as recorders of water fugacity than as a source of water. Ackermann et al., (1983) have grown synthetic pyropes under

mantle conditions and obtained a hydrated, fluid inclusion rich garnet. However, it is not clear that this represents a structural, dissolved hydrous component or whether it is related to the fluid inclusions and as such is part of a second phase. The amount of water they obtained was similar to that I observed, however. This is the only experimental study of water solubility in pyrope available, and until further work is done the relationship between water fugacity and observed water content is unknown. Other factors will also play an important role, including temperature and oxygen fugacity. It is now worthwhile to undertake such experimental studies since these results indicate that water can be an important stable dissolved component in mantle garnets. The observed higher water contents in the Colorado Plateau samples compared to the South African samples are a strong indication that the garnets accurately reflect the water content of the mantle, which appears to be much higher under the Colorado Plateau (Hunter and Smith, 1981; McGetchin and Silver, 1972).

ACKNOWLEDGMENTS

I would like to gratefully acknowledge the donors of many of the samples used in this study: Joe Ritchey, UCLA (Garnet Ridge), Mary Johnson and the Harvard Museum (Wesselton), Doug Smith, Univ. of Texas (Green Knobs), the U.S. National Museum (Roberts Victor), Harry Green and Robert Borch, U.C., Davis, (Lesotho), L.T. Silver, Caltech (Kimberly), and G.J. Wasserburg, Caltech (Solomon Islands). Doug Smith, L.T. Silver and Ed Stolper, Caltech, provided helpful suggestions and discussions. This work supported in part by NSF Grants EAR-79-19987 and EAR-83-13098.

REFERENCES

Ackermann, L., Cemic, L. and Langer, K. (1983) Hydrogarnet substitution in pyrope: a possible location for "water" in the mantle. Earth and Planetary Science Letters, 62, 208-214.

Aines, R.D. and Rossman, G.R. (1984) Water in minerals? A peak in the infrared. Journal of Geophysical Research, Red, in press.

Champion, D.E., Albee, A.L., Chodos, A.A. (1977) Reproducibility and operator bias in a computer controller system for quantitative electron microprobe analysis. Proceedings of the Tenth Annual Conference of the Microbeam Analysis Society, Las Vegas, 1975, 55A-55F.

Cohen-Addad, C., Ducros, P. and Bertaut, E.F. (1967) Étude de la substitution de groupement SiO_4 par $(OH)_4$ dans les composes $Al_2Ca_3(OH)_{12}$ et $Al_2Ca_3(SiO_4)_{2.16}$ $(OH)_{3.36}$ de type Grenat. Acta Crystallographica, 23, 220-230.

Green, W.H. and Guegen, Y. (1983) Deformation of peridotite in the mantle and extraction by kimberlite; a case history documented by fluid and solid precipitates in olivine. Tectonophysics, 92, 71-92.

Hunter, W.C. and Smith, D. (1981) Garnet peridotite from Colorado Plateau diatremes; hydrates, carbonates, and comparative geothermometry. Contributions to Mineralogy and Petrology, 76, 312-320.

McGetchin, T.R. and Silver, L.T. (1970) Compositional relations in minerals from kimberlite and related rocks in the Moses Rock dike, San Juan County, Utah, American Mineralogist, 55, 1738-1771.

McGetchin, T.R. and Silver, L.T. (1972) A crustal-upper-mantle model for the Colorado Plateau based on observations of crystalline rock fragments in the Moses Rock dike. Journal of Geophysical Research, 77, 7022-7037.

Nixon, P.H. and Boyd, F.R. (1979) Garnet bearing lherzolites and discrete nodule suites from the Malaita alnoite, Solomon Islands, S.W. Pacific, and their bearing on oceanic mantle composition and geotherm. In: The Mantle Sample: Inclusions in Kimberlites and other volcanics. F.R. Boyd and H.O. Meyer, eds. Proceedings of the 2nd International Kimberlite Conference, American Geophysical Union, 2, 400-423.

Sclar, C.B., Carrison, L.C., and Stewart, O.M. (1967) High pressure synthesis of a new hydroxylated pyroxene in the system $MgO-SiO_2-H_2O$ (abstract). Transactions of the American Geophysical Union, 48, 226.

Smith, D. and Levy, S. (1975) Petrology of the Green Knobs diatreme and implications for the upper mantle below the Colorado Plateau. Earth and Planetary Science Letters, 29, 107-125.

Switzer, G.S. (1977) Composition of garnet xenocrysts from the Kimberlite pipes in Arizona and New Mexico. Smithsonian Earth Sciences, 19, 1-21.

Chapter 6

Radiation Damage and Water in Minerals

ABSTRACT

The presence of trace amounts of water or hydroxide ion can dramatically affect the response of a mineral to radiation from both internal and external sources. In zircon, where radioactive decay of uranium causes structural damage (metamictization), water can enter the structure after a threshold of damage is reached and stabilize the metamict state by annealing local charge imbalance. In quartz, molecular water is positively correlated with the formation of citrine (yellow) color, and may stabilize vacancies. Amethyst (purple) color in quartz is negatively correlated with the presence of molecular water. This may be due to the reduction of the Fe(IV) color center by atomic hydrogen formed by radiolysis of the water. In topaz, special hydroxide sites correlate with the formation of a brown color center, but two other color centers (one brown, one blue) have no correlative hydroxyl species.

The common interaction of hydrous species in minerals and radiation damage appears to be due to the mobility of hydrogen, the ease with which hydrogen and oxygen species may be formed in silicate lattices, the number of possible hydrogen species, and the common occurrence of trace amounts of water in even nominally anhydrous minerals.

INTRODUCTION

Understanding the mechanisms of radiation damage in minerals is important to radiometric age dating as well as radioactive waste storage. Processes observed in crystalline solids can also be applied to understand those in glasses, where a lack of structural information complicates determining radiation damage mechanisms. In this paper I discuss the common interaction between the hydrous species and radiation damage in minerals, and discuss the implications for understanding generalized mechanisms of radiation damage.

Radiation damage in minerals may be divided into two categories, metamictization and oxidation-state changes. The distinction is not clear cut, but metamictization may be considered to arise primarily from the structural damage caused by α-particles and recoiling nuclei (Yada et al. 1981, Ewing and Headley 1983). Oxidation state changes can be caused by any type of ionizing radiation but do not need to be accompanied by the breaking of bonds or movement of nuclei in the structure. This type of radiation damage is common in minerals, especially those containing potassium or uranium or which have been in close contact with potassium bearing minerals over long periods of time. For example, a calculation by Ilene Reinitz of Caltech (personal communication, 1983) shows that a sample at the core of a typical potassium-feldspar pegmatite receives 28.7 mrads of γ-radiation over 100 million years. (This calculation assumed a cylindrical, potassium-feldspar body 3.6 m in diameter. The ^{40}K content is 6.75×10^{22} atoms per m^3, and the linear attenuation coefficient is 0.132 cm^{-1}.)

Studies in our laboratory have shown that hydrous components in minerals are frequently correlated in minerals with the extent and nature of radiation damage. This relationship also exists in glasses, where in most cases, the presence of the hydrogen species OH^-, H_2O, or H_2 inhibit the formation of color centers (Van Wieringen and Kats, 1957; Faile and Roy, 1970; Hartwig, 1976; Shelby, 1979). One color center, the so-called E' center in fused silica, is positively correlated with the presence of hydroxyl (Weeks and Lell, 1964). However, when samples are both irradiated and observed at -195°C, even hydrous silica glass becomes radiation damaged (Arnold and Compton, 1959). Upon warming, the color centers are destroyed.

A similar temperature-hydroxyl relationship is observed in smoky quartz (see Weil, 1975 for a review). The smoky quartz color center is caused by the simultaneous displacement of an electron and an alkali ion from the vicinity of an aluminum ion. However, when the aluminum is charge-compensated by a proton, the color center cannot form at room temperature because the proton diffuses back and destroys it. When irradiated at 77 K, Al-H centers can form smoky centers because proton diffusion is too slow (Mackey, 1963).

Hofmeister (1983) has shown that in feldspar, both water and Pb^{2+} must be present in order for radiation to form the amazonite (green) color. She hypothesizes that radiolysis of the water yields OH radials which oxidize the Pb^{2+} yielding the chromophore, Pb^{3+}. The water is regenerated through the reaction of H radical with a hole center, and subsequent recombination of the H^+ and OH^-. A second color center in

feldspar, the smoky center, does not form if any water is present. Hofmeister has shown that this center is similar to the smoky center in quartz, and hypothesizes that when water is present, its radiolysis yields hydrogen which diffuses and destroys the smoky center.

In this paper, I discuss three examples of minerals in which the radiation damage process is closely tied to the presence of hydrous species. As in the previously reported cases, the water or hydroxyl appears to aid radiation damage in some cases, while hindering it in others. I hope to show, however, that the mobility and reactivity of hydrogen species is the unifying factor.

EXPERIMENTAL METHOD

Water and hydroxyl concentrations were determined using infrared (IR) and near-infrared (NIR) spectroscopy, as described by Aines and Rossman (1984a,Chapter 2). Visible and NIR spectra were obtained on a CARY17I spectrometer, using calcite polarizers and techniques described by Amthauer and Rossman, 1984. IR spectra were collected using a Perkin-Elmer 180 and techniques described by Rossman (1975). A gold-wire polarizer was used for IR studies. Doubly-polished single-crystal slabs were used for all measurements.

RESULTS and DISCUSSION

Zircon

Zircons from the stream gravels of Sri Lanka share a common origin but range in uranium content from 20-8300 ppm eU. Non-metamict samples, containing less than 2000 ppm eU, have no detectable water. However, above 2500 ppm eU the zircons are metamict and contain easily detectable 'water' (J. Woodhead and G. R. Rossman, Caltech, in prep. 1984). This 'water' yields an isotropic, broad band in the IR spectra of single-crystal slabs (Fig. 1). These metamict samples also have broad, isotropic bands below 2000 cm^{-1} which replace the sharper, anisotropic bands seen in non-metamict samples. There is no detectable band at 1650 cm^{-1} which would be expected if the hydrous component were actually molecular water (Chapter 2, Aines and Rossman, 1984a). From this I deduce that the speciation is as OH^-. I have also seen a similar broad band in the spectrum of a metamict vesuvianite. These broad bands are caused by hydroxyl groups in a range of environments (Aines and Rossman, 1984b, Chapter 3).

Figures 2a and 2b show the behavior of this broad band after heating. Dehydration becomes rapid at 600°C, however, no recrystallization occurs until 800°. Figure 2b shows the 700° spectrum scaled to the same peak height as the original spectrum to show that there is a distinct loss of intensity in the lower-energy side of the broad band. This indicates that the hydroxyl groups involved in short hydrogen bonds are expelled preferentially (Aines and Rossman, 1984b, Chapter 3). The additional intensity at 2800-2400 cm^{-1} is due to overtone vibrations of

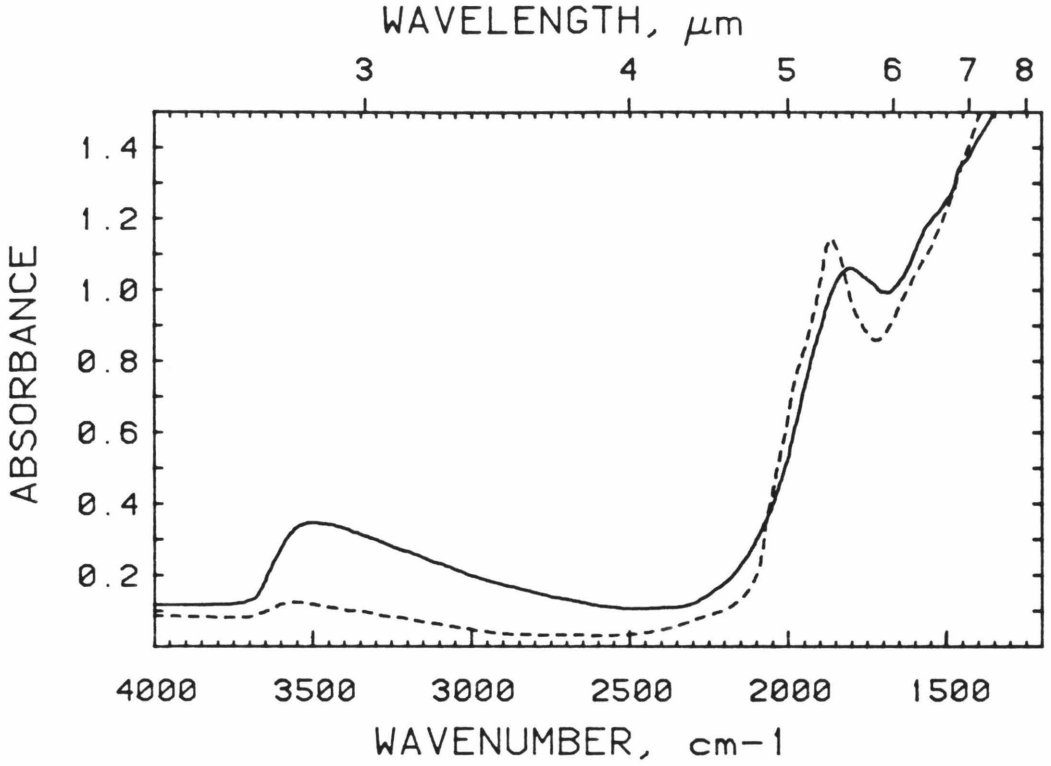

Figure 1. IR spectrum of a metamict zircon from Ceylon containing 6500 ppm eU. Solid trace-untreated. Dashed trace-heated to 800°C for 4 hours, causing partial dehydration and recrystallization. The broad band from 3650 to 2500 cm^{-1} is due to OH^{-}. Sample 0.307 mm thick.

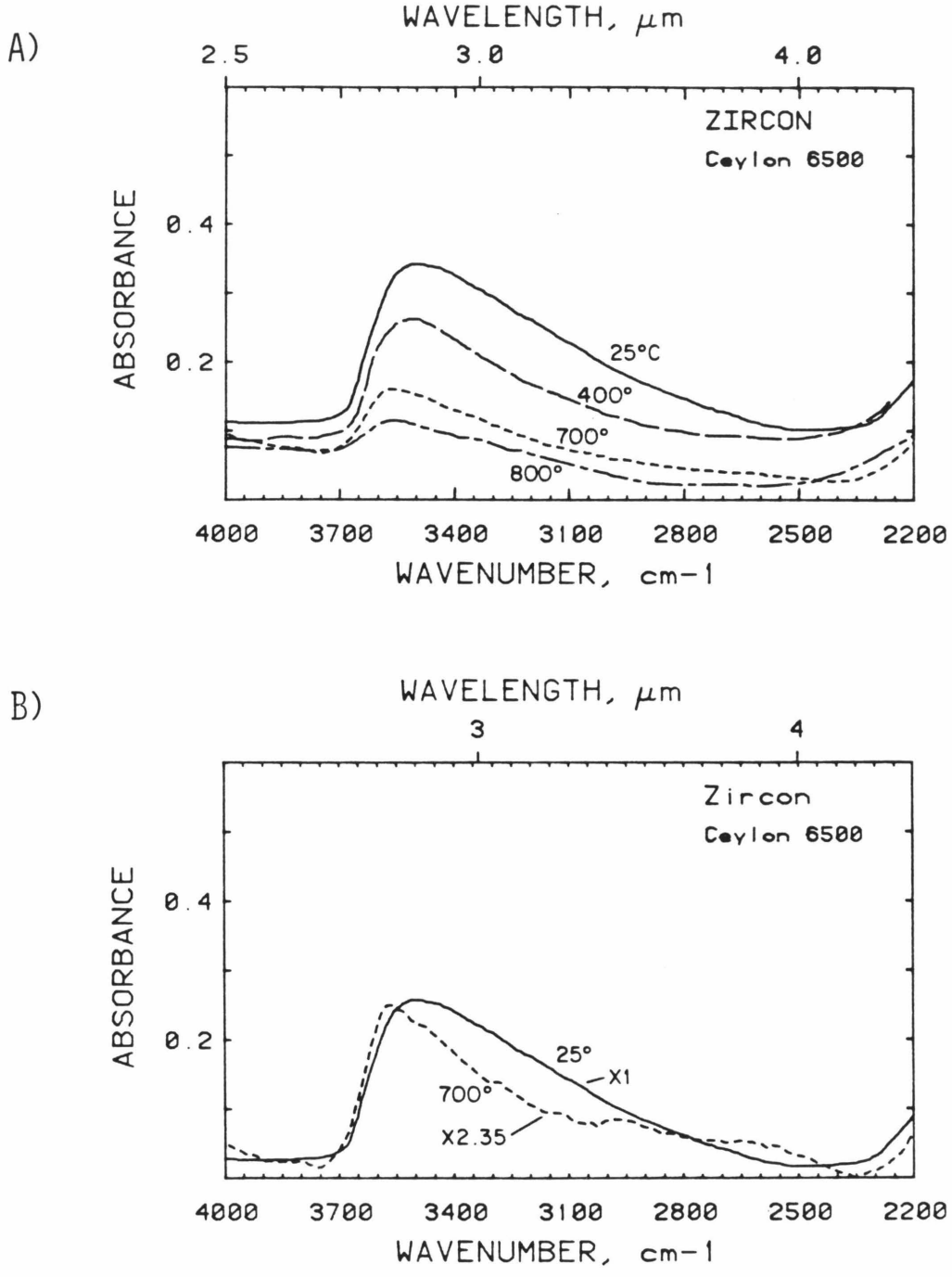

Figure 2. A) Single crystal IR spectra of the same sample as in Figure 1 after cooling from the indicated temperature. B) Comparison of the 25° and 700° spectra in figure 2a, with the 700° spectrum scaled to have the same peak absorbance as the original 25° spectrum.

the lattice. As slight recrystallization occurs, these modes increase in intensity.

The hydroxide in this zircon appears to be involved in local charge balance of the disrupted lattice. These samples are not recovered *in situ*, so the source is not well known, but it appears that they all start out anhydrous and water enters the lattice only after a threshold of radiation-damage (metamictization) occurs. Molecular water enters the crystal, and dissociates forming hydroxyl groups which satisfy local charge requirements. One possible reaction would be

$$\text{-Zr-O-Si-} \xrightarrow[\text{damage}]{\alpha\text{-particle}} \text{-Zr}^{+}\text{---}^{-}\text{O-Si} \qquad (1)$$

$$H_2O + \text{-Zr}^{+} \text{ --- } ^{-}\text{O-Si} \rightarrow \text{-ZrOH} + \text{HOSi-}.$$

The large number of possible similar reactions results in a variety of hydroxyl sites, and hence, the broad band. During recrystallization, the water reforms and is expelled, with the hydroxyl groups involved in short hydrogen bonds being expelled first. Most of the water is lost before any recrystallization becomes apparent in the infrared spectrum, indicating that water is actually stabilizing the metamict state.

Quartz: Amethyst-Citrine

Ionizing radiation produces three common colors in quartz: smoky (grey), amethyst (purple) and citrine (yellow). All three colors are strongly linked to the presence or absence of hydrogen impurities. Smoky quartz is a well known system (Weil, 1975) and will not be

discussed further. Amethyst and citrine are particularly interesting because both colors can occur in optically continuous single crystals of natural origin. Since these crystals have experienced uniform temperature and radiation histories, the color differences must be ascribed to the trace element concentrations or structural differences in the differently colored areas of the crystal. Amethyst coloration is known to be caused by the formation of Fe^{4+} centers from Fe^{3+} by radiation (Cox 1976, 1977). However, the depth of coloration is not a simple function of iron concentration (Dennen and Puckett, 1972; Lehmann and Bambauer, 1973). No change in the IR spectrum of quartz accompanies the formation of the Fe^{4+} centers, and no Fe(H) defect analogous to the Al(H) defect has been identified (Chakraborty and Lehmann, 1978.) Citrine coloration has not been decisively ascribed to a defect of known structure. This is partly due to the presence of at least two mechanisms which cause yellow coloration. The first of these is not true citrine; amethyst quartz may be heated to 300-400°C, precipitating iron into small clusters which cause a yellow-brown color. This is caused by an intense absorption at ~273nm (Stock and Lehmann, 1977). True citrine coloration is caused by radiation, and may be associated with the presence of high Li impurity content (Maschmeyer et al. 1980; Bukanov and Markova, 1969). Maschmeyer et al. suggest, based on EPR evidence, that the citrine color center is composed of a Li-Al hole center very similar to those causing smoky color, but that it is adjacent to a silicon vacancy. They hypothesize that one way to stablize such a vacancy is by incorporating H_2O in the Si site, with adjacent Si atoms moving to interstitial positions to minimize charge imbalance.

Figure 3 shows VIS, NIR and IR spectra of a single-crystal amethyst-citrine. This material is marketed under the name 'ametrine', and is from Bolivia, near the border with Brazil. The boundary between the two zones is optically sharp, and planar. The two colors appear to occur in the r and z growth zones, but I do not know zone is which color. Figure 3a shows that the amethyst color is caused by the typical absorption at 550 nm, leaving a window in the blue-purple region. The yellow citrine color is caused by the broad tail of an absorption in the ultra-violet region; this absorption peaks at about 240 nm, and is typical of natural citrine (Maschmeyer et al., 1980). Figure 3b shows that there is a remarkable difference between the two zones in the IR spectra. The citrine zone is dominated by a broad, isotropic band which is absent in the amethyst zone. This broad band correlates with absorption in the 1900 nm region which is characteristic of molecular water (Fig. 3c) and is due to small groups of water molecules trapped during rapid crystal growth (Aines et al., 1984; Aines and Rossman, 1984a, Chapter 2). These groups are not large enough to be considered fluid inclusions, probably ranging in size from ~ 5 to several hundred molecules.

The exact origin of the Bolivian 'ametrine' has not been revealed, so I have examined the color-H_2O relationships in a suite of known origin. These samples are found in quartz veins in deeply weathered granitic rock near Hyderabad, India, and have not been treated in any way. This was personally verified by R. H. Currier (Arcadia, CA), from whom I obtained the samples. These crystals contain a variety of amethyst and citrine zones, but are also often slightly altered and contain fluid inclusions. The same result is found as for the Bolivian

Figure 3. (Next two pages) A) Bolivian amethyst-citrine single crystal. Citrine-dashed trace. Amethyst-solid trace. Unpolarized. Sample 5.05 mm thick. B) IR spectra of same zones in crystal, 1.04 mm thick. Run at 77 K, polarized E$\perp$C. C) NIR expanded view of spectra in 3A, same conditions, showing the characteristic absorption due to molecular water.

3A)

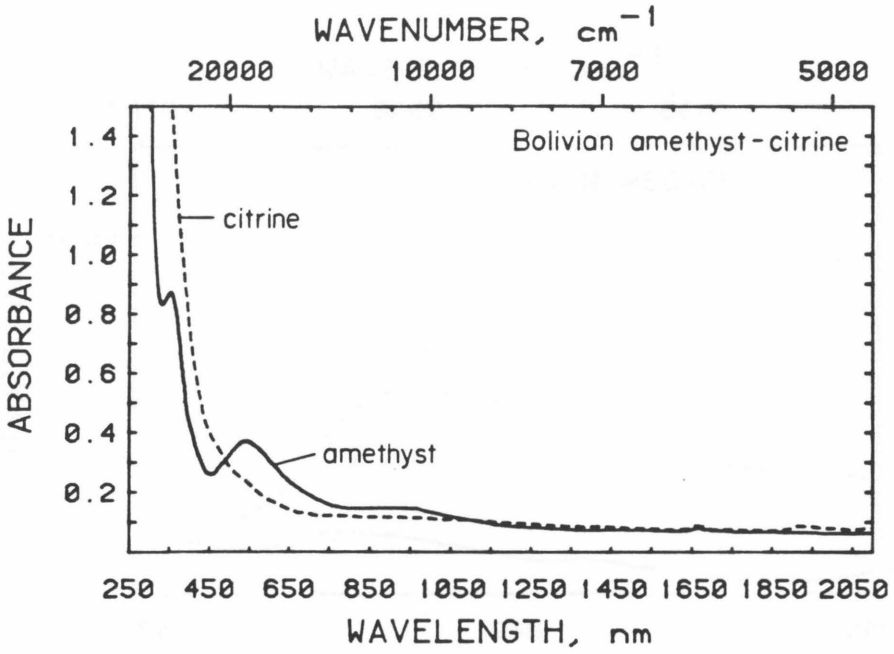
WAVENUMBER, cm⁻¹
20000
10000
7000
5000
Bolivian amethyst-citrine
citrine
amethyst
ABSORBANCE
1.4
1.2
1.0
0.8
0.6
0.4
0.2
250 450 650 850 1050 1250 1450 1650 1850 2050
WAVELENGTH, nm

3B)

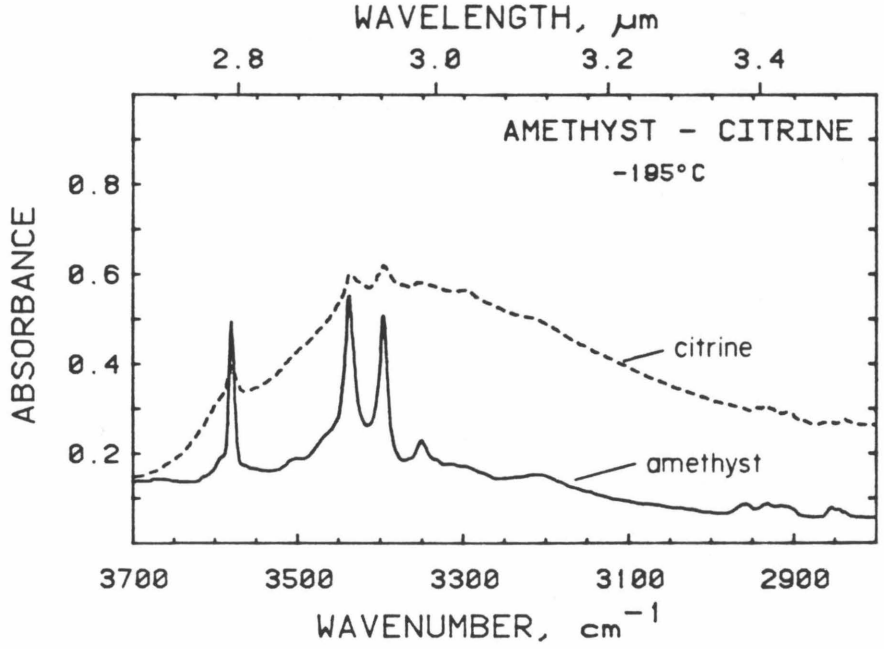
WAVELENGTH, μm
2.8
3.0
3.2
3.4
AMETHYST - CITRINE
-195°C
citrine
amethyst
ABSORBANCE
0.8
0.6
0.4
0.2
3700
3500
3300
3100
2900
WAVENUMBER, cm⁻¹

3C)

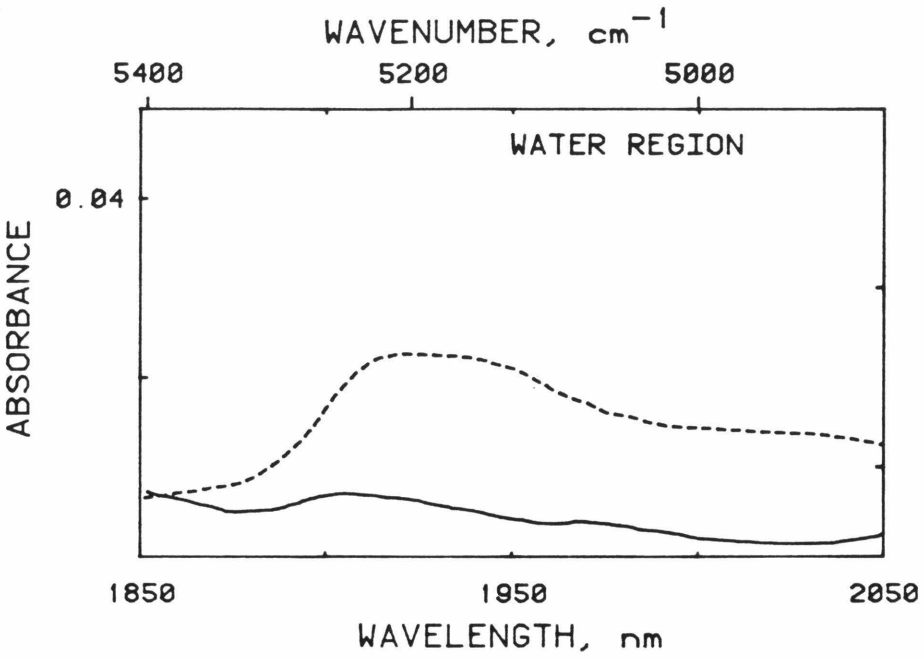
WAVENUMBER, cm⁻¹
5400
5200
5000
WATER REGION
0.04
ABSORBANCE
1850
1950
2050
WAVELENGTH, nm

samples, however. Figure 4 shows the inverse correlation between absorption at 550 nm (amethyst color) and absorption at 1920 nm (H_2O) for the Indian and Bolivian samples. The Indian samples can contain amethyst and citrine areas in the same growth zone (r or z), but the H_2O-correlation is independent of that. Amethyst only occurs in low H_2O zones. The minimum H_2O concentration for the Indian samples appears to correspond to a background due to fluid inclusions (water groups much larger than those previously discussed, Aines and Rossman, 1984a, Chapter 2).

It has been suggested that the citrine color center is related to lithium content, based on the intensity of the Li(H) defect IR absorption at 3396 cm^{-1} (Kats, 1962; Bukanov and Markova, 1969; Maschmeyer et al., 1980). However, in the Bolivian ametrine samples this peak is clearly less intense in the citrine sector than in the amethyst sector. However, Kats (1962) points out that this peak is only an indicator of Li(H) defect concentration and does not respond to Li(Al) defects.

One final piece of evidence may be obtained from the experience of the Soviet efforts at producing synthetic amethyst. They found that in order to obtain flawless amethyst, the crystals must be grown slowly (0.3-0.8mm/day) and in a Na-free solution (Balitsky, 1977). These slow growth rates correspond to those shown to result in a minimum uptake of total hydrogen under the same conditions (350°C, basal growth) for Bell Labs synthetic quartz (Figure 5; Kirby, 1984). Aines et al. (1984) have shown that 'water' speciation is entirely as hydroxyl at these low concentrations, and that higher concentrations result from the

Figure 4. (Next page) Relationship between peak intensity at 550 nm (amethyst) and 1920 nm (molecular H_2O) for amethyst-citrine. Measured using unpolarized spectra. 550 nm baseline drawn from 450 to 700 nm as a straight line, 1920 baseline from 1870 to 2100 nm. Symbols - triangle, amethyst zone in a growth sector containing only amethyst; cross, citrine; circle, amethyst or colorless in a sector containing citrine. Filled symbols, Bolivian samples (Fig. 3).

4)

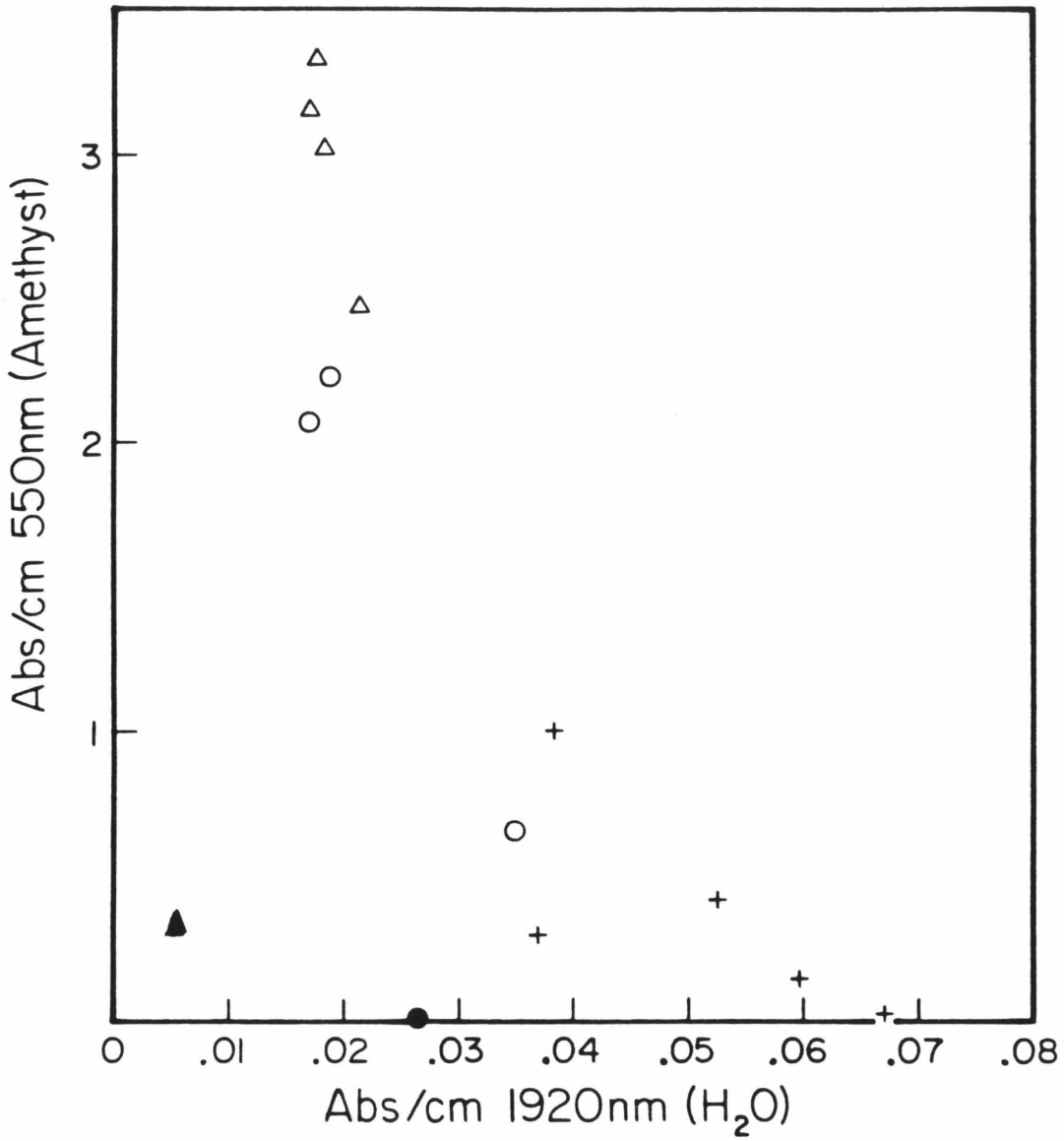
Abs/cm 550nm (Amethyst)
3
2
1
0
.01
.02
.03
.04
.05
.06
.07
.08
Abs/cm 1920nm (H_2O)

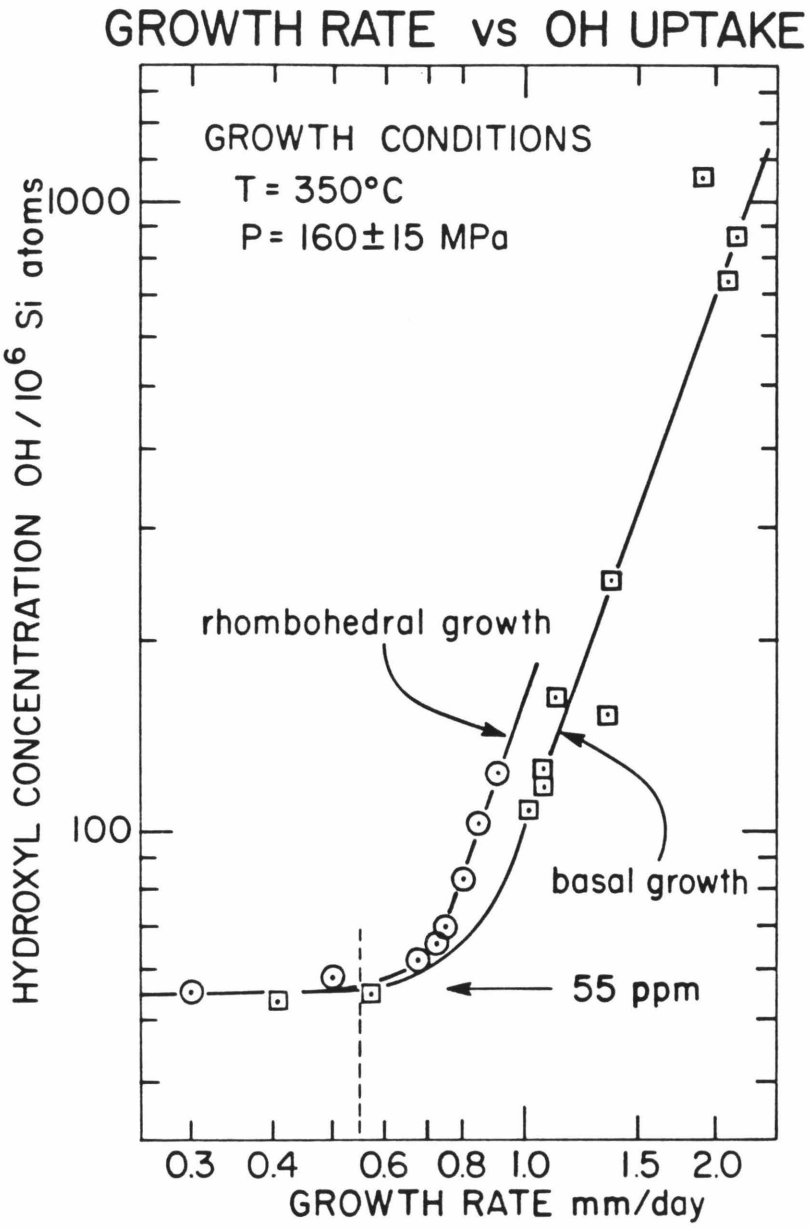

Figure 5. Growth rate versus total OH uptake (includes OH^- and H_2O), for Bell Labs synthetic quartz from Kirby, 1984.

additional incorporation of molecular water. This molecular water is incorporated in the Bell Labs crystals in a 5:1 atomic ratio with sodium. Apparently the successful Soviet technique involves complete elimination of molecular water from the amethyst starting material.

The evidence presented here suggests that the presence of molecular water strongly favors the formation of the citrine color center by ionizing radiation, and that the amethyst color center's formation is suppressed by the presence of molecular water. The citrine correlation is entirely consistent with the suggestion of Maschmeyer et al. that molecular water stabilizes the Si defect which is an integral part of the citrine color center.

The inverse correlation between amethyst color and molecular water may be explained by hypothesizing that radiolysis of water produces atomic hydrogen that may freely move through the quartz reducing the Fe^{4+} color centers to Fe^{3+}. The production of hydrogen through water radiolysis is well known (e.g. Dragnić and Dragnić, 1971, p. 38), and atomic hydrogen has been detected by EPR in synthetic quartz (Weeks and Abraham, 1965), natural 'rose' quartz (Rinnenberg and Weil, 1972), synthetic CaF_2 (Hall and Schumacher, 1962) and the mineral brasilianite (Hill and Lehmann, 1978). In all cases except the brazilianite, the hydrogen was unstable above 77 K, but in brasilianite it can persist to 450 K. The low stability of atomic hydrogen in quartz is probably a function of its extreme reactivity and mobility. However, the water from which hydrogen is formed must apparently be dispersed throughout the mineral and not in fluid inclusions which can trap the radicals produced by radiolysis. The Soviet amethyst effort was successful when

molecular water was completely excluded, eliminating hydrogen formation during irradiation. In the amethyst-citrine natural samples, the amethyst cannot form where too much molecular water is present, and either citrine or no coloration results.

Topaz

Irradiation can produce two common colors in topaz: brown and blue. The blue color does not appear to be related to hydrogen in any way. However, there is a strong correlation between the brown color and anomalous OH sites. Topaz contains one (OH^-, F^-) site and should yield an IR spectrum containing one peak due to hydroxyl. However, it is common for topaz to exhibit a number of absorptions in the O-H stretching region and some of these absorptions in the O-H stretching region correlate with the brown coloration in zoned, irradiated samples (Fig. 6). In Figure 6, the anticipated stretching mode is at 3650 cm^{-1} and the anomalous peaks occur at 3460 and 3425 cm^{-1}. The remainder of the absorptions are sum and difference modes centered on the 3650 cm^{-1} fundamental; the low frequency set disappears when cooled to 77 K, and this has been done to obtain the remainder of the topaz spectra in this paper.

The brown coloration in natural topaz is due to two components, a peak at 460 nm and a broad tail extending from the ultra-violet region into the visible region (Fig. 7a). Additional irradiation of natural brown topaz from the Thomas Mts. rhyolite (Utah) causes an increase in both components; the increased components are shown in Figure 7b. The Thomas Mountains samples are very fluorine rich, and accordingly

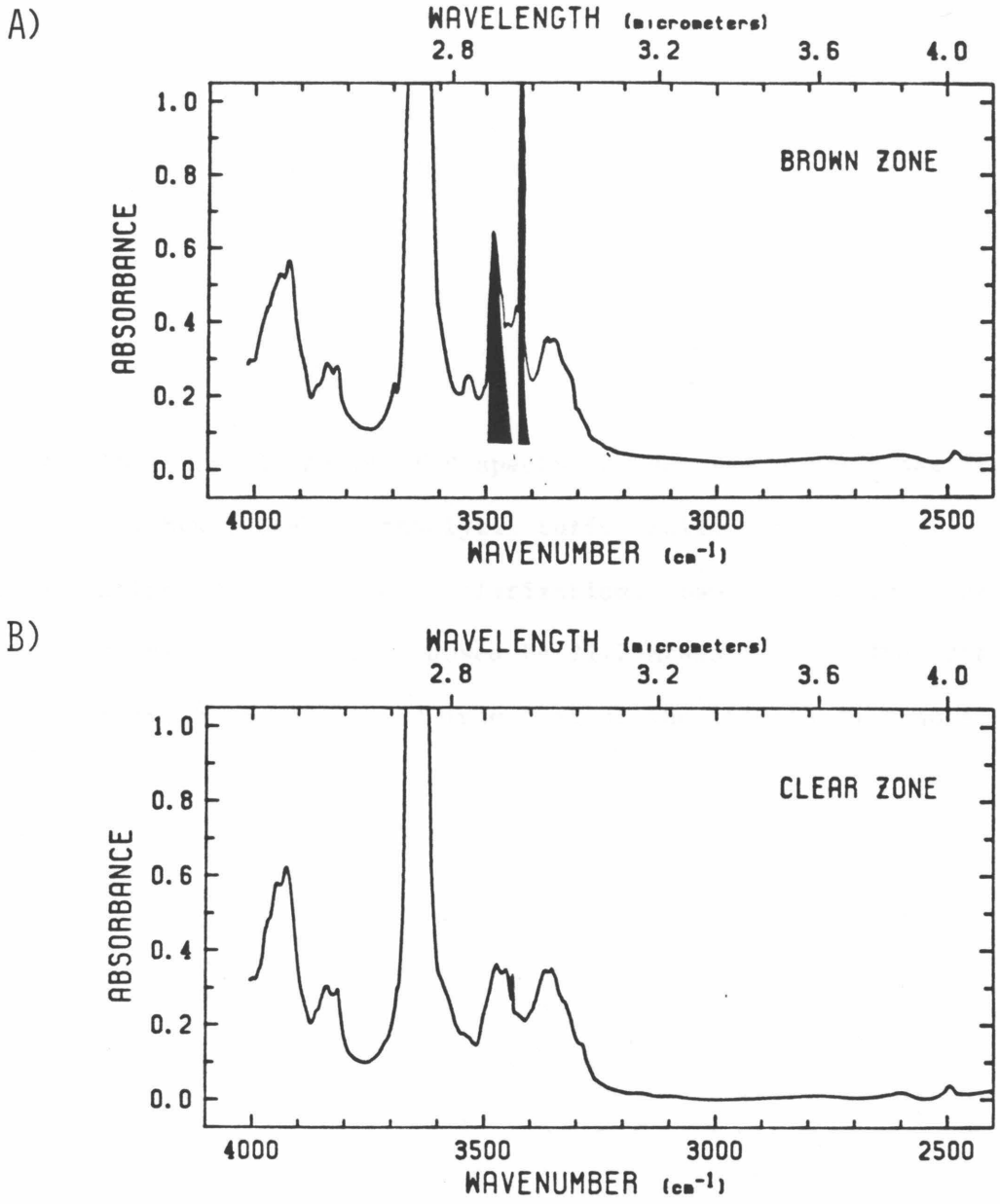

Figure 6. Comparison of brown (A) and colorless (B) zones in an irradiated Brazilian topaz. Polarized in α direction, sample 0.70 mm thick. Run at 307 K. The peaks unique to the brown zone are shown in black.

Figure 7. (Next page) A) VIS-NIR spectra of natural brown topaz from the Thomas Mts., Utah, a rhyolytic tuff. Solid trace-β polarization, Dashed trace-α polarization. Sample 7.00 mm thick B) The increase in coloration caused by 21.7 Mrads ^{137}Cs. The original spectrum has been subtracted from that of the irradiated sample.

7A)

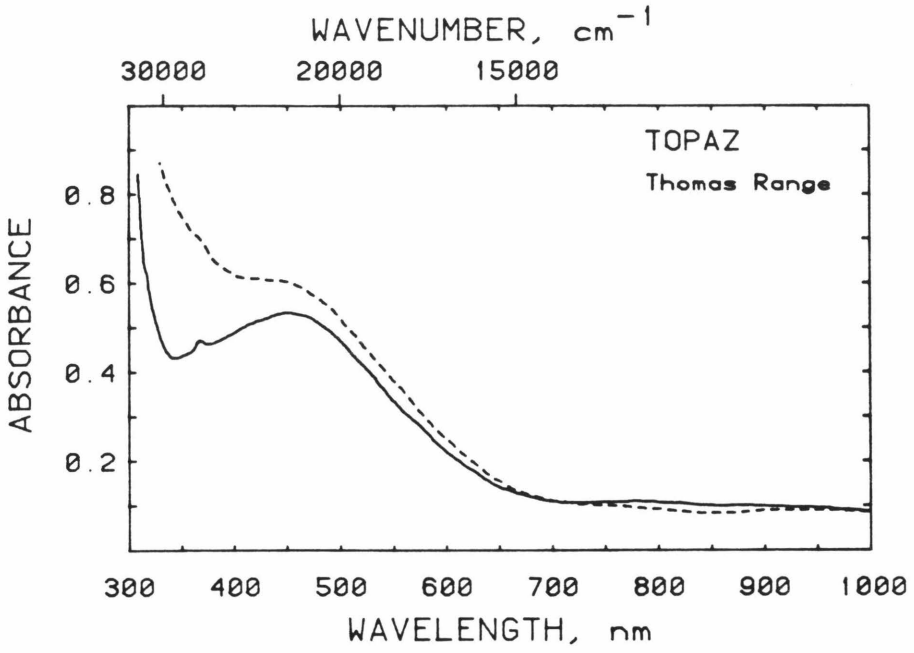
WAVENUMBER, cm^{-1}
30000
20000
15000
TOPAZ
Thomas Range
ABSORBANCE
0.8
0.6
0.4
0.2
300
400
500
600
700
800
900
1000
WAVELENGTH, nm

7B)

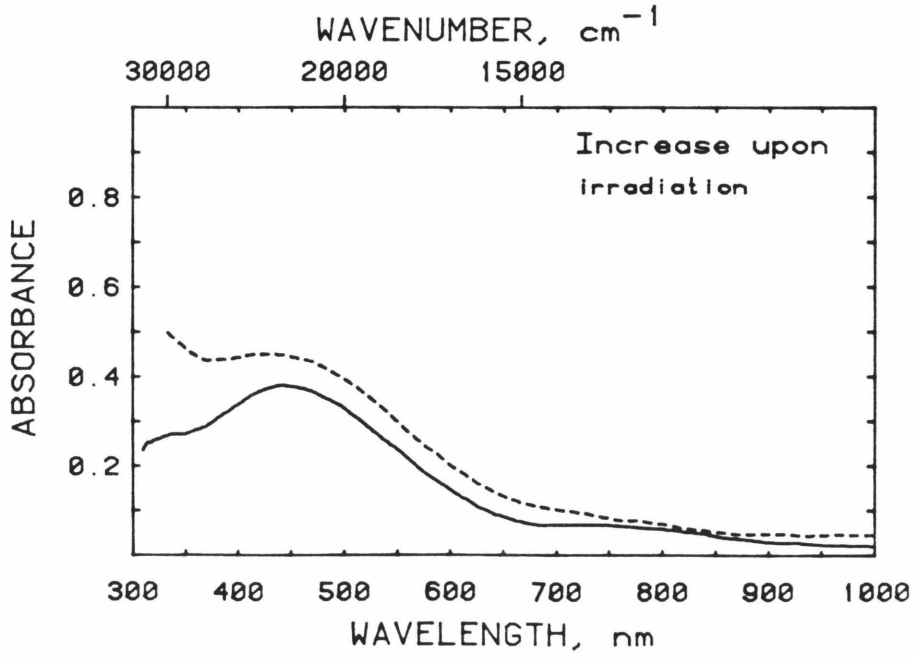
WAVENUMBER, cm^{-1}
30000
20000
15000
Increase upon
irradiation
ABSORBANCE
0.8
0.6
0.4
0.2
300
400
500
600
700
800
900
1000
WAVELENGTH, nm

hydroxyl poor. The anticipated fundamental OH^- absorption at 3650 cm^{-1} is dominated by anomalous absorptions in the 3400-3450 cm^{-1} region (Fig. 8a). The infrared spectrum undergoes a marked change after irradiation, with the 3400-3450 peaks undergoing a net decrease in intensity, although one component increased (Fig. 8b). There was no net change in the 3650 cm^{-1} fundamental.

In order to further examine these relationships, I have studied an e^- irradiated topaz sample from Brazil containing 2 shades of brown, and a light blue zone. As is usual in irradiated topaz the boundaries between the colors are sharp and planar, although some smaller areas can exist which also have sharp boundaries. In this crystal, all the color boundaries are co-planar with the prism faces of the sample. The VIS-NIR spectra after irradiation are shown in Figure 9a. The same brown-producing absorptions are seen as in the Thomas Mts. samples, and an additional absorption resulting in the blue color is seen at 640 nm. The differences in the optical region are accompanied by differences in the infrared. Although both the brown and blue zones contain a large number of anomalous IR absorptions, they are more intense in the brown zone and are dominated by absorptions in the 3400-3450 region as in the Thomas Mts. samples. (The lighter brown zone is intermediate in behavior in the infrared to the two shown.) These spectra were collected at 77 K to eliminate the difference bands which at 300 K occur as mirror images (around the 3650 fundamental) to the high frequency peaks in the 3800-4200 cm^{-1} region at 77 K.

This sample was bleached using two methods; 4 hrs of direct sunlight and 10 minutes at 550 K. The sunlight bleaching only affected the 460

Figure 8. (Next page) A) IR of untreated topaz from Thomas Mts. shown also in Figure 7. The anticipated peak at 3650 cm^{-1} is dominated by the peaks at 3400-3450 cm^{-1} caused by anomalous OH species. Sample 1.37 mm, solid trace-β plarization. Dotted trace-α polarization. Run at 307 K. B) The difference in the IR spectrum after irradiation (see Fig. 7) showing a decrease in the majority of the 3400-3500 cm^{-1} absorptions which is associated with the formation of the brown color.

8A)

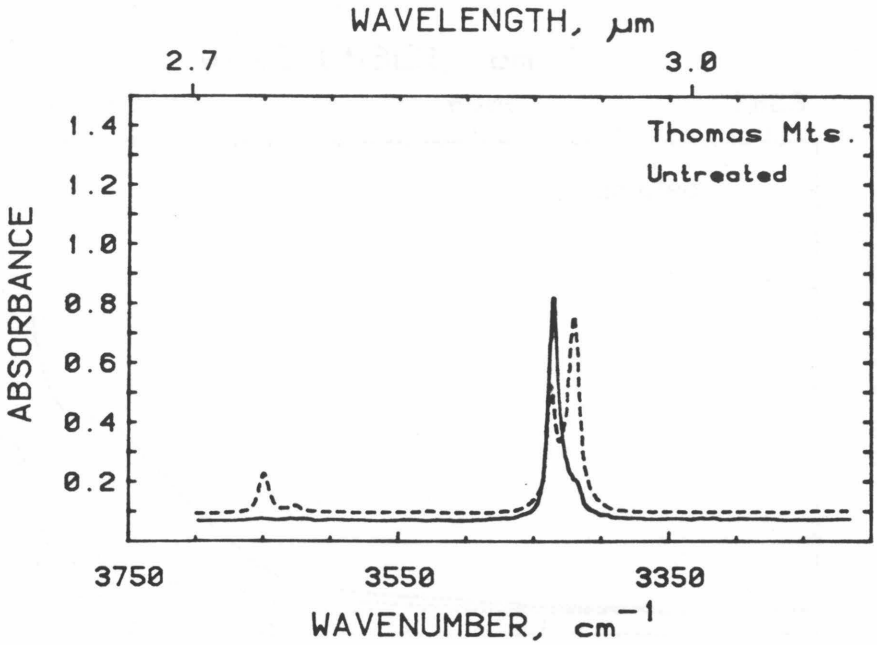
WAVELENGTH, μm
2.7
3.0
Thomas Mts.
Untreated
ABSORBANCE
1.4
1.2
1.0
0.8
0.6
0.4
0.2
3750
3550
3350
WAVENUMBER, cm⁻¹

8B)

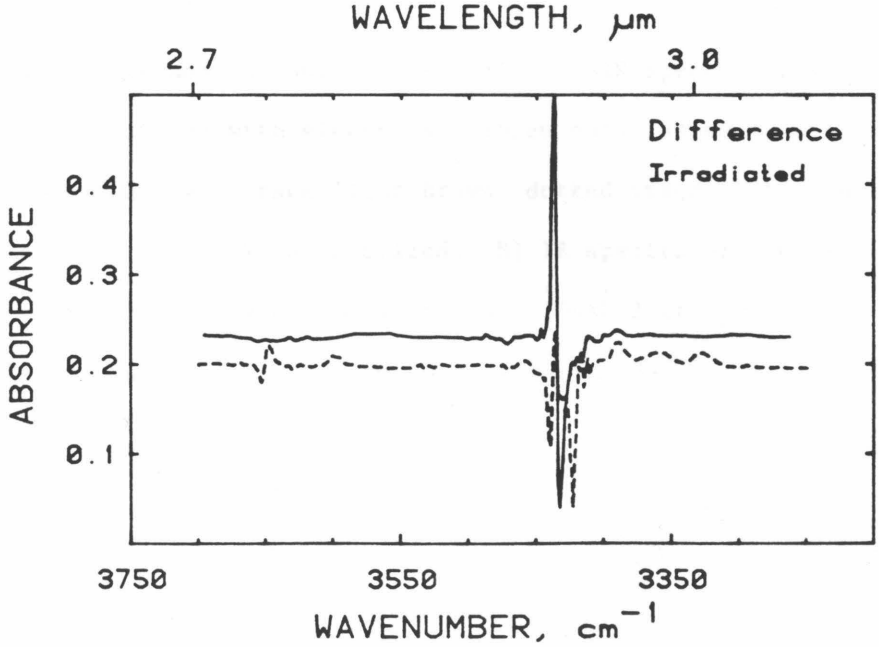
WAVELENGTH, μm
2.7
3.0
Difference
Irradiated
ABSORBANCE
0.4
0.3
0.2
0.1
3750
3550
3350
WAVENUMBER, cm⁻¹

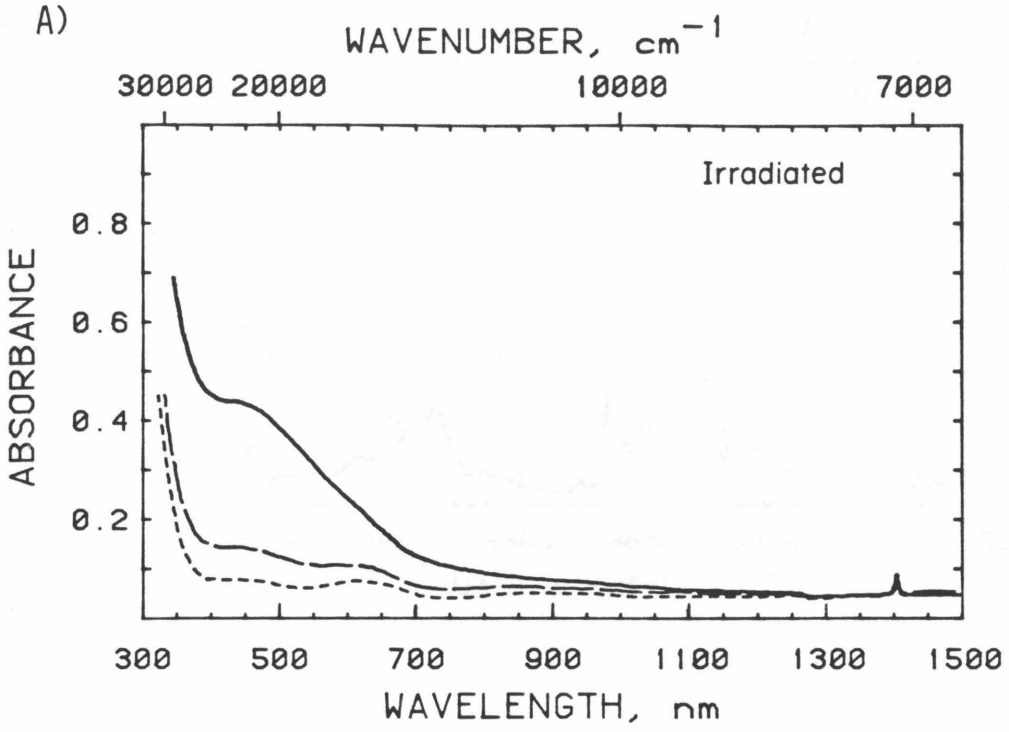

Figure 9. (This and following page) A) VIS-NIR spectra of Brazilian topaz irradiated with electrons. Three color zones exist; solid trace-brown; dash trace-light brown; dotted trace-light blue. Sample 1.0 mm thick, α polarized. B) IR spectra of the brown zone at 77 K. Solid trace-β polarization. Dashed trace-α polarization. C) Light blue area, same as (B).

9B)

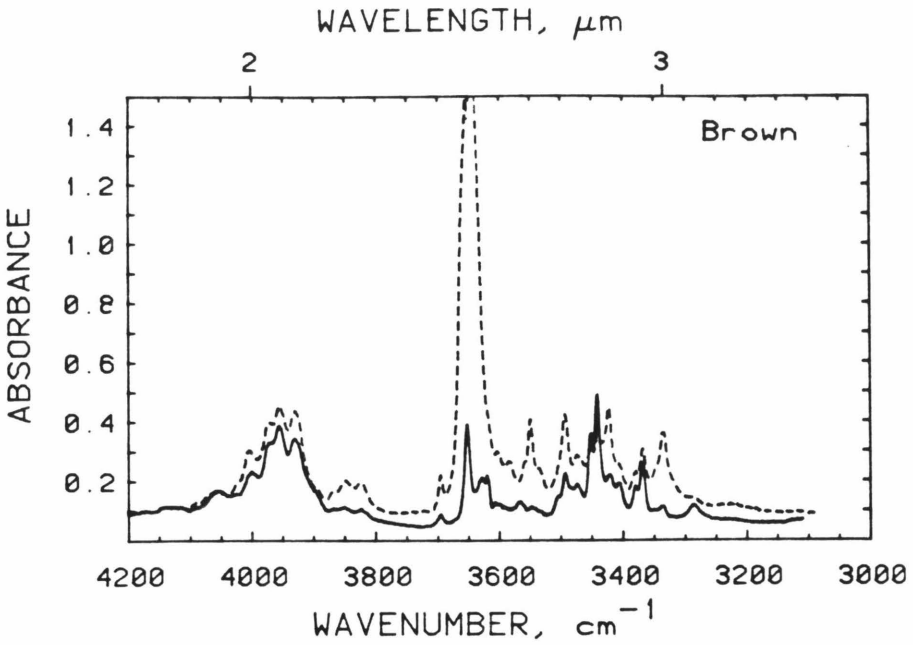
WAVELENGTH, μm
2
3
Brown
ABSORBANCE
1.4
1.2
1.0
0.8
0.6
0.4
0.2
4200
4000
3800
3600
3400
3200
3000
WAVENUMBER, cm⁻¹

9B)

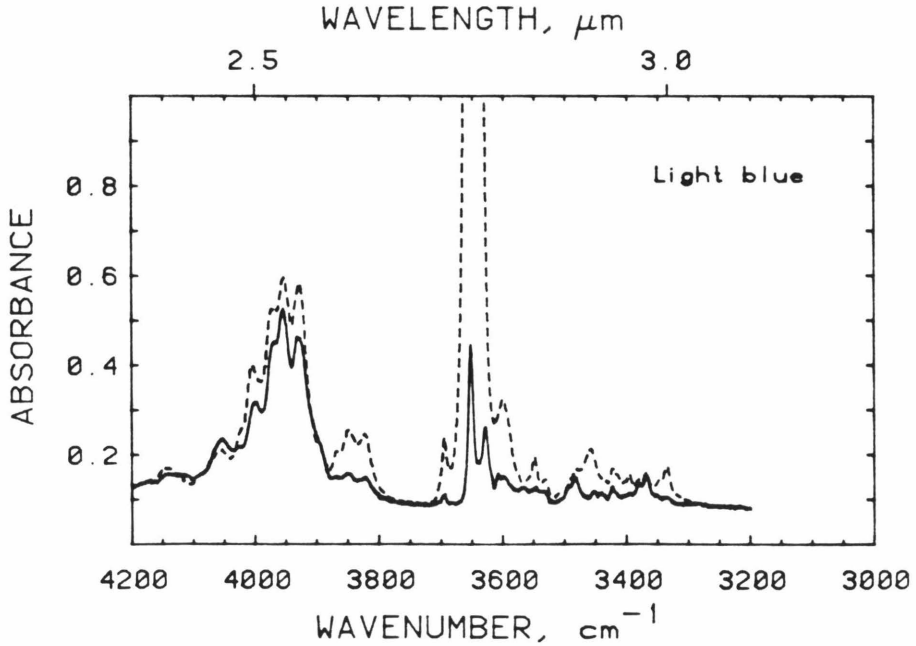
WAVELENGTH, μm
2.5
3.0
Light blue
ABSORBANCE
0.8
0.6
0.4
0.2
4200
4000
3800
3600
3400
3200
3000
WAVENUMBER, cm⁻¹

nm peak (Figure 10) and had no effect on the infrared spectra of any of the color zones. The effect on the 460 nm peak was the same in all color zones.

Heating the sample for 10 minutes at 500 K resulted in dramatic changes in both the visible and infrared spectra. All traces of brown color disappeared. Figure 11 shows the changes in the IR region (bleached minus unbleached). The effects in the 3300-3450 cm^{-1} region are opposite those seen in the Thomas Mts. sample after irradiation, as might be expected. There is also increased absorption in the 3500 cm^{-1} region, where no absorptions occur in the Thomas Mts. samples. Figure 12 compares the changes in the three color zones. There is a definite correlation between the intensity of the IR changes and those in the VIS-NIR region.

It appears that the radiation damage center associated with the anomalous hydrous components is only the more stable brown color caused by the absorption tail from the ultraviolet region. Neither the blue color, nor the less stable (sun-bleachable) brown component resulting from the absorption at 460 nm is associated with a hydrous species. Dickinson and Moore (1967) correlated an ESR active center with a yellow-brown radiation produced color in topaz. They assign this hole center to an O^- attached to Si, surrounded by 6 F^- atoms. It is not clear which of the two brown colors observed in this study that might represent, since they present no optical spectra. However, this is a very similar kind of hole center to that causing the smoky color in quartz, in which both an election and a proton diffuse away from the hole center. This could be the mechanism responsible for the coupling

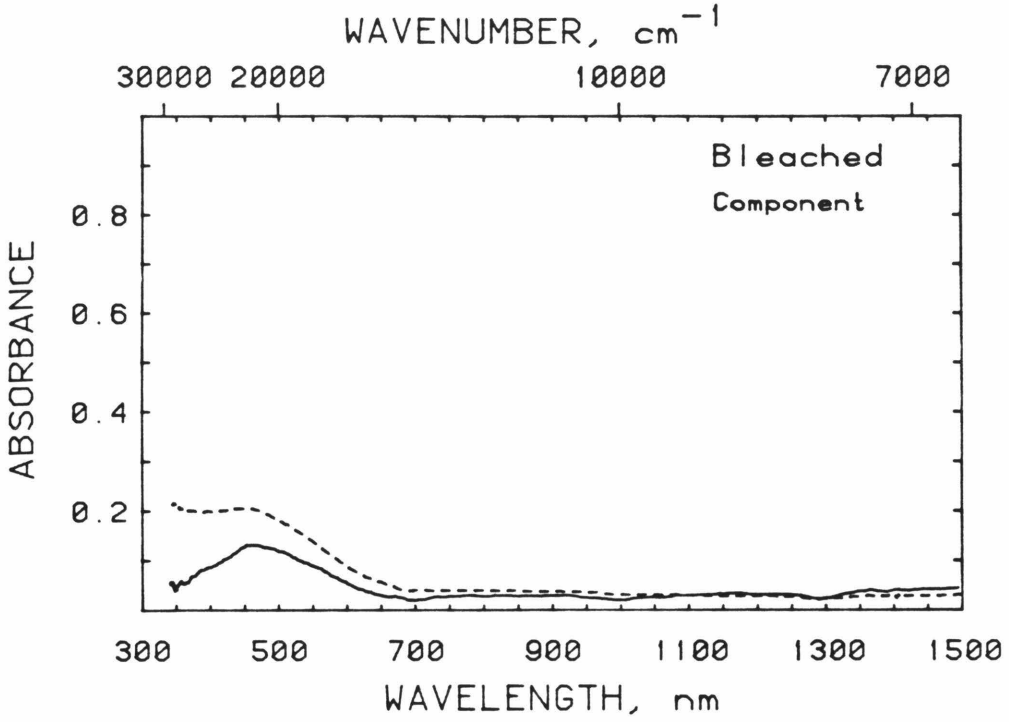

Figure 10. The component bleached from the brown zone of the sample in Figure 9 by 4 hrs of direct sunlight (difference spectrum, untreated minus bleached). Solid trace-β, dashed trace-α.

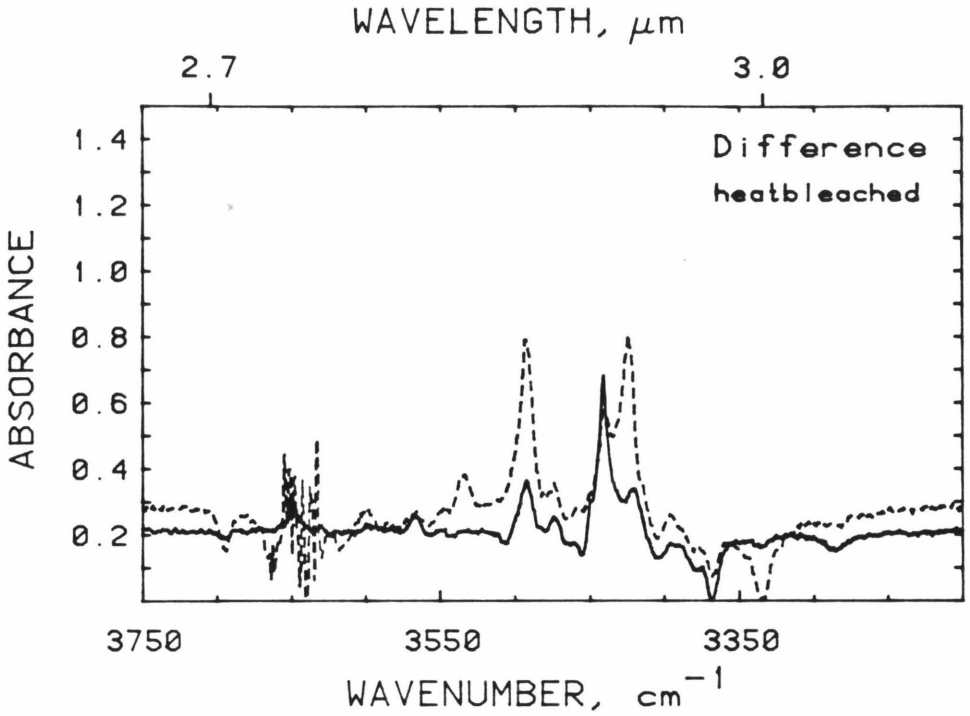

Figure 11. Changes in the IR spectrum of the e^- irradiated Brazilian topaz (brown zone) brought on by heating for 10 minutes at 500 K. Bleached spectra minus unbleached (positive deviations represent and increase in intensity during bleaching). Obtained at 77 K. Solid trace-β, dashed trace-α. Sample 1.0 mm thick.

Figure 12. (Next page) Comparison of changes in the VIS-NIR region with those in the IR after heating of e^- irradiated topaz. VIS-NIR difference is unbleached minus bleached, the opposite of the IR. Upper trace-brown zone; middle trace-light brown zone; lower trace-light blue zone. Both IR and VIS-NIR spectra and β-polarized, sample 1.0 mm thick. IR spectra obtained at 77 K, VIS-NIR at 300 K.

12A)

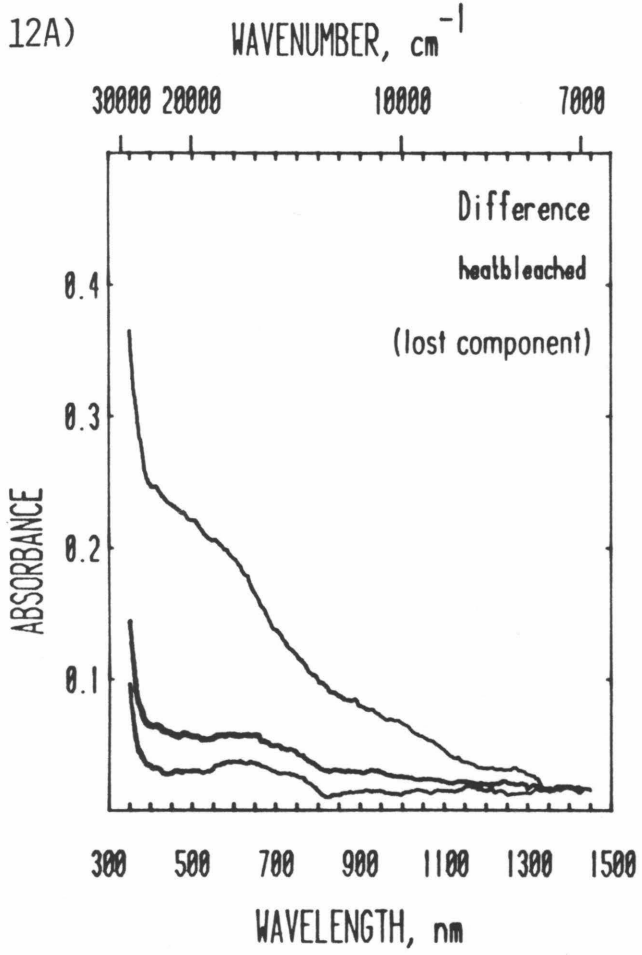
WAVENUMBER, cm-1
30000 20000 10000 7000
Difference
heatbleached
(lost component)
0.4
0.3
0.2
0.1
ABSORBANCE
300 500 700 900 1100 1300 1500
WAVELENGTH, nm

12B)

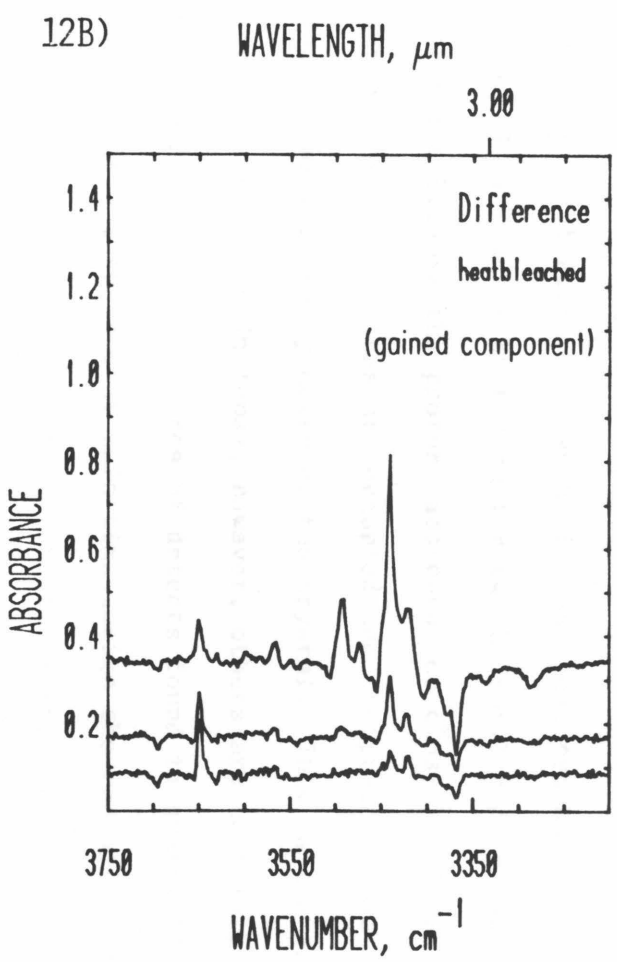
WAVELENGTH, μm
3.00
Difference
heatbleached
(gained component)
1.4
1.2
1.0
0.8
0.6
0.4
0.2
ABSORBANCE
3750 3550 3350
WAVENUMBER, cm-1

of radiation damage to the hydrous component in topaz; an (OH^-, F^-) site containing F^- could not form such a hole center. However, the anomalous nature of the participating hydrous component suggests that there is an additional hydroxyl site. One such site has been proposed by Parise et al (1980). They suggest that normally two hydroxyl groups cannot occupy adjacent sites because the protons approach too closely. However, there are samples where such sites are occupied and the protons move to new positions, lowering the symmetry of the crystal. This is the only known anomalous hydrogen site in topaz, however, others are certainly possible. For example, the types of defects found in quartz (Kats, 1962) may occur. I can not at this time assign the radiation-active proton species to a specific site in the topaz structure.

CONCLUSIONS

Although the presence of a hydrous component can apparently hinder (smoky quartz, amethyst) or help (amazonite, zircon, topaz) the course of radiation damage, it is now possible to identify some actual mechanisms responsible for the interaction and observe that the mobility and reactivity of hydrogen species in silicates are responsible for the relationship between radiation damage and hydrous species. Whether this appears to help or hinder the damage depends on the viewpoint. In the cases discussed here, hydrogen species are involved in annealing local and long distance charge imbalances, and as such are hindering total radiation damage despite the possibility that a new color (for instance) may result from this process. The mobility of protons and atomic hydrogen at room temperature make it possible for a small amount of a hydrous component to control the radiation behavior of a crystal. This coupled with the large number of possible hydrogen species, makes hydrogen a unique participant in the radiation damage process.

ACKNOWLEDGMENTS

I would like to thank Drs. Jim Woodhead and Leon Silver (Caltech) for helpful discussions and collaboration in the study of zircon metamictization. R. H. Currier (Arcadia, CA) provided and carefully described the history of the Indian amethyst-citrine samples. Other samples were provided by Kurt Nassau, Bell Labs, and by Vince Manson of the Gemological Institute of America, (Santa Monica, CA). J. B. Parise provided helpful discussions on topaz and kindly shared his samples with us. This work funded, in part, by National Science Foundation grants EAR-7723147, EAR-79-19987, EAR-83-13098.

REFERENCES

Acocella, J., Takata, M., Tomozawa, M., Watson, E.B., and Warden, J.T. (1982) Effect of γ radiation on high-water-content glasses. Journal of the American Ceramic Society, 65, 407-410.

Aines, R.D. and Rossman, G.R. (1984a) Water in minerals? A peak in the infrared. Journal of Geophysical Research (in press).

Aines, R.D. and Rossman, G.R. (1984b) The significance of infrared band shapes and positions in hydrogen-bonded systems. In preparation, 1984.

Aines R.D., Rossman, G.R., and Kirby, S. (1984) Hydrogen speciation in synthetic quartz. Physics and Chemistry of Minerals, in press.

Amthauer, G. and Rossman, G.R. (1984) Mixed valence of iron in minerals with cation cluster. Physics and Chemistry of Minerals (in press).

Arnold, G.W. and Compton, W.D. (1959) Radiation effects in silica at low temperatures. Physical Review, 116, 802-811.

Balitsky, V.S. (1977) Growth of large amethyst crystals from hydrothermal fluoride solutions. Journal of Crystal Growth, 41, 100-102.

Bukanov, V.V. and Markova, G.A. (1969) The smoky and citrine colors of natural quartz. Doklady Akadamii Nauk SSSR. Translations, Earth Science Sections, 187, 115-117, (translated from vol. 187, 647-647).

Chakraborty, D. and Lehmann, G. (1978) On the fine structure in the infrared spectra of clear natural quartz, amethyst, citrine, and synthetic quartz crystals. Zeitschrift für Naturforschungen, 33a, 290-293.

Cox, R.T. (1976) ESR of an S=2 center in amethyst quartz and its possible identification as the d^4 ion Fe^{4+}. Journal of Physics, C: Solid State Physics, 9, 3355-3361.

Cox, R.T. (1977) Optical absorption of the d^4 ion Fe^{4+} in pleochroic amethyst quartz. Journal of Physics, C: Solid State Physics, 10, 4631-4643.

Dennen, W.H. and Puckett, A.M. (1972) On the chemistry and color of amethyst. Canadian Mineralogist, 11, 448-456.

Dickinson, A.C. and Moore, W.J. (1967) Paramagnetic resonance of metal ions and defect centers in topaz. Journal of Physical Chemistry, 71, 231-240.

Dragnić, I. and Dragnić, Z. (1971) The Radiation Chemistry of Water. Academic Press, New York.

Ewing, R.C. and Headley, T.J. (1983) Alpha-recoil damage in natural zirconolite ($CaZrTi_2O_7$). Journal of Nuclear Materials, 119, 102-109.

Faile, S.P. and Roy, D.M. (1970) Mechanism of color center destruction in hydrogen impregnated radiation resistant glasses. Materials Research Bulletin, 5, 385-390.

Hall, J.L. and Schumacher, R.T. (1962) Electron spin resonance of hydrogen atoms in CaF_2. Physical Review, 127, 1892-1912 and 131, 2839.

Hartwig, C.M. (1976) The radiation-induced formation of hydrogen and deuterium compounds in silica as observed by Raman scattering. Journal of Chemical Physics, 66, 227-238.

Hill, F. and Lehmann, G. (1978) Atomic hydrogen in the mineral brasilianite $NaAl_3(PO_4)_2(OH)_2$. Zeitschrift für Naturforschungen, 33a, 1484-1486.

Hofmeister, A.M. (1983) A spectroscopic and chemical study of the coloration of feldspars by irradiation and impurities, including water. Thesis, California Institute of Technology.

Kats, A. (1962) Hydrogen in alpha-quartz. Philips Research Reports, 17, 133-195 and 201-279.

Kirby, S.H. (1984) Hydrogen-bonded hydroxyl in synthetic quartz: analysis, mode of incorporation, and role in hydrolytic weakening. Physics and Chemistry of Minerals, in press.

Lehmann, G. and Bambauer, H.U. (1973) Quartz crystals and their colors. Angewandte Chemie International, 12, 283-291.

Mackey, J.H. Jr. (1963) EPR study of impurity-related color centers in germanium doped quartz. Journal of Chemical Physics, 39, 74-80.

Maschmeyer, D., Niemann, K., Hake, H., Lehmann, G., Raüber, A. (1980) Two modified smoky quartz centers in natural citrine. Physics and Chemistry of Minerals, 6, 145-156.

Parise, J.B., Cuff, C., and Moore, F.H. (1980) A neutron diffraction study of topaz; evidence for lower symmetry. Mineralogical Magazine, 43, 943-944.

Ribbe, P.H. and Gibbs, G.V. (1971) The crystal structure of topaz and its relation to physical properties. American Mineralogist, 56, 24-30.

Rinnenberg, H. and Weil, J.A. (1972) EPR studies of Ti^{3+}-H^{+} centers in X-irradiated α-quartz. Journal of Chemical Physics, 56, 2019-2028.

Rossman, G.R. (1975) Joaquinite: the nature of its water content and the question of four-coordinated ferrous iron. American Mineralogist, 60, 435-440.

Shelby, J.E. (1979) Radiation effects in hydrogen-impregnated vitreous silica. Journal of Applied Physics, 50, 3702-3706.

Stock, H.D. and Lehmann, G. (1977) Phenomena associated with the diffusion of trivalent iron in amethyst quartz. Journal of Physics and Chemistry of Solids, 38, 243-246.

Van Wieringen, J.S., Kats, A. (1957) Paramagnetic resonance and optical investigation of silicate glasses and fused silica, coloured by X-rays. Philips Research Reports, 12, 432-454.

Weeks, R.A. and Lell, E. (1964) Relation between E' centers and hydroxyl bonds in silica. Journal of Applied Physics, 35, 1932-1938.

Weeks, R.A. and Abraham, M. (1965). Electron spin resonance of irradiated quartz: atomic hydrogen. Journal of Chemical Physics, 42, 68-71.

Weil, J.A. (1975) The aluminum centers in α-quartz. Radiation effects, 26, 261-265.

Yada, K., Tanji, T., Sunagawa, I. (1981) Application of lattice imagery to radiation damage investigation. Physics and Chemistry of Minerals, 7, 47-52.

Chapter 7

The High Temperature Behavior of Trace Hydrous Components in Silicates.

Abstract

I have studied the high temperature behavior of water and hydroxide in quartz, feldspar, topaz, zircon, muscovite, cordierite, and beryl using high temperature infrared spectroscopy. With this technique I can observe directly processes such as dehydration and changes in hydrogen speciation. In muscovite, no changes in speciation occur prior to dehydration at 750°C, whereas in topaz there is an interconversion of hydroxyl sites at 500°C. In metamict zircon there is a preferential loss of strongly hydrogen-bonded hydroxyl (from a continuum of sites) during a continuous dehydration occurring from 400° to 900°C. There may be minor changes in the O-H region spectrum of natural quartz at the $\alpha - \beta$ transition point, but a reversible broadening of the numerous hydroxyl peaks makes this difficult to quantify. In feldspar, there is a loss of one type of molecular water at ~200°C, and at 600° to 800° a second water type converts irreversibly to a new hydrous species.

Results typical to all minerals studied are a temperature broadening of the infrared absorption peaks, a shift to lower wavenumbers with temperature, and a slight increase in integral intensity accompanying dramatic decreases in peak height brought on by broadening. Lattice modes also broaden and shift to lower wavenumbers, typically with temperature coefficients of about .03 $cm^{-1}/°C$. Temperature coefficients for O-H stretching peaks range from 0 to 0.045 $cm^{-1}/°C$.

The most important result of this study is the observation that in some minerals trace hydroxyl and water speciation and properties at temperatures of geologic interest can be dramatically different from the speciation properties at 25°C.

Introduction

Studies of minerals and their properties usually utilize measurements at or near 25°C. This is experimentally convenient but may only provide a limited insight into the properties of minerals at the elevated temperatures typical of conditions of geologic interest. Trace "water" in silicates can have a substantial effect on the properties of minerals (e.g. Aines and Rossman, 1984a,d, Chapters 2 and 6; Kekulawala et al., 1978; Hobbs, 1981), but because of the reactivity and mobility of hydrous components in minerals it cannot be assumed that the high temperature speciation and sites of hydrous components are the same as those at room temperature. Accordingly, I have undertaken a study of trace hydrous components at elevated temperature in order to understand the types of behavior that may be expected of trace water under geologic conditions.

I have used infrared spectroscopy in this study because of infrared (IR) spectroscopy's sensitivity to O-H bonds, and because spectra may be obtained at elevated temperatures, allowing direct interpretation. This technique has been used previously largely to study glasses (e.g. Wedding, 1975; Stein and Shankland, 1981) and minerals (Aronson et al., 1970; Shankland et al., 1979) in order to determine their thermal conductivity. Studies of hydrous components at elevated temperature are limited to glasses (Wedding, 1975), $Mg(OH)_2$ (Freund, 1970, 1974), and other synthetics (Freund, 1974; Aines and Rossman, 1984c, Chapter 3 and references therein). We have previously reported on the high temperature behavior of water and carbon dioxide in cordierite and beryl (Aines and Rossman, 1984b, Chapter 8) and will report additional aspects of that study here. The theoretical basis for peak shifts and shape

changes caused by temperature changes is discussed in Aines and Rossman, (1984c, Chapter 3).

I use the term trace water to refer to hydrous components of any species when that species has not been identified. The only oxygen-hydrogen species in minerals for which firm evidence exists are hydroxyl (OH^-) and molecular water (H_2O) (Aines and Rossman, 1984a, Chapter 2). Other possible hydrogen species in silicates are oxonium, H_3O^+, silicon hydride groups, SiH, and atomic and molecular hydrogen. Although these have been proposed to exist based upon bulk analytical evidence, the only ones firmly established to exist are atomic and molecular hydrogen which may be formed by intense radiolysis of minerals (see Aines and Rossman, 1984d, Chapter 6, and references therein). Unfortunately, these species have no IR manifestation and are undetectable in my studies. However, an important goal of high temperature work is to closely examine whether such exotic species as those above may exist at high temperatures and convert to water and hydroxyl at low temperatures.

Experimental Method

High Temperature Apparatus

Spectra were obtained at high temperature by placing the sample in a small tube furnace, along the length of which the beam from the spectrometer could pass. The samples were mounted on stainless steel apertures which completely filled the cross-section of the furnace, allowing light only to pass through the sample. The furnace is contained in a vacuum dewar with KCl windows for the beam to pass through; this eliminates heating of the spectrometer and also avoids oxidation of furnace parts. Details of the construction of each of these parts follow.

Furnace. The furnace and sample assembly are shown schematically in Figure 1. The furnace tube is mullite, 4.5" long with a 0.9" ID and 1.0" OD. The exterior is grooved to accept the windings; the interior is smooth. The furnace is wound with 8.75 ft of Pt(80%)-Rh(20%) wire designed to be operable to 1400°C. The total electrical resistance is 14.0 ohms at 25°C. An applied a-c potential of approximately 80 volts is required to operate at 1200°C. The furnace temperature is controlled via the sample thermocouple (see below) using an Omega model 49 10A proportioning controller. This provides stable control from ~300° to 1200°C. Below 300° the thermal mass of the furnace limits response time, and fluctuations of 10-15°C over 20 minutes can occur.

Power for the furnace is supplied via an isolation transformer, the input voltage of which is limited by a Variac transformer to reduce thermal shock on the mullite tube and windings during the heat-up period. The furnace can reach 1200°C in about 5 minutes.

The exterior of the furnace tube is surrounded by a 0.3" thickness of alumina fiber tube (Zircar type ALC). The furnace is press-fitted into the tube. This assembly is supported in the dewar within a stainless steel tube 2.75" in inside diameter by 5" in length. The furnace is suspended (and alignable) within this tube by means of eight stainless steel screws arranged radially in the stainless steel supporting tube. The ends of the furnace are insulated by 1/2" thickness alumina fiber board discs (Zircar type SALI) with 0.9" diameter central holes which line up with the furnace tube. These discs are held in place by nichrome wires attached to the outside projections of the alignment screws in the stainless steel tube.

Figure 1. Schematic diagram of the furnace and sample assembly. View is cut-away and partially exploded. This portion of the apparatus is contained within the vacuum dewar.

A) Permanent thermocouple, cemented to furnace wall at center point.
B) Sample thermocouple, welded to aperture next to sample or cemented to the sample.
C) Furnace winding. Alumina insulating beads are used to keep the bare wire from contacting the steel support structure.
D) Fuse made of furnace winding wire.
E) Mullite furnace tube.
F) Alumina insulating tube. Furnace tube is a press-fit into this.
G) Stainless steel support tube. This tube is suspended from the lid of the dewar by a second s.s. tube (shown cut off here.)
H) Screws (radial to support tube) support and align the furnace. There is a 0.2" gap between the s.s. support tube and the furnace insulation.
I) Alumina insulating discs to mask black body radiation from exterior of furnace. These are held in place by nichrome wire wrapped around the support screws.
J) Nichrome wire to hold discs.
K) Machinable alumina cone to mask unwanted black body radiation from interior of furnace, and s.s. aperture.
L) Ceramic ring cemented in furnace center to align and support the sample. Permanent thermocouple is cemented between this ring and the furnace wall.
M) Movable ceramic ring, loose press fit to the furnace wall. This ring is inserted after the sample mount, and holds the sample mount snugly against the permanent ring.
N) Sample assembly. Sample is held on s.s. aperture with s.s. strips spotwelded in place; these also hold the sample thermocouple.

1)

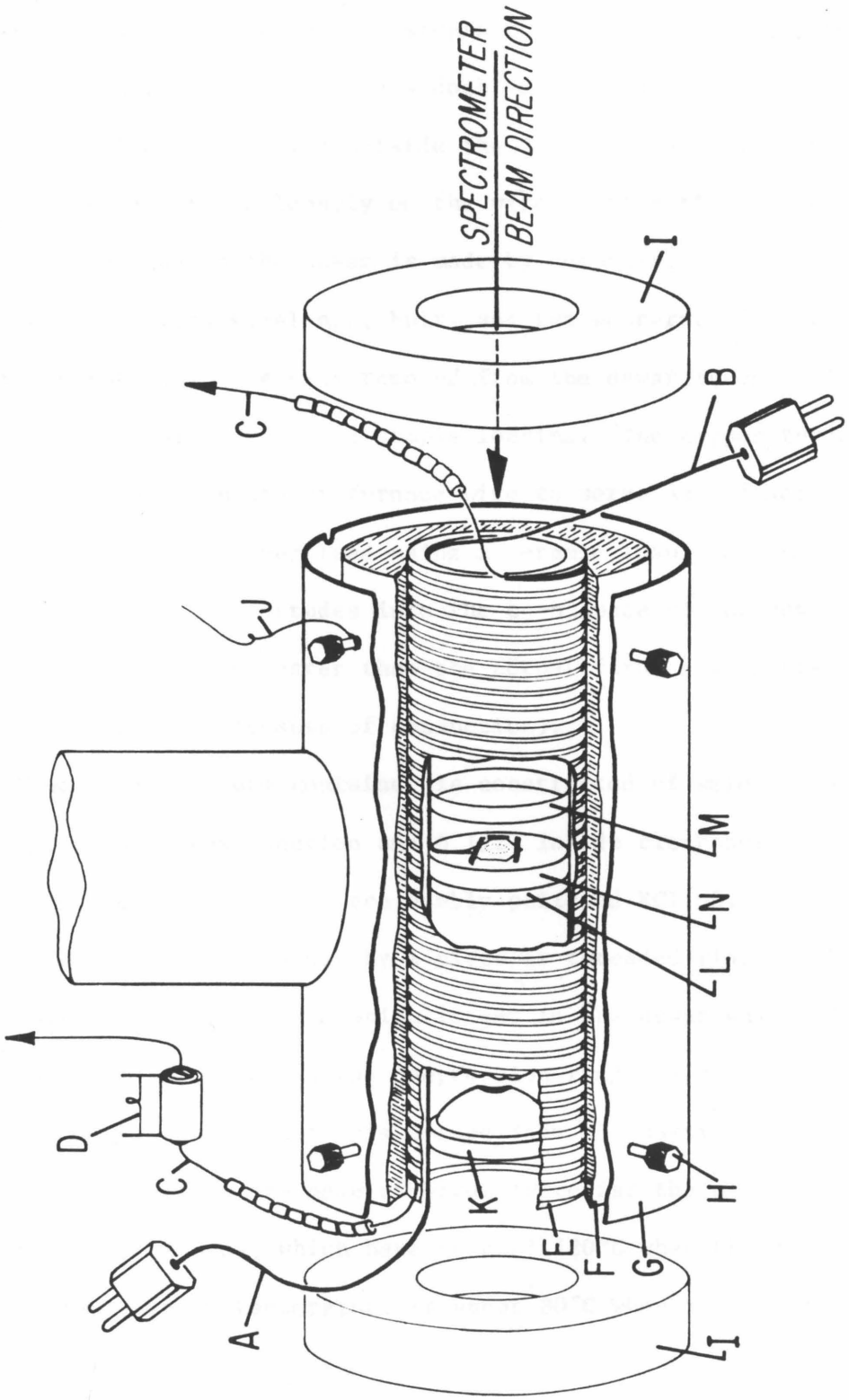

Electrical connections are made by passing the wires through grooves cut in the end discs, or by passing the wires through the central opening (this is done for the sample thermocouple). The power to the furnace windings is led in on a doubled section of the winding wire to avoid heating of the wire outside the furnace. This is insulated using alumina beads strung loosely on the wire. Connection to the copper power leads inside the dewar is made by compressing the wires together using a stainless steel nut, bolt, and two washers. In this way the furnace tube may be easily removed from the dewar assembly for maintenance, alignment, and sample loading. The copper furnace leads have an inserted piece of furnace wire to serve as a fuse; this wire is connected to the copper lead using a ceramic insulator and stainless steel screws. It protrudes into the open space of the dewar and is designed to heat up faster than the actual furnace windings (which lose heat more rapidly because of conduction).

Dewar. The vacuum container is constructed of welded 1/4" aluminum, with a square cross-section and 6 1/2" inside clearance. The windows for the spectrometer beam are doubly polished KCl, 0.2" by 1" round. They are held on the dewar by a circular threaded ring which compresses the window onto an O-ring which is set in the dewar wall. An additional O-ring is placed between the compression ring and the window to avoid breaking the window, but this O-ring does not participate in the vacuum seal. The O-rings are made of Viton to resist the occasional high window temperatures, which have reached 120°C when the vacuum is poor. The normal window temperature is about 80°C when the furnace is at 1200°C.

Vacuum connections to the dewar are made through a 1/2 inch valve for pumping, and a 1/4 inch valve which is normally used to attach the vacuum gauge. Two liquid nitrogen traps are placed in the vacuum line, one oriented upstream to catch pump oil, and one oriented downstream to catch volatiles evolved from the furnace. These volatiles are primarily organics associated with alumina cement used to bind insulation and sample mounts. Normal vacuum for the system is 0.02 Torr. During initial heating cycles the combination of cements and water absorbed on the fiber ceramics frequently causes the pressure to rise to 0.1 Torr, which results in greater heating of the dewar walls and windows.

Electrical connections are made through the lid of the dewar, which also supports the furnace assembly by means of a stainless steel tube which holds the stainless steel furnace support tube mentioned previously. Four thermocouples pass through epoxy fittings which are O-ring sealed to the dewar, allowing changes in the type of thermocouple. Power connections are made by a permanent epoxied electrical feed through with 8 leads, five of which are for future use. The lid is sealed to the body of the dewar by an O-ring seal, and electrical ground continuity is maintained by two locking screws passing through the lid into the body of the dewar. The lid, electrical connections, thermocouples, and furnace assembly form a single unit which may be removed from the dewar for sample mounting and alignment.

Sample Assembly. The samples used are oriented, doubly polished single crystal slabs. These are mounted on a circular stainless steel aperture (type 303) which is machined to allow maximum light passage through irregularly shaped samples. Typical apertures are 5 to 20 mm^2; apertures smaller than 5 mm^2 result in problems with the black body

correction. The aperture disc is 0.1" thick and just slightly (.005") smaller in diameter than the inside of the furnace. The sample is held over the aperture by straps made of .001" stainless steel shim stock, spot welded onto the aperture disc.

The sample disc is held upright and centered in the furnace by two machinable ceramic rings which are easy press-fits into the furnace tube. An additional ceramic piece is used to mask off black body radiation from the stainless steel disk. This disc is placed in the end of the furnace tube through which light exits toward the detector. It has a conical hole in the center which is shaped to allow maximum light from the sample to pass through.

A minimum of two thermocouples are used in each run. One is permanently mounted on the inside of the furnace tube at the center position. The second is mounted on the sample disc, adjacent to the sample. When the sample is sufficiently thick, an additional thermocouple may be mounted on the sample, in the beam path. Typical thermal gradients measured in this way across the radius of the furnace have not exceeded 10°C. The thermocouples used are chromel-alumel with ceramic insulation sheathed in stainless steel with an outside diameter of .020" (from Omega Engineering). The thermocouple is grounded to the sheath at the tip. This is then grounded to the case of the dewar through the stainless steel tube supporting the furnace.

Spectrophotometer

A Perkin-Elmer model 180 spectrophotometer is used to collect infrared spectra. This model is uniquely suited to the task of high temperature spectroscopy because of its optical and detector system.

The beam passes through the sample and reference before being monochromatized by a diffraction grating. Since only this monochromatic beam strikes the detector, the amount of black body radiation from the sample which strikes the detector is minimized. This avoids saturating the detector. The black body emission is subtracted from the spectrophotometer beam by a double chopping system, which alternately measures the transmitted and emitted light, subtracting the latter electronically. This removes the necessity of having an emitting reference material at the same temperatures, which would never be an adequate reference because no two materials have identical emission properties.

The accuracy with which the black body emission is subtracted from the signal may be quantitatively measured by checking the apparent phase relationship of the sample and reference beam. Since there is no emitter in the reference beam, if the subtraction is not made accurately there appears to be either a positive or negative amount of energy in the sample beam relative to the reference, when the spectrophotometer beam is blocked before the sample. In other words, the emission spectrum is the only one present and should be accurately subtracted from itself, yielding zero signal. This condition is easily obtainable up to 1200°C provided that the stainless steel aperture has been adequately masked off, and the detector "sees" the sample emissions and only limited emissions from the rest of the furnace. When black body emissions are too large, for instance if the furnace were run with no thermal baffles, the detector saturates. A thermopile dector is used and if too much energy strikes it, the apparent phase-shift problem occurs.

The furnace dewar is mounted in the sample compartment in an X-Y-Z translation stage to allow accurate positioning. Typical absolute transmission using this system is about 12%, the losses largely due to window reflection, collimation of the focused beam by the furnace parts, and the restriction of the aperture. Quantitative results may be obtained down to about 0.01% transmittance.

The spectrophotometer is interfaced to a DEC MINC-11 computer system which is used to collect both spectra and kinetics data (absorbance vs. time). This interface directly utilizes the PE-180 digital absorbance and frequency information, allowing quantitative measurements up to absorbances of 2. The spectra and data in this paper were checked against standard absorption screens and are accurate to within 2% of the stated absorbance value.

The most significant component in the spectral baseline of this system is due to organics which accumulate on the KCl dewar windows. The windows are the coolest part of the system and condense material outgassed from the furnace cements and insulation. This results in several sharp C-H stretching bands near 2900 cm^{-1}. The baseline is checked frequently and subtracted by computer from the spectra. In practice, the windows require replacement infrequently, typically after about 30 hrs at 900°C

The most significant problem in this system is caused by samples cracking under thermal stress. This results in light leakage and effectively limits the maximum amount of light that can be absorbed. This problem limited my work in silicate crystals to 800-900°C. We have successfully obtained spectra of glasses routinely at 1200°C (Aines, Stolper, and Rossman in preparation).

Results and Discussion

Muscovite

The hydroxyl in muscovite is not a 'trace' hydrous component, but I have included it in this study in order to understand the type of behavior to be expected from a single, well defined hydroxyl site at high temperature. This is required to verify that the effects observed in other mineral systems are not spurious effects of temperature.

Figure 2 shows the reversible aspects of the changes in the O-H stretching band with temperature. The peak shifts slightly and there is a slight decrease in integrated intensity. Upon cooling the original spectrum is once more obtained. (The 'cooled' temperature in this run is 40°C because of heating by the spectrometer beam; this varies somewhat from sample to sample and depending on the type of thermal baffles in place.) When heated to 750°C dehydration occurred. Figure 3 shows that no new O-H absorptions form during dehydration. There is only a monotonic decrease in intensity of the original band. The 757° spectrum in Figure 3 was obtained during active dehydration.

The lack of new absorptions, and hence observable intermediate species, is in contrast to a 1970 study by Freund of the dehydration of $Mg(OH)_2$ (see also Freund, 1974). He observed just prior to dehydration a slight broadening of the O-H peak and interpreted this as evidence of proton tunneling between OH sites. This is one way to form H_2O molecules which are the observed dehydration species. There is no evidence of such a process in muscovite, and no reason to believe that H_2O molecules are not formed by simple diffusional hopping of H^+ to an adjacent OH^- site. These H_2O molecules would be free to rapidly diffuse out of the sample, which was thin at the outset of the experiment

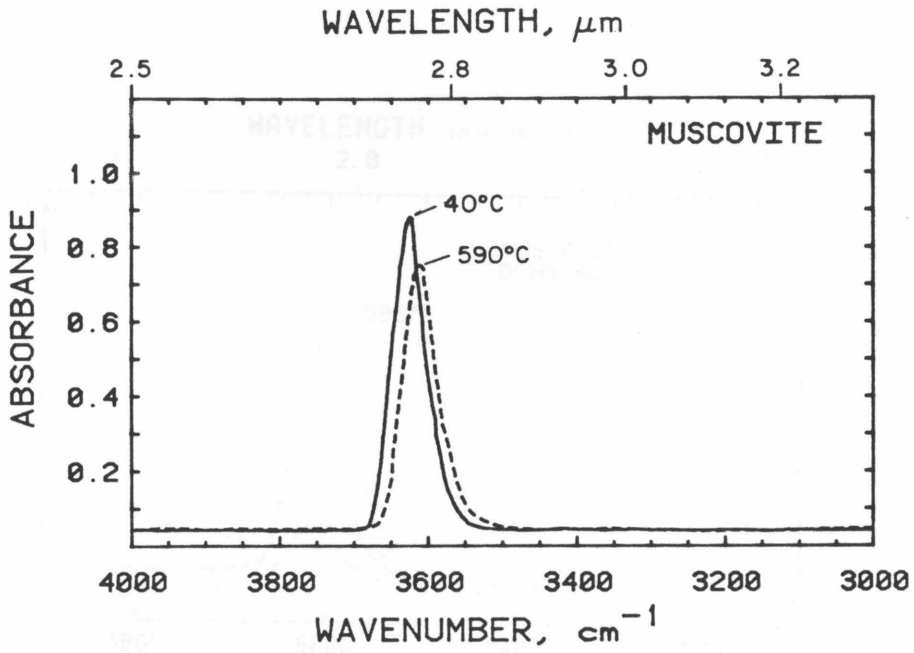

Figure 2. Infrared spectra of an 11 μm thick cleavage flake of muscovite showing thermal effects on the O-H stretching absorption. Spectra obtained at the indicated temperatures. Slight broadening and shift to lower frequency is completely reversible upon cooling. Spectra obtained in the β polarization, $\bar{E} \| \underline{a}$, the minimum O-H intensity direction.

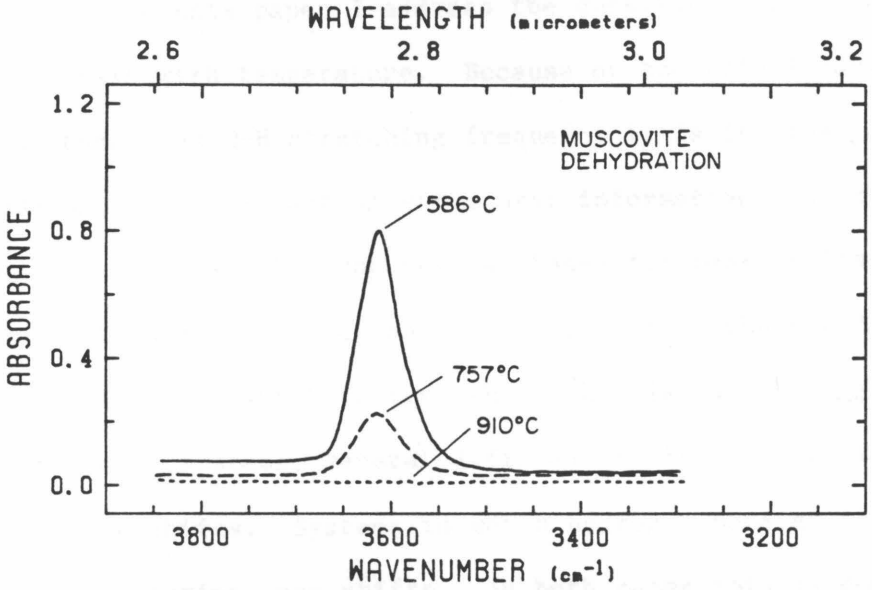

Figure 3. Dehydration of the same sample as Figure 2. The sample recovered after 910° had exfoliated, leaving a center remaining thickness of about 2 μm.

(6 μm), and exfoliated to 2 μm sheets during dehydration (see also Figure 20b).

Cordierite and Beryl

We have previously reported on changes in H_2O site and the dehydration mechanism of these minerals (Aines and Rossman, 1984b, Chapter 8). In this paper I address the question of peak shifts in these minerals with temperature. Because of the relationship between O-H-O distance and O-H stretching frequency it is interesting to examine the possibility of extracting structural information from thermally induced peak shifts. The theoretical bases for peak shifts of several kinds are discussed in Aines and Rossman, (1984c, Chapter 3), but very few data exist with which to test these theories which suggest that for hydrogen-bonded systems, several different mechanisms should result in positive peak shifts. Systems in which hydrogen bonding is unimportant should have negative peak shifts. In both cases this is due to the average increase in O-O, and hence O-H-O, distance with temperature. In hydrogen-bonded systems it has been suggested that as O-H-O distance increases, so should the absorption frequency because the hydrogen bond strength decreases (Freund, 1974; Aines and Rossman, 1984c, Chapter 3, and references therein).

In our study of beryl and cordierite, examples of both positive and negative peak shifts were found. However, the positive shifts occur in minor, unidentified peaks, bending modes, or in rotational-vibrational combination bands. The shifts in the combination bands are caused by black body excitation of low energy bands to successively higher states (Wood and Nassau, 1967). Figure 4 shows the cordierite type II

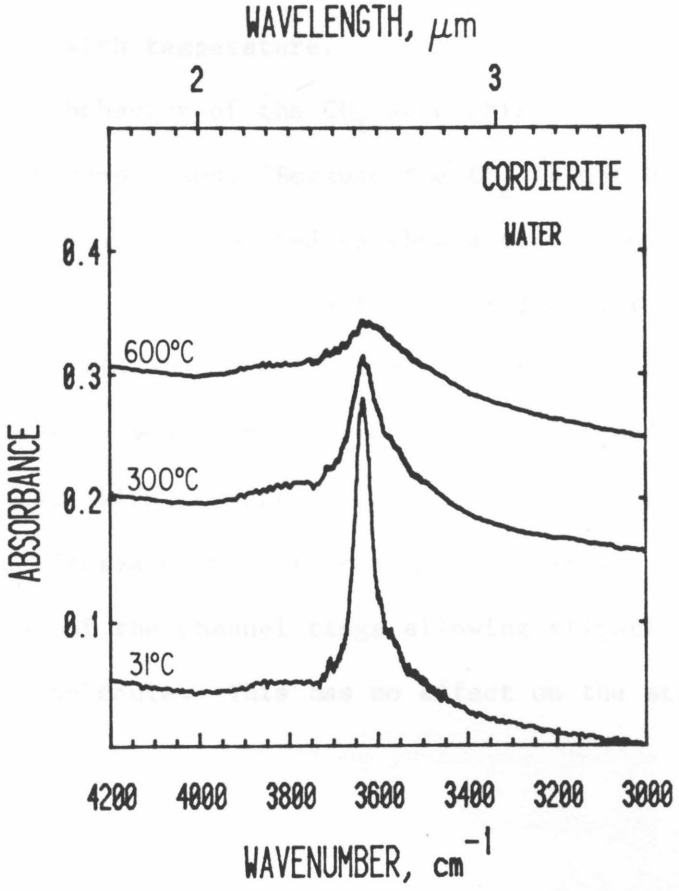

Figure 4. Cordierite type II asymmetric stretching mode. Sample used in Aines and Rossman,(1984b, Chapter 8). 60 μ thick, polarized in β. No shift in peak position with temperature is seen.

asymmetric stretching band behavior with temperature. There is no peak shift observable, within error. Figure 5 shows peak shifts for three absorptions in beryl. The type II asymmetric stretch in beryl shows no peak shift, as in cordierite. However, the two other indexed H_2O stretching absorptions show substantial negative shifts, as does a lattice overtone at 1870 cm^{-1}. In all three the rate of shift with temperature increases with temperature.

Figure 6 shows the behavior of the CO_2 stretching and rotational-combination bands for comparison. Because the CO_2 is not bonded to the cordierite lattice, it is not expected to show a stretching vibration peak shift. No shift is seen in the central peak due to the asymmetric stretch. However, the side bands which appear to be rotational (librational) combination modes shift toward each other and the stretching fundamental, with temperature. Apparently the frequency of the librational mode decreases with temperature, possibly due to expansion or rotation of the channel rings allowing slightly more free 'rocking' of the CO_2 molecule. This has no effect on the stretching frequency, however.

Quartz

Quartz is known to undergo numerous changes in its O-H vibrational spectrum upon heating (Kats, 1962). These changes involve the interconversion of numerous OH defects which occur in a charge compensating role for aluminum and alkali substitutions in quartz. The effect of heating on a natural hydrothermal quartz crystal is shown in Figure 7. This crystal contains only OH^- groups and no molecular H_2O. This is typical of relatively high temperature quartz (e.g. Aines and

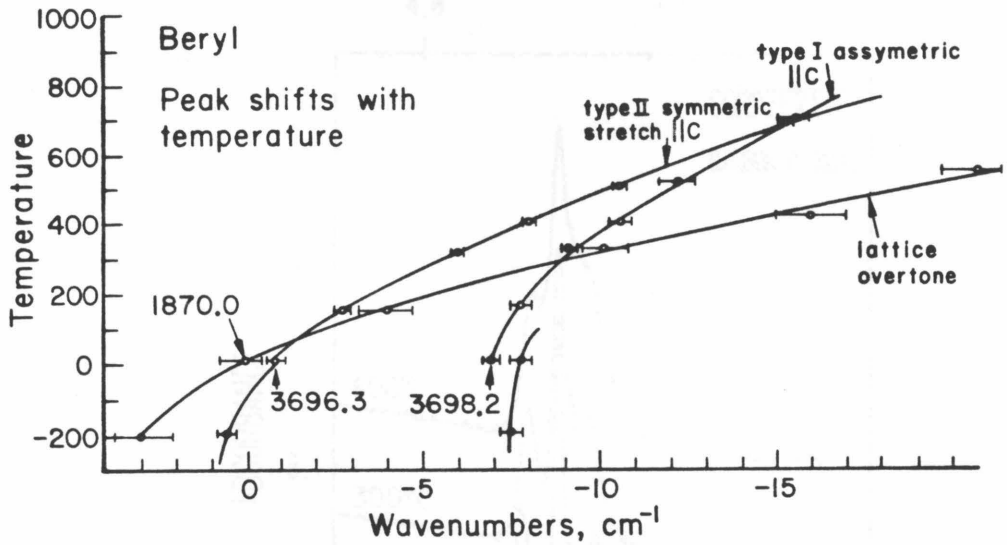

Figure 5. Peak shifts for 3 absorptions in beryl, same sample used in Aines and Rossman,(1984b, Chapter 8). 25°C values are shown in the graph. The offsets in the two water curves at 25°C are apparently due to the fact that the -196°C spectra were run after the sample had been heated to 750°C, oxidizing some of the iron in it. Error bars are 95% limits based on estimated error in peak measurement. Curves have been drawn to fit the data smoothly.

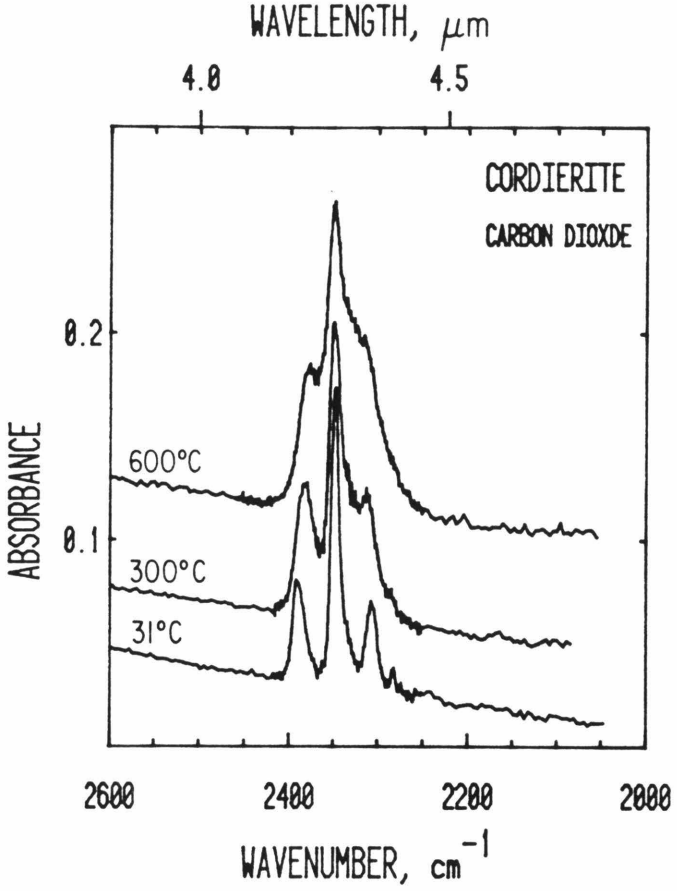

Figure 6. Cordierite CO_2 absorptions. β and γ polarizations are mixed by a twin in the sample, however, the predominant direction is β. See Aines and Rossman, (1984b, Chapter 8). Sample 16 μm thick. (Under perfectly polarized conditions, the central stretching mode is polarized in γ and the rotational-combination modes in β.)

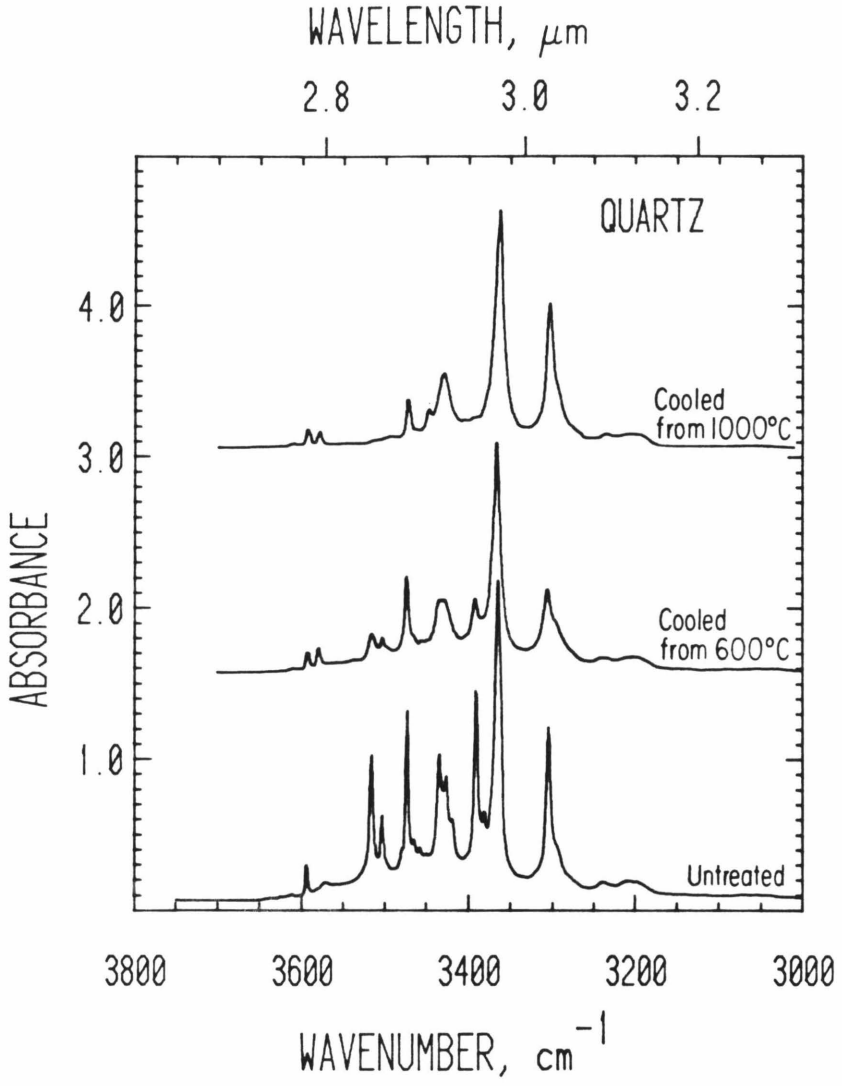

Figure 7. Natural, flawless quartz crystal from Hot Springs, Arkansas. 5.07 mm thick, polarized E⊥C. Spectra obtained at -196°C after cooling from indicated temperatures.

Rossman, 1984a, Chapter 2). The major changes in Figure 6 result from a net dehydration of the crystal. The most stable defects are Al(OH) defects, which result in the three most intense peaks in the top spectrum of Figure 7.

I have investigated the in situ high temperature spectra of this sample in order to determine whether the kinetics and mechanisms of the defect interconversions could be observed, and whether the α - β transition results in an observable change in the O-H vibration spectrum.

Thermal broadening of peaks is an important effect on the spectroscopy of OH defects in quartz, as seen in Figure 8. At -196°C 22 absorptions may be identified (this is typical in natural quartz; see Kats, 1962). At 577°C the spectrum has merged into a nearly featureless continuum, making it difficult to differentiate reactions among the O-H defect species. Accordingly I was unable to directly observe at high temperature the changes documented in Figure 7.

Details of the changes in the spectrum over the range of the α - β transition are seen in Figure 9. The temperatures in this experiment are known to within $\pm$ 1/2°C. This was accomplished by drilling a small hole in the center of the sample, and cementing a thermocouple into it directly in the center of the illuminated area. This yielded an average temperature for the section of the sample actually being observed, which was approximately 3 x 5 mm in cross section. The thermocouple mounted on the stainless steel aperture was as much as 2° hotter than the sample, and the rim of the sample aperture (at the wall of the furnace) registered up to 10° hotter than the sample. These low gradients make me confident that the data in Figure 9 actually represent the α and β

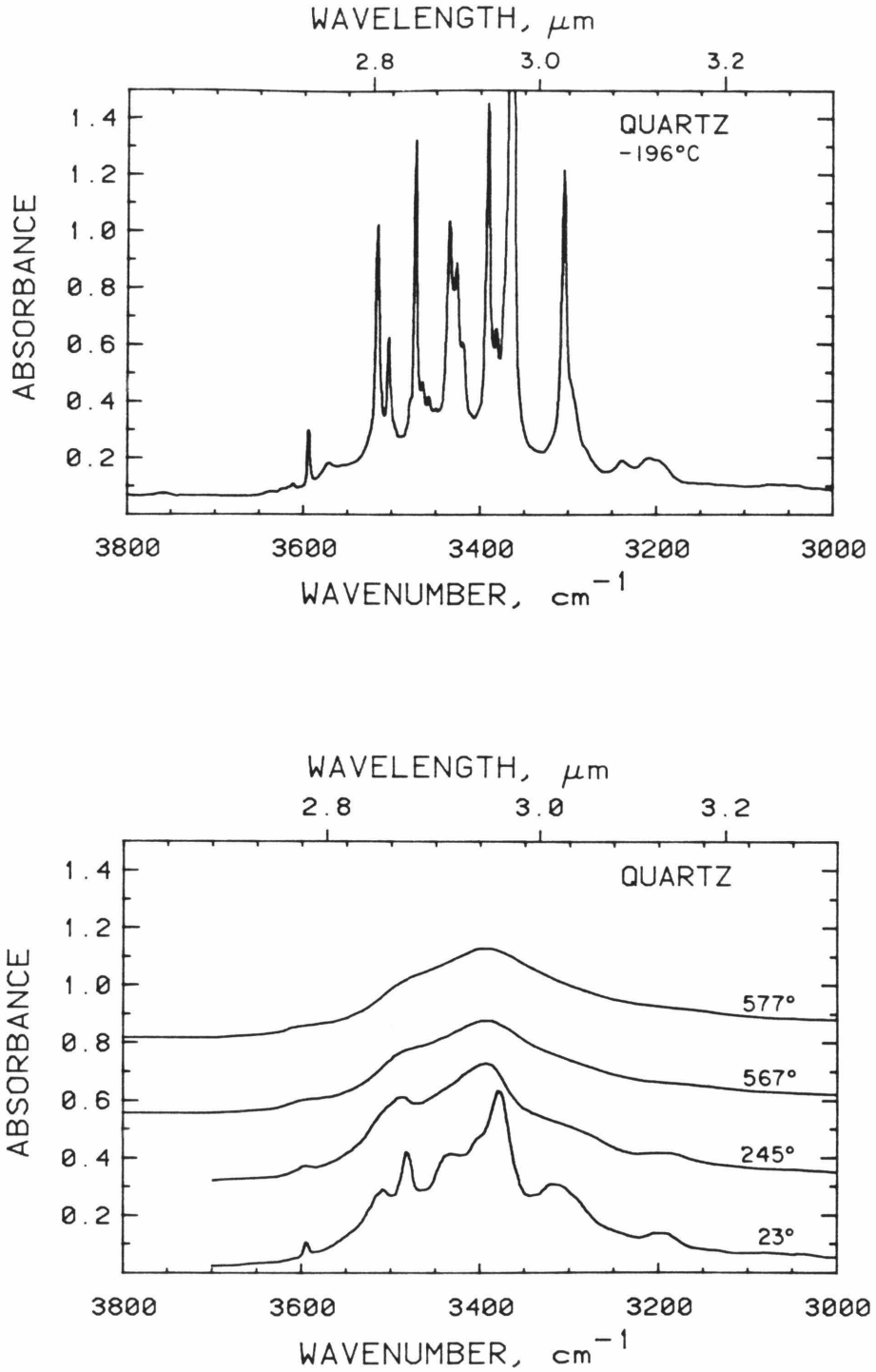

Figure 8. Spectra of the same sample as Figure 7, taken at temperature during the cycle up to 600°. A) -196°C before heating, B) Heating up to 600°C, through the α-β transition of 573°C. Polarized E⊥C.

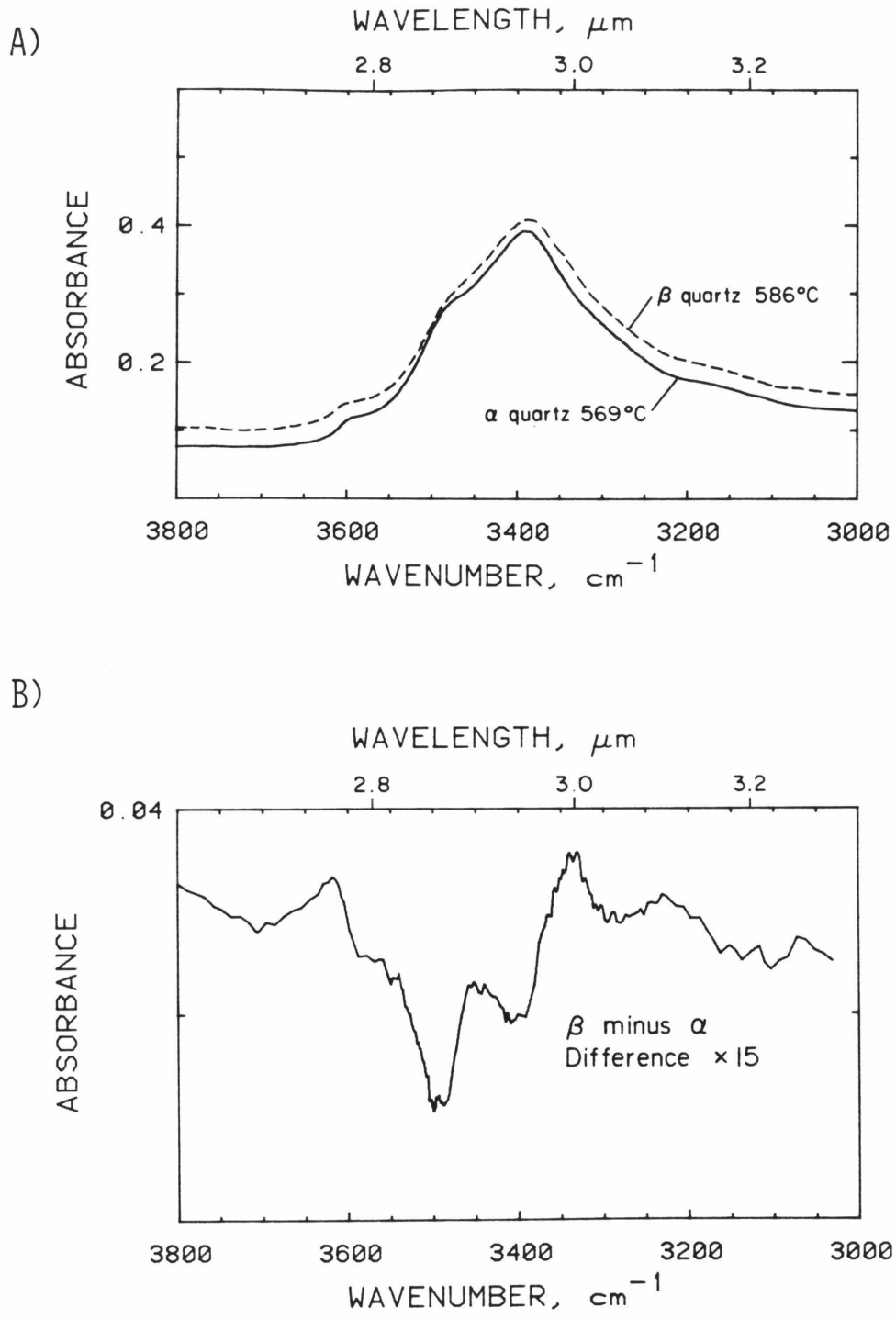

Figure 9. A) Infrared spectra of α and β quartz, same sample as Figures 7 and 8. B) Difference between β and α spectra shown in (A), expanded vertically 15 times.

phases without temperature gradients causing partial conversion. The changes seen in Figure 9a are reversible, and the β minus α difference is seen in Figure 9b, expanded 15 times. These differences are very small, and it is not clear whether they are a function of the phase change, or only of temperature change. The major areas where intensity is lost, 3400 and 3500 cm^{-1}, correspond roughly to the major peaks in the 23°C spectrum (Figure 8b) shifted to lower frequency by temperature. These peaks are due to Al(H) and Li(H) defects, respectively (Kats, 1962; Aines and Rossman, 1984a, Chapter 2). Careful profiling in 2°C increments through the α - β transition showed that these changes are continuous over a 20° range, and are similar to changes occurring over that temperature range below the transition point. Therefore it is not possible to identify them uniquely with the transition. However, the α - β transition is also known to occur over a temperature range of 10° to 15°C (Van Goethem, et al., 1977; Wright and Lehmann, 1981), consisting of a continuous increase in the effective area actually consisting of β quartz. From this one might also expect changes in the IR spectrum to also occur over this range. (Using a Mettler TA 2000 differential scanning calorimeter I have determined that the α - β transition in this sample occurs over a range of 570 to 575°C when heating at 0.2°/minute. The peak in the transition is at 573.5°C). Dolino et al. (1983) review the current literature on the α - β transition, and present high temperature IR spectra in the far-infrared which show a low frequency mode associated with the transition.

Metamict Zircon

Metamict zircons from Ceylon contain a hydrous component, while zircons from the same locality that are not metamict are anhydrous (Woodhead, Rossman, and Silver in preparation). The hydrous component in the metamict samples causes a broad, asymmetric absorption in the infrared and has been interpreted as hydroxyl groups in charge-balancing roles in the disrupted lattice, for instance H_2O forming SiOH and ZrOH groups from a broken Si-O-Zr bond (Aines and Rossman, 1984c,d, Chapters 3 and 6). I have examined the relationship between the dehydration of this hydrous component and the onset of recrystallization during heating. Figure 10 shows the hydroxyl broad band during heating. Dehydration occurs more or less continuously above 400°C, but is rapid above 600°C. The low-frequency side of the band is lost preferentially, indicating that hydroxyl groups involved in short hydrogen bands (e.g., Aines and Rossman, 1984c, Chapter 3) are being lost preferentially. No recrystallization occurs until 800°C, when most of the hydrous component is gone. This lack of recrystallization prior to dehydration may indicate that the hydroxyl groups are stabilizing the metamict state, and must re-form water before the bonds in the zircon lattice can re-form. The loss of the low-frequency component of the broad band at low temperatures indicates that the hydroxyl groups involved in short hydrogen bonds, and hence high energy bonds, are expelled first.

It has been noted in broad bands in glasses that there is a reversible change in the band shape with temperature. The band shifts to higher energies, and loses integral intensity, both completely reversible and not associated with dehydration (Wedding, 1975; Aines, Stolper, and Rossman in preparation). There is a suggestion that some

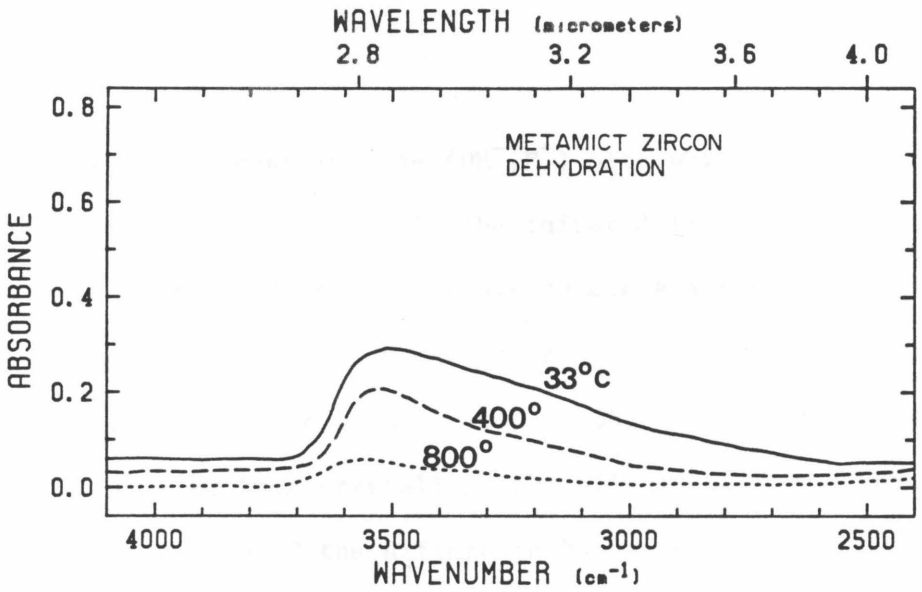

Figure 10. Metamict zircon from Ceylon, sample #6500 from Aines and Rossman,(1984d, Chapter 6). Sample 0.3 mm thick, spectra are unpolarized.

reversible changes of this kind also occur in zircon, but dehydration occurs too rapidly to verify it. It is not as pronounced an effect in glasses if it is present, however. There is no difference in the zircon spectrum from 33° to -196°, while in hydrous glasses there is a pronounced increase in the low-frequency area of the band over this temperature interval.

Topaz

Topaz classically contains one (OH^-,F^-) site which should result in a single OH stretching absorption in the infrared (Ribbe and Gibbs, 1971). However, topaz frequently shows numerous absorptions in the 4000 to 3000 cm^{-1} region. Many of these are sum and difference modes centering on the fundamental OH stretch at 3650 cm^{-1}. This is the absorption resulting from crystallographically identified "normal" hydroxyl site. At -196°C the difference bands related to this fundamental disappear (Aines and Rossman, 1984d, Chapter 6) and a number of "anomalous" secondary OH absorptions may be identified in the 3640 to 3200 cm^{-1} region (Fig. 11). These anomalous OH absorptions appear to be caused by hydroxyl groups; I have not observed a diagnostic H_2O band at 5200 cm^{-1} in the near-infrared region (Aines and Rossman, 1984a, Chapter 2) in any topaz with or without the anomalous OH absorptions.

Neutron diffraction work by Parise et al. (1980) has revealed a second type of hydroxyl site in topaz. When two hydroxyl groups occupy adjacent (OH^-, F^-) sites, the protons approach too closely in the normal symmetry position, and instead are deflected to new positions. The original O-H vector lies between the α - γ directions, but when the protons are deflected to new sites the O-H vector will be in the α - β

Figure 11. (Next page) OH absorptions in topaz caused by hydroxyl groups not in the crystallographically defined (OH^-,F^-) site. A) -196°C spectra comparing colorless topaz from Minas Gerais, Brazil to light brown topaz from the Thomas Mountains, Utah. The Brazilian sample is probably from a granitic pegmatite, typical of the region; thickness 0.6 mm. The Thomas Mts. topaz occurs in vugs in rhyolite tuff; thickness 1.37 mm. The primary OH absorption at 3650 cm^{-1} is not shown. B) Comparison of the Brazilian sample in (A) before heating, and the difference (untreated minus heated) showing absorptions lost after heating. No change occurred in the 3650 cm^{-1} primary absorption. Both A & B: dotted trace, α polarized, solid trace β polarized

11A)

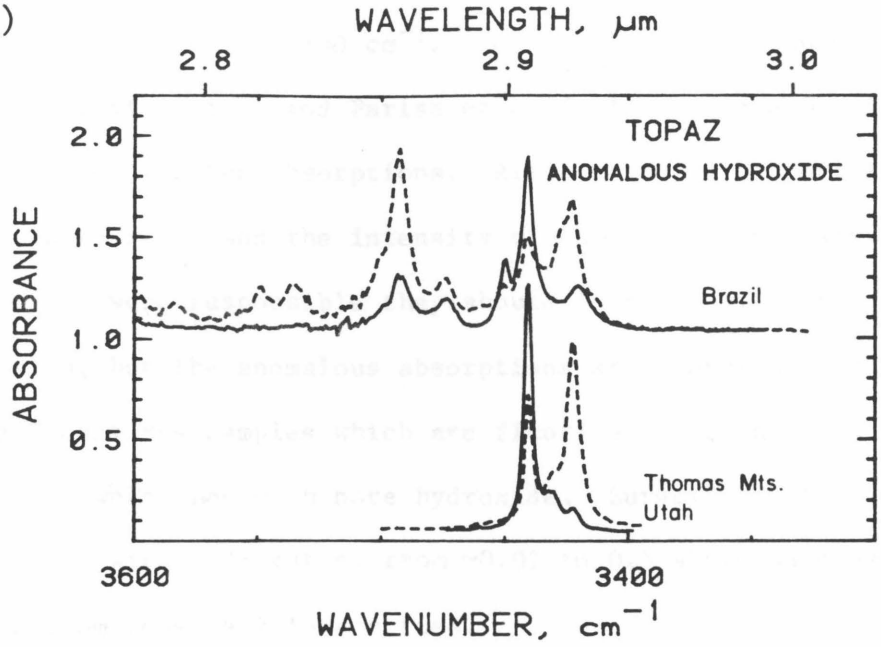
WAVELENGTH, μm
2.8
2.9
3.0
TOPAZ
ANOMALOUS HYDROXIDE
Brazil
Thomas Mts.
Utah
ABSORBANCE
2.0
1.5
1.0
0.5
3600
3400
WAVENUMBER, cm⁻¹

11B)

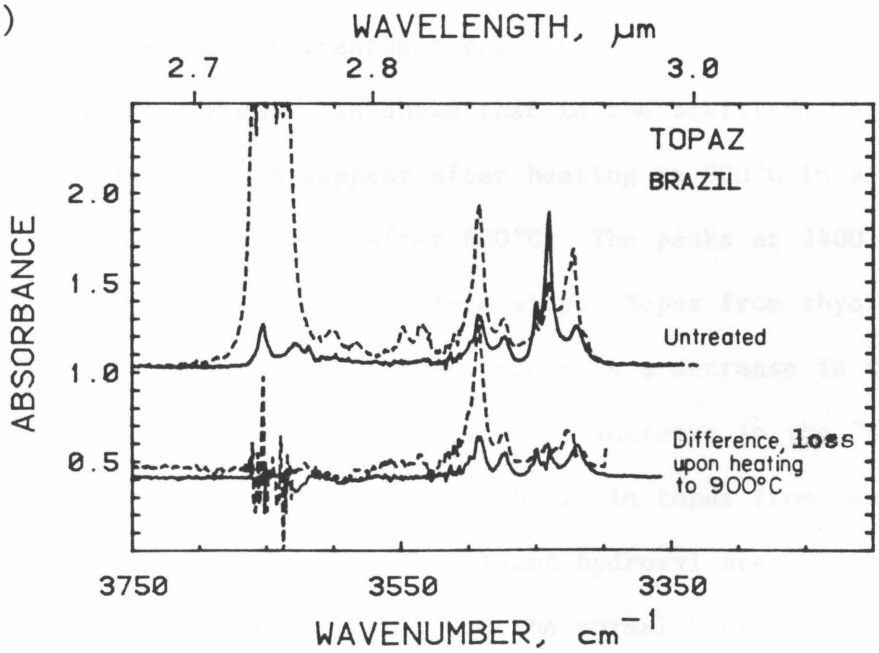
WAVELENGTH, μm
2.7
2.8
3.0
TOPAZ
BRAZIL
Untreated
Difference, loss upon heating to 900°C
ABSORBANCE
2.0
1.5
1.0
0.5
3750
3550
3350
WAVENUMBER, cm⁻¹

plane. This is the same polarization behavior observed for the anomalous peaks at ~3400 to 3450 cm^{-1}. However, there are numerous absorptions in that region, and Parise et al.'s lower symmetry site could only account for two absorptions. Also, there is no correlation between OH/(OH+F) ratio and the intensity of the anomalous peaks. If paired hydroxyls were responsible they should increase with the OH/(OH+F) ratio, but the anomalous absorptions are approximately the same in the Thomas Mts samples which are fluorine-rich, and the Brazilian topaz which has much more hydroxide. Survey work of many topaz localities with OH/F ratios from ~0.02 to 0.5 shows no consistent variation in anomalous peak intensities.

Despite the inability to assign these absorptions to specific OH sites, their thermal behavior is of interest. Aines and Rossman (1984d, Chapter 6) have shown that these absorptions are integrally related to radiation damage and thermal treatment results in re-equilibration of hydrogen among sites. Figure 11b shows that in the Brazilian topaz, the peaks at 3450 to 3500 cm^{-1} disappear after heating to 900°C in air for 18 hours; no change was observed after 600°C. The peaks at 3400 to 3450 cm^{-1} showed little reduction in intensity. Topaz from rhyolites behaves differently, however. In these, there is a decrease in the 3440 cm^{-1} "anomalous" peaks concurrent with an increase in the "normal" peak at 3650 cm^{-1}. Figure 12 shows this change in topaz from San Luis Potosi, Mexico. In this sample, the dominant hydroxyl species is the one resulting in the 3440 cm^{-1} peaks, and the normal hydroxyl is subsidiary. Upon heating to above 400°C, however, the peaks can be observed changing intensity simultaneously (Fig. 12). The "anomalous" site is being converted into the "normal" site. In Figure 13 the

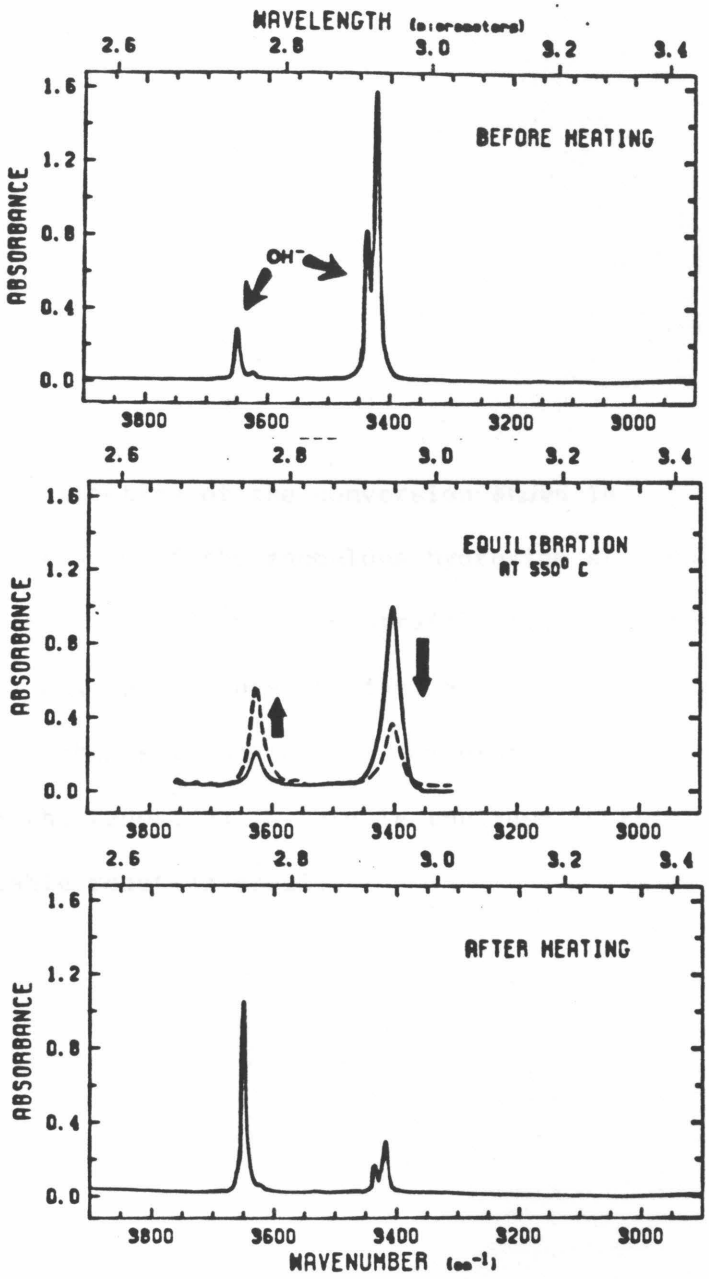

Figure 12. Equilibration of hydroxyl sites in topaz from a rhyolite tuff, San Luis Potosi, Mexico. Sample 0.72 mm thick, polarized in the α direction. At 550°C, the anomalous hydroxide at 3400 cm^{-1} is seen converting to the normal hydroxide site.

Figure 13. (Next page) Kinetics of the conversion shown in Figure 12. The absorbance of the anomalous hydroxide at 3400 cm^{-1} in α is plotted against $(time)^{1/2}$. The straight line relationships between absorbance, and hence concentration, and $t^{1/2}$ are consistent with a diffusional mechanism. Successive temperature plots are all from the same run; the reduction in rate is thus due to the reduction in available reacting species.

13)

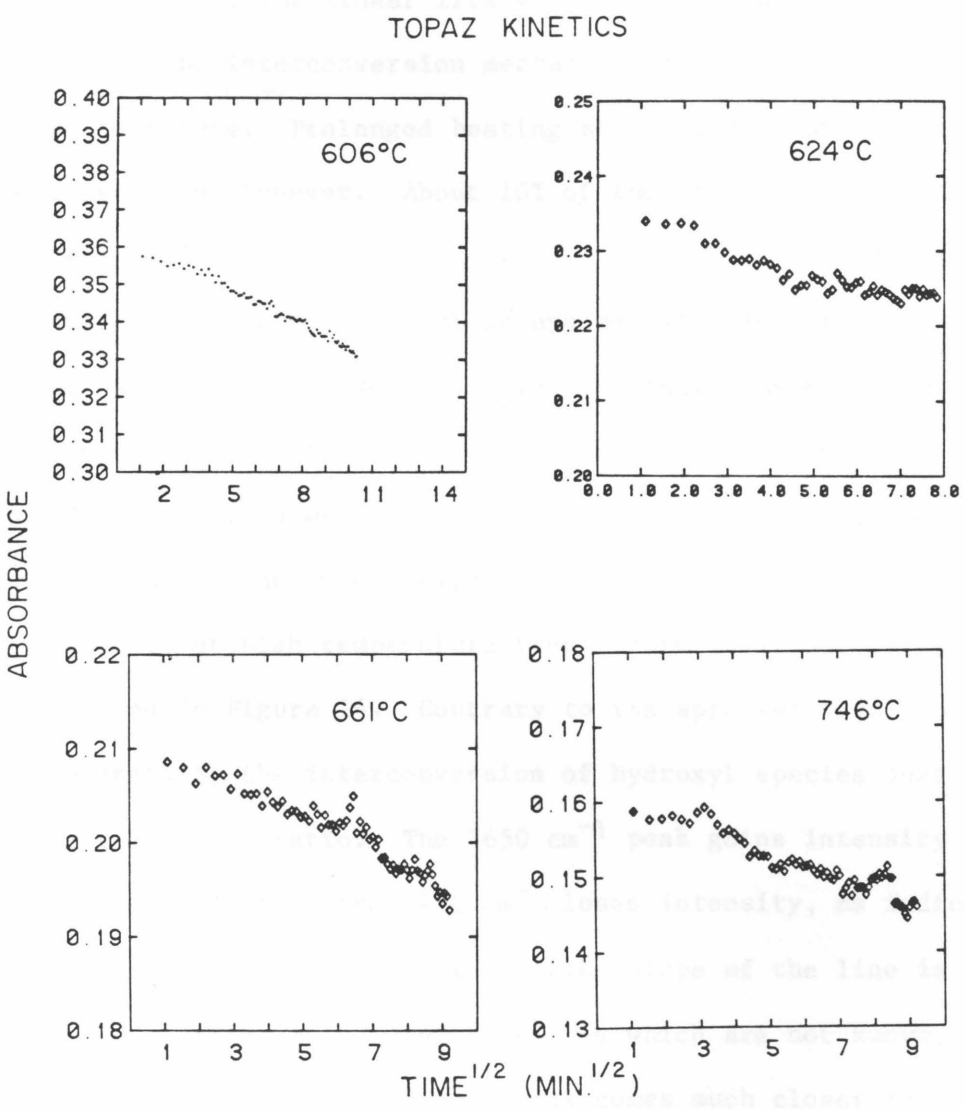
TOPAZ KINETICS
606°C
624°C
661°C
746°C
ABSORBANCE
TIME$^{1/2}$ (MIN.$^{1/2}$)

intensity of the 3400 cm^{-1} peak is plotted against $(time)^{1/2}$ at four temperatures run successively on the same sample. The rate slows as the number of groups available to react becomes smaller at the higher temperatures. As such, an activation energy cannot be obtained from these data. However, the linear fits when plotted against $t^{1/2}$ are consistent with the interconversion mechanism rate-limiting step being diffusional in nature. Prolonged heating at 900°C did not result in complete conversion, however. About 10% of the original intensity at 3400 cm^{-1} remained.

This interconversion of hydroxyl groups was also investigated in a Thomas Mts. sample by stepwise sequential heating. The sample was held at temperature for 18 hours, then cooled, and the intensities at 3650, 3436, and 3419 cm^{-1} in α were measured. By making the measurement at 25°C I could measure the intensities of both the 3436 and 3419 cm^{-1} peaks which merge at high temperature (see Figure 16). The results of this are plotted in Figure 14. Contrary to the apparent result observed at high temperature, the interconversion of hydroxyl species does not exactly occur in a 1:1 ratio. The 3650 cm^{-1} peak gains intensity slightly more rapidly than the 3436 cm^{-1} loses intensity, as indicated by the lack of straight line behavior. (The slope of the line is related to the relative molar absorptivities which are not known, but appear to be similar.) The 3619 cm^{-1} peak comes much closer to a 1:1 conversion into the 3650 cm^{-1} peak.

The suggestion from this experiment is that there is an additional thermally unstable hydrous component in the topaz which also converts into the hydroxyl responsible for the 3650 cm^{-1} peak. I have not identified this species. It is not a major species, judging by the

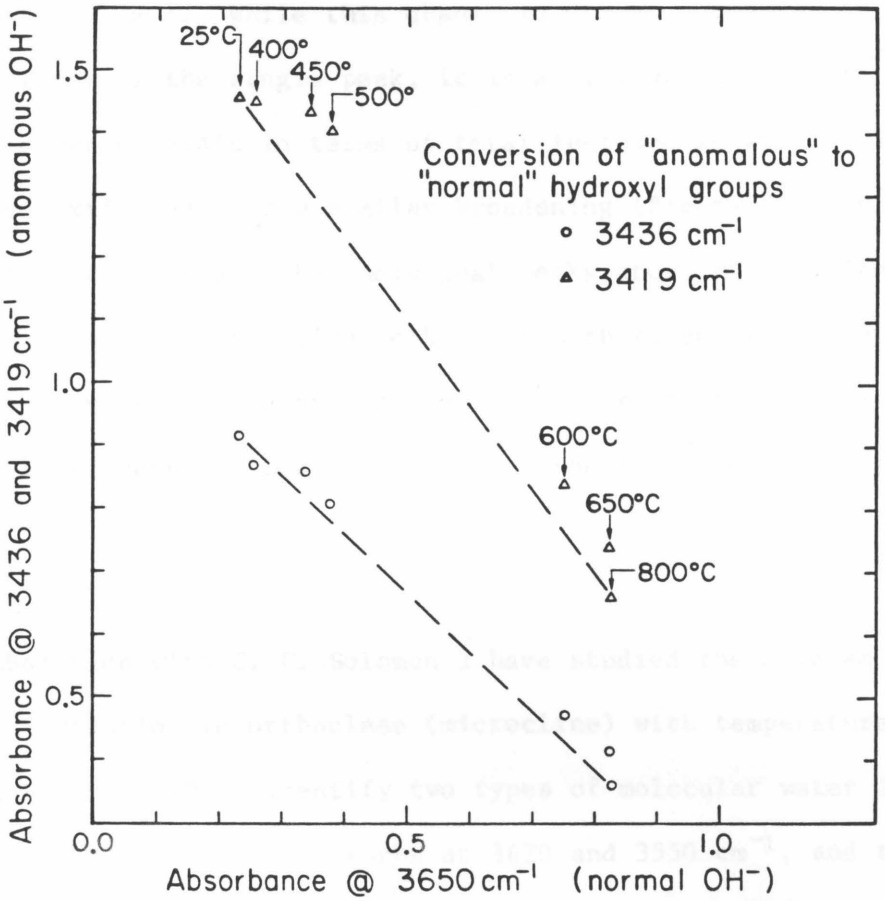

Figure 14. Quantitative comparison of the peak heights of the two major anomalous OH peaks at 3436 and 3419 cm^{-1} in α, with peak height at 3650 cm^{-1} (normal hydroxyl) during a sequential heating experiment on topaz from the Thomas Mts., Utah. Sample 3 mm thick. Sample was held for 18 hours at the indicated temperatures, in air. Peak height measurements were then made at 25°C.

minor deviation in Figure 14; however, I have not observed any additional absorptions in the rhyolite topazes which behave in this way.

The primary ("normal") OH absorption in topaz has a pronounced thermal shift, seen in Figure 15. The peak shifts 40 cm^{-1} lower in energy from -196° to 750°C. The increase in half-width is also large, from 5 cm^{-1} to 30 cm^{-1}. While this change is dramatic because of the initial sharpness of the single peak, it is a similar increase to those seen in the other minerals in terms of total increase in width. The anomalous hydroxide peaks show similar broadening (Figure 16) making it impossible to differentiate the individual peaks above 400°C. These peaks also show a strong negative peak shift with temperature. It is not clear whether the two major peaks merge because of broadening or because the high frequency peak shifts under the low frequency peak.

Feldspar

In collaboration with G. C. Solomon I have studied the changes in trace water speciation in orthoclase (microcline) with temperature. Solomon and Rossman (1984) identify two types of molecular water in orthoclase (Fig. 17). Type I absorbs at 3620 and 3550 cm^{-1}, and type II at 3440 and 3280 cm^{-1}. Both are due to molecular water, identified by the 5200 cm^{-1} characteristic band (not shown).

Substantial changes occur in the spectra of water in orthoclase upon heating. Figures 18a and b show that the type II water is lost by 400°C. Solomon and Rossman have identified this water as occupying a very open site or defect, able to readily exchange. The rapid, low temperature loss confirms this. The type I water persists to 660°C. This water type has been identified by Solomon and Rossman, and

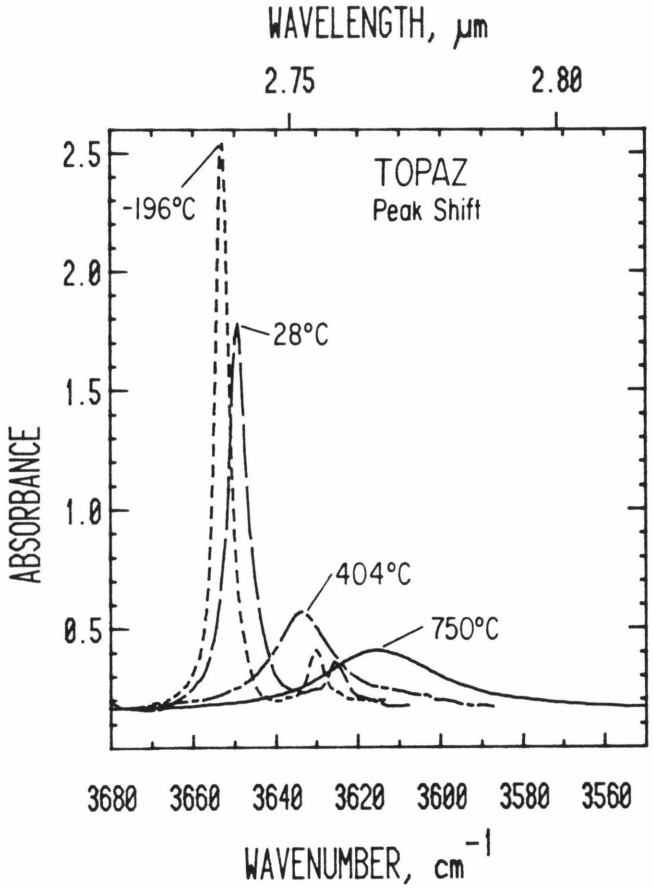

Figure 15. Change in shape and position of the primary topaz OH absorption with temperature. Spectra from same experiment as Figure 14. Peaks have been scaled to reflect the peak intensity at 28°C after cooling from 750°C, since at each increasing temperature this peak grew in intensity. Polarized in α.

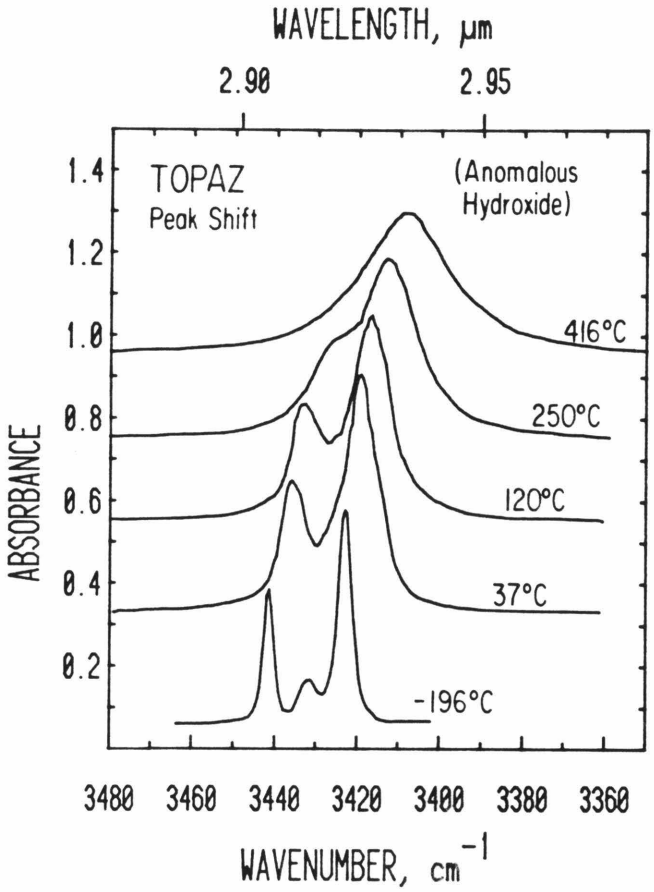

Figure 16. Change in shape and position of the secondary OH absorptions with temperature. Same experiment as Figure 14. These spectra were obtained during the course of heating the sample from 37° to 416° over 15 minutes. No reaction occurred over this time. -196°C spectrum was run separately. Polarized in α.

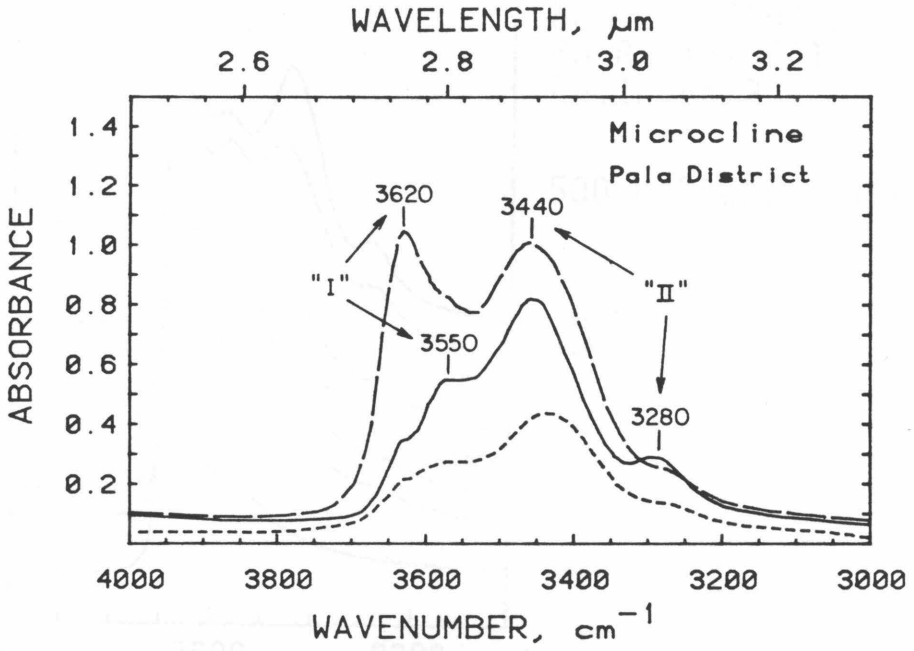

Figure 17. Molecular water species in orthoclase feldspar as identified by Solomon and Rossman, 1984. Sample 0.38 mm thick, gemmy microcline (no fluid inclusions or turbidity) from the White Queen Mine, Pala, CA. Solid trace - α, dotted trace - β.

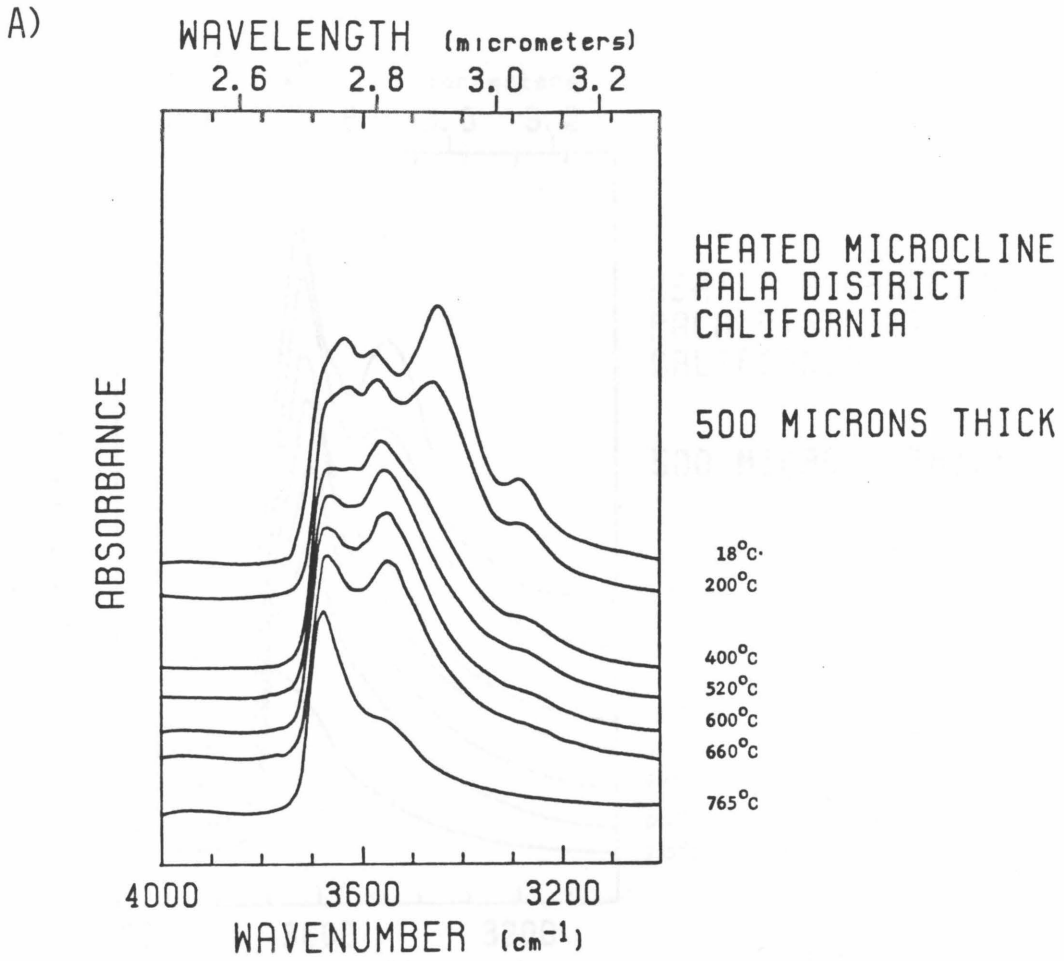

Figure 18. (This and next page) High temperature spectra of the sample in Figure 17. A) α polarization; B) γ polarization. Plotted 0.5 mm thick.

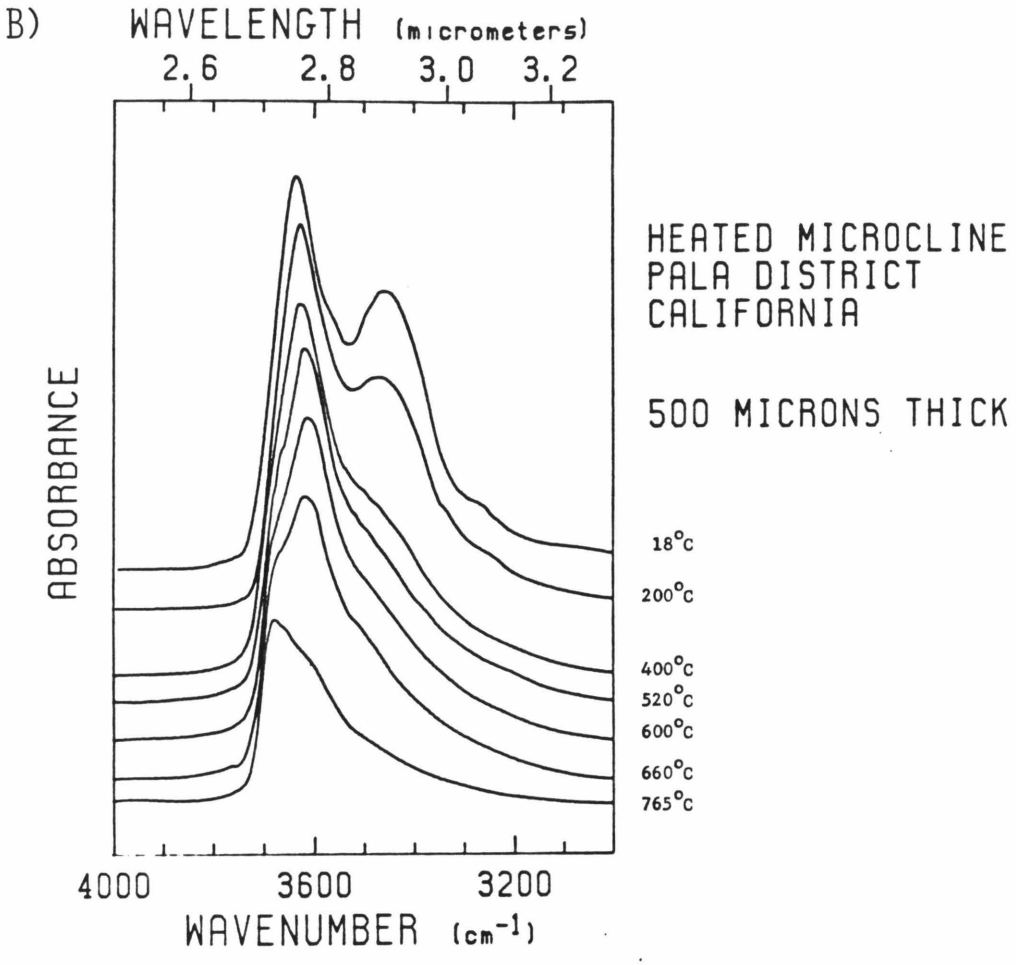
B)
WAVELENGTH (micrometers)
2.6
2.8
3.0
3.2
ABSORBANCE
HEATED MICROCLINE
PALA DISTRICT
CALIFORNIA
500 MICRONS THICK
18°C
200°C
400°C
520°C
600°C
660°C
765°C
4000
3600
3200
WAVENUMBER (cm-1)

Hofmeister (1984) as "structural," that is, oriented and occupying a well defined site in the feldspar structure. This is the water that Hofmeister has identified as taking an integral role in the formation of amazonite (green) color in conjunction with lead and irradiation.

Above 520°C a new component becomes apparent in both polarizations of the feldspar spectra. This is a nearly isotropic band centered near 3690 cm^{-1}. The spectra of Figure 18 do not conclusively demonstrate whether this is a new component, or whether the type I water peak at 3670 cm^{-1} simply shifts far enough to lower energy to expose the 3690 cm^{-1} band. The formation of this new band is irreversible, however, and in Figure 19 the spectra of the sample cooled from 770°C are compared to the original spectra. Clearly a new hydrous species has been created; the 3620 cm^{-1} peak could not have concealed the new peak. This is the first instance I have encountered of a major new species being formed irreversibly upon heating. The identity of this species is not known.

It seems unlikely that this feldspar originally crystallized at high temperature, or the type II water would not have been incorporated, and type I would have reacted to form the new species seen here. However, both water types in the original sample may have formed during the slow transition to maximum microcline during cooling. Our experiment was not able to duplicate the slow cooling rate or water confinement that would be expected in a pegmatite, so we cannot verify this experimentally.

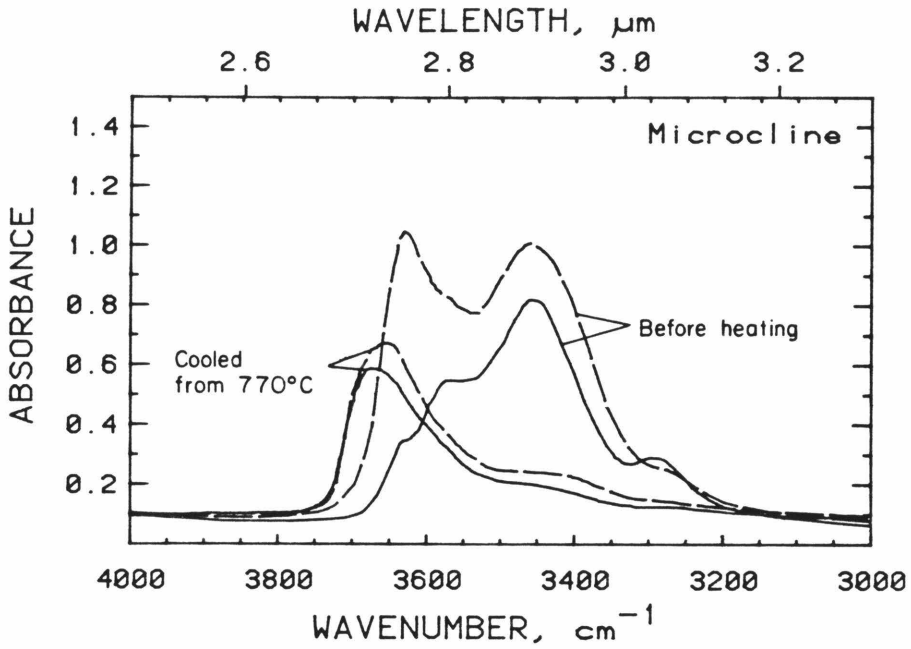

Figure 19. Comparison of the before and after heating spectra of the White Queen microcline showing the loss of both water types and the formation of a new, unidentified hydrous species. Spectra obtained at 25°C.

Lattice Modes

During the course of high temperature observations of O-H absorptions, some information on the thermal behavior of lattice modes was also collected. Figure 20 shows thermal effects in quartz and muscovite. In both minerals lattice modes broaden and shift to lower frequencies with temperature. In muscovite, the three bands that are on scale do not broaden greatly, while the off-scale absorption (near 1000 cm^{-1}) broadens considerably. In spectra taken during dehydration (at 750°C) this region was completely opaque, apparently due to structural changes in the mica.

Conclusions

High temperature observation of water and hydroxide in minerals has revealed a wealth of reactions and behaviors. In muscovite and quartz, hydroxyl groups appear much the same structurally at high temperature as at 25°C. In zircon, progressive and apparently coupled dehydration and recrystallization occurs in metamict material. Cordierite and beryl both form an intermediate, gas-like H_2O species prior to dehydration. In topaz and feldspar, irreversible changes in hydrogen speciation are observed.

For topaz, feldspar, beryl, and cordierite an understanding of the 25°C behavior of their trace hydrous components proves to be insufficient to understand those components at temperatures of geologic interest. The high temperature hydrogen speciation and sites differ in both reviresible and irreversible fashions. The irreversible changes observed in topaz and feldspar may provide information about the thermal history of the sample

Figure 20. (Next page) Thermal effects on lattice infrared modes. A) Quartz 5.07 mm thick, polarized E⊥C. Same sample as Figures 7-9. B) muscovite, 11 μm thick, polarized in β. Same sample as Figures 1 and 2.

20A)

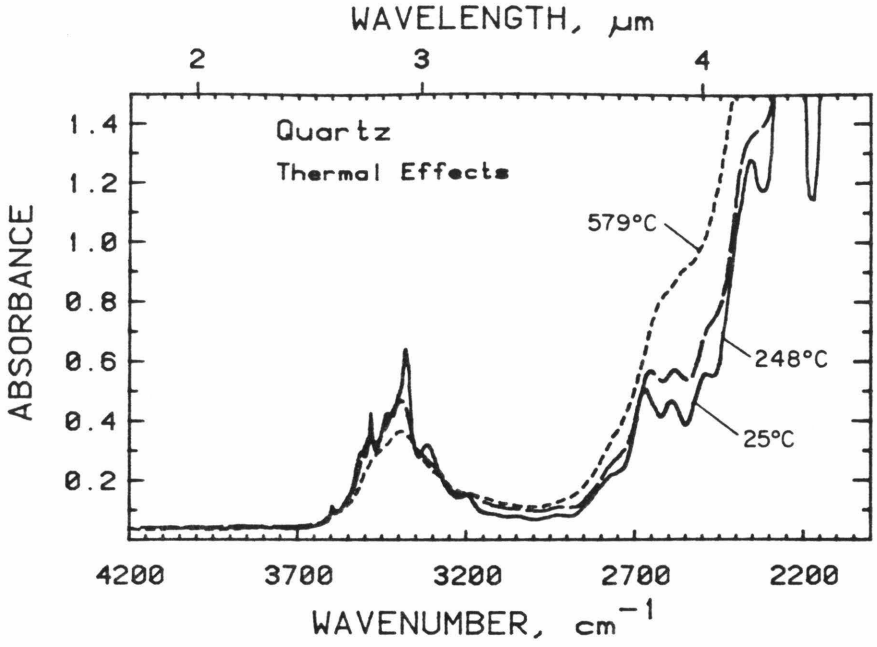
WAVELENGTH, μm
2
3
4
Quartz
Thermal Effects
579°C
248°C
25°C
ABSORBANCE
1.4
1.2
1.0
0.8
0.6
0.4
0.2
4200
3700
3200
2700
2200
WAVENUMBER, cm⁻¹

20B)

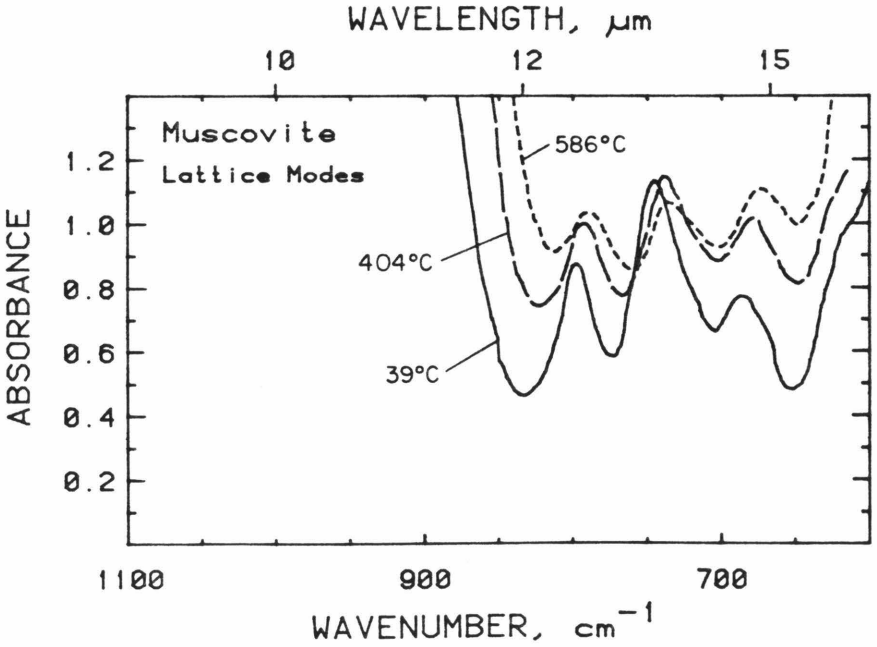
WAVELENGTH, μm
10
12
15
Muscovite
Lattice Modes
586°C
404°C
39°C
ABSORBANCE
1.2
1.0
0.8
0.6
0.4
0.2
1100
900
700
WAVENUMBER, cm⁻¹

In all cases I have studied, O-H stretching absorptions in minerals show negative shifts with temperature. This indicates that hydrogen-bonding considerations are not controlling the peak shifts, since that should result in predominantly positive shifts. The O-H bonds are behaving as simple diatomic oscillators instead (Aines and Rossman, 1984c, Chapter 3). Integral IR intensities generally decrease slightly with temperature, as is expected as O-H-O distance increases, and the net dipole first derivative decreases. Broadening in all sharp O-H absorptions occurs to about the same extent (same number of $cm^{-1}/°C$), indicating that it is due to scattering by lattice modes and not quantum mechanical changes in hydrogen bonding with temperature.

Acknowledgments

I would like to thank G. Cleve Solomon (Caltech) for his help, collaboration, and discussion on the problem of water in feldspar. Jim Woodhead and L. T. Silver (Caltech) provided similar assistance with zircon. The zircon experiment was run by Chris Finch, and the quartz experiment by Martin Ruzek, while they were undergraduate research assistants. Their help is gratefully acknowledged. This work was supported in part by National Science Foundation grants EAR-79-19987 and EAR-83-13098.

References

Aines, R.D. and Rossman, G.R. (1984a) Water in minerals? A peak in the infrared. Journal of Geophysical Research, in press.

Aines, R.D. and Rossman, G.R. (1984b) The high temperature behavior of water and carbon dioxide in the channels of cordierite and beryl. American Mineralogist, in press.

Aines, R.D. and Rossman, G.R. (1984c) The significance of infrared band shapes and positions in hydrogen bonded systems. (ms. 1984)

Aines, R.D. and Rossman, G.R. (1984d) Radiation damage and water in minerals. (ms. 1984)

Aronson, J.R., Bellotti, L.H., Eckroad, S.W., Emslie, A.G., McConnel, R.K., and von Thüng, P.C. (1970) Infrared spectra and radiative thermal conductivity of minerals at high temperatures. Journal of Geophysical Research, 75, 3443-3456.

Dolino, G., Bachheimer, J., Gervais, F., and Wright, A.F. (1983) La transition α-β du quartz: le point sur quelques problemes actuels: transition ordre-désordre ou displacive, comportment thermodynamique. Bulletin de Minéralogie, 106, 267-285.

Freund, F. (1970) Infrared spectra of $Mg(OH)_2$ at elevated temperatures. Spectrochemica Acta, 26A, 195-205.

Freund, F. (1974) Ceramics and thermal transformations of minerals. In, The Infrared Spectra of Minerals, V.C. Farmer, ed., pp. 465-482. Mineralogical Society of London.

Fruwert, J., Kowasch, E., and Geisler, G. (1966) Temperature dependence of the intensity of infrared bands. Zeitschrift für Physicische Chemie, 232, 415-417.

Hobbs, B.E. (1981) The influence of metamorphic environment upon the deformation of minerals. Tectonophysics, 78, 335-383.

Hofmeister, A.M. (1984) A spectroscopic and chemical study of the coloration of feldspars by irradiation and impurities, including water. Thesis, California Institute of Technology, Division of Geological and Planetary Science.

Johari, G.P. and Chew, H.A.M. (1983) O-H stretching vibrations in ice clathrate. Nature, 303, 604-605.

Kats, A. (1962) Hydrogen in alpha-quartz. Philips Research Reports, 17, 133-195 and 201-279.

Kekulawala, K.R.S.S., Paterson, M.S., Boland, J.N. (1978) Hydrolytic weakening in quartz. Tectonophysics, 46, T1-T6.

Neszmelyi, A., and Imre, L. (1968) Evaluation of IR absorption band intensities in measurements above room temperature. Spectrochemica Acta, 24A, 297-300.

Parise, J.B., Cuff, C., and Moore, F.H. (1980) A neutron diffraction study of topaz; evidence for lower symmetry. Mineralogical Magazine, 43, 943-944.

Ribbe, P.H. and Gibbs, G.V. (1971) The crystal structure of topaz and its relationship to physical properties. American Mineralogist, 56, 24-30.

Shankland, T.J., Nitsan, V., and Duba, A.G. (1979) Optical absorption and radiative heat transport in olivine at high temperature. Journal of Geophysical Research, 84, 1603-1610.

Solomon, G.C. and Rossman, G.R. (1984) Water in feldspar. I. Submitted to American Mineralogist.

Stein, J. and Shankland, T.J. (1981) Radiative thermal conductivity in obsidian and estimates of heat transfer in magma bodies. Journal of Geophysical Research, 86, 3684-3688.

Van Goethem, L., Van Landuyt, J., Amelinckx, S. (1971) The α-β transition in amethyst quartz as studied by electron microscopy and diffraction. Physica Status Solidii (a), 41, 129-137.

Wedding, B. (1975) Measurements of high temperature absorption coefficients of glasses. Journal of the American Ceramic Society, 58, 102-105.

Wood, D.L. and Nassau, K. (1967) Infrared spectra of foreign molecules in beryl. Journal of Chemical Physics, 47, 2220-2228.

Wright, A.F. and Lehmann, M.S. (1981) The structure of quartz at 25 and 590°C determined by neutron diffraction. Journal of Solid State Chemistry, 36, 371-380.

Chapter 8

The High Temperature Behavior of Water and Carbon Dioxide in Cordierite and Beryl

(Text of article accepted for publication in
The American Mineralogist,
George Rossman coauthor)

Abstract

We have studied the behavior of molecular water and carbon dioxide in the channels of cordierite and beryl at temperatures up to 900°C using high temperature infrared spectroscopy. Above 400°C water that is structurally bound in the channels begins partitioning into an unbound state with the characteristics of a gas. The process is fully reversible and involves both type I and type II water in both minerals. Dehydration occurs after most of the water is in this unbound state, and channel cations are no longer coordinated by the type II water molecules. These cations can then move to the walls of the channels or be expelled from the channel, opening the channel for dehydration of the water contained in it. This behavior is contrasted with that of muscovite, in which the hydroxide shows no change in speciation and only slight changes in its spectroscopic properties at temperatures below the dehydration point. CO_2 in the channels of cordierite does not undergo major changes in bonding at high temperatures. Although all the water in the cordierite was released, about 40% of the CO_2 remained after heating to 800°C. Heating to 900°C was required to expel all CO_2. This is indicative of the tighter wedging of CO_2 in the channels. Because of an equilibrium among type I, type II, and unbonded gaslike water at high temperature, the concentration of type I alone serves as an indicator of the water fugacity. The type II concentration only responds to the number of channel cations and need not be considered in water fugacity calculations. Cordierites with greater numbers of channel cations will effectively close to re-equilibration at higher temperatures, making them more suitable as indicators of water and carbon dioxide fugacity.

Introduction

The potential use of cordierite as a water and carbon dioxide fugacity indicator in rocks has generated much current interest in the thermodynamics and structural properties of the gases contained in its channels. Cordierite and beryl are also of interest as models for extremely small channel zeolites and for the behavior of water trapped in small cavities in other minerals. We report here studies of the behavior of the channel water and carbon dioxide in these two minerals at temperatures up to 900°C. The primary tool used in this study was high temperature infrared spectroscopy on oriented, natural, single crystals.

Cordierite and beryl are structurally similar, containing $(Si,Al)_6O_{18}$ and Si_6O_{18} rings which define channels parallel to the c axis. The most common contents of these channels are water, carbon dioxide, and alkali cations (Wood and Nassau, 1967; Armbruster and Bloss, 1980; Cohen et al., 1977; Hawthorne and Cerny, 1977; Zimmermann, 1981). In both minerals water can assume two orientations in the channel (Wood and Nassau, 1967; Goldman et al., 1977). Type I water has its H-H vector parallel to c, and type II has its H-H vector perpendicular to c (Figure 1). The presence of an alkali cation seems to predispose any adjacent water molecule to reside primarily in the type II orientation, while in the absence of a cation the type I orientation is preferred. These positions are not rigid. Carson et al. (1982) used NMR to demonstrate that indivdual water molecules can hop between the two orientations in cordierite. A rotational IR spectrum is observed in beryl (Wood and Nassau, 1967) which is also consistent with motion of this type. The

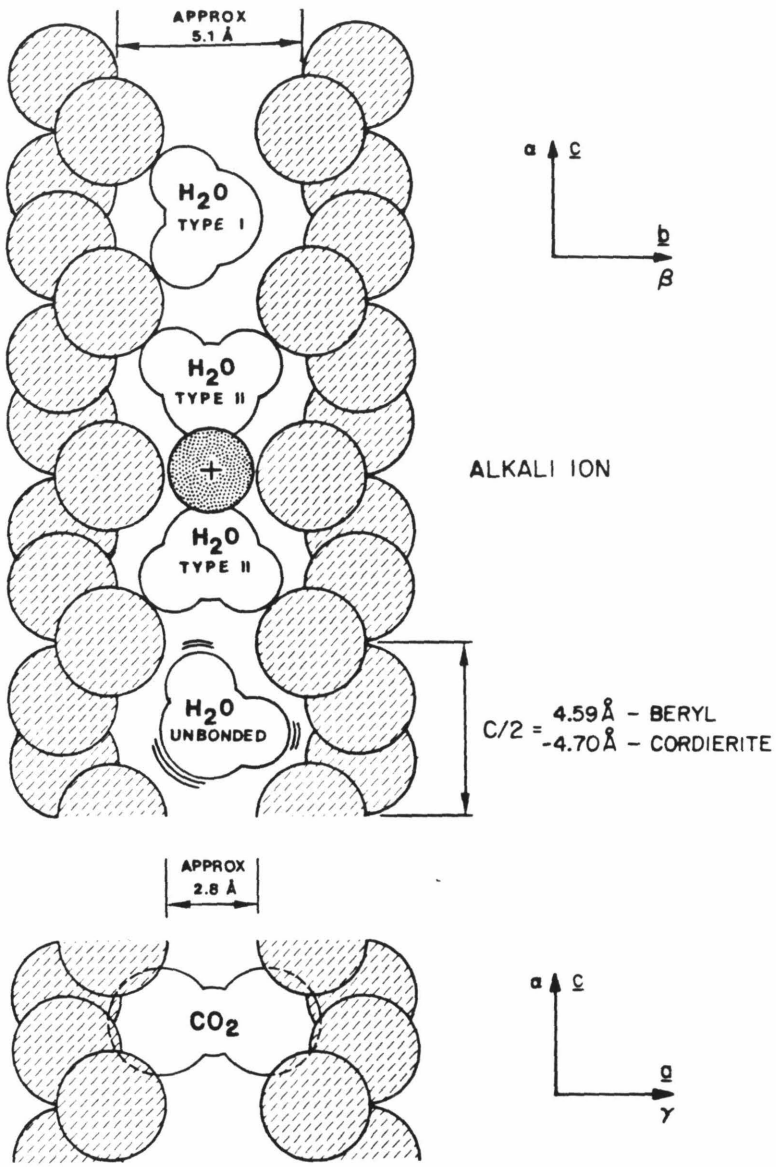

Figure 1. Schematic representation of the orientations of channel constituents.

fact that type I and type II water molecules are distinct on an IR time scale (about 10^{-12} seconds) but indistinct on an NMR time scale (about 10^{-6} seconds) indicates a residence time in the bonded state that is somewhere between these values at room temperature.

The crystallographic and thermodynamic status of water in cordierite will have a substantial effect on any attempt to use cordierite as a water fugacity indicator. Experimental work (e.g. Johannes and Schreyer, 1981; Armbruster and Bloss, 1982) has emphazised Mg-cordierite with no channel cations and no type II water. The theoretical model of the H_2O-cordierite system by Martignole and Sisi (1981) also considers only one water site. A thermal release study by Zimmerman (1981) of the gases contained in cordierites from different origins did not consider the presence of multiple water sites or the influence of channel cations on release patterns. The relationship between the two types of water, channel cations, and also carbon dioxide in the channels must be understood before these studies can be confidently applied to natural systems. Such an understanding can be advanced by studying the channel constituents at the temperatures of cordierite formation.

Experimental Method

Single crystal samples of previously studied cordierite (Goldman et al., 1977) and beryl (Goldman et al., 1978) were used. The cordierite, #5 in Goldman et al. (1977), is from a metamorphic pegmatite near Manitouwadge, Ontario, Canada (Pye, 1957). The beryl, #8 in Goldman et al. (1978), is from Brazil. Analytical data for the cordierite are given in Table 1 (pg 271); additional data are contained in Goldman et al. (1977). Data for the beryl are contained in Goldman et al. (1978). Both samples are homogeneous

at microprobe detection limits.

Infrared spectra were obtained in the 4000 cm^{-1} to 1200 cm^{-1} region using a Perkin-Elmer model 180 grating infrared spectrophotometer using techniques described by Goldman et al. (1977) for room temperature spectra. The same doubly polished oriented single crystal slabs were used for all measurements. At higher temperatures similar methods were used, but the sample was mounted in an evacuated, $Pt_{80}Rh_{20}$ wound tube furnace which is placed in the spectrophotometer. The beam from the spectrometer passes through KCl windows in a vacuum jacket and down the length of the tube furnace, which is 2.5 cm in diameter and 12 cm long. Approximately 10 mm^2 of sample, in the form of an unsupported section, 20-40 m thick is exposed to the spectrometer beam. The sample, mounted on a stainless steel aperture using stainless steel straps, sits in the middle of the furnace. The sample temperature reported for these experiments is measured in the stainless steel sample mount adjacent to the sample since the sample is too fragile to support a thermocouple. In experiments with a 5 mm thick quartz slab with thermocouples mounted in the sample, the aperture was 10°C hotter than the sample.

One doubly polished beryl slab was used. This was an ac section 40 μm thick. Two cordierite slabs were used; one optimized for H_2O observation, a bc ($\beta\alpha$) section 60 μm thick, and one optimized for CO_2 observation, an ab ($\gamma\beta$) section 16 μm thick. The ab section contained a simple {130} twin. About 20% of the slab was not an ab section, therefore, and the polarizations E∥a and E∥b are mixed slightly.

Spectra obtained from the beryl, the bc cordierite and the muscovite section were digitized to produce Figures 2, 3, and 6. Data from the ab cordierite section were collected in digital form using a computer interface and were used directly to produce Figures 4 and 5. This was necessitated by the low intensity of the H_2O bands and the CO_2 rotational bands in this section, which was optimized for the CO_2 stretching peak.

The effects of black body radiation by the furnace and sample are eliminated by double chopping of the spectrometer beam; the pure emission spectrum of the sample and furnace is subtracted electronically from the observed absorption spectrum, yielding the actual absorption spectrum. This subtraction becomes impractical above 900°C because the intensity of the black body radiation becomes much greater than that of the spectrometer beam. This causes the thermopile detector to behave nonlinearly, and is evidenced as an apparent phase shift in the sample and reference beam. This phase shift was checked at all temperatures and is not an important factor until 800°C; above this the absorbance measurements become increasingly non-linear. All absorbance values reported here and shown in the figures are accurate to within approximately ± 2%, verified using standard absorption screens.

Results

Infrared spectra were obtained in the 3600 cm^{-1} region where stretching modes of water occur, in the 1600 cm^{-1} region where the bending mode occurs, and in the 2300 cm^{-1} region where CO_2 absorbs. Beryl was studied between -180° and 700°C and cordierite was studied between 35° and 915°C.

Beryl

Figure 2 shows the ε-spectrum (E$\parallel$ c) of the beryl between 35° and 700°C. The peaks are indexed according to Wood and Nassau (1968). For type I water, absorptions occur at: 3694 cm^{-1} in ε, (ν_3, asymetric stretching), 3555 cm^{-1} in ω, (ν_1, symmetric stretching), and 1595 cm^{-1} in ω, (υ_2, bending). For type II water, the corresponding absorptions occur at: 3655 cm^{-1} in ω, 3592 cm^{-1} in ε, and 1628 cm^{-1} in ε. Both type I and type II water are present, which is consistent with the alkali content of this sample (Goldman et al., 1977.) Figure 1B also shows an overtone absorption of a lattice mode, at 1929 cm^{-1}. No CO_2 absorptions were detected in the infrared spectrum of this sample.

At high temperatures, the peaks broaden slightly and decrease in intensity. The broadening is attributable to an increase in the range of O-H ••O distances in the environments of the H_2O molecules brought on by thermal motion. At 330°C the intensity of the original peaks is diminished, and a new component is added to the spectra. There is a broad band of equal intensity in both polarizations, centered at approximately 3650 cm^{-1}. This band was not apparent at 160°C. The intensity of this band increases with temperature at the expense of the sharp peaks of type I and type II water. The two water types appear to be partitioning into the state represented by the broad band. This partitioning is reversible. Upon cooling the broad band disappears and the spectra of the two water types are identical to those obtained before heating. Although both type I and type II water partition into the state resulting in the broad band, there is only evidence of a single broad band. The two water types do not partition equally into

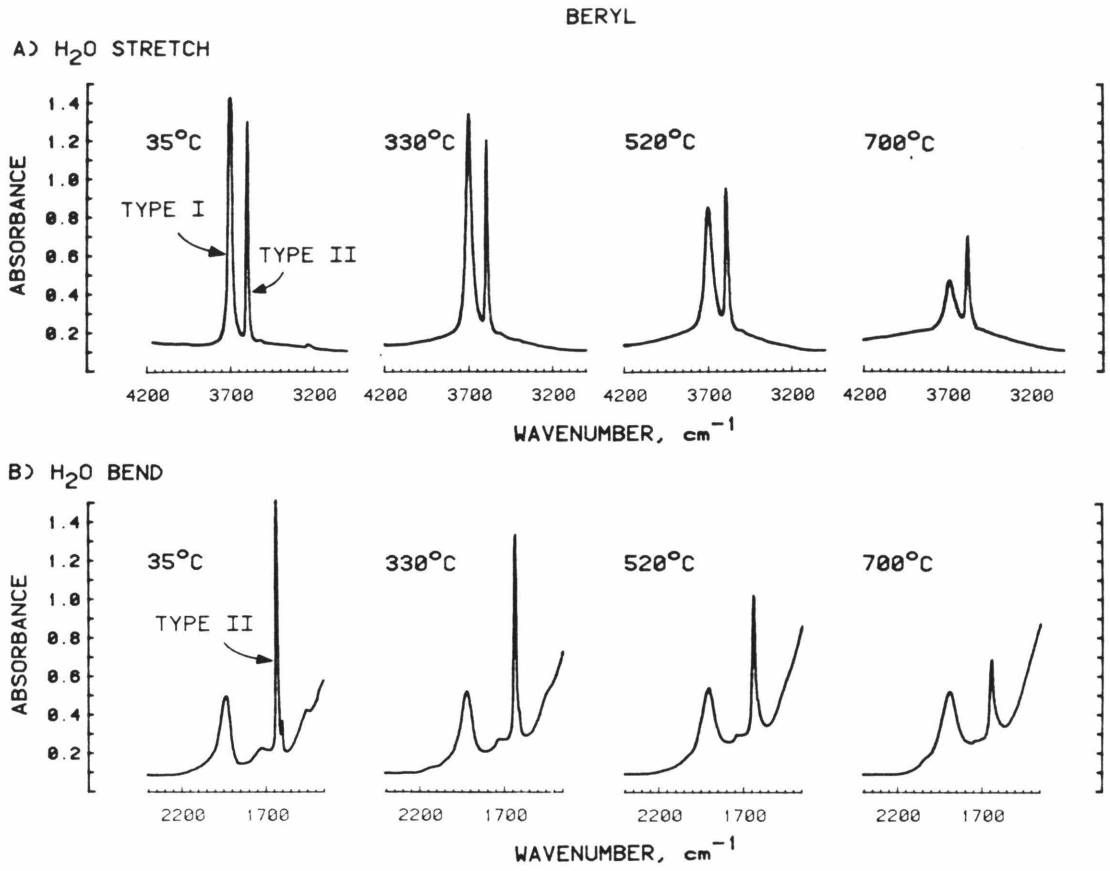

Figure 2. Infrared spectra of a 40 μm thick single crystal of beryl. Polarized E∥c. A) O-H stretching region, B) H-O-H bending region. Labels indicate sample temperature at time of measurement. The broad band in the H_2O stretching region, centered at ~3600 cm^{-1}, is apparent at 330° but is best seen at 700°C.

this third state; type I water enters it at lower temperatures as is evidenced by the more rapid loss of intensity of the type I stretching peak in Figure 2. It is not possible to resolve a broad band in the bending region (1600 cm^{-1}) although the peak intensities there show similar decreases to the stretching peaks. The loss of intensity in the sharp peaks is not due to broadening, because the integrated intensity of the peaks decreases at the same rate that the integrated intensity of the broad band increases.

The sample remained at 700°C for 2 hours. When cooled and measured at 35°C, some dehydration had occurred as indicated by a loss of intensity of 15% for both water types. The relative intensities remained approximately the same as before heating.

Cordierite

The cordierite H_2O spectra (Figure 3) show the same features observed in the beryl spectra, but the peaks are broader and less well defined in cordierite. The indexing of the peaks, according to Goldman et al. (1977) follows the same pattern as for beryl. For type II water, absorptions occur at: 3632 cm^{-1} in β, (ν_3, asymmetric stretching), 3574 cm^{-1} in α, (υ_1, symmetric stretching), and 1630 cm^{-1} in α, (ν_2, bending). For type I water absorptions occur at: 3689 cm^{-1} in α, (asymmetric stretching), the exact position of the ν_1 symmetric stretch is not assigned, but it occurs in β, and the bending mode appears in β as a triplet centered near 1600 cm^{-1}. Figure 3B shows a silicate lattice overtone at 1880 cm^{-1} similar to that in beryl, Figure 2B. The increased complexity of this band is presumably due the lower symmetry of the $(Si,Al)_6O_{18}$ rings in cordierite.

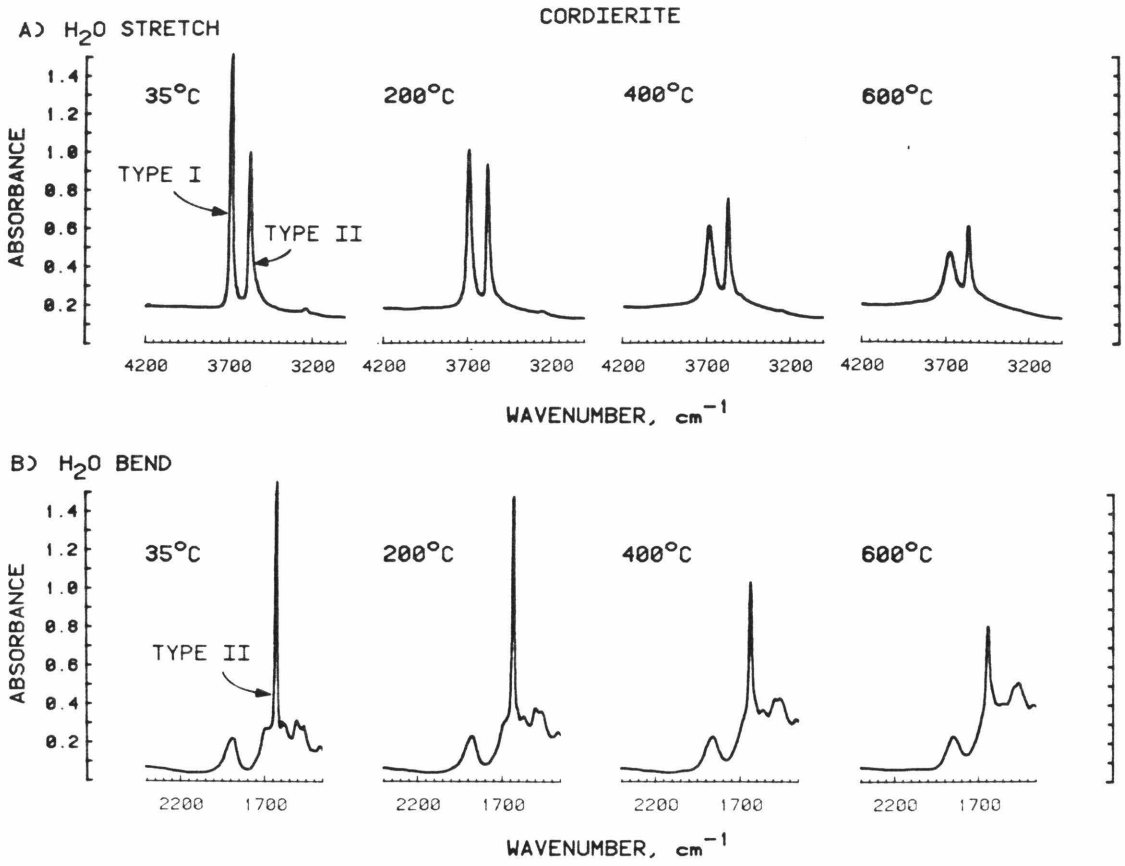

Figure 3. Infrared spectra of a 60 μm thick single crystal of cordierite (optimized for H_2O observations). Polarized E$\parallel$c (α). A) O-H stretching region, B) H-O-H bending region. Labels indicate temperature of sample at time of measurement. The broad band is centered at ~3600 cm^{-1} as in beryl, but is spread over a wider range of energies and therefore is less intense at 3600 cm^{-1} (see Figure 4).

In cordierite the reversible formation of the broad band at high temperatures occurs in an analogous fashion to beryl, but it begins at a lower temperature (200°C) as does dehydration (600°C). The same reversal in type I/type II peak intensities occurs as the temperature increases. The lower dehydration temperature of cordierite allowed us to observe it going to completion. At 600°C the integrated intensity ratio of sharp peak (types I & II) to broad band is about 3:1 (Figure 3A). At 800°C dehydration occured too rapidly for us to obtain a complete spectrum from the bc slab, however, the sharp peak to broad band ratio was approximately 5:1. As the crystal dehydrated this ratio remained approximately constant. Type I and Type II waters were lost at the same rate.

The ab section allowed us to obtain information on the isotropy of the broad band state. In the room temperature γ polarization ($E \| a$) there are no absorption features due to water identified as type I or II. The high temperature broad band state is isotropic, however, and is clearly seen in γ at 655°C (Figure 4). (The sharp peaks seen in the γ spectrum are due to the slight mixing of polarizations and to minor unidentified OH species.) At 655°C dehydration was occurring slowly. At 755°C dehydration occurred more rapidly and was complete in 2 hours. Upon cooling, all the bands attributable to types I & II water were gone.

This cordierite sample also contains CO_2 in the channels, as is evidenced by a sharp peak at 2348 cm^{-1} in γ (as assigned by Armbruster and Bloss, 1982). This peak is due to asymmetric stretching of CO_2 and its polarization indicates that the CO_2 molecule is oriented with its long axis parallel to the a axis of the crystal. This orientation has

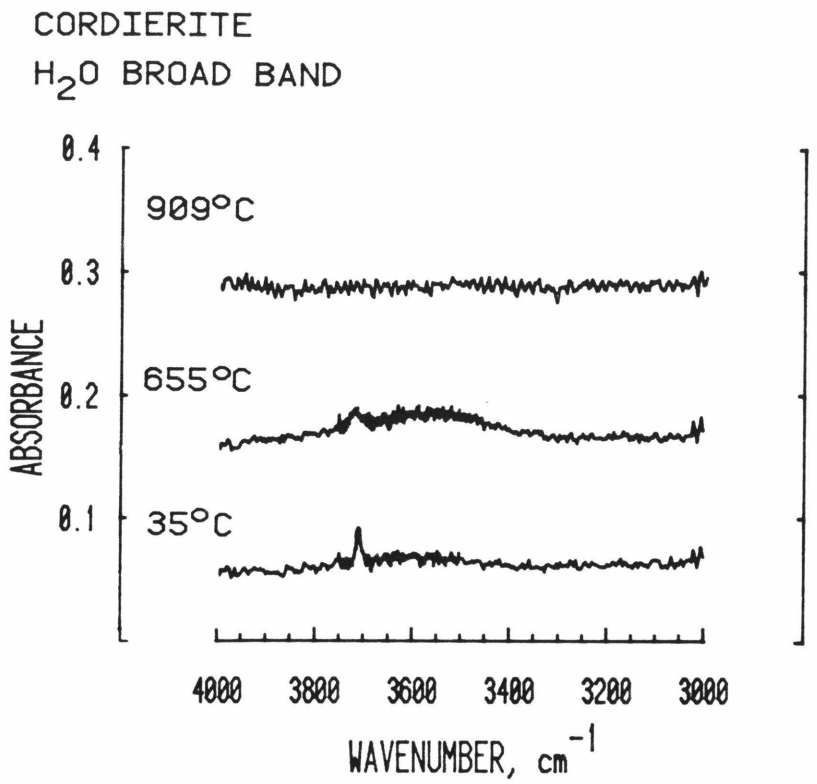

Figure 4. Infrared spectra of a 16 μm thick single crystal of cordierite. Polarized E$\parallel$a (γ). The broad absorption present at 655° disappears after the sample dehydrates at 755°C. The 909°C spectrum shows that the high temperature broad band absorption is caused by H_2O and that it disappears after dehydration. Labels indicate temperature of sample at time of measurement. Peak at 3740 cm^{-1} is caused by a minor, unidentified hydrous species. Baseline corrected to remove elements of the β spectrum mixed in by a twin in the sample.

also been suggested on the basis of structural criteria (Johannes and Schreyer, 1981) and optical properties (Armbruster and Bloss, 1982) and is consistent with the orientation of CO_2 in beryl (Wood and Nassau, 1967). Two sidebands occur at 2307 cm^{-1} and 2390 cm^{-1} in β. These have the characteristics of rotational, or more likely librational, sum and difference combination bands involving both the stretching motion and a coupled, hindered rotation.

The spectra of CO_2 in the γ and β directions are shown in Figure 5. These directions are slightly mixed by the twin in the sample. Room temperature observation of the untwinned portion of the sample indicates that the side bands are completely polarized in β, and the fundamental completely in γ. High temperature spectra require a large aperture, so the twinned sector had to be included in those measurements.

At high temperatures the only change apparent in the CO_2 spectrum in both polarizations is a broadening of the peaks. The integrated intensity in γ increases about 50% as the sample is heated. In γ the broadening is asymmetric, with a lower energy shoulder becoming prominent. It appears that the rotational bands center on this shoulder, and not the sharper peak, at high temperature. No broad band behavior is observed. Upon cooling from below 650°C the spectra are identical to the original spectra. Beginning at 700°C some decarbonation occurs. As mentioned previously, the ab section was held at 755°C for 2 hours until all the H_2O was gone. Only 20% of the CO_2 was lost. The sample was then heated in increments of 10° to 915°C, losing CO_2 more rapidly at each step. After 20 minutes at 915° no CO_2 remained. The decarbonation rate could also be observed in the bc section, using the rotational bands. This section was heated from 600° to 800°C quickly,

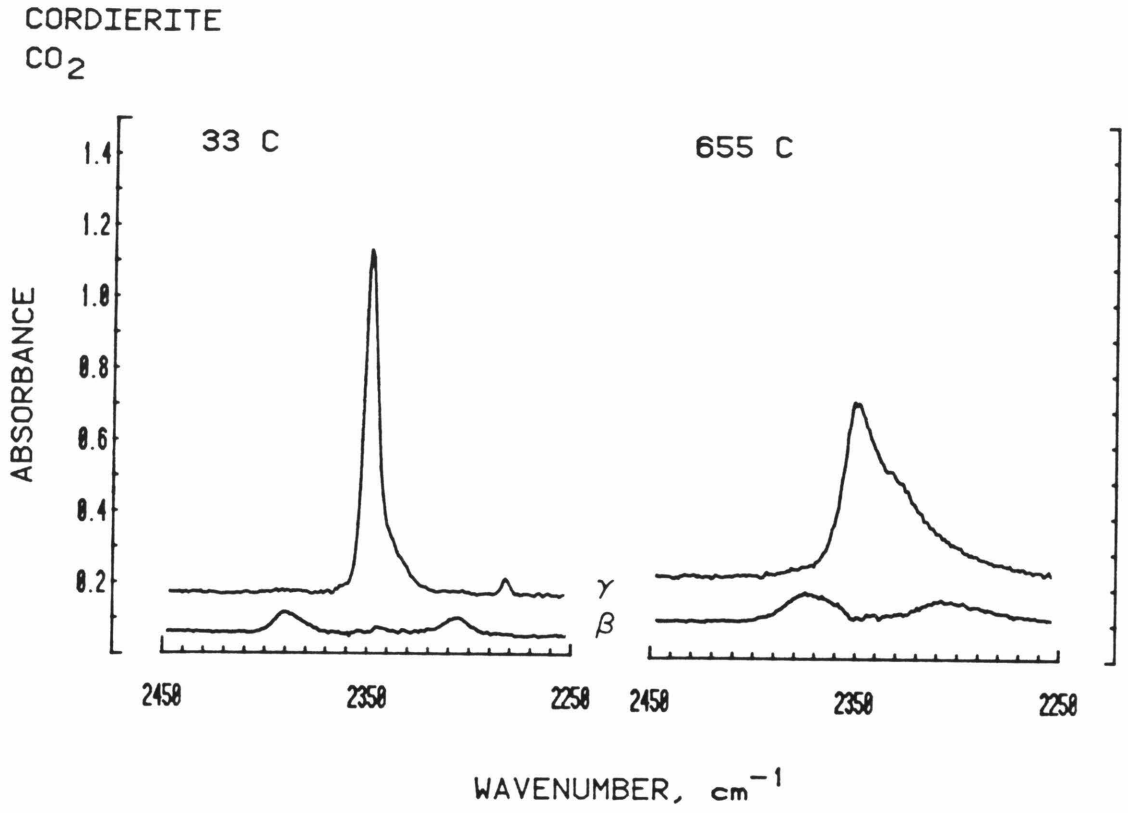

Figure 5. Infrared spectra of a 16 μm thick single crystal of cordierite, the same crystal as Figure 4, showing the absorptions due to CO_2. Polarized E∥a (γ) and E∥b (β). Labels indicate sample temperature at time of measurement. β spectra have been baseline corrected to remove elements of the γ spectra mixed in due to a twin in the sample. γ spectra are uncorrected.

and allowed to remain at 800°. This procedure resulted in a greater loss of CO_2 (60%) at 800°C than was observed in the 10° stepwise heating of the ab section (30%).

For the purposes of comparison we also include the high temperature spectra of muscovite (Figure 6). The single hydroxide group gives a single peak, and no broad band is observed at high temperature. The peak shifts slightly to lower energies (from 3625 cm^{-1} to 3612 cm^{-1}), and is slightly broadened at high temperature. The integrated intensity is approximately constant. At 700°C the sample was observed during dehydration, and no spectroscopic changes other than loss of intensity occured during this process. We have also observed topaz, quartz, and feldspar at high temperatures and seen no evidence of the formation of a broad band, or of large intensity decreases prior to dehydration. This indicates that the many of the changes observed in the beryl and cordierite spectra, in particular the formation of the broad band, are not general characteristics of high temperature.

Discussion

Speciation of water at high temperature

The formation at high temperature of a state of water which yields a broad band IR spectrum is most easily explained by postulating that water can exist in beryl and cordierite in both bound and unbound states. The bound states are types I and II. The unbound state has the characterisitics of a gas, with a typical gas IR spectrum which is broad and isotropic. The formation of this gas-like state is reversible, with the type I/type II ratio the same before and after heating. This suggests that although the gas-like water molecules are not bound, they are

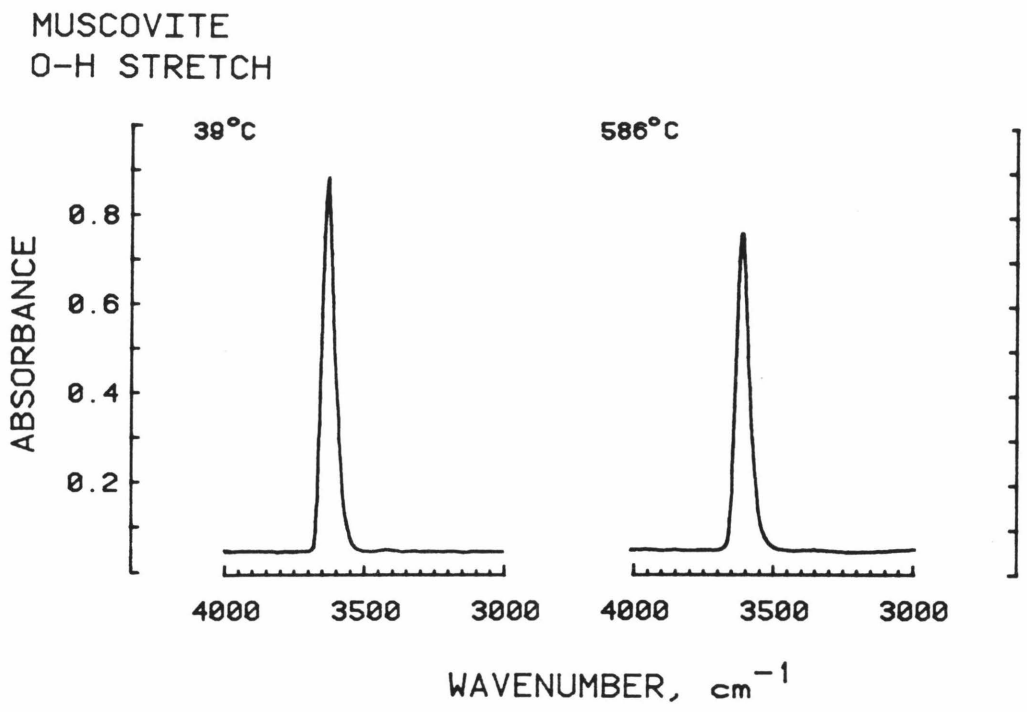

Figure 6. Infrared spectra of a single crystal cleavage flake of muscovite 11 μm thick. The 586° spectrum was obtained 150° below the dehydration point. Polarized approximately E$\parallel$a. Labels indicate temperature at time of measurement.

confined to the ring voids that they occupy at low temperature. The motion of the gas-like molecules is distinct from the fluctional motion that Carson et al. (1982) observed in cordierite, and from the motion resulting in the librational bands in beryl (Wood and Nassau, 1967). These motions are restricted to the plane defined by the type I - type II orientations (the bc plane in cordierite), and would only result in the interconversion of the two types. The formation of the gas-like state results in a water molecule that can assume any orientation in the channel.

Our observation of gas-like water is consistent with high temperature x-ray diffraction work on cordierite done by Hochella et al. (1979). They refined the structure of an Mg-rich cordierite (poor in channel cations) at 24°, 375°, and 775°C. At 375° the peak in the electron density map ascribed to oxygen in channel water broadens in the a direction, the large axis of the cavity. At 775°C the peak disappeared, but it reappeared upon cooling, with some dehydration having occured. Hochella et al. attribute the disappearance at 775°C to thermal motion, which is consistent with our postulated gas-like state. At this temperature the water is almost completely in the broad band state. The broadening at 375°C could either be due to type I - type II interconversion motion, or to the formation of the gas-like state.

Dehydration mechanism

The close association between the formation of the gas-like H_2O state in cordierite, and the onset of dehydration, is probably not coincidental. Just below the point of dehydration (600°C) the ratio of unbound to bound water is 3:1 (Figure 3). During dehydration at 700° to

800°C (not shown) it is higher, 5:1 or greater. Both values are approximate due to difficulty integrating the overlapping bands. In beryl, which is known to dehydrate at higher temperatures than cordierite, (e.g. Brown and Mills, 1983), the partitioning of bound into unbound states is delayed relative to cordierite. At 700°C in beryl the ratio of unbound to bound water is only 2:1 (Figure 2), and only minor dehydration occured.

This close association between the unbound water and dehydration can be explained using a model involving the hydration of channel cations. It is now accepted that the intermediate size channel cations such as Na^+ and Fe^{3+} reside in the center of the $(Si,Al)_6O_{18}$ rings in both minerals (Hawthorne and Cerny, 1977; Hochella et al., 1979; Brown and Mills, 1983). This is the most restricted point in the channel. These cations are then coordinated by two type II water molecules, one above and one below in the channel (Goldman et al., 1977; Hawthorne and Cerny, 1977). Our data suggest that the dehydration of beryl and cordierite proceeds when these coordinating water molecules are partitioned into the gaslike state. We propose that the coordinating water molecules hold the cation in its central position, where it completely plugs the channel. When the water molecules are partitioned into the gas-like state and are removed from their coordinating positions, the cation is released and moves into the larger part of the channel, releasing the other contents of the channel. Such motion of Fe^{3+} to the walls of the channels in dehydrated cordierite was proposed by Goldman et al. (1977) on the basis of optical spectra.

When enough of the channel cations are simultaneously not coordinated, dehydration can occur. We interpret the pervasive cracking of both

minerals at temperatures above the normal dehydration point as due to build up of gas pressure in the channel as larger continuous volumes with unplugged cations form. If, however, the dehydration point is not exceeded greatly, the equilibrium between diffusion down the channel and the release of coordinated channel cations allows dehydration to occur without cracking.

Decarbonation mechanism

During heating of cordierite, no CO_2 is lost before H_2O, but a substantial amount remains after all the H_2O is gone. This is probably due to tight wedging of CO_2 in the cavity, as described by Johannes and Schreyer (1981). This tight wedging appears to cause CO_2 to diffuse slowly along the channel, and considerably higher temperatures are required to remove CO_2 than H_2O, 900° vs 750°C. The different rates of CO_2 loss in the two sections we studied appear to be due to the heating rates. The section heated rapidly to 800° lost considerably more CO_2 up to that point than the one heated gradually to that point. One explanation for this is that some CO_2 is swept out by the H_2O in the rapidly heated sample, but that when the heating rate is more gradual water diffuses down the channels without carrying CO_2 with it. Zimmerman's (1981) data support this. Using mass spectrometric analysis of the gas released from continuously heated cordierites he observed smooth water release curves, with release generally beginning at around 500°C and reaching a maximum near 700°C. In contrast CO_2 and CH_4 were released in two pulses, the first corresponding to the initial release of water, and the second not occuring until 900°C.

CO_2 does not appear to undergo any changes in speciation or bonding prior to decarbonation. Our observations are consistent with simple diffusional loss, but at a much slower rate than H_2O. This reflects the fact that CO_2 is wedged in the larger part of the channel while H_2O is held in largely by weak hydrogen bonds and the cations plugging the channel. The effective length of the linear CO_2 molecule is 4.96Å (Wood and Nassau, 1967), while the effective diameter of the H_2O molecule is only 3.40Å (Langer and Schreyer, 1976).

Several questions remain concerning the high temperature behavior of CO_2. We do not have satisfactory explanations for the appearance of the low energy shoulder in the γ spectrum, or for the behavior of the rotational-librational bands which center on it and grow in intensity along with it. Certain possibilities may be ruled out, however. The shoulder does not represent a broad band state, since it only appears in γ. Likewise, the librational bands are only in β. This means the CO_2 molecule is to some degree in a state of different energy, but it is still highly oriented. When coupled with the rapid equilibration and reversibility of the sharp band to shoulder conversion, this orientation of the CO_2 molecule suggests that it remains in the same channel site at high temperatures.

Orientation of water and its effect on the structure

Early models of water in cordierite and beryl emphasized rigid positions. It is apparent that this is not the case, and that depending on the time scale of the observation water in cordierite can be in motion in two ways: the hopping between types I and II seen by Carson et al., and the random motion of the gaslike state proposed here. The room temperature predominance of rotational bands that are consistent

with the hopping motion, and the lack of rotational bands corresponding to motion in other directions, indicates that it is the predominant motion at low temperatures. In beryl, an additional motion at room temperature has been observed by Rehm (1974) using microwave spectroscopy, this being the rotation of type I molecules around the crystallographic c axis such that the water always occupies symmetrically equivalent positions in the channel. In both minerals the random motion of gas-like water molecules predominates at high temperatures, but it may occur to a small extent at all temperatures. These motions appear to contribute to the difficulty in resolving the positions of water molecules by diffraction techniques. It is not possible to directly reconcile the neutron diffraction data taken at room temperature by Hochella et al. (1979) with the IR data by appealing to these motions, however. They report positions which cannot be considered to be averages over the positions and motions described here. It seems likely that the extreme differences in time scale for IR vs diffraction measurements (10^{-12} vs $\sim 10^{3}$ seconds) allows for the diffraction methods to be observing a long term average not predictable by spectroscopic methods.

The apparent effect of channel H_2O on the structure and properties of cordierite can be substantial (Stout, 1975; Hochella et al., 1979) but as Langer and Schreyer (1976) have pointed out, the absorption energies of the stretching modes indicate a lack of strong hydrogen bonds. We suggest that the coupling mechanism between the lattice properties and the presence of water is the coordination of channel cations by water. By holding the cations in the intra-ring position type II water can have a substantial effect on the structure in an indirect fashion.

Implications for the use of cordierite as a petrogenetic indicator

An important limitation in the use of cordierite as a water fugacity indicator is the difficulty in accounting for both type I and type II water. The required task of experimentally calibrating the entire range of possible H_2O, CO_2, and alkali contents for cordierite would be immense, and some simplification is called for. We suggest that since the low temperature type I/type II ratio reflects accurately the high temperature ratio, it is only necessary to consider the concentration of type I water in order to arrive at the original water fugacity. Type II water, as well as type I, is originally incorporated in an equilibrium form with the gas-like state, and two type II waters will coordinate each channel cation at low temperature. This leaves the remaining sites to be filled by type I H_2O or CO_2, as well as possible exotic species like the rare gases. The equilibrium at high temperatures between type I, type II, and gas-like water assures that the final low temperature concentration of type I water is an accurate reflection of the original H_2O fugacity.

The ease with which type I and type II waters may be distinguished using IR spectroscopy makes this the ideal technique for petrologic application of cordierite as an H_2O-CO_2 fugacity indicator. We suggest the following method. Since type II H_2O seems to only respond to the number of channel cations, it is not considered and the number of sites taken up by it are subtracted from the total available sites. These sites are filled by type I H_2O, CO_2, other constituents, or they are empty. A simple model ignores the other constituents because of the complexity of their partitioning into the crystal. This leaves type I H_2O, CO_2, and empty sites to be considered, and these are exactly the

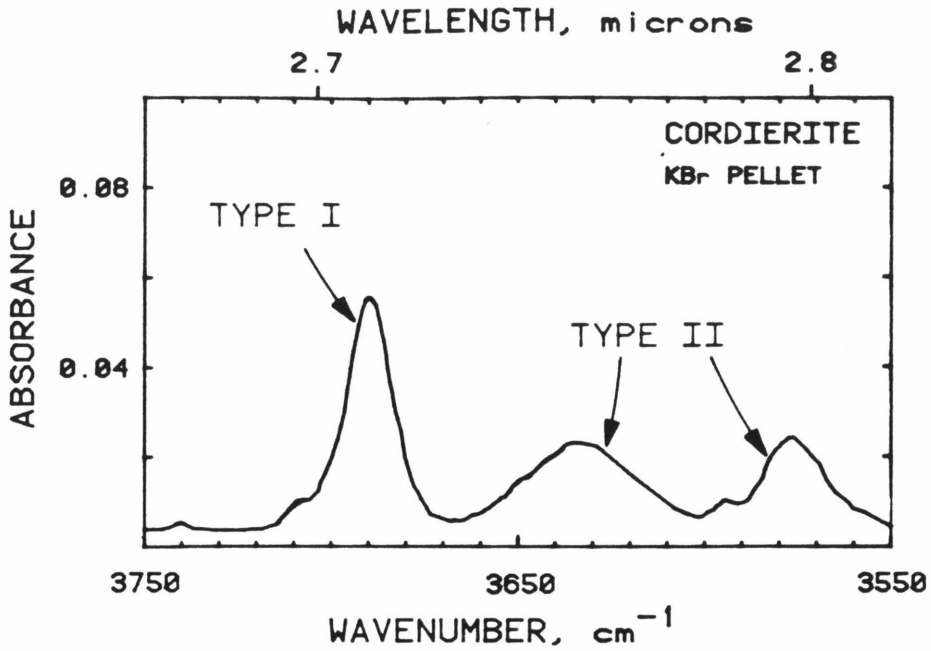

Figure 7.

Infrared spectra of cordierite powder, 2.07 mg in 200 mg of KBr pressed into a 1 cm radius pellet. Baseline due to H_2O trapped in the KBr has been subtracted. Spectra of this type could be used to measure H_2O concentration and speciation in cordierite.

parameters considered and calibrated by Johannes and Schreyer (1981). The implicit assumptions in this technique are: 1) there are no important channel constituents aside from H_2O, CO_2, and cations of intermediate size; 2) all channel cations are coordinated by two type II H_2O molecules; 3) once the sites filled by type II H_2O are removed from consideration, the remaining sites are filled by H_2O and CO_2 as if there were no channel cations or type II H_2O present.

The concentration of the important channel constituents, that is, types I and II H_2O, CO_2, and empty sites, will be easily determined by IR spectroscopy. The powder spectrum of the cordierite used in this study is shown in Figure 7. The two water types are well resolved from each other. CO_2 (not shown) also is resolved at 2348 cm^{-1}. Only 2 mg of sample are required for this technique, and our experience indicates that it can be a quantitative technique provided uniform sample handling procedures are followed. All that is required are good calibrations of molar absorptivities. Two major advantages to this technique over bulk analytical techniques are: 1) the type I/type II H_2O ratio and the type I H_2O/CO_2 ratio may be very accurately determined, and 2) very small samples, or even petrographic thin sections may be used in the measurement, allowing studies of disequilbrium and zonation. This will also allow the hydrous impurities common in cordierite (e.g. Zimmerman, 1981) to be rigorously excluded from the measurement.

The formation of variable lengths of interconnected open channel due to the partioning of type II water into the unbound state will have a substantial effect on the observed closing temperatures and equilibration rates for cordierite. The diffusion rates for H_2O and CO_2 through a channel that is mostly plugged will be much lower than the rate through

a channel that is mostly open. As the length of interconnected open stretches approaches the thickness of the mineral grain, rapid equilibration is expected to occur. This has been observed by Goldman et al. (1977) who found that finely ground cordierite dehydrates at about 500°C while large crystals do not dehydrate until 800°C, and that the difference could not be attributed solely to diffusional path lengths. Selkregg and Bloss (1980) describe a cordierite with high Na and Be content which is resistant to dehydration, presumably because the number of plugs still in the channel at any temperature is higher than for other cordierites. The differences in dehydration temperatures reported by Zimmerman (1981) (400° to 800°C for crushed samples) are probably not due to the origin of the cordierites, as he suggests. It is more likely that they are a reflection of the channel cation content of the samples, which were not reported.

CO_2 also probably acts as a partial plug in the channels, and may affect H_2O equilibration rates. The much lower diffusion rates for CO_2 movement through the channels indicate that water will be more readily equilibrated experimentally in cordierite than CO_2. This is in agreement with the findings of Johannes and Schreyer (1981), who found that CO_2 moved in and out of synthetic, alkali-free cordierite at a much lower rate than H_2O, and that increased CO_2 content inhibited H_2O equilibration in high pressure, high temperature hydrothermal equilibration studies. Because of the interplay between diffusion and the coordination of channel cations, it should be more difficult to experimentally introduce equilibrium amounts of H_2O and CO_2 into cordierites with channel cations

present, and conversely the best natural cordierites for use as petrogenetic indicators will be those with high channel alkali contents because they will have comparatively high closing temperatures.

Acknowledgments

We would like to thank R. H. Currier for the cordierite, W. Johannes and W. Schreyer for providing analyzed samples of synthetic cordierite and for helpful discussions concerning the use of cordierite as a petrogenetic indicator, and E.M. Stolper for a critical review. This work was funded in part by NSF Grant EAR 79-19987.

Table 1. Cordierite Analytical Data

		wt. %
	Na_2O	0.33
	MgO	10.44
	Al_2O_3	33.31
	SiO_2	48.88
	K_2O	0.02
	CaO	0.13
	TiO_2	0.09
	MnO	0.15
	FeO	5.29
Subtotal		98.44
	H_2O type I	0.81*
		0.77**
	H_2O type II	0.43**
	CO_2	0.42*
Total		100.06†

*H_2O and CO_2 concentrations determined spectroscopically using powdered sample. Powder ε type I H_2O = 210 ± 10, ε CO_2 = 6000 ± 500 (ℓ mole^{-1} cm^{-1}). Standards were two synthetic cordierites provided and analyzed by W. Johannes and W. Schreyer, their #s 97A and 98A.

**H_2O type I and II concentrations using single crystal ε values of 204 and 256 (ℓ mole^{-1} cm^{-1}) from Goldman et al. (1977).

†Calculated using %H_2O from single crystal calibration (**).

References

Armbruster, T. and Bloss, F.D. (1980) Channel CO_2 in cordierites. Nature 286, 140-141.

Armbruster, T. and Bloss, F.D. (1982) Orientation and effects of channel H_2O and CO_2 in cordierite. American Mineralogist 67, 284-291.

Brown, G.E. and Mills, B.A. (1983) High temperature crystal chemistry of a hydrous alkali beryl from the Harding pegmatite, New Mexico. (In Press, American Mineralogist).

Carson, D.S., Rossman, G.R., and Vaughan, R.W. (1982) Orientation and motion of water molecules in cordierite: a proton nuclear magnetic resonance study. Physics and Chemistry of Minerals 8, 14-19.

Cohen, J.P., Ross, F.K., and Gibbs, G.V. (1977) An X-ray and neutron diffraction study of hydrous low cordierite. American Mineralogist 62, 67-78.

Goldman, D.S., Rossman, G.R., and Dollase, W.A. (1977) Channel constituents in cordierite. American Mineralogist 62, 1144-1157.

Goldman, D.S., Rossman, G.R., and Parkin, K.M. (1978) Channel constituents in beryl. Physics and Chemistry of Minerals 3, 225-235.

Hawthorne, F.C. and Cerny, P. (1977) The alkali metal positions in Cs-Li beryl. Canadian Mineralogist 15, 412-421.

Hochella, M.F. Jr., Brown, G.E. Jr., Ross, F.K., and Gibbs, G.V. (1979) High-temperature crystal chemistry of hydrous Mg- and Fe-cordierites. American Mineralogist 64, 337-351.

Johannes, W. and Schreyer, W. (1981) Experimental introduction of CO_2 and H_2O into Mg-cordieriete. American Journal of Science 281, 299-317.

Langer, K. and Schreyer, W. (1976) Apparent effects of molecular water on the lattice geometry of cordierite: a discussion. American Mineralogist 61, 1036-1040.

Martignole, J. and Sisi, J. (1981) Cordierite-garnet-H_2O equilibrium: a geologic thermometer, barometer, and water fugacity indicator. Contributions to Mineralogy and Petrology 77, 38-46.

Pye, E.G. (1957) Geology of the Manitouwadge area. Ontario Department of Mines Reports 66, part VIII, 1-114.

Rehm, H.J. (1974) Paraelektrische Resonanz und dielektrische Dispersion von Wasser in Beryll-Einkristallen. Zeitschrift für Naturforschungen 29A, 1558-1571.

Selkregg, K.R. and Bloss, F.D. (1980) Cordierites: compositional controls of Δ, cell parameters, and optical properties. American Mineralogist 65, 522-533.

Stout, J.H. (1975) Apparent effects of molecular water on the lattice geometry of cordierite. American Mineralogist 60, 229-234.

Wood, D.L., and Nassau, K. (1967) Infrared spectra of foreign molecules in beryl. Journal of Chemical Physics 47, 2220-2228.

Zimmermann, J.L. (1981) The liberation of H_2O, CO_2, and hydrocarbons from cordierites: kinetics, structural sites, and petrogenetic implications. Bulletin Mineralogie 104, 325-338.

Chapter 9

Summary

Hydrogen species in minerals.

It is extremely common for nominally anhydrous minerals to contain hydrogen; a quick perusal of almost any set of chemical analyses of minerals will reveal this. During the course of this work I have investigated both specific and general mechanisms which allow hydrogen to enter minerals. Although there are a variety of individual ways that this occurs, the mechanisms and species involved can be reduced to only a few that are generally important. Since the species of hydrogen must be determined before the solution mechanism can be proven, I will first review the proven hydrous species, then look at the mechanisms which allow them to enter minerals.

Alteration and Fluid Inclusions

Alteration and fluid inclusions are actually separate phases contained within minerals, but they are commonly the source of the water seen in chemical analyses of minerals. IR spectroscopy has proven to be very effective at identifying these and distinguishing them from trace hydrogen which is more of interest to this work. The techniques for distinguishing included hydrous phases and alteration are demonstrated in Figure 4, Chapter 4 (page 110). One of the most interesting sources of water of the general incipient alteration type is water that is adsorbed onto the surface of a freshly broken grain. This can presumably amount to a layer several molecules thick, and may be geologically important in extremely fine-grained rocks. In Chapter 4 I showed that for garnets this is unlikely to exceed 0.05 wt. % for grains

averaging 25 μm in diameter, but this may still be a significant amount in a mantle-derived sample and should be expected to increase as grain size decreases. This must be taken into consideration when analyzing for water as well as when considering possible sources and reactions of water in nature. In particular, water on grain surfaces may be important in controlling the deformation behavior of dunites and quartzites.

The spectroscopy of fluid inclusions is discussed in Chapter 2. Presently our understanding is limited to identifying large (greater than about 200 molecules) vs. small (less than about 5) groups of water molecules. This distinction is sufficient to aid in understanding water speciation in low-temperature quartz, which falls between those limits. The study of fluid inclusions will be interesting to pursue further, particularly with regard to mixtures of fluids since IR spectroscopy is very sensitive to many of the common and exotic components of fluid inclusions. An interesting question is the number of molecules required to coexist before they constitute a fluid inclusion; my work suggests that we should only consider the groups larger than about 200 molecules to be fluid inclusions, since they behave as separate phases and have the characteristics of fluid.

Molecular H_2O

Trace molecular water occurs in two general forms: groups of molecules which appear to have been trapped during rapid growth, and individual water molecules which occupy voids in the crystal structure. The latter type is that seen in zeolites and clays, for

instance. This is an interesting form of trace water because it can be truly dissolved, whereas the trapped groups of water molecules are metastable. This dissolved water occurs in beryl, cordierite, feldspar, and nepheline. It can be identified by the characteristic absorption at 5200 cm^{-1} in the near-infrared, and by the the anisotropic nature of its infrared absorption which is due to the crystallographic orientation of the water molecules.

Hydroxyl, OH^-

Hydroxyl groups appear to be the most common form for trace hydrogen in minerals. Minor IR absorptions attributable to hydroxyl occur so frequently that it is surprising to find a sample which does not exhibit them. In most cases it is difficult to determine the site of such a hydroxyl group because the symmetry information available is limited to the oxygen-hydrogen vector. However, it is possible to obtain quite a bit of information about bonding from the position and shape of the stretching absorption (Chapter 3). It is typical for trace hydroxyl to occupy fairly large sites in which there is very little hydrogen bonding; the hydrogen is simply behaving as a mono-coordinated cation. The existence of hydroxyl species is best determined from the existence of the combination bend+stretch mode at about 4500 cm^{-1} in the near-infrared.

Hydrogarnet, H_4O_4

The replacement of a silicate tetrahedron by four hydroxyl groups has come to be called the hydrogarnet substitution because it was first

identified in garnets, and may in fact be restricted to that mineral. The factors which may influence the existence of this substitution in a mineral are discussed in Chapter 4 and are complex, however it is unlikely that this substitution does not occur in other orthosilicates. Because of the impossibility of linking two H_4O_4 tetrahedra and the extreme structural changes that would be associated with linking a H_4O_4 tetrahedron with a SiO_4 tetrahedron, it seems possible that this substitution may be restricted to orthosilicates. Brief survey work of the orthosilicates olivine, zircon, and sphene has revealed common groups of O-H stretching absorptions. Their identity has not yet been determined, but they may be due to hydrogarnet substitution. Vesuvianite almost certainly can contain this substitution, based on the similarity of some of its O-H absorptions with those identified as hydrogarnet-derived in grossular.

H_3O^+, H, H_2, and SiH

One of the primary goals of this study was to identify the possible hydrogen species in minerals. The species listed here have from time to time been suggested to be important in minerals, but there is no supportable evidence that they occur to a significant extent. With the exception of molecular and atomic hydrogen, which occur as short-lived intermediates of radiolysis (Chapter 6), there is no evidence that they exist at all. When the case-history of reported occurrences is examined, they are found to be based on either bulk analysis or spectroscopic evidence which is better explained by the existence of water or hydroxyl. This is particularly true of molecular hydrogen,

which is theoretically undetectable in the IR. However, several reports may be found in the literature of it yielding an absorption at 4000 to 4200 cm^{-1} (Chapter 1). My work indicates that most O-H bonds yield an absorption in this region due to a combination of lattice bending modes with O-H stretching, and examination of the relative intensities of the reported molecular hydrogen bands indicates that they are in fact due to this sort of O-H absorption. H_3O^+ has been shown to occur only in extremely acidic environments not reproducible in silicates, although it may occur in some minerals from evaporite deposits. SiH has occasionally been suggested to occur in minerals and glasses, but the spectroscopic evidence for its existence is incomplete and its existence must be considered an unresolved question.

Solubility and solubility mechanisms of hydrogen.

In order to be able to predict the concentration, speciation, or site of hydrogen incorporation in a mineral it is necessary to understand the mechanisms by which hydrogen may be dissolved. Only three mechanisms appear to be important.

First, molecular water can occur (as described above) in voids in the crystal structure. The solubility limit in this case is related to the number of voids in the structure and the volume change associated with water occupying the voids. This volume change appears to be negligible in beryl and cordierite, so there is anticipated to be no pressure dependence on the solubility of water in these minerals. The volume change is not known for the solution of water in feldspar, and

the exact site of the water in feldspar has not been determined so the solubility limit is not known. It was shown in Chapter 7 that at 1 bar, molecular water is not stable above 600°C in feldspar.

Second, hydroxyl can occur in a charge-balancing role for another substitution, for instance AlO_3OH for SiO_4, or even completely neutralizing another substitutional ion, such as the LiOH net substitution that commonly occurs in natural quartz. In this case the solubility is limited by the concentration of the associated ion or ions. Hydrogen in this instance is behaving as a simple cation; it is only unique in that it is only mono-coordinated to oxygen. Hydroxyl may also of course substitute for flourine.

Third, hydroxyl may occur as the hydrogarnet substitution. This substitution is unique in that it is the only demonstrated form in which hydrogen actually changes the structure of a mineral. The solubility of this form of hydrogen would appear to be strongly controlled by the positive volume of solution, however its occurrence in mantle garnets suggests that there are other factors participating. Perhaps the hydrogarnet substitution is very compressible, which could make it very important in the mantle. The experimental work required to determine this has not yet been done. At one bar, hydrogen is extremely soluble in grossular garnet, since it is possible to make a silica-free garnet. In nature, the realistic limit appears to be about 2 wt. %, which corresponds to about one H_4O_4 tetrahedron per every 12 SiO_4 tetrahedra. This is potentially the most efficient mechanism for dissolving hydrogen in silicates.

It has been suggested, particularly in the case of hydrolytically

weakened quartz, that hydroxyl may structurally occur in minerals through the hydrolysis of Si-O-Si bonds by water to form Si-OH HO-Si groups. I have found no evidence for this occurring even in comparatively 'wet' synthetic quartz. However, the occurrence of this reaction in silicate glasses suggests that it may yet be discovered to occur in crystalline materials, and it appears that a similar reaction is responsible for the uptake of hydroxyl by metamict zircon (Chapter 6). Because of the range of bond lengths and hydrogen bond strengths that may be expected from this type of hydroxyl site, I anticipate that the IR spectra of such hydroxyl would be composed of a broad band similar to that seen in zircon.

One potentially valuable application of the study of trace hydrogen in minerals is the development of water fugacimeters, that is mineral-water systems in which the water concentration has been calibrated against temperature and oxygen-hydrogen fugacities. In order for such a system to be usable it must be simple, and the best candidate is cordierite which is currently being calibrated experimentally by Werner Schreyer and W. Johannes. In order to use even a simple system like this, however, it is necessary to have a relatively complete understanding of the hydrogen siting and speciation. For instance, in cordierite it appears that only one of the two water types present provides useful information on water fugacity (Chapter 8). The hydrogarnet substitution is a possible water fugacimeter for the mantle, but its application appears even more complicated than that of cordierite (Chapters 4 and 5).

Reactions and interactions of hydrogen in minerals.

The common interaction of trace hydrogen with physical properties of minerals appears to be related to the extreme mobility of hydrogen at temperatures of geologic importance, and the ease with which it may form species of different charges in the oxygen framework of silicate minerals. Hydrolytic weakening appears to occur through the catalytic breaking of Si-O-Si bonds by water (Chapter 2), with the water only dissociating to hydroxyl groups at the instant the mobile defect plane passes. Similar reactivity is seen in radiation damage mechanisms. Here this is good evidence that atomic hydrogen may occur as a highly reactive intermediate (Chapter 6), and hydroxyl appears to play a common role in annealing local charge imbalance caused by oxidation state changes and the breaking of bonds. This role is only possible because of the mobility of protons, which may move rapidly through diffusional jumps between oxygens. It is the ubiquitous occurrence of a convenient charge-balancing species that makes hydrogen important in radiation damage mechanisms; no other ion can move rapidly enough to participate in as many reactions. Hydrogen is also unique in that it occurs mono-coordinated to oxygen, which is partially responsible for its ability to break Si-O-Si bonds in crystals and melts. The reaction of H_2O with an Si-O-Si bond need only affect that bond and requires no additional charge compensation to occur, making the reaction rapid and easily reversible.

Conclusion

The goals outlined in Chapter 1 have certainly not all been fulfilled. However, there is now a solid foundation of understanding of the behavior of trace hydrogen in minerals, and this understanding is predictive in that we now know what species may occur, the controls on their concentrations, some possible reactions they may undergo, and some mechanisms which may be important in affecting mineral properties. The spectroscopic tools for studying hydrogen are now well established. The high temperature work which I have begun is perhaps the most promising area for future work because of the ability to directly observe properties and reactions at conditions of geologic interest. Along with the development of mineral systems as water fugacimeters this appears to be a field of research poised for rapid advancement.